MICROFLUIDIC PLATFORMS AND MULIVARIATE ANALYSIS FOR IMMUNE CELL SIGNALING STUDY

A Dissertation
Presented to
The Academic Faculty

by

Luye He

In Partial Fulfillment
of the Requirements for the Degree
Doctor of Philosophy in
Chemical and Biomolecular Engineering

Georgia Institute of Technology
December of 2017

MICROFLUIDIC PLATFORMS AND MULTIVARIATE ANALYSIS FOR IMMUNE CELL SIGNALING STUDY

Approved by:

Dr. Hang Lu, Co-Advisor
School of Chemical Engineering
Georgia Institute of Technology

Dr. Mark Styczynski
School of Chemical Engineering
Georgia Institute of Technology

Dr. Melissa Kemp, Co-Advisor
Department of Biomedical Engineering
Georgia Institute of Technology
Emory University

Dr. Victor Breedveld
School of Chemical Engineering
Georgia Institute of Technology

Dr. Cheng Zhu
Department of Biomedical Engineering
Georgia Institute of Technology
Emory University

Date Approved: Nov. 13th, 2017

To my grandparents and parents

ACKNOWLEDGEMENTS

First, I would like to thank my co-advisors, Dr. Hang Lu and Dr. Melissa L. Kemp, who show great leadership in creating an intellectual, collaborative, and rigorous research environment with continuous willing and effort to improve. They have allowed me the freedom to explore subjects that satisfy my curiosity and interest, while being critical, constructive, supportive and optimistic to my effort. They have been very patient with my struggles, while encouraging me to live to my potential. From them I have learned how to do research, solve problems and attitude in face of unknown. I also would like to thank all my committee members, Dr. Cheng Zhu, Dr. Victor Breedveld, and Dr. Mark Styczynski for their expertise, advice and guidance through this process.

Also, I would like to thank all the members of the Lu Lab and Kemp Lab for their companion and help. I would like to mention in particular: Dr. Hyundoo Hwang, who taught me all the tricks that made my microfluidics worked and shared selflessly ideas that made my project possible; Dr. Ariel Kniss, who worked with me closely on the T-cell project and gave so many good suggestions during subgroup meetings; Linda Kippner as the best lab manager who is fun and also taught me how to make cells happy; andDr. Guillaume Aubry, Dr. Charles Zhao, Tel Rouse, Fangyuan Zhou for being good friends besides awesome colleagues; Kaitao Li and Baoyu Liu from Dr. Zhu's lab for their insightful discussion and generous help during difficult time.

I want to also thank all my friends here in GT, who have helped me through the days. Finally and most importantly, I want to thank my family for their love, encouragement, and sacrifice by letting me devote my best years to this unique experience.

TABLE OF CONTENTS

LIST OF FIGURES

LIST OF APPENDIX FIGURES

SUMMARY

Cell-mediated immunity is a critical component of an adaptive immune system, where immune functions are mostly mediated through the coordination of T cells. The understanding of fundamental T cell signaling processes involved in cell-mediated immunity has underlined recent advancement of cancer immunotherapy. While conventional methods (including lipid bilayer, biomembrane force probe (BFP) and microwell, *etc*) remain important tools in studying these fundamental signaling processes, the lack of either control (e.g. microwell) or throughput (e.g. BFP) poses substantial challenges in effective study of highly dynamic and heterogeneous cellular signaling processes. This thesis responded to these challenges through development of microfluidic tools and multivariate data analysis methods to solve problems related to immune cell signaling study. In Chapter 2, a microfluidic platform able to deliver programmable dynamic stimulus to interrogate T cell signaling was developed. This platform was applied to probe system property of T cell signal transduction pathways, which showed T cell calcium signaling pathway behaved as low-path filter and was highly heterogeneous among T cell population. In Chapter 3, a microfluidic system to precisely manipulate and synchronize cell interaction of large number of cell pairs was developed. This system provided simultaneous real-time signaling imaging and organelle tracking at temporal density with single cell resolution. In addition, new image-derived metrics were developed to quantify calcium response and mitochondria movement. In Chapter 4, the cell interaction microfluidic system was applied to study how subtle differences in antigen structures translate to distinct T-cell effector functions through early signaling processes such as

calcium and mitochondria during T-cell antigen recognition. Using an altered peptide ligands (APLs) and a hybridoma cell line model, this work recapitulated prior findings of T cell calcium dynamics responding to differences in antigen potency with sensitivity of single amino acid change, while remained inert to changes in antigen concentration. Lastly, a partial least square regression model was developed, which highlighted mitochondrial positioning as a strong predictor of calcium response during T-cell antigen recognition. In summary, this thesis, microfluidic tools were developed to provide precise control of cell microenvironment and interaction, which enabled *in vitro* real-time live-imaging of cell signaling events at large sample size with single cell resolution. Combined with advanced statistical techniques to interpret these data, this work shed new insights into signaling processes relevant to immune cells, which had not been resolved using conventional techniques and population-based statistics. These results demonstrated the new methodology of using microfluidic tools and multivariate analysis to investigate fundamental cellular and molecular process, which was critical for understanding of immune system and future engineering of rational therapies.

CHAPTER 1. INTRODUCTION

1.1 Thesis Motivation

1.1.1 From Study of Immunology to Applied Arm of Bioengineering

Immunology studies the functions of immune system, the major role of which is to distinguish self from foreign material (1). The immune system protects human beings from infectious diseases and cancer, while maintains tolerance to self-antigens in order to absorb necessary nutrition and to avoid autoimmunity. The disruption of this balanced system has severe consequences, manifested in immunodeficiency (as in the case of AIDS) in one way and auto-immune disease (such as multiple sclerosis) in the other.

Faced by our immune system is seemingly an impossible mission. The immune system must recognize millions of antigens which circulate our body and harbor in our living environment with both breadth and precision (2). In order to conquer such tasks, our immune system has evolved to be an extremely sophisticated system, which is composed of tens of immune cell types each in charge of a specific function, hundreds of cytokines and chemokines that mediate distinct immune responses, and essentially unlimited possibilities of antibodies to neutralize same number of different kinds of antigens. With development of genetics and molecular biology tools, we are closer to understanding the essence of immune system than ever before, shaping immunology into an applied arm of bioengineering that can be modified, manipulated and redesigned to cure diseases.

1.1.2 Understanding of Immune-Cell Signaling Process Underlines Development of Immunotherapy

Recently, people have realized the potential of augmenting endogenous immune system in curing cancer (3–5). Novel therapies such as Chimeric Antigen Receptor (CAR) T-cell therapy and Check Point Inhibition are translating clinical practice of cancer treatment. In CAR T-cell therapy, endogenous T cells were extracted from patients and were engineered to express artificial receptors that had better affinity towards cancer antigen than native T cell receptors. These cells were then reintroduced into the patient, which were better equipped at eliminating cancer cells. In Checkpoint Inhibition Therapy, it was discovered that cancer cells utilized PD-1/PD-L1 signaling pathway in order to escape T-cell surveillance. By blocking this signaling pathway, this therapy relieved the suppress of cancer cells on T cells and improved elimination of cancer cells following recognition of cancer antigens (6). Combining CAR T-cell therapy with Check Point Inhibitors has resulted in promising results in treatment of some solid forms of cancer (7). These achievements will be impossible without the understanding of cellular and biomolecular foundation of the immune system. Understanding of fundamental signaling mechanisms involved in immune functions provides knowledge for points of medicine interference, which is critical in future advances of rationally designed therapy (8–11).

1.1.3 Novel Experimental Tools are Needed for Precise Manipulation of Single Cells

However, studying immune cell signaling presents substantial challenges. While *in vivo* studies in whole animals were useful in assessing the interaction and efficiency of certain therapy with the organism holistically, direct observation of cellular signaling processes is difficult, if not impossible. In order to observe fundamental cellular signaling processes and to interrogate these processes using molecular tools, it is preferable to isolate the process of interest in single cells. However, because cells are small with diameters of

only 5μm to 20μm, precise manipulation and perturbation of these single cells are very difficult with macroscopic tools. In addition, many immune cell types that circulate the body are non-adherent, which poses extra challenge to monitor their signaling processes compared to adherent cell types.

1.1.4 Novel Modelling Techniques are Needed for Interpretation High-Dimension Cell Signaling Data

Different from studies where only a few features were measured at sparse time points, real-time imaging of large cell sample size will allow measuring of multiplex signaling features simultaneously at high temporal density. The next challenge is to interpret the resulting high dimensional dataset. With multiple features and each feature containing tens of time points, uncovering important relationship by manual examination is impractical (12). Simple statistics based on population means and variance are insufficient, and more advanced statistical techniques are needed.

1.2 Review of Immunology

1.2.1 Basic Concepts in Immunology

The immune system can be largely divided into innate immunity and adaptive immunity (1). Innate immunity is the first line of defence, composed of cells derived from the myeloid lineage including dendrite cells, macrophages, eosinophil, etc. Innate immunity cells from innate immunity are equipped with general pattern recognition receptors to recognize pathogen-associated molecular patterns (PAMPs), evolution-conserved in many pathogens (13–16). Pathogens that enter the body are initially

recognized and controlled in a non-specific manner by the innate immune system, which usually induce an inflammatory response. Antigen presenting cells (APCs) of innate immunity (e.g. dendritic cells) then initiate the adaptive immune response by activation of lymphocytes in secondary lymphoid tissues. Lymphocytes which originate from lymphoid lineage of bone marrow include T cells, B cells and natural killer cells. Unlike innate immune cells, these cells are equipped with unique antigen receptors which are only able to recognize antigens with certain molecular motif (17). A specific antigen selects out corresponding clone of lymphocytes, which proliferate in peripheral lymphoid organs and differentiates into effector cells. Upon maturation to effector cells, they are ready to eliminate pathogen and infected cells through the production of antibody (B cells) or targeted killing (cytotoxic T cells) (18).

1.2.2 Cell-Mediated Immunity

Unlike the humoral immune response, where antibodies produced by B cell exert their protection in extracellular fluid, cell-mediated immunity is achieved through direct cell-cell contact between immune cell partners. Examples of cell-mediated immunity includes: activation of naïve T cells in response to antigens presented on antigen presenting cells (APCs), T cell-mediated cytotoxicity (CD8 T cells), activation of macrophage and B cells by helper T cells (CD4 T cells) (19–21). A hallmark of cell-mediated interaction is the formation of supramolecular activation complex (SMAC) or the immunological synapse (IS) (22–25), which is a circular cluster of T-cell receptors (TCR), antigen packaged within the peptide-major histocompatibility complex (pMHC), co-stimulatory

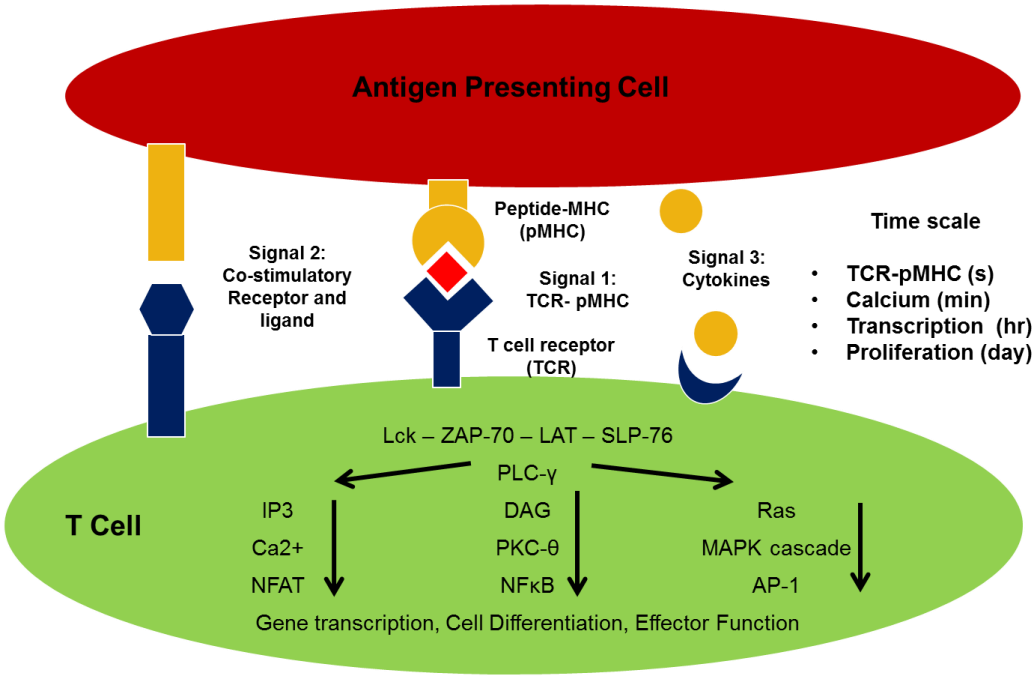

Figure 1-1 T cell signaling during antigen recognition

T cell interacts with antigen presenting cells (APCs) through 3 categories of signals: (1) T cell receptors (TCR) recognize specificity of antigen conveyed through peptide-MHC (pMHC) (signal 1). (2) Co-stimulatory molecules modulate signal 1 either positively or negatively. (3) Different cytokines are secreted by APCs to further modulate T cell function. All 3 signals converge in T cells to trigger cascades of signaling events that eventually leads to transcriptional, translational changes and cell differentiation. The time scale of these events spans from second to days.

receptors and their corresponding ligands formed at the interface between a T cell and an APC. The formation of IS accompanies reorientation of the cytoskeleton, which polarizes the T cell by local reorganization of the cortical actin cytoskeleton, reorientation of microtubule-organizing center (MTOC) and the Golgi apparatus. The reorganization and polarization of T cell is critical in performing many effector functions of T cells, exemplified in cytotoxic T cells' target secretion of cytotoxic granules at the side of cell contact onto the target cells (26). Despite the importance of cell-mediated immunity,

signaling processes involved in this process, such as IS formation and their function, have not been fully understood yet, which are still ongoing research topics.

1.2.3 Antigen Recognition by T-Cell Receptor

An antigen-specific receptor on a T cell, known as the T-cell receptor (TCR), recognizes an antigen in the form of a peptide bound to a major histocompatibility complex (pMHC) on an antigen presenting cell (APC) (27–29) (Figure 1-1). T cell receptors are generated by rearranging of receptor gene segments in T cells, which give rise to more than a million of unique biochemical structures capable of recognizing essentially any antigen (30–32). MHCs (MHC class I and MHC class II (33–35)) are expressed in all nucleated cells, whose main function is to mount intracellular antigens onto cellular surface in order to interact with cells from the immune system (36–41). Thus, MHCs provide the portal for the immune system to gauge the health of somatic cells and take proper reaction based on the interaction with the repertoire of antigens. The TCR-pMHC interaction is extremely specific and sensitive: a trace amount of agonist antigen presented on antigen presenting cells (APCs) can induce full activation of T cell clone (42, 43), while subtle structural difference within peptide sequences leads to distinct effector functions (44–50). However, it is still yet to understand how T cells are equipped with such high sensitivity and specificity.

1.2.4 T-Cell Signaling During T-Cell Antigen Recognition

Three kinds of signals participate in T-cell antigen recognition and convert information received from extracellular space into intracellular biochemical signals (51–54) (Figure 1-1): Signal 1 is the recognition of peptide-MHC (pMHC) complex on APC

by T-cell receptor on T cells (55–62); Signal 2 is delivered on cell surface by co-stimulation factors including CD28, CTLA-4, and CD40L, *etc*; Signal 3 is delivered through extracellular fluid in form of cytokines, and small molecules (H_2O_2, etc). All three signals are required in proliferation, differentiation and effector functions of T cells: for example, Signal 1 alone leads to inactivation (anergy) of T cell clone; Signal 2 alone has no effect on T cells; and various forms of Signal 3 lead to differentiation into different T cell effector types.

For Signal 1, antigen recognition by the T-cell receptors and its co-receptors lead to sequential phosphorylation of several kinases and scaffold protein: Src-family kinases (63, 64), tyrosine kinase ZAP-70, LAT (linker of activated T cells) and SLP-76 (65, 66). These scaffold proteins recruited and activated phospholipase PLC-γ (67), which is the converging point with signaling from co-stimulatory interaction (such as CD28-B7.1 (62)). Activated PLC-γ generates the second messenger diacylglycerol (DAG) and inositol trisphosphate (IP_3), which triggers a triads of signaling cascades(68–71): IP_3 triggers ER Ca^{2+} release, activating NFAT through calcineurin; DAG recruits protein kinase C-θ, activating NFκB through CARMA; and DAG recruits RasGRP to active Ras, which stimulates mitogen-activated protein kinase (MAPK) relay and induces expression of the transcription factor AP-1. The transcription factors NFκB, NFAT, and AP-1 act together to induce specific genes transcription, leading to cell proliferation and differentiation. While the structure of signaling pathway during T-cell antigen recognition is known, it is not known how early signaling events (such as calcium, *etc.*) encodes information transmission from receptor ligation to downstream transcriptional and translational activities. Besides the canonical signaling pathway listed here, mitochondria are also

considered in participating in T cell antigen recognition (72–74). However, there the exact role of mitochondria is still unclear (75–78).

1.3 Review of Conventional Technology in Cell Signaling Studying

1.3.1 Lipid Bilayer for Studying Formation of Immunological Synapse

In order to study IS formation, a method relying on artificial lipid bilayer had been developed (22, 23). In this method, an artificial membrane lipid bilayer was deposited onto a glass slide, after which various molecules including peptide-MHC complex, B7.1, and other adherent molecules were added onto the lipid bilayer to mimic the surface of a target cell. Then T cells were deposited onto the lipid bilayer, and time series imaging was performed in order to study the dynamics of IS formation in T cells stimulated by molecules presented on the lipid bilayer. This method provided a bottom-up method in studying cell signalling by allowing fine tuning of the composition of the lipid bilayer, which yielded much insight regarding the dynamic of IS formation. However, this artificial bilayer could not mimic all biomolecular and mechanical properties of an antigen presenting cell (APC), which limited the interpretation of such results in intact cells. In addition, constructing a lipid bilayer was labor-intensive and low-throughput in nature. While the top-down orientation in this method was useful in providing a planar view for imaging IS formation, it was less optimal for studying signaling processes that happened in perpendicular direction to cell interface, such as in studying the movement of organelles.

1.3.2 Biomembrane Force Probe for Precise Control of Cell Interaction

In order to study mechanical properties of molecular interaction, force spectroscopy using biomembrane force probe (BFP, also known as adhesion frequency assay) was developed (79–82). In this method, molecules to be investigated (peptide-MHC, *etc.*) were coated on a microbead, which was further biochemically anchored onto a red blood cell. Then both the red blood cell and the T cell were separately captured on two micropipettes, which were further held by two mechanical arms to make contact between the T cell and the microbead. The adhesion between TCR and its ligand (peptide-MHC) caused elongation of the red blood cell, the tension of which could be measured as two cells were pulled apart until separated. The BFP method was highly sensitive in resolving force of molecular interactions down to single molecular interaction in pico-newton range. Besides measuring molecular interaction, BFP was also used to study signaling dynamics in interacting cells (83, 84). However, despite good control on cell contact, the throughput of this method was limited. Collection of data on multiple cells was done in a serial fashion, while quality of cells might deteriorate over long experiments procedure.

1.3.3 Microwell Plate Method for Forming Cell Contact Pairs

Because lymphocytes are non-adherent cells, positioning two cells together to study cell-cell interactions poses additional difficulties. Early studies of immune cell interactions was conducted in microwell plates (85–87). In this method, antigen presenting cells (APCs) were grown into confluency at the bottom of a microwell plate and incubated with peptide antigen of interest. Next, T cells suspension were added into the plate and centrifuged down onto the bottom of plate to force contact with APCs. However, due to randomness in seeding and contact of cells, it usually required manual searching of the plate in order to image cell pairs. More importantly, information of signaling events during centrifuging

operation was unavailable to an investigator because measurements could not be taken during centrifuging. Lastly, this method was not compatible with cell signaling interrogation by stimuli delivery, because exchange of media into microwell plates would cause disturbance and loss of established cell position.

1.3.4 Technical Challenges Unmet by Conventional Technologies

While each technology above has its unique niche and remains useful tools in studying signaling processes of immune cell signaling, there are still experimental needs that are unmet by these developed technologies. Specifically, an ideal technology should achieve following goals: 1. capture live non-adherent cells at fixed locations for microscopic imaging; 2. maintain a good control of microenvironment (media, temperature, pH, etc) for cells; 3. image cells at cellular and sub-cellular resolution; 4. monitor large amount of cells simultaneously for statistical analysis; 5. deliver dynamic chemical cues to perturb cell signaling without disturbing cell location; 6. precisely control cell-cell interaction for signalling study. Such a platform will be a good alternative if not a better tool than established methods for *in vitro* live-cell real-time imaging of signaling processes relevant to cell-mediated immunity, which will be a useful addition to the toolbox of immunologists and cellular/molecular biologists.

1.4 Review on Application of Microfluidics in Cell Signaling Study

1.4.1 Advantages of Microfluidics in Single Cell Analysis

Microfluidics provides a potential solution to these challenges (88, 89). First of all, microfluidics operates on micrometer scale, similar to that of a cell, which allows effective

manipulation of single cells (90, 91). Secondly, microfluidics enables fast mass and energy transport either for maintaining microenvironment or providing flexible perturbation: 1. large surface-to-volume ratio of microfluidic device enables fast heat exchange, which allows tight temperature control; 2. use of PDMS makes microfluidics gas permeable to exchange of CO_2 and O_2 with ambient environment, which maintains media pH and facilitates cellular energy production through oxidative phosphorylation (92). 3. continuous flow removes waste and replenishes nutrients for *in vitro* cell culture. 4. microfluidics provides means to deliver chemicals stimuli in order to perturb or initiate cell signaling (93); 5. microfluidics reduces the labor involved in experimental process and makes automation possible. The following are reviews of current microfluidic approaches that have been developed for single-cell analysis.

1.4.2 Microfluidics for Capturing and Arraying Cells

Capturing and arraying non-adherent cells in a microfluidic device is the first step in studying cells signaling. Several microfluidic devices were developed for this task. A microfluidic microwell was a microwell plate fabricated at micrometer scale, where each well had single cell capacity (100 to 400 μm^2). In this method, cell suspension was flowed over the space above microwells, followed by sedimentation of cells into microwells under the force of gravity (94–97). However, despite the simple concept of this design, topologically it was difficult to ensure the flatness of the bottom side of the wells, which was bonded to a glass slide, rending high quality imaging difficult. Some microfluidic cell capture devices were based on electrical methods (98, 99). While these methods provided more deterministic cell movement, they usually required sophisticated fabrication techniques (for example, to incorporate electrodes on chip). More importantly, electrical

based methods generally required specific electrolyte buffer, which were not necessarily compatible with cell media. Hydrodynamic approaches had the advantages of simple device fabrication and operation, because they used cell media itself as operation fluid. By estimating the fluid resistance in microfluidic array, high-throughput cell arraying was achieved (100–102). For example, in the Dr. Hang Lu's and Dr. Melissa L. Kemp's labs, microfluidic devices based on hydrodynamic method have been previously developed for arraying of single T cells (103, 104).

1.4.3 Microfluidics for Delivering Stimulus to Cells

Once immune cells are captured on-chip, the next challenge is to stimulate cells through delivery of soluble chemical cues. Several microfluidic devices were developed to achieve this goal. Early approaches established spatial gradients and exposed cells in different locations with different stimulus concentration (105–108). However, each cell could only receive time-invariant stimulus with spatial stimulus gradient, which limited the use of such methods if time-varying stimulus was desired to mimic naturally dynamic extracellular signal received by cells. Active valve components were required to generate temporally changing stimulus (109–118). Multilayer devices with separate layer for pneumatic valve and cell array offered more control on flow in microfluidic channel, thus suitable for delivering temporal stimulus (116). However, multilayer devices were generally difficult to fabricate, thus a single-layer device with pneumatic valves on the same layer with the cell array became an attractive alternative (119). In order to interrogate T cell signaling using external soluble cues, there is a need to develop a microfluidic platform which is able to deliver dynamic stimulus to anchored live T cells.

1.4.4 Microfluidics for Cell Interaction Study

Immune cells communicate not only through exchanging biochemical cues in extracellular space, they also interact through direct cell-cell contact. In order to study cells in interaction with each other, various microfluidic approaches have been developed. As in cell capturing and arraying, microfluidic microwells were also used for cell interaction studies (120, 121). While simple to fabricate and straightforward to use, there was still little control on contact of two different cell types because two immune cell types were randomly seeded into the wells. On the other hand, cell pairing devices based on dielectriophoresis (DEP) were used to achieve deterministic cell pairing (122). Again, electrical-based method raised concern about compatibility of electrolyte buffer with cell sample, not to mention fabrication complexity which was required to incorporate electrode on chip. Lastly, hydrodynamic approaches remained attractive alternatives, but extending single cell capture to cell interaction was not trivial. One interesting design used cells themselves as movable plug to control the loading of the second cell type: once the first type cells adhered to the surface and started to migrate away, the plug on flow path was removed to attract the second cell type (123). However, the first cell type was required to adhere to a surface before the second cell type could be loaded, which prolonged device operation time. Another design used sequential opening of two side channels to load two cell types onto each side of a channel to facilitate cell contact (124). However, this method could not guarantee contact of cells and had limited throughput (about 5 cell pairs). Several methods for cell interaction used a reverse flow mechanism (125), achieving high-throughput (about 100 cell pairs) and deterministic cell interaction, and were used for cell signaling monitoring (126). Lastly, several designs utilized deformable property of PDMS to achieve

cell interaction and signaling studies (127). In order to study early signaling processes during antigen recognition, there is a need to develop a microfluidic platform that enables precise control of immune cell interaction.

1.5 Review on Application of Advanced Modeling Techniques in Cell Signaling Study

In data-derived modelling, the choice of modelling depends on the availability of data. In biological experiments where population statistics were measured with one variable changed at a time, use of simple statistical techniques such as sample mean and variance, ANOVA, and simple regression are sufficient. However, as new technologies bring down the cost of obtaining data, more advanced statistical tools are required to interpret multivariate data and time series data. Luckily, many advanced statistical tools have been developed in other disciplines in order to cope with the expansion of data in those fields such as in control engineering, manufacture, statistics, *etc* (128). More advanced modelling and statistical techniques, inlcuding multivariate analysis, principle analysis techniques (PCA), and time series analysis, have been developed and applied to interpret multivariate and time series data in these fields.

Similarly, with more and more real-time data on large sample size are enabled by new technologies, biological experiments also start to generate larger and larger size of data, such as in genomics (129). The advanced statistical techniques developed in other field has been applied in biological studies. Among these techniques, partial least square regression is useful in identifying important relationships among large number of variables (130), which has been applied to signaling studies (131, 132).

1.6 Thesis Structure

In Chapter 2, to study the effect of reactive oxygen species (ROS) in T cell calcium signaling, a microfluidic platform capable of delivering dynamic stimulus to T cells was developed. On-chip valve was used to generate dynamic chemical stimulus from binary inputs in order to perturb T cells signaling. Using this device, the system property of T cells signaling network regarding calcium and ROS was studied.

In Chapter 3, a microfluidic system was developed to enable synchronized interaction between two immune cell partners. Operation of this device did not alter natural signaling process and provided a high-throughput way to study T-cell signaling during antigen recognition. A cell tracking algorithm was also developed to facilitate analyzing of cell signaling data.

In Chapter 4, the microfluidic system developed in Chapter 3 was applied in studying how antigen potency and dose modulate calcium response and mitochondria movement during T-cell antigen recognition. New metrics were developed to quantify calcium dynamics and mitochondria movement. A partial least square regression model was also developed to identify important time points and metrics that relate to calcium-mitochondria interactions during antigen recognition.

In Chapter 5, the contribution of this thesis to various domains is reviewed. Future research directions that follow naturally from the work of this thesis are discussed.

CHAPTER 2. DEVELOPMENT OF A MICROFLUIDIC PLATFORM FOR DELIVERYING DYNAMIC STIMULI TO INTERROGATE T CELL SIGNALING

Parts of this chapter were adapted from He, L, Kniss, A*, et al., An automated programmable platform enabling multiplex dynamic stimuli delivery and cellular response monitoring for high-throughput suspension single-cell signaling studies. Lab on a Chip, 2015. 15(6): p. 1497-1507.*

2.1 Introduction

T lymphocytes are a critical component of the adaptive immune response. Activation of T cells induces rapid signaling through multiple kinase cascades to alter gene expression and ultimately leads to rapid proliferation and cytokine release (133, 134). The dynamic feature of these signaling pathways is essential for full functionality of T cells (135, 136). Dysregulation of T cell intracellular signaling has been implicated in a multitude of diseases such as asthma (137), allergic reactions (138), autoimmunity (139), lupus (140), and tumor immunity (141). Although many components of the T-cell receptor signaling network have been identified, the signal transduction properties of these dynamic processes are difficult to be discerned with conventional experimental methods, which typically measure cellular response to a simple stimulus concentration step change.

To better understand the dynamic network structure and dominant feedback controls in complex biological systems, system identification methods, originally developed in control engineering, have recently been applied (142–145). By stimulating

cells with a dynamic input signal and measuring the gain and delay of the output signal, the signal transduction properties of a particular signaling pathway can be analyzed (146). However, this approach requires short timescales; for example, calcium signaling has a time scale of seconds to minutes (147), an event too fast to interrogate for experiments done in bulk. Moreover, due to heterogeneity among cells, conventional population-average assays can mask individual cell dynamics (147, 148). The successful adoption of a systematic engineering approach relies on simultaneous delivery of biologically relevant dynamic stimuli and measurement of high-throughput readouts at single cell resolution.

Microfluidics offer new opportunities to study cellular signaling dynamics (104, 149–152). One such microfluidic design used for studying chemotaxis generates a spatial rather than temporal chemical gradient (153). Other designs have utilized oscillatory chemical signals to enable frequency response analysis of cellular signaling properties (142–144, 154). Most of these experimental setups rely on macro-scale external components to achieve fluid switching (143, 155), and the damping associated with a large dead volume in these setups limits temporal resolution. More importantly, these schemes do not allow dynamic changes in concentration. While one previous work has shown a scheme capable of generating temporal variation in concentration (156), this implementation is rather complex with multiple layers and requires numerous syringe pumps to operate. One further impediment is that non-adherent cells often shift out of place under flow condition, rendering these technologies not compatible with suspension cells such as T cells.

An experimental platform that enables the delivery of dynamic chemical signals varying in both time and concentration level is introduced in this chapter. This platform

incorporates hydrodynamic cell traps to enable a high-throughput readout of single T cells using time-lapse microscopy (104). In addition to the versatile range of signals it can deliver, the fabrication and operational simplicity makes it a convenient tool for end-users. Initially developed for T cell signaling studies, this platform can be generalized to a variety of cell types including adherent cells and can be applied to a broad range of problems in single-cell analysis, such as in pharmacology, immunology, stem cell and cancer research.

2.2 Material and Methods

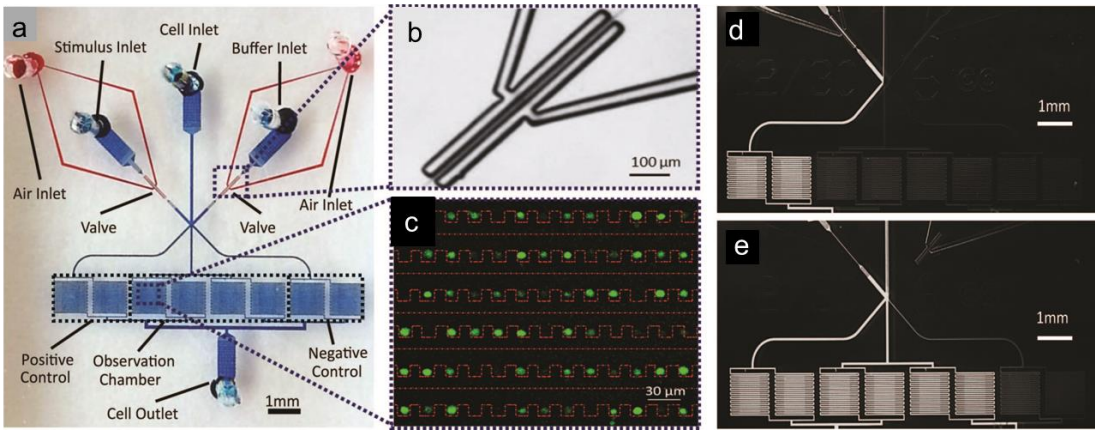

Figure 2-1 Device design

(a) Micrograph of microfluidic device: pneumatic valves (red) and fluid flow module (blue). (b) Enlarged bright field image of pneumatic valves when actuated. (c) False color image of Jurkat cells (green) trapped in cell chamber (red dot line). (d & e) Fluorescent image of alternate switching between fluorescein solution (bright) and PBS (dark).

2.2.1 Device Design

Our device consists of a single-layer PDMS that is plasma bonded onto a standard glass slide (Figure 2-1 a). It is composed of two functional modules: pneumatic valves to generate stimulatory signals and cell trap arrays to facilitate high-throughput imaging.

We use two sets of on-chip pneumatic valves (Figure 2-1 b), which are key to generating versatile dynamic signals. By integrating the valves on-chip, we eliminate pressure fluctuations associated with using external macro-scale switch valves and tubing. This feature enables stable flow and faster response time of the system. The design is all in a single-layer (157), avoiding the time-consuming and labor-intensive processes of fabricating multiple layer devices (158). Each set of valves forms a two-sided clamp on each of the two solution inlets (spacing of 10 μm between valve and channel of 10 μm in width). By alternate actuation of the two valve sets, we can modulate the laminar interface between co-flowing streams (Figure 2-1 d & e)(157). The flow then splits into multiple cell trap arrays downstream. Cells in the middle four chambers are exposed to the dynamic stimuli created by the fluid switching, while cells in each of the two side chambers experience constant stimuli as a positive or negative control (Figure 2-1 a, d & e).

Because of the small dimensions of flow channels (width of 30 μm and height of 15 μm), on-chip filters upstream from the cell chambers were included in the design to prevent debris from clogging the cell traps. The cell trap arrays were adopted from a previous design from our lab (104), where cells are passively trapped via hydrodynamic focusing (Figure 2-1 c). Due to the small inner volume of the device, we chose to use a pressure source to provide for a more stable flow, as opposed to a flow source.

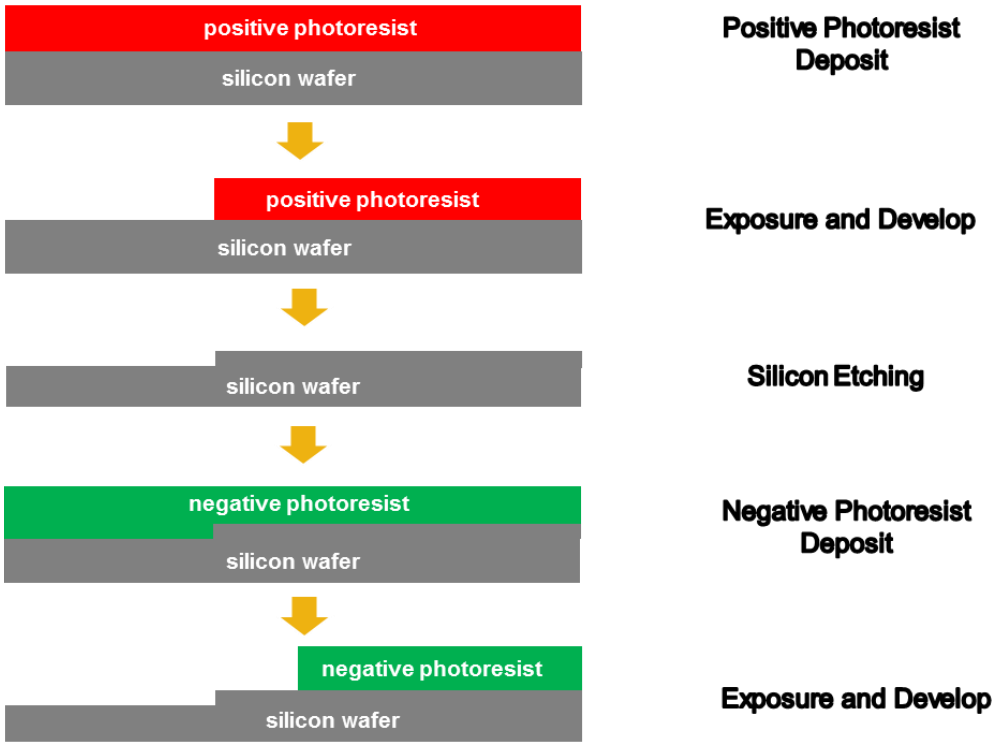

Figure 2-2 Microfabrication process for two-layer hybrid master

2.2.2 Device Fabrication

To make a device, polydimethylsiloxane mixture (*PDMS*, Sylgard 184, Dow Corning, Midland, MI) was cast over a hybrid two-layer master. The microfabrication process of the hybrid two-layer master is shown in Figure 2-2. The bottom layer of the master is 2 μm high and was etched on a new silicon wafer by deep reactive-ion etching (DRIE). The process ensured the high uniformity of this shallow layer, which is difficult to achieve using photoresist spin coating. The top layer of the master is 15 μm high and was spin-coated onto the bottom silicon feature using negative photoresist (SU-8 2015, Microchem, Newton, MA) and processed by standard UV photolithography. The master was treated with tridecafluoro-1,1,2,2-tetrahydrooctyl-1-trichlorosilane vapor (United

Chemical Technologies, Bristol, PA) in a vacuum desiccator for 12 hours to prevent adhesion of PDMS during the molding process. PDMS mixture (A and B in 20:1 ratio) of 1 mm thick was first poured onto the master and partially cured in a 75 °C oven for 15 minutes. Then, another layer of 4 mm PDMS mixture (A and B in 10:1 ratio) was added onto the bottom layer and incubated for another 4 hours. The difference in stiffness offers both mechanical support (top layer) and elasticity for the pneumatic side valves (bottom layer). The PDMS was peeled off from the master and cut into individual devices. Holes were punched with 19-gauge needles and the PDMS devices were plasma bonded onto a clean glass slide.

2.2.3 Experimental Setup

All solutions and cell suspension were prepared and contained in 15 mL tubes (Falcon tube, BD biosciences, San Jose, CA). Tubes were connected to the device through polystyrene tubing (PE4, Scientific Commodities). Pneumatic valves were initially filled with water at 30 psi through the valve inlet; during the experiment, valves were alternatively actuated at 50 psi. To prime the device and create a liquid environment, filtered 2% bovine serum albumin (BSA, Fisher Scientific) in 1X phosphate buffered saline (PBS, Boston BioProducts) were pressurized simultaneously from all ports into the device using a pressure around 5 psi. This priming step removed any air bubbles and prevented undesired adhesion of cells to channel walls. To load cells after priming the device, the cell inlet was replaced with tubing connecting to the cell suspension, while all other ports stayed connected to priming solution. The cell suspension was driven into device by applying 1 psi at the cell inlet and no pressure at the outlet. Pressures were adjusted at stimulus and buffer inlets to keep priming solution flowing into device, which ensured unidirectional

loading of cells to trapping chambers. After cells were loaded, priming solutions at stimulus and buffer inlets were replaced by stimulus solution and cell media, respectively. After closing the cell inlet by pinching the tubing, stimulus and buffer were driven to their respective inlets by constant a pressure between 1 and 5 psi to stimulate cells with dynamic signal. The pressure source was provided by an air compressor regulated through solenoid valves in a customized pressure control box. A custom Matlab (MathWorks) GUI controlled these solenoid valves that modulate the actuation or shutoff of pressure.

2.2.4 Cell Culture and Treatments

The Jurkat E6-1 human acute T cell lymphoma cell line (American Type Culture Collection) was cultured in RPMI 1640 Medium without Phenol Red and with L-glutamine (Sigma-Aldrich) at 37°C in a humidified 5% CO2 incubator. The media was supplemented with 10 mM HEPES buffer, 1 mM sodium pyruvate, 100 units/mL penicillin-streptomycin (Cellgro), 1X MEM Nonessential Amino Acids, and 10% fetal bovine serum (Sigma-Aldrich). Cytoplasmic Ca2+ concentration was monitored using Fluo-3, AM, cell permeant (Life Technologies). Cells were incubated for 40 minutes with 5 µM Fluo-3 and 0.05% w/v Pluronic F127 at 37°C before being washed 3 times with PBS and resuspended in white RPMI. Cells were loaded into the device at $0.5x10^6$ cells/mL for approximately 20 minutes before they received stimulation.

2.2.5 Time-Lapse Microscopy and Image Analysis

Once cells were loaded in the device, images were acquired with a Nikon Eclipse Ti inverted fluorescent microscope using a FITC filter cube (Omega XF22). Time-lapse microscopy was performed using Elements Software (Nikon) with frame rates of 0.1 Hz to

avoid photo bleaching of the Ca^{2}+ dye, Fluo-3. Images were analyzed in an automated fashion using custom Matlab (MathWorks) scripts. Analyzed cells were manually chosen based on presence in the first and final frame. The mean fluorescence intensity was calculated for each region of interest (ROI) with the removal of background fluorescence at each time point.

2.2.6 Characterization of Stimulus Profiles at Various Flow Rates, Temporal Resolutions and Concentration Levels

To assess the performance of our device in various experimental conditions, we experimentally characterized the chemical stimulus profiles at various flow rates, temporal resolutions and concentration levels. We recorded the fluorescent intensity acquiring images (Infinity 3, Leica) at a frame rate of 5 Hz. Image analysis was done using custom MATLAB (MathWorks) scripts. With these scripts, we manually identified a ROI for each row and calculated the mean intensity in that ROI for all frames.

To visualize the effect of flow rates on stimulus profiles within the cell trapping chamber, we pressurized fluorescein solution (0.05 mg/mL, Sigma-Aldrich, St. Louis, MO) and PBS into the device at various pressures: 1, 2, and 3 psi, while alternating these two solutions at a constant frequency of 50 mHz. We also repeated this experiment with fluorescein isothiocyanate conjugate bovine serum albumin of 10 mg/mL (FITC-BSA, Sigma-Aldrich, St. Louis, MO) solution (Appendix Figure A-1).

To characterize the temporal resolution of stimulus profiles, we alternated fluorescein solution (0.05 mg/mL) and PBS at 4 frequencies: 5, 10, 100, 500 mHz, while pressurizing both solutions at 3 psi. The alternation was automated by a customized

pressure control box and controlled through a customized Matlab GUI communicating to the box.

To characterize the stimulus profiles at various concentration levels, we alternated fluorescein solution (0.05 mg/mL) and PBS at 10 relative durations to generate 10 corresponding concentration levels (pure PBS as 0, pure fluorescein solution as 10 and the other 9 combinations for corresponding intermediate levels), while both solutions were pressurized at 2 psi. At each concentration level, pulse duration of one solution was fixed at base pulse duration, while pulse duration of the other solution was varied. Base pulse duration of 50, 100, 200 and 500 ms were tested. By combining the base pulse with a range of scalar multiples (0-9) of basic pulse duration, 10 concentration levels were produced. Each concentration level was held for 10 sec by repeating the relative duration of binary pulses.

2.2.7 Quantification of Effective Molecular Dispersion in a Cell Trapping Chamber

In order to quantify the effective dispersion of stimulus molecule in our device, we delivered a plug of 500 ms of four fluorophore solutions in PBS background: fluorescein (0.05 mg/mL), FITC-dextran average molecular weight 4000 Da (MW 4000, 5 mg/mL), FITC-BSA (10 mg/mL) and FITC-dextran mw 70000 (12.5 mg/mL) at five discrete pressures at 1, 2, 3, 4 and 5 psi and measured the fluorescence intensity as a function of both travelled distance and time (159). Video recording and image analysis follow the same setup as stated previously.

To extract parameters that describe the dispersion pattern, we use the Matlab curve fitting toolbox to fit the time series values of fluorescence intensity by a Gaussian in the form of Eqn.1 (159).

$$y = f(x) = d + a \times \exp\left(-\left(\frac{x-b}{c}\right)^2\right) \quad (1)$$

Extracted parameters include background signal (*d*), peak intensity (*a*), time to reach peak intensity at the center of row *n* (b_n), and a parameter to measure the decay rate of Gaussian (*c*) (Figure 2-5). Mean flow velocity is estimated using Eqn. 2 (159).

$$U = \frac{distancebetweenmidpointofrow20\ androw1}{b_{20} - b_1} \quad (2)$$

The effective dispersion coefficient, D_{eff}, is calculated using Eqn. 3 (159),

$$D_{eff} = \frac{c^2 U^2}{4b} \quad (3)$$

Because D_{eff} should be measured after transient regions (159, 160), only parameter values at row 20 were used to compute D_{eff}. This process was repeated for all five pressures of each molecule. Under Taylor dispersion assumption, D_{eff} is a linear function of $\frac{U^2 w^2}{D}$ as in Eqn. 4(159),

$$D_{eff} = \frac{kU^2 w^2}{D} \quad (4)$$

in which k (a constant) is only dependent on the geometry of the channel cross section. We plot D_{eff} against $\frac{U^2w^2}{D}$ to estimate k, in which w is channel width and D is molecular diffusivity. We also plot D_{eff} against U^2 as in Eqn. 5,

$$D_{eff} = k'U^2 \tag{5}$$

in which k' is a simple correlation to compare dispersion of different molecules under same flow rate. Finally, the standard deviation of Gaussian is related to c as $stdev = \sqrt{\frac{c^2}{2}}$. The rise time is estimated as twice this standard deviation, which accounts for 95% of the area under the Gaussian. Results are summarized in Appendix Table A-1.

2.3 Results and Discussion

2.3.1 Effect of Flow Rate on Stimulus Profile

In our device, chemical stimuli are delivered in forms of alternating fluid boluses. Taylor and Aris described how transport of these signals can be affected by dispersion in long straight channels (161, 162). In order to understand the actual chemical micro-environment experienced by cells in our microfluidic device, we empirically examined what controls the flow and transport behavior and how much the flow in our device deviates from Taylor-Aris model.

We first examined the effect of flow rates on stimulus profiles. Figure 2-3 (a to c) shows the resulting spatial-temporal profiles of average ROI fluorescent intensity driven by various pressures. Increased flow velocities under large driving pressures (Figure 2-3)

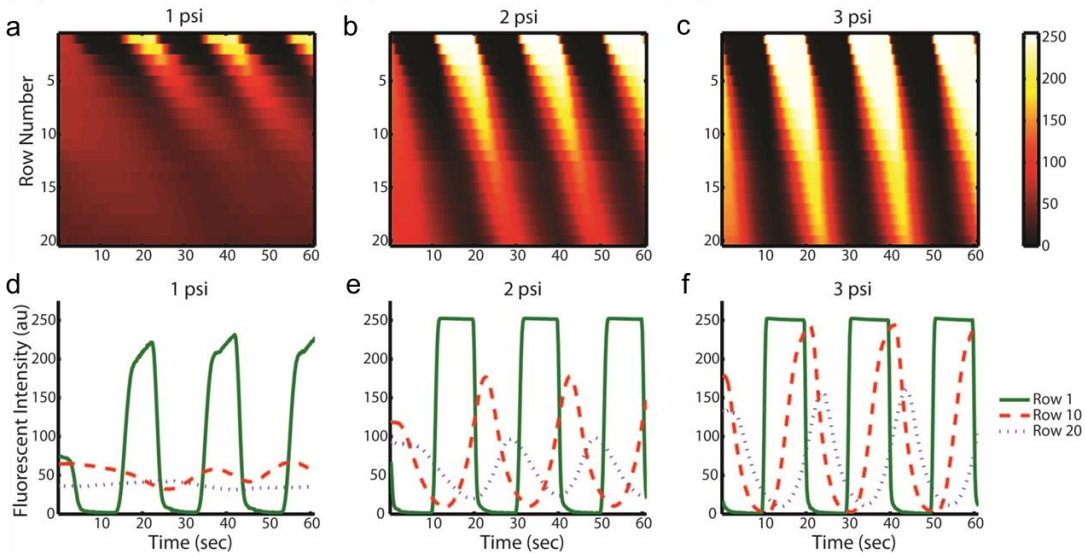

Figure 2-3 Effect of Flow Rate on Stimulus Profile

Stimulus profiles are affected by flow rates as driven at (a & d) 1psi, (b & e) 2psi, (c & f) 3psi. Profiles were generated by alternatively delivering fluorescein solution and PBS at 50 mHz at all driving pressures. Top panels: heatmaps of spatial (Y axis) and temporal (X axis) fluorescent intensity (color bar) in single observation chamber. Bottom panels: The corresponding average ROI fluorescent intensity (Y axis) plots as function of time (X axis) shows the evolution of plug-like waveforms to Gaussian-like waveforms.

result in less lag throughout the trap array. In spite of possible cell loading variation among each row, the lag per row is roughly constant and predictable at each pressure condition, which is important for robust operation. This result indicates that rise time and delay in our device can be easily tuned by adjusting the driving pressure.

To characterize dispersions in the device, we used several fluorescent solutes. As expected, dispersion of all fluorophores causes continuous evolution of the stimulus profile from an initial plug-like waveform to a final Gaussian-like waveform (Figure 2-3, d to f, Appendix Figure A-1). At high flow rates, due to shorter residence time, the stimulus profile is less dispersed than that at low flow rate. This feature enables simultaneously

stimulation of cells with signals of the same temporal features (i.e. same frequency of rise and fall) but various shapes (e.g. square-wave or Gaussian-like). This feature may be beneficial in the early screening of experimental conditions of interest, when the ability to quickly sample wide range of signals in a single experiment is important.

2.3.2 Temporal Resolution of Stimulus Profile

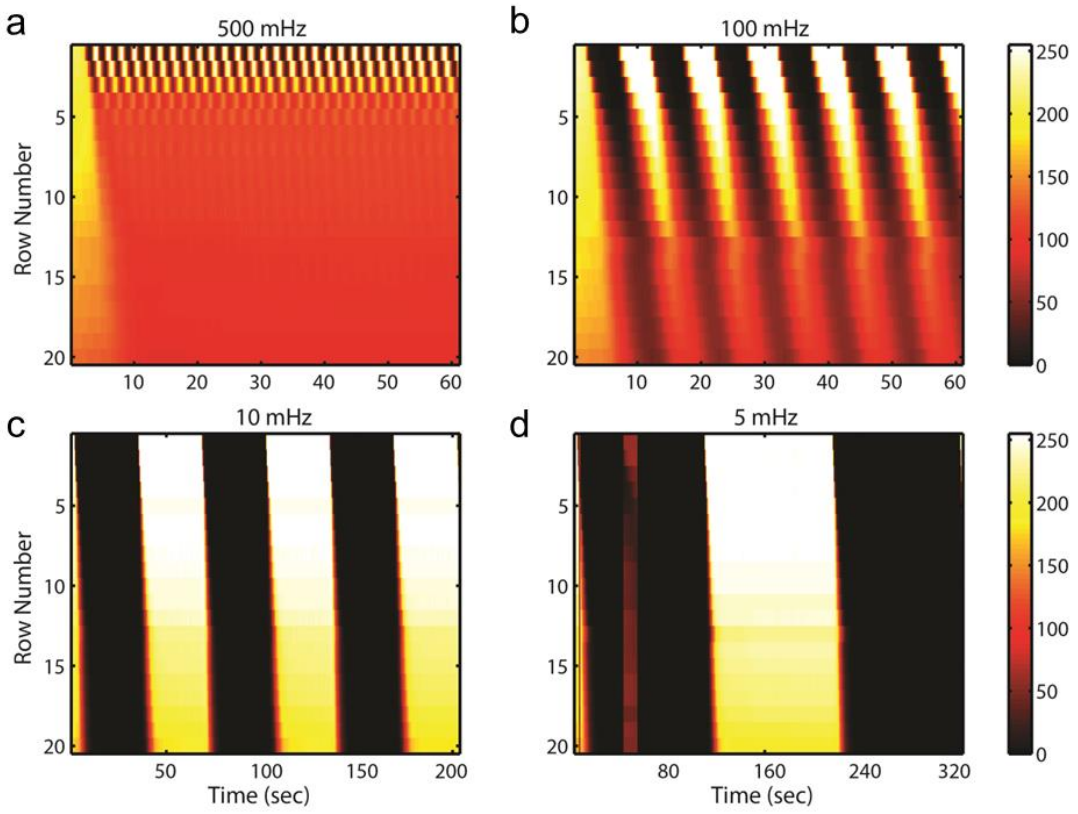

Figure 2-4 Temporal Resolution of Stimulus Profile

The temporal resolution is revealed by stimulus profiles oscillating in wide temporal ranges: (a) 500 mHz (2 s), (b) 100 mHz (10 s), (c) 10 mHz (100 s) and (d) 5 mHz (200 s). Profiles were generated by alternatively delivering fluorescein solution and PBS at driving pressure of 3 psi. Heatmaps show spatial (Y axis) and temporal (X axis) average ROI fluorescent intensity (color bar) in single observation chamber.

One goal of our device is to interrogate cells with stimulus signals spanning wide timescales. To assess its achievable temporal resolution, we visualized the stimulus profiles by alternating fluorophore solutions with PBS at various frequencies.

Figure 2-4 depicts the resulting spatial-temporal profiles of fluorescein intensity at various frequencies. Depending on the frequency, dispersion affects fluorescent profiles to different extents. At frequencies slower than 10 mHz (period longer than 100 sec), the effect of dispersion becomes less apparent. This is because residence time (8 sec at driving pressure of 3 psi) becomes much smaller compared to the timescale of alternating period. At frequencies faster than 500 mHz, waveforms are only resolved in the first few rows, dynamic signals become homogenized into an average, constant level stimulus as they pass along the chamber. As discussed in last section, the resolution of the high frequency stimulus signal at bottom rows can be improved by increasing the flow rate. However, in practice, extreme high flow rates should be avoided to minimize the detrimental effects of shear stress on trapped cells and to prevent cells from being pushed through the cell trap.

Moreover, since chemical cues transported *in vivo* are also subject to the same physical limitations posed by dispersion, we argue T cells are unlikely to utilize chemical signals with timescales shorter than 2 seconds to encode distinguishable information (146). If this hypothesis holds true, then the temporal resolution of our device should be sufficient for dynamic studies of T cell signaling pathways.

2.3.3 Molecular Diffusivity Dependence of Dispersion

While the standard technique to perform device characterization is to use soluble fluorophores (with molecular weight ranging from low hundreds to thousands), some

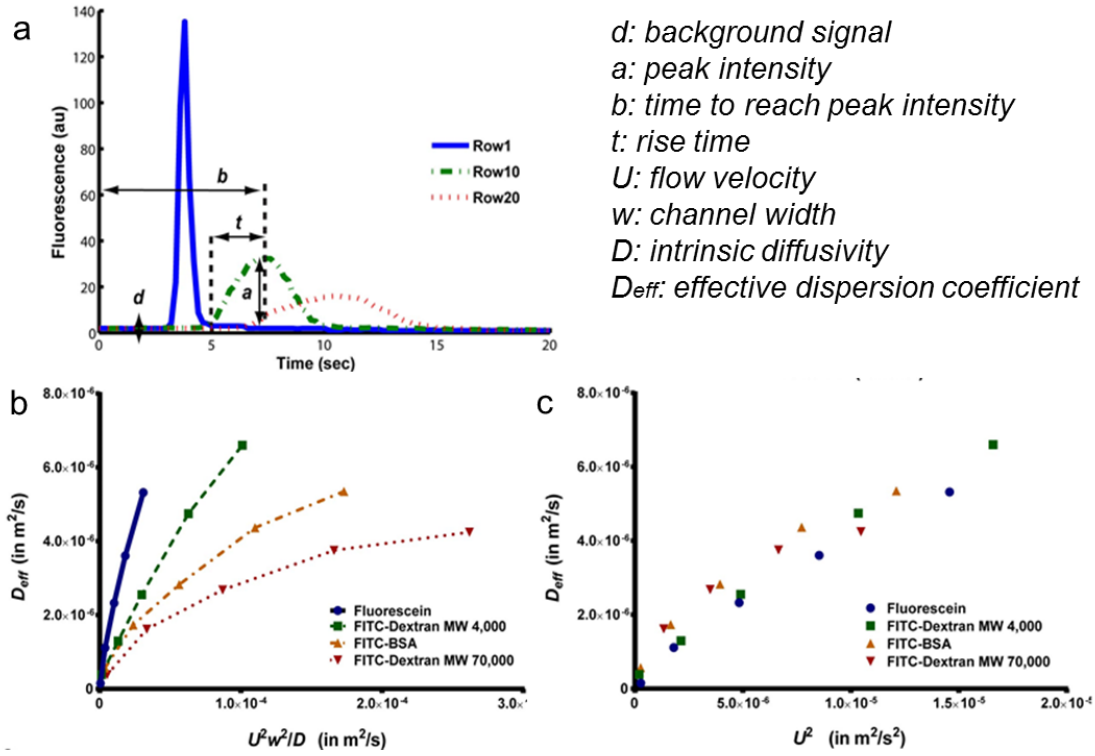

Figure 2-5 Quantification of the effective dispersion in a cell trapping chamber

(a) A 500 ms pulse of fluorescein solution was delivered in PBS background. A Gaussian fit was applied to the spatial-temporal intensity function to extract parameters that described effective dispersion: *a* is peak intensity, *d* is background intensity, *b* is peak time, *t* is rise time. (b) Effective dispersion of various fluorophores shows large deviation from Taylor's model, which predicts constant slope *k* for all molecules. (c) Under the same flow velocity, molecules with smaller intrinsic diffusivity have larger effective dispersion in accordance with the Taylor dispersion model. Nevertheless, the effect of complex flow pattern dominates in shaping effective dispersion, rendering effect of molecular diffusivity not apparent.

biologically relevant stimuli are non-fluorescent and are often of small molecular weight (e.g. H_2O_2). As such, their dispersion patterns cannot be measured easily. To study how molecular weight (and more directly molecular diffusivity) affects stimulus profiles, we analyzed the dispersion patterns of various fluorophores with distinct molecular sizes and

shapes: fluorescein (MW 332), FITC-dextran (MW 4,000), FITC-BSA (MW 66,000), and FITC-dextran (MW 70,000).

We find that similar conclusions can be made for profiles of other fluorophores as those for fluorescein (Appendix Figure A-1): (1) the stimulus profiles continuously evolve as a function of residence time (flow rate), and (2) the stimulus signal can be generated across wide timescales with an upper bound resolution of 2 seconds.

We first tested how similar the dispersion pattern is to the Taylor-Aris model (161, 162). In the Taylor-Aris model, the effective dispersion coefficient is a linear function of U^2w^2/D (159), where the slope *k* is only dependent on cross-section geometry as in Eqn. 4. This model predicts that molecules with smaller diffusivity have a larger D_{eff}. The cell chamber in our design is a "leaky" serpentine channel where flow splits and recombines (104).This "leakiness" did not result in dramatic changes in the concentration profiles, i.e. we did observe the Gaussian-like dispersion profile as in Taylor dispersion (161, 162). Next, we quantified how the flow in our device deviated from the Taylor model. Tayor-Aris model predicts that the parameter *k* is largely dependent on geometry and independent of (or a very weak function of) molecular weight.

In order to experimentally measure and quantify the dispersion patterns of various fluorophores, we used the framework by Bontoux *et al* (159). We delivered a short pulse of fluorophore solution of 500 ms, the shortest pulse we can generate that gives reliable fluorescent measurements (Figure 2-5 a and Eqn. 1). We measured and calculated mean flow velocity (U), effective dispersion coefficient (D_{eff}) and rise time (t) at various locations in a cell chamber (Appendix Table A-1). The rise time serves as a direct measurement of

the extent of dispersion patterns. Figure 2-5 b plots the experimentally determined D_{eff} against U^2w^2/D for each fluorophore molecule (159). This result shows that k is not constant; it follows the order of the molecular weight and diffusivity, indicating that the dispersion deviates significantly from Taylor's model. We repeated this experiment and found consistent results across experiment repeats (Appendix Figure A-2), thus the deviation from theory was unlikely caused by experiment-to-experiment variation. It is also interesting to note that the value of *k* is between 0.2 and 0.01 (Figure 2-5 b), which is much larger than the prediction of 0.003 in Taylor's model (159, 160), indicating the complex flow path significantly increases the extent of dispersion.

We next ask to what extent and how molecular weight contributes to the effective dispersion because stimuli molecules may not be fluorescently labeled. When plotting D_{eff} against U^2w^2/D, the lumped term makes it difficult to assess the contribution of each variable to D_{eff}. In order to isolate the contribution of intrinsic diffusivity, we compare D_{eff} for various fluorophores as a function of U^2(Eqn. 5). Fluorophores with higher molecular diffusivity (usually smaller molecular weight) have a smaller D_{eff} as in Taylor dispersion (Eqn.4). Accordingly, we would predict that stimuli with small molecular weight such as H_2O_2 are less dispersed compared to the fluorophores tested. Indeed, Figure 2-5 c shows that molecules with smaller diffusivity have less dispersion. This implies that the observed patterns are worst-case scenarios for experiments that require well-defined temporal patterns throughout the trap array. Additionally, the observed dependence on molecular diffusivity is much smaller than that in Taylor dispersion (as in Eqn. 4). We speculate that because the complex flow pattern unselectively increases the extent of dispersion regardless of molecular size, the effect of flow splitting and recombination dominates over

the effect of molecular diffusivity in the observed dispersion pattern. This renders the effective dispersion almost only is a function of flow velocity, which is convenient to control experimentally.

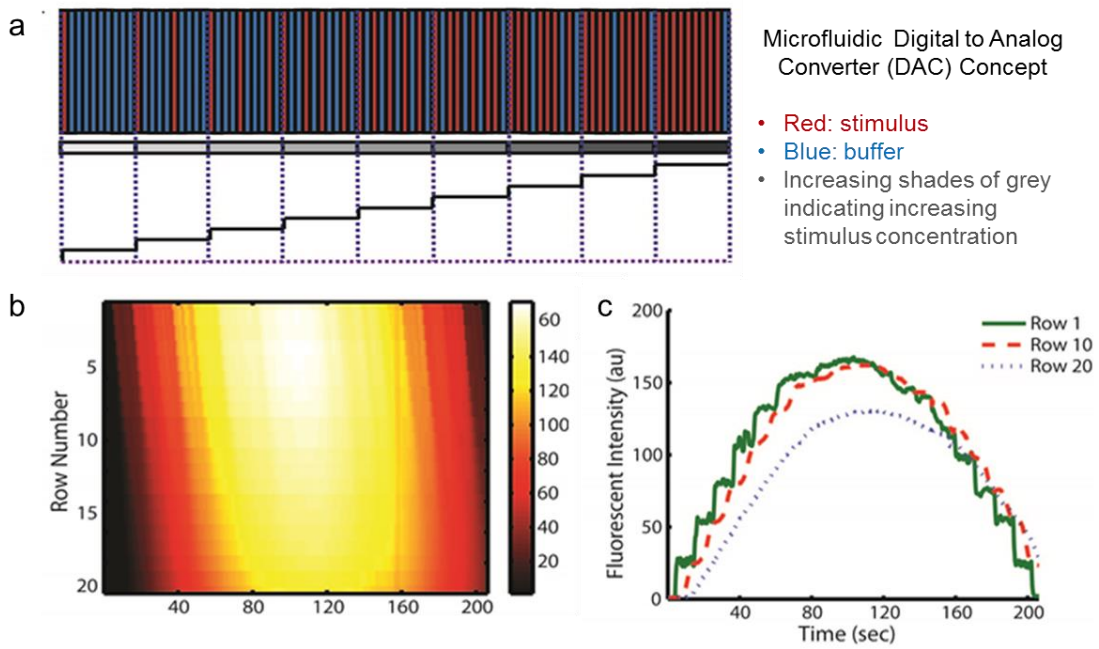

Figure 2-6 Dynamic stimulus varying in both time and concentration is automatically generated using only stimulus and buffer

(a) Schematic for signal synthesis by pulse-density modulation. Each color bar represents a base pulse duration: stimulus (red) and buffer (blue). Nine relative durations of binary solutions are delivered and converted to 9 corresponding stimulus concentration levels by controlling dispersion in microfluidic channels. (b) & (c) A ramp signal with 10 concentration level is generated using FITC-BSA solution and PBS using a base duration of 50 ms. (b) The spatial temporal heat map of average ROI fluorescent intensity within a cell chamber. (c) The corresponding fluorescent intensity profile shows the evolution of waveform from a step-like waveform to a linear waveform.

2.3.4 Generating Dynamic Stimulus Profile of Varying Concentration

Our goal is to deliver dynamic stimuli with arbitrary waveforms that can simultaneously vary in time and concentration. This is analogous to pulse-density modulation in signal processing where the amplitude of analog signal is represented by relative density of digital signal. Similarly here, we modulate the relative pulse duration of stimulus and buffer to encode various concentration levels. By controlling the dispersion in the microfluidic channel, binary pulses can be homogenized into uniform concentration of various levels.

To demonstrate this idea, we generated a ramp signal with 10 concentration levels (Figure 2-6 a). Pure buffer corresponded to a signal of 0 and original prepared stimulus solution corresponded to a signal of 10. In order to generate other concentration levels, we first defined a base pulse duration. We applied the base pulse duration to either stimulus or buffer, and assign the other solution a relative duration corresponding to each concentration level. For example, we first defined a base pulse of 100 ms; to generate a signal of 1, we delivered 100 ms of stimuli and 900 ms of buffer; to generate a signal of 2, we delivered 100 ms of stimuli and 400 ms of buffer; to generate a signal of 9, we delivered 900 ms of stimulus and 100 ms of buffer, etc. Each concentration level lasted for 10 second by repeating the corresponding combinatory pattern of pulses. We repeated this experiment at four different base pulses: 50 ms, 100 ms, 200 ms and 500 ms (Figure 2-6 b, c & Appendix Figure A-3)

For base pulse durations of 50 ms and 100 ms (Figure 2-6 b, c, and Appendix Figure A-3 a), the device generated a step-like profile with 10 distinguishable concentration levels in the first row. This step-like waveform continuously dispersed out to be a more linear profile as it propagated through the chamber. However, for base pulse duration of 200 ms

and 500 ms (Appendix Figure A-3 b & c), we saw prominent oscillations at the first row. This indicated that signals with period longer than 2 sec (200 ms x 10) cannot be homogenized by the time it reached the first row of trapping chamber, which was consistent with previous results on temporal resolution of stimulus profiles. Since temporal resolution is the product of base pulse duration multiplied by total number of concentration levels, the shorter the base pulse duration, the more concentration levels can be discerned. The minimal base pulse duration is ultimately limited by mechanical properties of the valve actuation and switching speed between two solutions, which is below 50 ms in our device. Nevertheless, even using a base pulse duration longer than 200 ms, a ramp can be created. This implies that our device can support wide dynamic range of base pulse duration, temporal resolution and total concentration levels. Since there are 40 cell trapping sites on each row, a small region of the trap is sufficient to collect large number of cellular responses. Depending on the time span, temporal resolution, and total concentration levels required by a particular experiment, proper base pulse duration and portion of the trapping chamber can be chosen for cellular responses under the same desired stimulus waveform.

Since there are only two input solutions, our device substantially simplifies experimental operation by eliminating the need to prepare multiple solutions and switch solutions of discrete concentrations manually during experiments. The synthesis and delivery of dynamic signal to trapped cells are automated by a Matlab GUI controlled pressure box, both of which are custom made. Desired stimulus waveform can be easily programed on spot in the Matlab GUI. Finally, as signal generation module is independent from the cell trapping module, the cell trapping module can be replaced to adapt to most cell sizes and types.

2.3.5 Calcium Signaling in Response to Dynamic Stimulation of H_2O_2

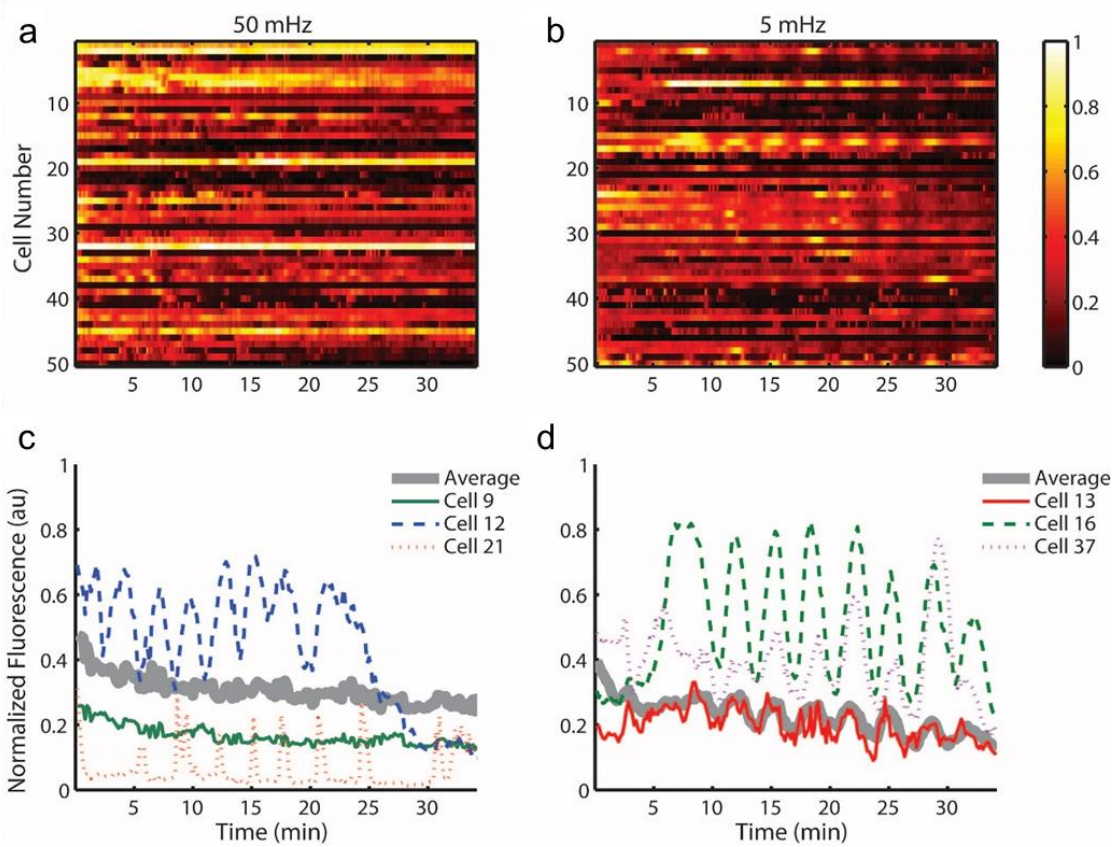

Figure 2-7 Cytoplasmic calcium signaling synchronizes with low frequency oscillating stimulus

Heat map of 50 cells responding to (a) 50 mHz and (b) 5 mHz stimulation of 100 μM H_2O_2. Single cell traces are graphed from selected cells responding to (c) 50 mHz and (d) 5 mHz stimulation of 100 μM H_2O_2. The population synchronized to the stimulus at 5 mHz, while response heterogeneity exists among population under each stimulation condition.

Ca^{2+} is actively sequestered in the endoplasmic reticulum (ER) until T cell activation triggers its release (163). Upon stimulation, cytoplasmic Ca^{2+} concentration has been shown to oscillate through time, which is thought to be the result of stochastic distribution of receptor proteins within the membrane (164, 165). This dynamic calcium

signaling ultimately leads to nucleation of NFAT and production of cytokine interleukin-2 (IL-2) (134). Studies suggest a role of ROS in T cell activation, especially involved in calcium flux that follows TCR recognition (166–168).

We used our device to examine the response of Jurkat cells to dynamic stimulation by alternating 100 μM H_2O_2 solution with white RPMI media. Cytoplasmic Ca^{2+} concentration was monitored using fluorescence microscopy of Fluo-3 while cells experienced stimulation at a frequency of either 5 mHz or 50 mHz. Individual cell traces were analyzed over time, and a heat map of fluorescent intensity from 50 cells is shown in Figure 2-7 a & b. The heat maps clearly show heterogeneity within the population of cells and select individual cell traces are shown in Figure 2-7 c & d. The 5-mHz signal entrained some cells within the population to exhibit cytoplasmic Ca^{2+} concentration oscillations at approximately the same frequency. In contrast, the cells experiencing 50 mHz stimulation do not appear to exhibit oscillations of cytoplasmic Ca^{2+} concentration at the same frequency as the driving frequency. These results suggest the calcium signaling pathway of Jurkat cells acts as a low-pass filter, not responding to stimulation at high frequencies while synchronizing to low frequency signals. The cut-off frequency of this particular pathway was shown to be between 50 mHz and 5 mHz.

Given these results, we demonstrated the value of this device to generate biologically relevant signals in order to interrogate cellular signaling pathways and probe its signal transduction properties. With a full spectrum of frequencies sampled, this device is capable of gathering the experimental data necessary for frequency response analysis and provide a more systematic approach to analyzing the underlying feedback control in a complex biological network.

2.4 Conclusions

Here we present an automated platform capable of simultaneously delivering an arbitrary dynamic stimulus and enabling single cell resolution measurements for high throughput T cell signaling studies. We thoroughly characterized the stimulus profile at various flow rates, temporal resolution and concentration levels. We also developed a quantitative method to determine the effective dispersion from the complex flow pattern in our microfluidic device. This result helped us to generalize our conclusion obtained from the dispersion pattern of fluorophores to arbitrary, non-fluorescent stimulus of interest. Finally, we investigated the role of ROS in Jurkat human T cells' calcium signaling network by stimulating cells with two dynamic patterns of H_2O_2 signals. Our results would not be observable in population-average based, bulk experiments and emphasized the unique value of our platform to enable the study of cellular signaling. We envision this platform to be applied to broad single-cell analyses, such as in pharmacokinetics, personalized medicine, fundamental immunology, stem cells and cancer research.

CHAPTER 3. DEVELOPMENT OF A MICROFLUIDIC PLATFORM FOR MONITORING EARLIEST SIGNALING EVENTS ASSOCIATED WITH IMMUNE CELL-PAIRING

3.1 Introduction

In cell-mediated immunity, information about the current status of the host is contained within the presence of specific molecules and is relayed between various immune cell types through direct cell-cell contact (1, 21). This contact-dependent information relay persists through the entire adaptive immune response: starting with dendritic cells' presentation of pathogen antigen to prime naïve T cells (20, 52), followed by CD4+ T cells' recruitment of macrophages or naïve B cells (169–172), and terminated by CD8+ T cells' elimination of infected cells or cancer (173–176). While it is known that different antigens cause T cells to differentiate into different effector functions, it is still not entirely clear how a T cell's intermediate signaling pathway transmits differences in the pMHC-TCR interaction into differential downstream translational changes (55–58). In one study, altered peptide antigens with various potencies presented using antigen presenting cells (APCs) caused hierarchical IL-2 production and cell apoptosis in T cells (177). Thus the cell line and antigen system used in this study provided an optimal model system to study how early signaling processes encodes information in order connect antigen with cell fate decision. In another study, simultaneous external calcium influx and mitochondria translocation towards immunological synapse (IS) were observed during T cell activation by antibody conjugated microbeads (25). With calcium and mitochondria's involvement in many important cellular signaling processes and availability of robust

fluorescent indicator, monitoring changes in intracellular [Ca2+] and mitochondrial position provide useful readouts for intermediate signaling processes as potential link antigen recognition to effector functions.

However, our ability to study these early signaling processes during T cell activation was limited by the technical challenges of visualizing these process in real-time for non-adherent immune cells. While much of the signaling events related to IS formation was elucidated using artificial lipid bilayer systems (19, 22–24, 178), the top-down orientation in this technique was not best for imaging organelle movement orthogonal to IS plane. Force spectroscopy using biomembrane force probe (BFP) offered paramount control on cell interaction (79–82), but the throughput of experiments was limited as only one pair of cells could be put into contact at a given time. In methods based on microwell plate, cell interactions were forced by centrifugation, which made it impossible to synchronize timing of cell contacts or to image cell signaling at the time of initial contact (85–87). An ideal system should allow imaging of cellular and subcellular probes in real time for the entire process through precise control of cell interaction timing, while a side-on orientation of cells is preferred in order to utilize better horizontal resolution of microscope to monitor relative motion of mitochondria to IS (24, 179).

Microfluidics provides finer cell manipulation and easier environment control compared to conventional methods, so they are better orientated to meet needs of this study (180, 181). Recent modified microfluidic microarray designs improved cell contact control compared to earlier designs (182), but required a more complicated device fabrication and operation procedure while still adopted an up-down orientation and device (183). Dielectrophoresis (DEP) and other electrical methods used specific electrolyte buffer,

which raised concerns of compatibility with cell sample and possible inference with signaling processes (184). Several hydrodynamic approaches demonstrated controlled contact between different cell types with various performance (126, 185, 186). Notably, Voldman *et al.* designed several devices based on hydrodynamic principle, with ones based on reversing flow (125, 126) and others that utilized deformability of PDMS material (127, 187). Recently with these devices, they studied T cell signaling and their interaction with other cell partners at high-throughput (126, 187). Inspired by a single cell trap array previously developed in our lab (104) and the deformability of microfluidic devices (127), here a microfluidic system was developed in order to monitor early signaling events in the experimental model (altered peptide antigens and transformed cell lines) used in this study. This chapter focuses on design, characterization and optimization of this microfluidic device, its operation protocol and image analysis, which allowed synchronized contact between multiple immune cell pairs and monitoring of calcium and mitochondria interaction through the entire T cell activation process.

3.2 Methods and Material

3.2.1 Microfluidic Device Fabrication

The microfluidic master was fabricated using conventional photolithography techniques with mask purchased from CAD/Art Services, Inc. A hybrid microfabrication process was developed to ensure the accuracy in fabricating critical features (Figure 3-1). The *front restriction* (6 μm) and *back restriction* (3 μm) features were etched onto a silicon wafer using deep reactive ion etching (DRIE, Vision RIE) (188). Negative photoresist (SU-8 2025, MicroChem, Newton, MA) were spin-coated and exposed to form remaining

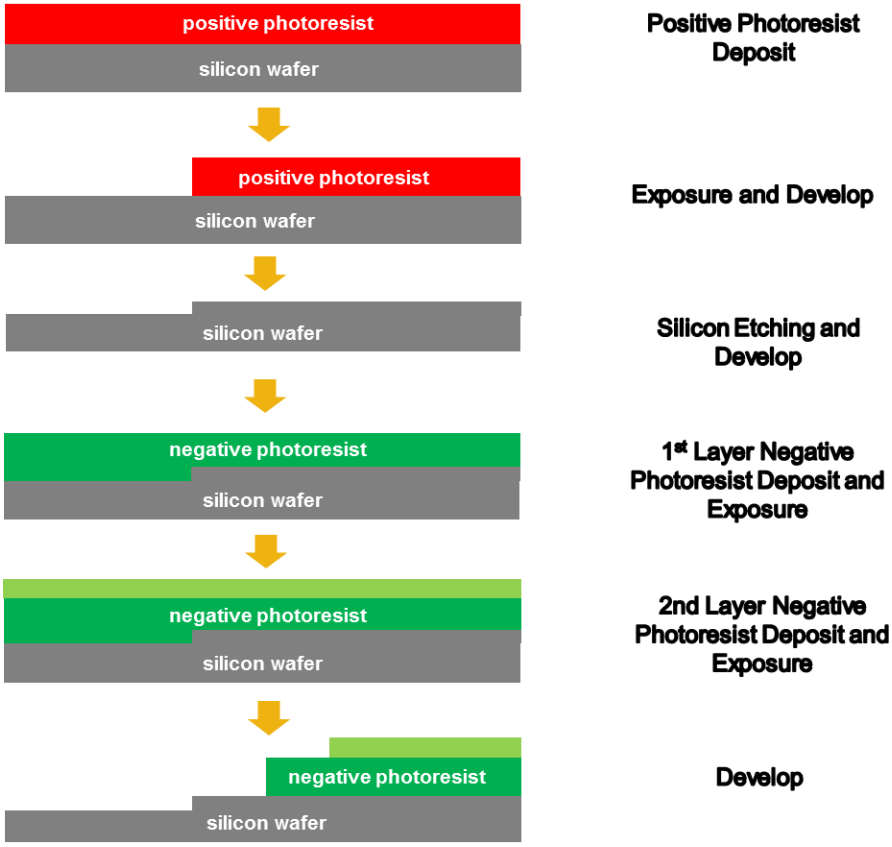

Figure 3-1 Microfabrication process for 3 layers master

features (30 μm in height). A finished master was treated with tridecafluoro-1,1,2,2-tetrahydrooctyl-1-trichlorosilane vapor (United Chemical Technologies, Bristol, PA) in a vacuum desiccator overnight to prevent adhesion of PDMS during future molding process. Two polydimethylsiloxane (PDMS, Sylgard 184, Dow Corning) layers were sequentially casted onto the master to mold the microfluidic structures. The first layer of 3 mm of PDMS (ratio of prepolymer: curing agent = 17:1) was partial cured in the 85 °C oven for 30 minutes, followed by another layer of 3 mm (ratio of prepolymer: curing agent = 10:1) with continuous curing for 2 hours at 85 C°. PDMS layers were removed, and fluid access holes

were made using 19-gauge needles (McMaster-Carr). The final device was made by plasma bonding of PDMS to a cover slip.

3.2.2 Cell Culture and Peptide Antigens

The 1B6 T cell hybridoma line used in these studies has been previously described (189) and consists of fusion of the 1B6 T cell clone with the TCR-negative fusion partner BW1100. Human fibroblasts (DAS) expressing I-As and B7.1 were used as antigen presenting cells (APCs) (190). Both 1B6 T cells and DAS cells were cultured in RPMI 1640 medium minus phenol red minus L-glutamine (Life Technologies, Carlsbad, CA), supplemented with 10% v/v FBS (Life Technologies), 1% HEPES buffer 1M solution (Cellgro, Manassas, VA), 1% sodium pyruvate 100mM solution (Cellgro), 1% MEM nonessential amino acids 100X solution (Cellgro), 1% Penicillin Streptomycin 50X solution (Cellgro), and 1% L-Glutamine 200mM solution (Cellgro). Three peptide antigens with C-terminal amides were synthesized in TFA salt at 95% purity (BioMatik, Cambridge, Ontario, Canada) with amino acid sequences of HSLGKLLGHPDKF(L144), HSLGKQLGHPDKF(Q144), HSLGKYLGHPDKF(Y144), respectively.

3.2.3 Cell Staining and Antigen Loading

In experiments to characterize device performances, DAS cells were incubated with 2μM of CellTracker Red (Life Technologies) and 1B6 T cells with 2μM of CellTracker Green (Life Technologies) for 30 minutes prior to loading onto device for imaging. In experiments involving antigenic peptide presentation, DAS cells were incubated with 4μg/mL or 0.4μg/mL of respective peptide in fresh regular media for 16 to 24 hours prior to staining with fluorescent dyes. In all experiments, DAS cells were dissociated from the

culture flask by gentle rocking following 10mM EDTA in PBS treatment. In all experiments, fresh cell culture media was used as cell culture media and imaging media.

3.2.4 Device Operation

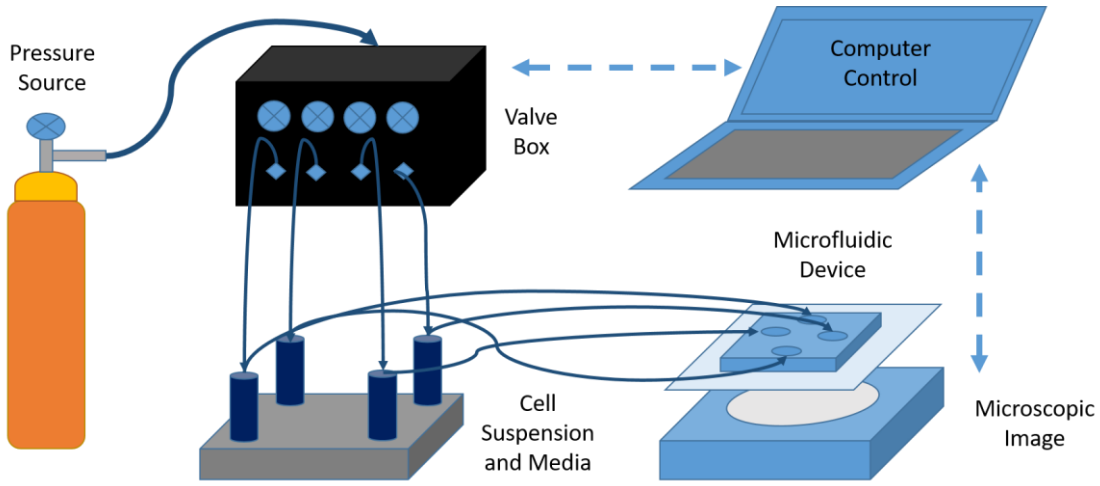

Figure 3-2 Experimental setup

Solid lines with arrow indicate flow direction (air or liquid). Dash lines with arrows indicate communication between equipment.

The experimental platform included a custom made microfluidic chip, 15 mL tubes (Falcon tube, BD biosciences, San Jose, CA) and polystyrene tubing (PE4, scientific Commodities) to contain and transport cell and media, an air tank or compressor as pressure source, a custom-made solenoid valve box as pressure regulator, and a custom Matlab GUI for control of the valve box (Figure 3-2). At the beginning of the experiment, 2% PBS BSA solution was pressurized at 4 psi into the outlet to degas the microfluidic chip and to prevent unspecific bonding of cells to channel walls. After the chip was primed, the stop pins at inlets were replaced with tubing connecting to 15mL tubes ready for delivery of cell

suspension/media onto chip. Cell loading procedure was illustrated in a four-step scheme (Figure 3-3). DAS cells were loaded from the left inlet into chip. A low-pressure difference of 0.1 psi between inlet and outlet retained cells in *front cell traps*, and prevented cells from squeezing through the *front restriction* (Figure 3-3 a). Once satisfactory loading of APCs was achieved, the media inlet was switched open while keeping other inlets closed to wash away extra APCs in channels. Then, 2 seconds of surging pressure at 4 psi was applied through media to expand the *front restriction* and push DAS cells to into the *cell*

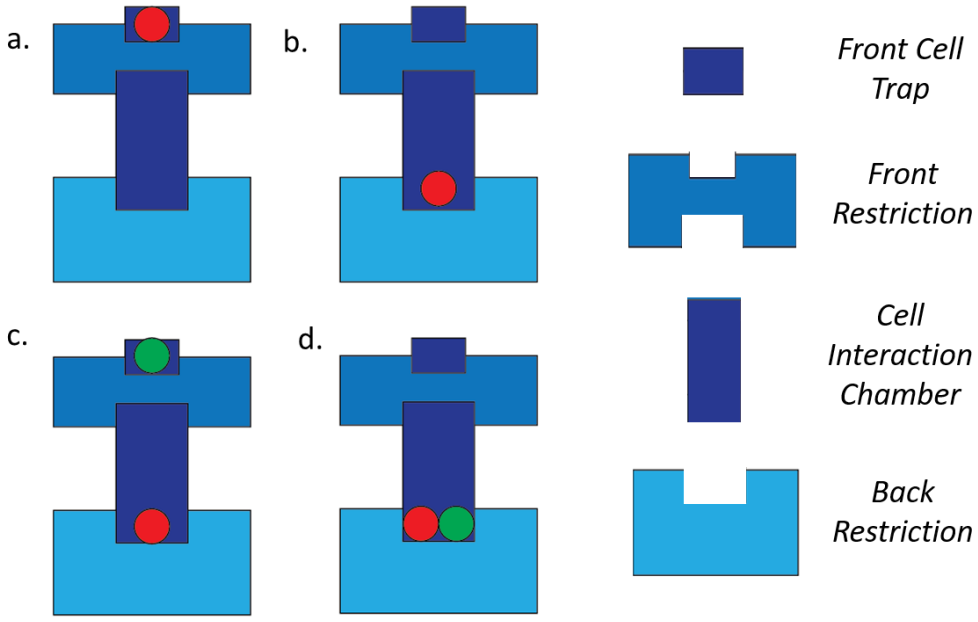

Figure 3-3 Device stepwise operation from top-down view

(a) APC cells were loaded from the left inlet into chip. A low-pressure difference of 0.1 psi between inlet and outlet retained cells in *front cell traps*, and prevented cells from squeezing through the *front restriction*. Once satisfactory loading of APCs was achieved, the media inlet was switched open while keeping other inlets closed to wash away extra APCs in channels. (b) Then, 2 seconds of surging pressure at 4 psi was applied through media to push APCs cells into the *cell interaction chamber*. A pressure difference of 0.1 psi was restored, and cells were retained in *cell interaction chamber* by *back restrictions*. (c & d) The same procedure was repeated for 1B6 T cells, and rendered two cell types into contact.

interaction chamber (Figure 3-3 b). The pressure difference of 0.1psi was restored and cells were retained in *cell interaction chamber* by *back restrictions*. The same procedure was repeated for 1B6 T cells, and rendered two cell types into contact (Figure 3-3 c and d, Supplemental Video 1).

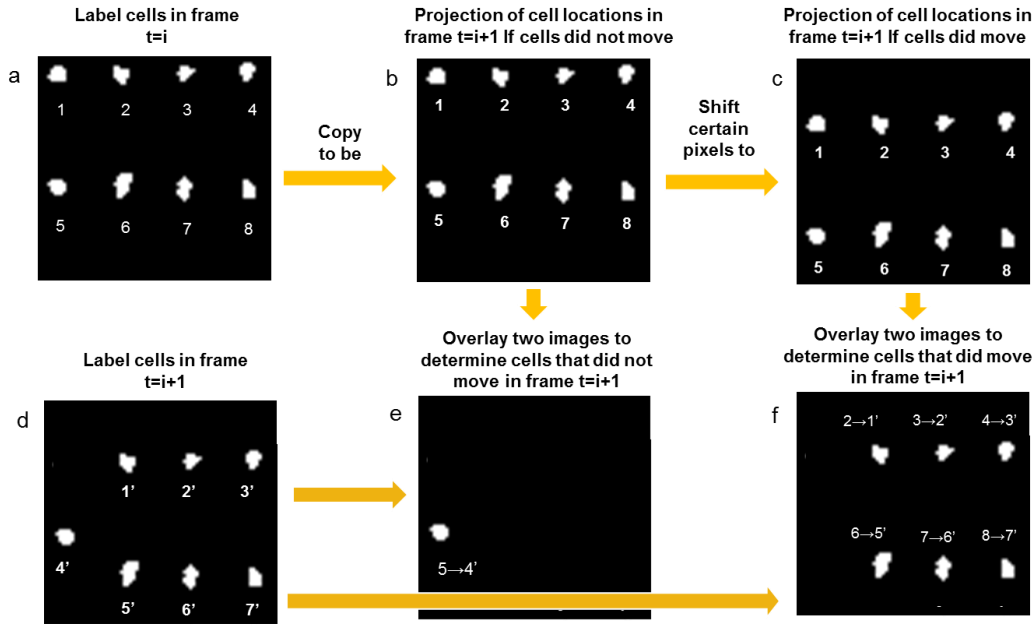

Figure 3-4 Cell tracking algorithm

Cell tracking was established between two adjacent frames in time. In the preceding frame, (a) Assigned identification number to cells based on masking. (b) Copied the preceding frame as if cells stay in the same location in next frame. (c) Shifted the preceding frames for certain distance as if all cells moved in the next frame. (d) Assigned identification number to cells of next frame based on masking. (e) Multiply (b) and (d) pixel wise, overlapping indicated cells actually stay in the same locations, associated both identification number. (f) Multiply (c) and (d) pixel wise, overlapping indicated cells actually moved for certain distance, associated both identification number.

3.2.5 Live Cell Imaging

In all live imaging experiments, cells were loaded on chip in pre-contact positions for 5 to 10 minutes prior to recording in order for temperature to equilibrate to 35 ± 2 C°. For all studies, CO_2 level was maintained at 5% using stage incubator on microscope to maintain constant pH. In experiments for device characterization, epi-fluorescent microscopy (Nikon Eclipse Ti-E) was used to image 1B6 T cells in *FITC* channel and APCs in *TRITC* channel at 10x magnification. Recording continued for 20 minutes at 15 second intervals, during which cells were triggered into contact at 2 minutes into the recording.

3.2.6 Image Analysis

In the calcium dynamics study, T cells calcium signals were tracked through recording. Several custom Matlab scripts (Appendix D.1.1 and Appendix D.1.2) were used to track movement of T cells (Figure 3-4), to extract calcium intensity based on fixed threshold (Appendix Figure B-1 and Appendix Figure B-2) and to calculate various metrics including *normalized peak fold change*, *area under curve* and *peak time*.

3.3 Results

3.3.1 Initial Design for Cell Interaction Study

In order to develop a microfluidic device to control interaction of immune cells, multiple versions of microfluidic designs were tested before the design was finalized. In the first design scheme (Figure 3-5 a), where APCs were allowed to adhere to the device cover glass before the other cell type was loaded. In this scheme, a co-laminar flow was used to coat the main channel with BSA protein (the green fluorescent FITC-BSA band

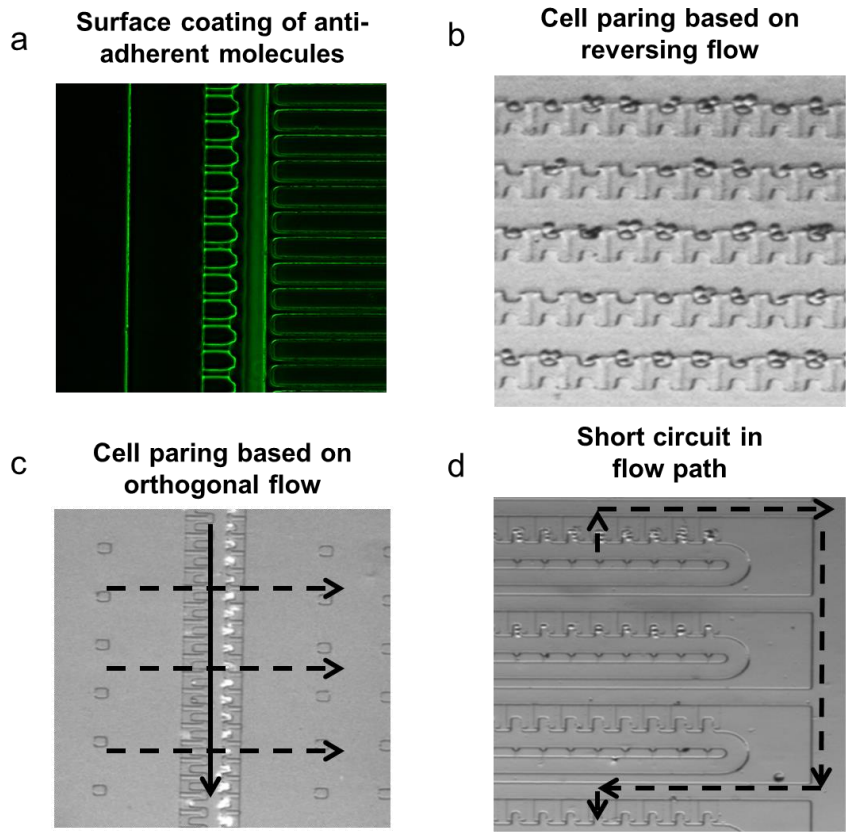

Figure 3-5 Several initial designs for cell interaction study

(a) The coating of anti-adherent molecules using laminar co-flow could not efficiently restrict the movement of cells in microfluidic channel. (b) Cell pairing based on reversing flow could not ensure tracking of cell identity and synchronized cell contact. (c) Cell paring based on orthogonal flow was sensitive to small disturbance during operation. (d) Modified version of (c) still could not control the movement of cells due to unanticipated short cut in fluid resistance circuit.

that spans vertically in center of Figure 3-5 a) to prevent the adherent cells from moving out of trap. However, the coating provided no guaranteed way to restrict the movement of APCs. Moreover, the APC adhering process took more than 20 minutes, making the experiment process time consuming and inefficient. In a later design (Figure 3-5 c), two cell types were separated loaded onto different sides of a straight channel, and then

delivered an orthogonal flow to push one type of cells from one side to the other. Due to the small fluid resistance in the single straight channel, cells moved too fast to be captured in trapping sites, and cells' locations were easily disturbed by even small movement of the device. In a modified version of this design (Figure 3-5 d), we combined orthogonal flow with the cell array (104) to increase the fluid resistance in the device. However, it was challenging to arrange flow resistance in channels to make cells moving into desired positions. Without fluid modelling, it was difficult to predict cell movement before actual testing. Other ideas were also tested based on reverse flow mechanism (125), however, it was difficult to track the identity of cells during reverse flow operation, and the contact of two cell types could not be synchronized (Figure 3-5 b). Our final design idea based on pressure-induced cell interaction was selected based on empirical tests on performances of multiple schemes.

3.3.2 Device Design

The general device design had four major goals: 1. precise control of contact timing between two immune cell partners; 2. single cell and subcellular resolution for cell signaling imaging; 3. imaging multiple cells simultaneously to extract statistical information; 4. imaging cell pairs in side-on orientation instead of more conventional top-bottom orientation. In our final design, the microfluidic device features four *cell trap arrays* for redundancy reason in case of clogging in individual array (Figure 3-6 a). Two cell types are loaded from two separate inlets to prevent undesired contact, while the media inlet and outlet are used to establish pressure difference in order to control cell movement. Each *cell trap array* contains 10 parallel *main channels* (W:45μm x H:30μm) connected head-to-end, with repetitive *cell interaction units* flanked by two adjacent channels (Figure

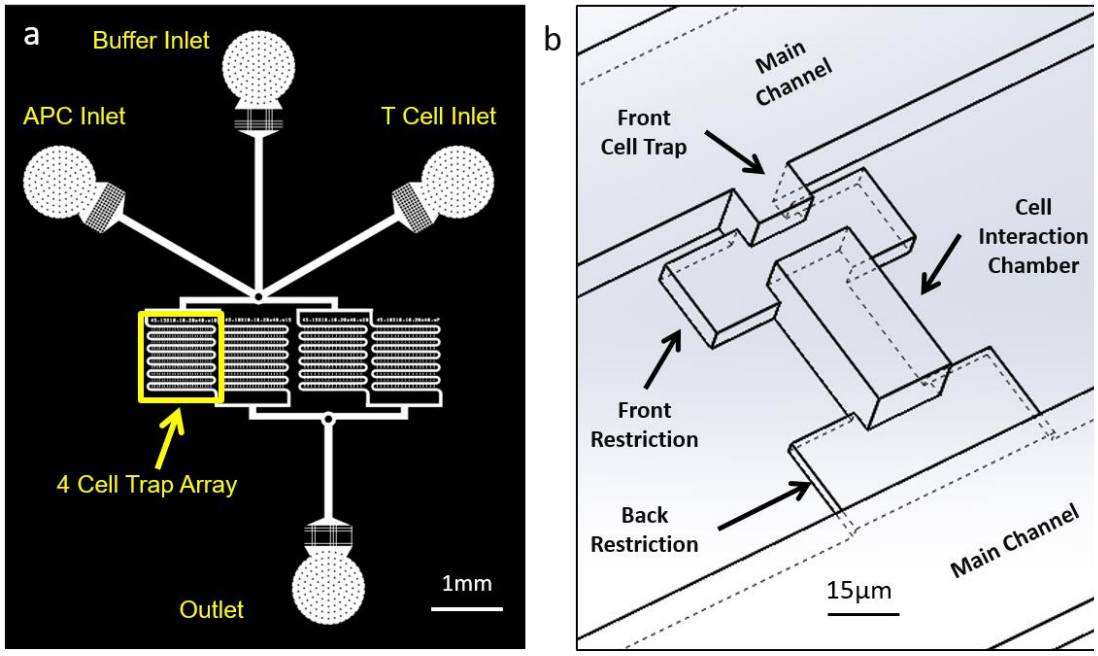

Figure 3-6 Microfluidic device design

(a) Overall layout of the microfluidic device. Yellow box, a *cell trap array*, which is composed of repetitive *cell interaction units*. (b) 3D Structure of a *cell interaction unit*. Each *cell interaction unit* is a multi-component structure consisting of a *front cell trap* (W:15 µm x D:10 µm x H:30 µm), a *front restriction* (W:30 µm x D:10 µm x H:6 µm), a *cell interaction chamber* (W:20 µm x D:40 µm x H:30 µm) and a *back restriction* (W:30 µm x D:20 µm x H:3 µm).

3-6 b). The *front restriction* and *back restrictions* were silicon etched features to ensure accuracy and uniformity, as their heights are critical in determining device performance through modulating fluid resistance across a *cell interaction unit*. Tan *et al.* had illustrated how ratio of fluid resistance in alternative flow paths affected hydrodynamic trapping of cells in microfluidic devices (191). Since this fluid resistance ratio was similar for all cell trapping units, this design allows uniform loading of large number of cells across the entire array (104). Because the *front cell trap* has only single cell capacity, once the trap is occupied by a cell, incoming cells are directed to next available units (191) (Figure 3-3 a).

When a user delivers a *transient positive pressure* (pressure difference of 3 psi to translocate DAS cells and 2 psi to translocate T cells) between device inlet and outlet, cells in *front cell trap* are transferred into *cell interaction chamber*, which had multiple cell capacity (Figure 3-3 b). This operation releases the capacity of the *front cell trap* and allows uptake of the next cell type (Figure 3-3 c).

3.3.3 Device Optimization

a

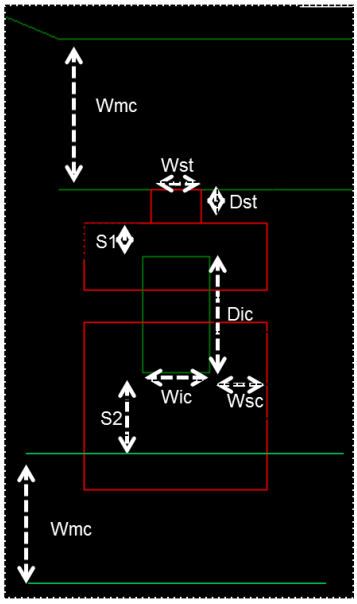

b

Device Dimensions	Cell Loading	Cell Squeezing	Cell Retain in Interaction Chamber
30µm-4µm-2µm	Bad, Rarely loaded	Bad	Good
30µm-4µm-4µm	Very Good, Near full trap loading	Bad	Bad, cells squeeze out of trap directly
30µm-6µm-3µm	Good, Depends on geometry	Good	Good
30µm-6µm-6µm	Very Good	Good	Bad, cells squeeze out of trap directly

Figure 3-7 Device optimization

(a) Device dimensions varied and tested during design optimization process. *Main channel* (Green parallel lines); *Cell interaction chamber* (Green rectangular); *Front cell trap* (Red small rectangular); *Front restriction* (Red median rectangular); *Back restriction* (Red large square); Width of *main channel* (*Wmc*); Width of *front cell trap* (*Wst*); Depth of *front cell trap* (*Dst*); Depth of *front restriction* (*S1*); Depth of *cell interaction chamber* (*Dic*); Width of *cell interaction chamber* (*Wic*); Depth of *back restriction* (*S2*); Width of *side wing* (*Wsc*). (b) Device dimensions of main channel – *front restriction* – *back restriction* and respective performance assessment.

In order to optimize the design performance, multiple device dimensions were empirically tested and then the device performance was determined experimentally (Figure 3-7 a). Among all dimensions, the height of *front restriction, back restriction* and the ratio between them were the most critical in determining device performance. To illustrate the importance of *front restriction* and *back restriction* heights and their ratio in device performance, several prototypes were fabricated with various ratios (*front restriction: back restriction*): 6μm to 6μm, 4μm to 4μm and 4μm to 2μm (Figure 3-7 b). In prototype where the *front restriction* to *back restriction* heights was 6μm to 6μm or 4μm to 4μm, cells tent to escape through the *back restriction* during transient positive pressure. In prototype of

4μm to 2μm, cells flowed along the *main channel* and were not directed into *front cell traps,* likely due to the higher fluid resistance across *cell interaction unit* compared to circumventing along the *main channel*. Only in prototype of 6μm to 3μm, cells flowed were loaded into *front cell traps,* translocated into *back restriction* and remained there after *transient positive pressure*.

3.3.4 Device Performance Characterization

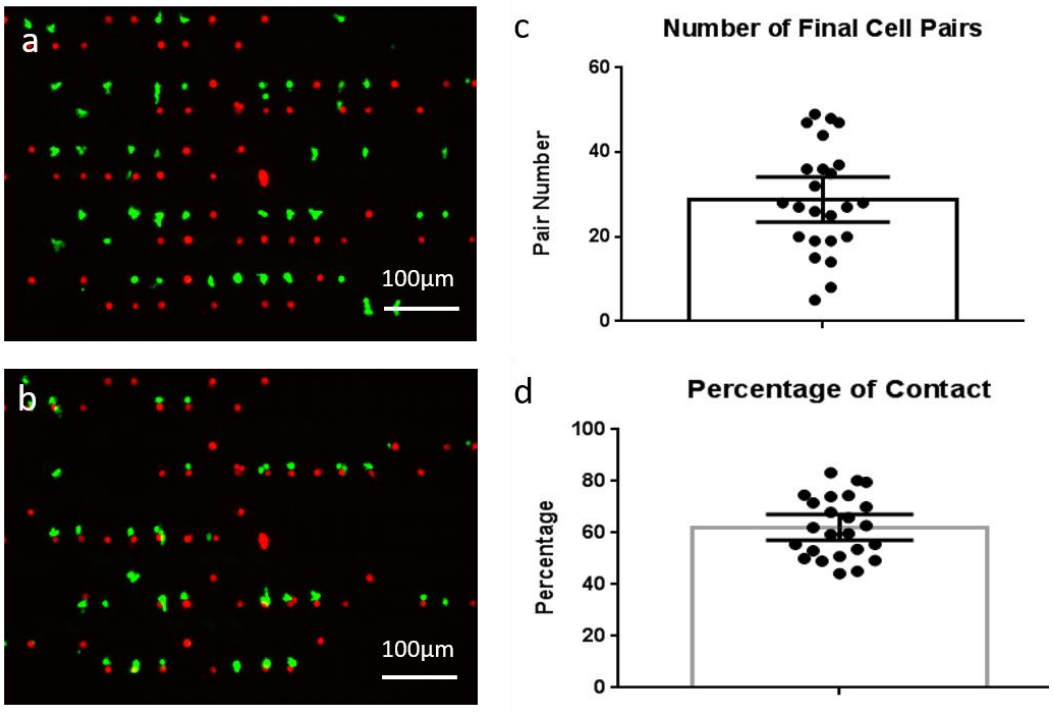

Figure 3-8 Device performance

(a) Representative image of cell loading before forced contact (Red: DAS cells, Green: 1B6 T cells). (b) Representative image of cell loading after forced cell contact. (c & d) Performance statistics. Each dot is a single experiment, imaged at 10x, including 4 regions of interest (ROIs). (c) Statistics of final number of *desired hetero-pairs*. Error bar: 95% confidence interval. (d) Statistics of *contact percentage* between pre-contact cell pairs to post-contact cell pairs.

Next the performance of this microfluidic platform was assessed. Cell pairs simultaneously contacted each other across the entire device within 1 second following application of *transient positive pressure* (Supplemental Video 1). Cell signaling imaging at single cell resolution was achieved at 10x magnification (Figure 3-8 a & b), while subcellular features required magnification of 20x and above (Appendix Figure C-2). At 10x magnification, 4 regions of interest (ROI) were imaged at 15 second interval to balance temporal resolution and imaging throughput. At this imaging setting, on average 30 (ranging from 20 to 60, Figure 3-8 c) *desired hetero-cell pairs* (defined as T cells that successfully contacted APCs in response to *transient positive pressure*) were obtained from each experiment. *Contact percentage*, defined as the percentage of hetero-cell pairs that transitioned from a separated pre-contact state into *desired hetero-cell pairs*, averaged 60% (range from 40% to 80%) in our experiments. At high magnification of 20x and above, when each field of view contained only a few *cell interaction units*, *contact percentage* became an important performance indicator by ensuring a relatively high certainty of successful cell interaction events (Figure 3-8 d).

3.3.5 Device Operation Does Not Affect T-Cell Calcium Response

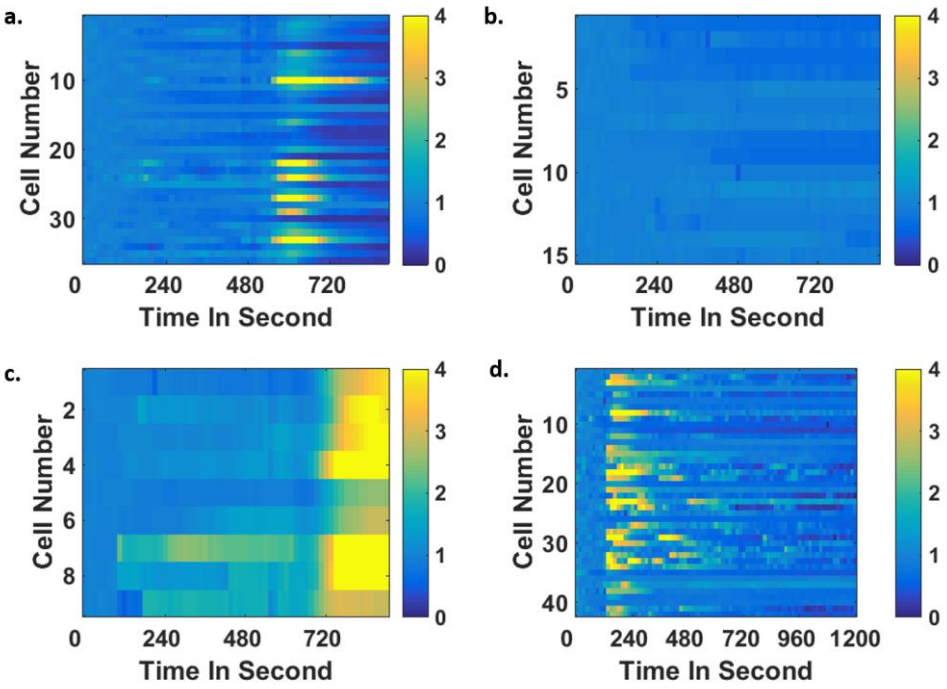

Figure 3-9 Device operation does not alter calcium signaling of T cells

Calcium signaling of 1B6 T cells in device with (a) no pressure surge delivered but stimulated using ionomycin; (b) pressure surge delivered but no ionomycin stimulation; (c) pressure surge delivered and ionomycin stimulated; (d) pressure surge delivered and stimulated with L144 presented on DAS cells.

In order to determine whether experimental operation alters natural cell signaling process, a series of control experiments were performed with the calcium signaling of 1B6 T cells as readout. First, a positive control for calcium signaling was established using ionomycin (Figure 3-9 a). Ionomycin is an commonly used ionophore to raise intracellular level of Ca^{2+} in T cells without engagement of TCRs (192). In this positive control experiment, 1B6 T cells were only loaded into the *front cell traps* and their calcium signaling were monitored under ionomycin stimulation. Some T cells responded to ionomycin with large calcium spikes as expected. Next, in order to test whether the

transient positive pressure would induce calcium spikes, 1B6 T cells were translocated from *front cell trap* to *cell interaction unit* under *positive transient pressure* (Figure 3-9 b). Despite mechanical stimulus experienced during *transient positive pressure* operation, these T cells maintained baseline calcium signaling. Then a third experiment was conducted to test whether T cells' signaling property was compromised by *transient positive pressure* operation (Figure 3-9 c). Again, T cells elicited strong calcium spikes in response to ionomycin stimulation after *transient positive pressure*, proving their signaling capabilities were not compromised by device operation. Finally, Figure 3-9 d showed a characteristic calcium signaling pattern of 1B6 T cells stimulated by L144 (agonist peptide) presented on DAS cells, which showed comparable calcium spikes to ionomycin stimulated cells.

3.3.6 T-Cell Calcium Signaling Requires Temperature Control

Kemp *et al.* had demonstrated hierarchical IL-2 production and apoptosis in 1B6 T cell population subject to various peptide antigens with known potencies of L144 > Y144 > Q144 (177). With the same cell line and peptide antigen system, it was hypothesized that more potent antigen would trigger stronger calcium dynamics in T cells. However, in primary experiments where temperature was not controlled and conducted at room temperature, 1B6 T cells showed minimal calcium response even to the agonist L144, the most potent antigen among three (Figure 3-10 a, Appendix Figure B-4 & Appendix Figure B-5). Moreover, trial-to-trial variation was large among independent repeats (Figure 3-10

b). These results indicate temperature control is necessary in signaling study of immune cells.

3.3.7 Experimental Protocol Optimization

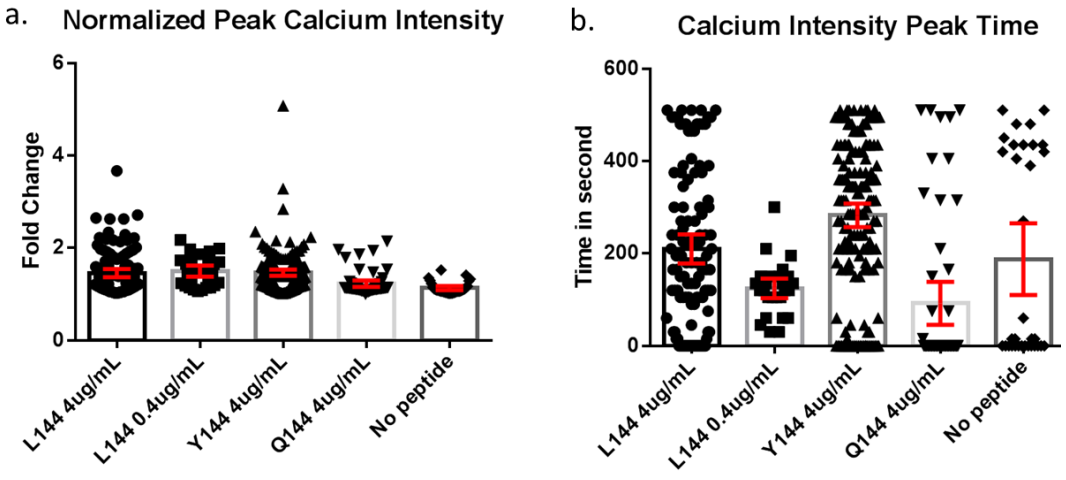

Figure 3-10 T-cell calcium signaling requires temperature control

(a) *Normalized peak calcium intensity* (arbitrary units in fold) is the peak calcium intensity normalized to pre-contact average. (b) *Peak time* (in seconds) is the time to calcium peak intensity since time of contact. X axis lists all experiment conditions. Column heights indicate mean value for each condition. Red bars indicate 95% confidence interval for each condition. L144 4μg/mL were pulled from 6 independent repeats; L144 0.4μg/mL from 1 independent repeat; Y144 from 6 independent repeats; Q144 from 2 independent repeats; and no peptide from 2 independent repeats.

Besides temperature was validated to be the most critical variable that affected calcium signaling, alternative cell dissociation method was also developed to eliminate effect of trypsin on antigen presenting (Appendix Figure B-6). Besides temperature and cell dissociation method, other factors involved in experimental procedure were also examined thoroughly. Among these factors, dye loading media including the choice of media, the duration of dye loading, and method of dye loading had the most significant

effect (Appendix Figure B-7 and Appendix Figure B-8). For example, a simple procedure of conditioning fresh cell culture media in a culture flask with breathing windows in CO_2 incubator before being used as dye loading media was proved to be very effective in maintaining health of cells. This unexpected effect might be related to equilibration of temperature and pH of the media, which produced less shock to cells compared to unconditioned media at room temperature. This result further emphasized the paramount importance of maintaining cell physiology condition in *in vitro* live cell imaging for signaling study.

3.4 Discussion and Conclusion

3.4.1 Discussion of Device Performance

The number of desired hetero-pairs was significantly lower than the number of individual cells of each type loaded into the array, mainly due to existence of prematurely-contacting-hetero-pairs, homo-pairs, singlet cells and losing cells during device operation (Figure 3-8 a & b).

These non-ideal situations were considered to be caused by pressure fluctuations. Because the resting pressure difference were merely 0.1 psi (besides *transient positive pressure* operation), fluctuations in the pressure source (provided by compressor for example) would lead to disturbance of cell positions. A more stable pressure source (compressed air tank instead of air compressors which had duty cycles) or a design with larger array (which has larger fluid resistance) would mitigate local pressure fluctuation, which might help improve the number of desired cell paring obtained.

Second, the wide range of desired hetero-pairs was also thought to be related to the state of cells: the designed procedure was more effective with viable and healthy cells, while unhealthy and apoptotic cells failed to be directed towards *front cell traps*. Even if some cells were loaded into *front cell traps*, these cells tended to pre-maturely squeeze through *front restrictions* before *transient positive pressure* operation, indicating healthy and non-healthy population had different mechanical property (Appendix Figure B-3 a).

Lastly, cells within a *cell trap array* adopted a zigzag distribution, as cells tended to skip the first *cell interaction units* while only occupied later units (Figure 3-8 a & b and Appendix Figure B-3 a & b). This phenomenon had also been observed in other hydrodynamic cell trapping device, where first several units (called dummy traps) mainly served to drain the flow in order to direct cells into cell trapping units (104). Nevertheless, other designs with these dummy traps removed resulted further receding of loading position, arguing for the usefulness of these dummy traps.

3.4.2 Conclusion

In this work, an integrated experimental platform was developed to examine the earliest signaling events (calcium and mitochondria dynamics) upon T cell contact with antigen presenting cells. Compared to multiwell plate assays, this platform ensured precise spatial and temporal control of cell contact, making simultaneous monitoring of large number of cell pairs possible. Compared to electrical based methods, this system used regular cell media to operate, eliminating concerns about compatibility of electrolyte with cell signaling. In addition, the side-on orientation is preferred than a top-down orientation in visualizing the relative motion of organelles with regard to the IS plane. Aside from the

microfluidic chip, the experimental setup allowed semi-automated manipulation of cell contact using pressure driven flow. This design stabilized position of cells in microfluidic chip during experiment process, which allowed translocation of device between working bench and microscopy stage without triggering undesired contact of cells. Because this setup is resistant to disturbance, signaling events during the entire antigen recognition before and after cell contact can be monitored in real time at high imaging quality. While there is still room for further improvement of device performance, our experimental system is adequate to provide new insights into signaling process involving T cell-APC interaction.

CHAPTER 4. EFFECT OF ANTIGEN POTENCY AND DOSE ON T CELL CALCIUM AND MITOCHONDRIA ACTIVITY

4.1 Introduction

Equipped with specific T cell receptors (TCRs), a T cell clone can distinguish antigens with a single amino acid difference in peptide sequence (44–50). In order to investigate how antigen-TCR interaction shapes T cells immune response, altered peptide ligands (APLs) were generated by introducing subtle molecular changes in original immunogenic peptides (193, 194). T cells stimulated by APLs showed differential phosphorylation status and cytokine patterns, leading to distinct functional phenotypes, including Th1/Th2 differentiation, anergy, *etc* (195–197). In a mouse model of experimental autoimmune encephalomyelitis (EAE), the TCRs responded to auto-antigenic myelin proteolipid (PLP) peptide 139–151 (HSLGKWLGHPDKF; W144) (198, 199). Besides W144, these TCRs were shown to be highly cross-reactive with increased potency to ligands L144 > Y144 > Q144 with substitutions at position 144 (200, 201). Compared to primary cells, these transformed cell lines were easier to obtain at large quantity with least batch-to-batch differences, so this system would be ideal in studying the effect of antigen potency and dose on calcium signaling and mitochondria activity. For example, using APLs and cell lines derived from this experimental model (198, 200–202), Kemp *et al.* showed differences in antigen potencies were transduced to phenotypic changes through combinatorial activation of kinases in a hybridoma T-cell clone (177). The downstream changes induced by APLs suggested early signaling events immediately

following TCR stimulation might also exhibit differential patterns, but these studies did not directly demonstrate it.

While several studies investigated calcium responses of T-cell population following APL stimulation (203–206), the results were based on imaging of unsynchronized contact between T cells and antigen presenting cells (APCs) due to difficulty in manipulating cell interaction. In addition, the top-down orientation only made it more challenging to assess the exact contact timing. Thus, a snapshot of calcium signaling in unsynchronized population may result in loss of important temporal features to simple averaging.

Mitochondria are believed to be involved in T-cell antigen recognition, although details of the mechanisms remain elusive. Quintana *et al.* reported simultaneous calcium influx and mitochondria translocation towards immunological synapse (IS) in T cells when stimulated by microbeads coated with anti-CD3 (25). They suggested mitochondria translocated to IS in order to take up extra calcium influx at proximity of CRAC (25), which was identified as the major calcium influx channel composed of STIM1 and Orai1 (207, 208). In contrast, Barr *et al.* showed STIM1-Orai1 accumulated at the distal pole of T-cell body rather than IS during T cell activation (209), while another study by Quintana *et al.* also observed heterogeneous distribution patterns of STIM1 and Orai1 among T cell population following antigen stimulation (210). These mitochondria studies are subject to the same technical constrains as in calcium studies mentioned above. Because mitochondria distributions in these studies were measured at different time points, it is difficult to discern whether different observations reflect the true heterogeneity of mitochondrial positioning, or was a consequence of a dynamic process captured at different times. Like in calcium study, live-time imaging was only performed on a few cell pairs in

these studies, raising questions on whether these observations were inclusive representatives of all behaviors in a population. Moreover, most of these studies used anti-CD3 or strong agonist antigen to stimulate T cells, how antigens potency modulates calcium response and mitochondria positioning in a synergistic fashion is unknown.

A technical barrier preventing addressing these questions is the ability to synchronize sufficient number of cell pair interactions for monitoring entire signaling processes before and after cell contact. With the microfluidic system designed in Chapter 3 to precise control synchronized interaction of multiple cell pairs, this system allows us to image mitochondrial migration with associated calcium response for the entire T cell antigen recognition process.

Once mitochondrial dynamics and calcium responses from multiple cell pairs are obtained, the next challenge is to interpret the resulting high dimensional dataset. Different from studies where only a few features were measured at sparse time points, uncovering important relationship among hundreds of possible variable pairs by manual examination is impractical (12). For example, we want to reveal relationship between antigen potency, calcium response and mitochondria positioning, which were measured using several image-derived metrics with each containing tens of time series points. Simple statistics based on population means and variance are insufficient, and more advanced statistical techniques are needed. Among current techniques, partial least square regression is useful in identifying important relationships among large number of variables (130), which has been applied to signaling studies (131, 132). Here, we developed a partial least square regression model to identify the most effective metrics and most important time points in answering how calcium dynamics and mitochondria positioning encode antigen potency.

4.2 Methods and Materials

4.2.1 Cell Culture and Peptide Antigens

The 1B6 T cell hybridoma line was generated by fusion of the 1B6 T cell clone with the TCR-negative fusion partner BW1100 in the laboratory of Vijay Kuchroo as previously described (189). Human fibroblasts (DAS) transfected with I-As and expressing B7.1 were used as antigen presenting cells (APCs) (190). Both 1B6 T cells and DAS cells were cultured in RPMI 1640 medium –phenol red –L-glutamine (Life Technologies, Carlsbad, CA), supplemented with 10% v/v FBS (Life Technologies), 1% HEPES buffer 1M solution (Cellgro, Manassas, VA), 1% sodium pyruvate 100mM solution (Cellgro), 1% MEM nonessential amino acids 100X solution (Cellgro), 1% Penicillin Streptomycin 50X solution (Cellgro), and 1% L-Glutamine 200mM solution (Cellgro). Three peptide antigens with C-terminal amides were synthesized in TFA salt at 95% purity (BioMatik, Cambridge, Ontario, Canada) with amino acid sequences of HSLGKLLGHPDKF(L144), HSLGKQLGHPDKF(Q144), HSLGKYLGHPDKF(Y144), respectively.

4.2.2 Cell Staining and Antigen Loading

To study T cell calcium response to antigen potency and dose, DAS cells were stained with 2μM of CellTracker Red for 20 minutes prior to loading onto device, after which 1B6 T cells were stained with 2.3μM of Fluo-4, AM (Life Technologies) for 20 minutes prior to loading onto chip and imaging. In study of calcium-mitochondria interactions, DAS cells were stained with 5μM Hoechst 33342 (Thermo Fisher Scientific) for 20 minutes prior to loading onto device, after which 1B6 T cells were stained with 2.3μM Fluo-4, AM and 120nM MitoTracker Red (Life Technologies) for 20 minutes prior

to loading onto chip and imaging. In all experiments, DAS cells were dissociated from the culture flask by gentle rocking following 10mM EDTA in PBS solution. In all experiments, fresh cell culture media was used as cell culture media and imaging media.

4.2.3 Live Cell Imaging

In all live imaging experiments, cells were loaded on chip in pre-contact positions for 5 to 10 minutes prior to recording in order for temperature to equilibrate to 35 ± 2°C. For all studies, CO_2 level was maintained at 5% using stage incubator on microscope to maintain constant pH. In studies of calcium-mitochondrial interaction, spinning disk confocal microscopy (microscope body: Nikon Ti-E with Perfect Focus 3; detector: Hamamatsu C9100-23b back-thinned EM-CCD) was used with 405, 488 and 561 nm laser lines at 20x magnification. Recording continued for 20 minutes at 30 seconds interval, during which cells were triggered into contact at 3 minutes into recording. 11 z-slices (from -9μm to 21μm relative to maximum projection at 0μm position) with 3 μm spacing were obtained for each cell pair for all three channels.

4.2.4 Image Analysis

In the calcium dynamics study, T cells calcium signals were tracked through recording. Several custom Matlab scripts (Appendix D.1.1 and Appendix D.1.2) were used to track movement of T cells (Figure 3-4), to extract calcium intensity based on fixed threshold (Appendix Figure B-1 and Appendix Figure B-2) and to calculate various metrics including *normalized peak fold change*, *area under curve* and *peak time*. In calcium-mitochondria interaction study (Appendix D.2.1), the *xyz* coordinates of pixel and intensity values of APCs, T cell and mitochondria were extracted from image *z* stacks to calculate

mitochondria net projection (Eqn. 1) and *moment of inertia* (Eqn. 2). *Intercellular vector* was defined as the vector from centroid of APC (DAS cell nucleus /Hoechst 33342) to centroid of T cell (calcium signal /Fluo-4). *Mitochondria vector* was defined as the vector from centroid of APC centroid to centroid of T cell mitochondria (mitochondria signal /MitoTracker Red). *Mitochondria net projection* was the dot product of these two vectors. For *mitochondria moment of inertia*, sum of distance (*d*) square of each mitochondria pixel (*I*) to the cell centroid (calcium centroid) was normalized to total mitochondria intensity ($\sum_{i=1}^{n} I$). In both metrics, all distances were intensity weighted and normalized to average of T cell pre-contact radius (*R*) to remove effect of cell sizes.

$$\textit{Mitochondria net projection} = \frac{\sum_{i=1}^{n} I \times \frac{\textit{mitochondria vector} \cdot \textit{intercellular vector}}{R \times |\textit{intracellular vector}|}}{\sum_{i=1}^{n} I} \quad (1)$$

$$\textit{Mitochondria moment of inertia} = \frac{\sum_{i=1}^{n} I \times \left(\frac{d}{R}\right)^2}{\sum_{i=1}^{n} I} \quad (2)$$

4.2.5 Partial Least Square Regression Model

A partial least square regression model was developed with SIMCA v12 (Umetrics). The data was collected from 218 T cells subjected to four peptide antigens (Appendix D.2.2). For each cell, three variables were derived summarizing calcium dynamics (*Peak fold change*, *Area under curve* and *Peak time*). A categorical variable for each peptide antigen was included as *peptide*. time series data of six mitochondria features and one calcium feature (*normalized calcium intensity* or *NC*) consisted of 38 time points each, each time point considered as an independent variable) were also included. The six mitochondria features were as follows (Appendix Table C-1): *mitochondria moment of*

inertia calculated on cell centroid (*MC*), *mitochondria moment of inertia calculated on mitochondria centroid* (*MM*), *mitochondria absolute projection* (*AP*), *mitochondria net projection* (*NP*), *mitochondria projection ratio* (*PR*), and *mitochondria intensity ratio* (*IR*). The initial model contained all 218 observations (cells) with all 270 variables was shown in Appendix Figure C-6. After optimization, the final model only contains 205 observations, where the outliers were removed according to DmodX criteria. The trimmed X block consisted of *NP* and *MC* between time points 7 to time points 14 (14 variables) and *normalized peak fold change* (*peakFold*) as Y variable. The validity and degree of overfitting was tested using SIMCA-P permutation test, with 50 iterations of shuffling the Y-block variable with respect to the X-block. The results of this analysis yielded background R^2Y of 0.02 and a Q^2Y of -0.15, establishing the significance of the final model fit.

4.3 Effect of antigen potency and dose on T cell calcium signaling

4.3.1 Effect of Antigen Potency on T-cell Calcium Signaling

With the microfluidic system validated, we first investigated T-cell calcium response to APLs of various potencies. Figure 4-1 illustrates the results from one of such trials, where T cells were subjected to the three antigen peptides of known potencies (L144 > Y144 > Q144) presented on APCs, with a condition of no peptide displayed as a control. The heatmaps show T cells responded strongly to L144 and Y144, while the population subject to Q144 and no peptide control elicited minimal response. Responding cells typically had a characteristic peak of Fluo-4, AM fluorescence immediately after contact, followed by decay in fluorescence intensity, with some cells showing multiple intensity

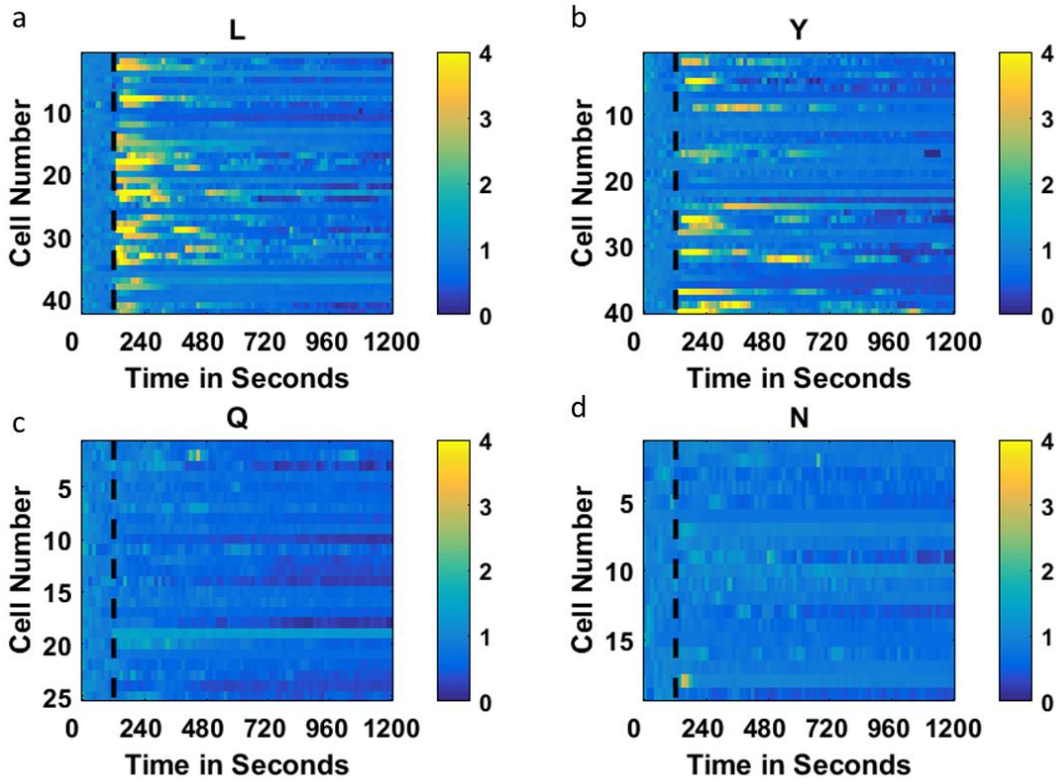

Figure 4-1 Peptide antigens of various potencies elicit differential calcium response in T cell population

Each panel represents cell signaling results from a separate experiment. Black dash line, time of contact. Heatmap, total calcium intensity of a cell normalized to pre-contact average total intensity. (a) L144, majority of T cells exhibited strong calcium response. (b) Y144, only half of cells exhibited strong calcium response. (c) Q144 and (d) no peptide, few cells showed strong calcium response.

peaks. When Figure 4-1 a is compared to Figure 4-1 b, the majority of T cells responded to L144, but only around half of the population responded to Y144. Interestingly, not only T cells either responded or not (binary response) within each condition, the percentage of responding cells in population also increased with more potent antigen (L144 > Y144). In addition, more potent antigen also induced faster and more cohesive response: T cells

responded to L144 immediately after contact, while the timing for calcium response to Y144 was less synchronized among population.

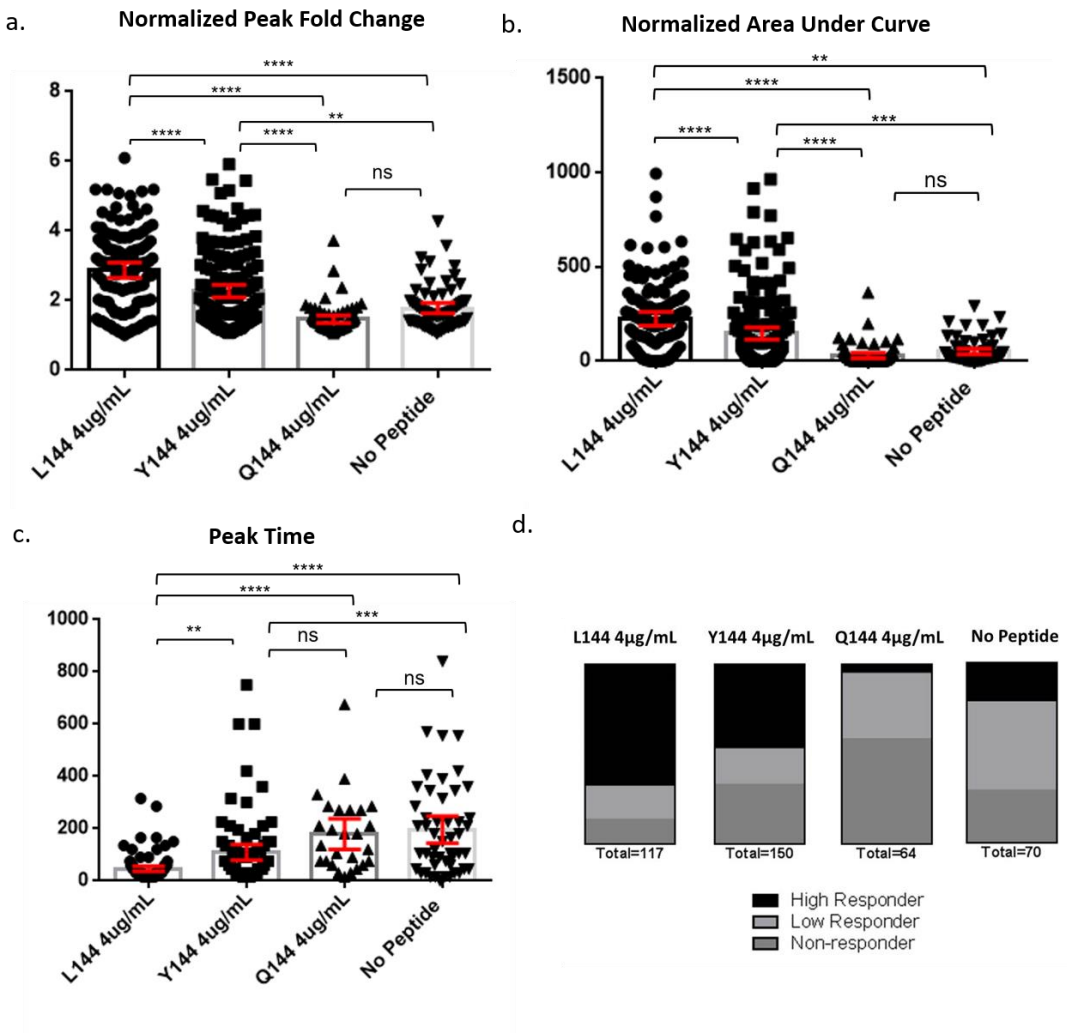

Figure 4-2 Effect of antigen potency on T-cell calcium dynamics

Results from all 4 repeats were combined. (a) *Normalized peak fold chan*ge as the maximum fold change of calcium intensity normalized to pre-contact intensity average. (b) *Normalized area under curve* as the total area under the normalized peak fold change curve. (c) *Peak time* as the time in seconds of the maximum fold intensity since time of contact. (d) Percentage of T cells in each responder category.

Because it was difficult to quantify the effect of antigen potency based on visual inspection, we devised three metrics in order to compare calcium responses statistically: *peak fold change*, *area under curve,* and *peak time* (also see 4.2.4 Image Analysis). *Normalized peak fold change* was the maximum peak intensity divided by average value of pre-contact state intensities of each cell. If there were multiple peaks for a given cell (Figure 4-1, some cells in L144 and Y144), the peak with highest fold change was used. *Normalized area under the curve* measured the integrated area under the normalized intensity of each cell. *Peak time* was the time when each cell reached its maximum intensity since the time of contact. For example, if T cells had continuously declining calcium intensity after contact with APCs, the *peak time* would be negative and *peak fold change* < 1. Figure 4-2 (combined all four repeats) and Figure 4-3 (listed each repeat separately) showed results from 4 independent repeats, where in each repeat T cells were subject to all 4 conditions (L144, Y144, Q144 and no peptide). In Figure 4-2 a and b, *normalized peak fold change* and *area under the curve* both demonstrate a hierarchical response, in accordance with the trend of peptide potencies and translational responses observed by Kemp *et al*. (4). In Figure 4-2 c, *peak time* showed L144 group responded fast and coherently, while T cells subjected to less potent peptide responded slower and less coherent, which was consistent with existing literature (205).

In Figure 4-2 a and Figure 4-3 a, it appeared from visual inspection that L and Y groups had mean *normalized peak fold change* above 2, while Q and no peptide group had mean *normalized peak fold* change below 2. Thus, by choosing a threshold of 2 for peak fold change, T cells were readily separated into three groups: high responders with peak fold change >2, low responder with peak fold change 1< but <2 and non-responders with

peak fold change <1. Figure 4-2 d shows the fraction of each category when subject to peptide antigen of each potency. Collectively, results from Figure 4-1 and Figure 4-2

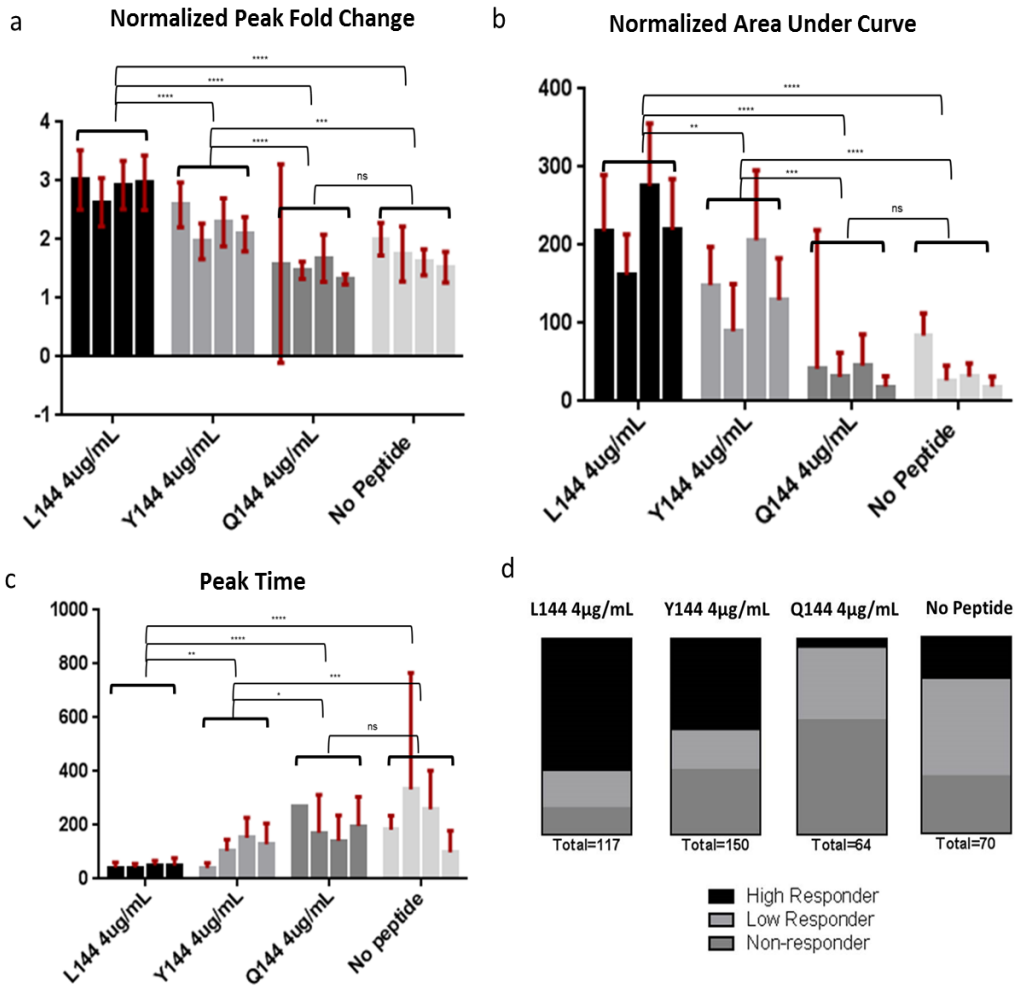

Figure 4-3 Effect of antigen potency on T-cell calcium dynamics was consistent across four independent repeats

Results from 4 repeats were listed separately, showing consistency across repeats subject to same condition. (a) *Normalized peak fold change* as the maximum fold change of calcium intensity normalized to pre-contact intensity average. (b) *Normalized area under curve* as the total area under the normalized peak fold change curve. (c) *Peak time* as the time in seconds of the maximum fold intensity since time of contact. Red bar: 95% confidence interval. (d) Percentage of T cells in each responder category.

suggest that peptide antigen potency modulates the fraction of high-responder in T population. Instead of gradually increasing response, our result is better explained by a digital response model (20): individual T cell exhibits a none-or-all response, but the percentage of high-responders reflects peptide antigen potency the population is subject to.

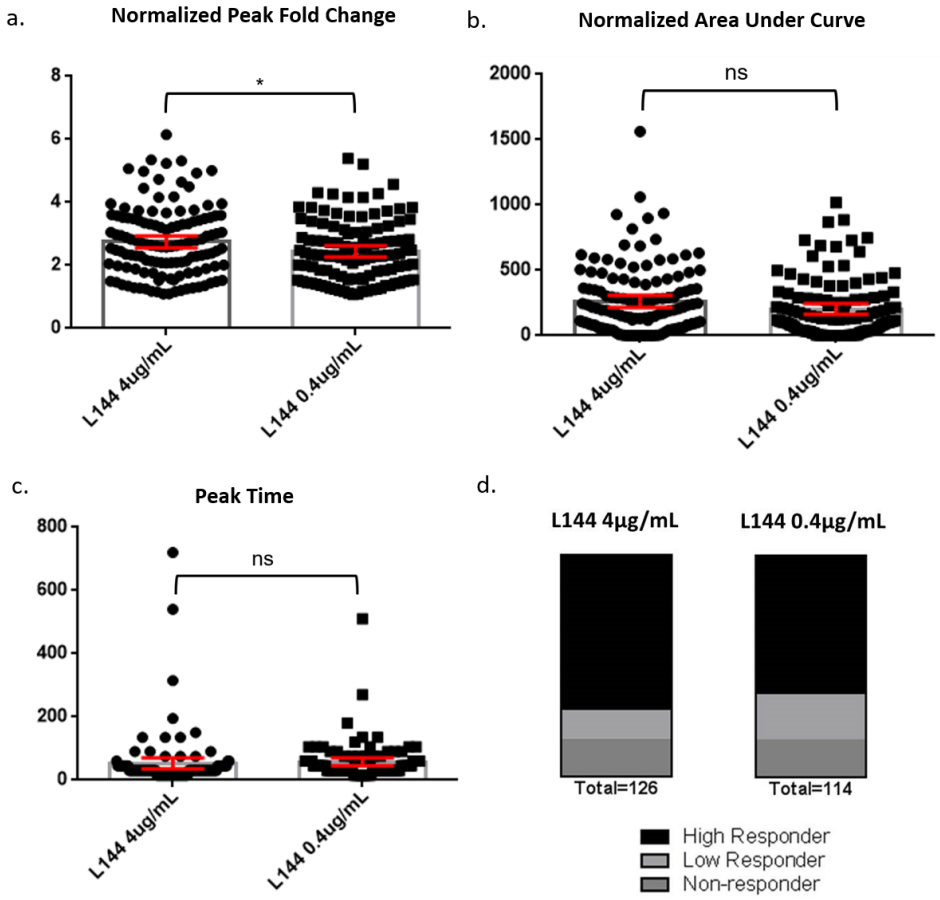

Figure 4-4 Effect of antigen dose on T-cell calcium dynamics

(a) *Normalized peak fold* change as the maximum fold change of calcium intensity normalized to pre-contact intensity average. (b) *Normalized area under curve* as the total area under the normalized peak fold change curve. (c) *Peak time* as the time in seconds of the maximum fold intensity since time of contact. (d) Percentage of T cells in each responder category.

4.3.2 Effect of Antigen Dose on T Cell Calcium Signaling

Next, we studied the effect of antigen dose on T cell calcium dynamics. Given prior reports showed kinase phosphorylation levels, apoptosis, and IL-2 production were related

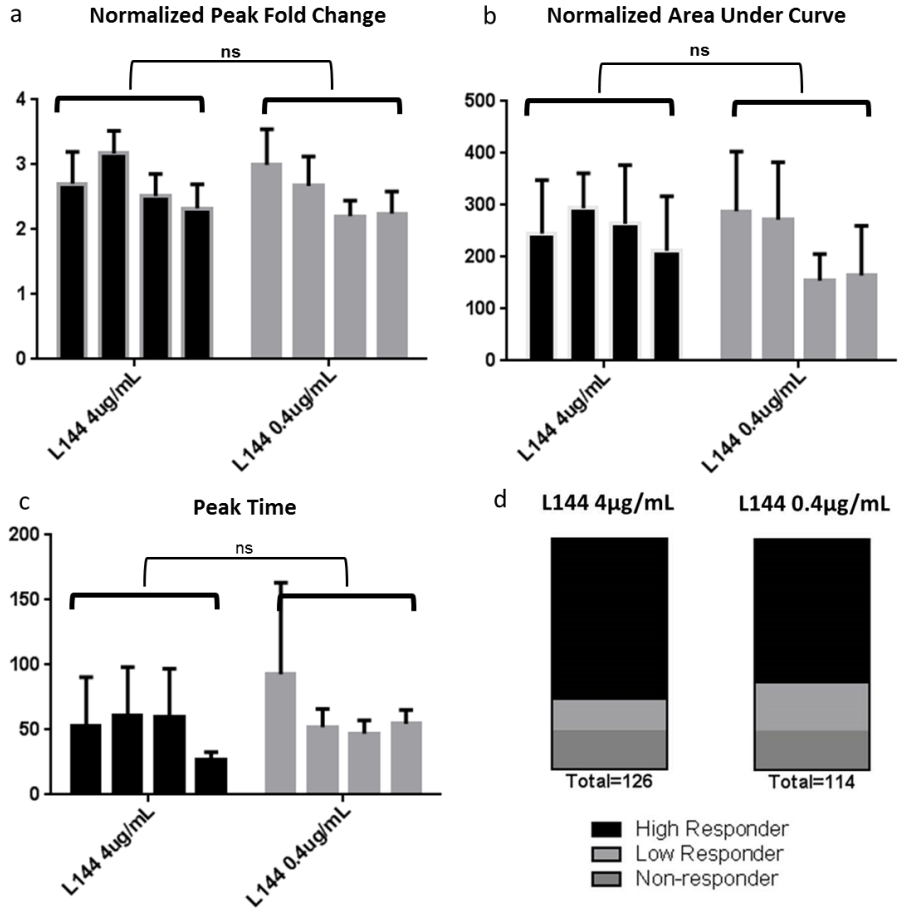

Figure 4-5 Effect of antigen dose on T-cell calcium dynamics was consistent over four independent repeats

(a) *Normalized peak fold change* as the maximum fold change of calcium intensity normalized to pre-contact intensity average. (b) *Normalized area under curve* as the total area under the *normalized peak fold change* curve. (c) *Peak time* as the time in seconds of the maximum fold intensity since time of contact. (d) Percentage of T cells in each responder category. Red bar: 95% confidence interval.

to peptide dose available for APC uptake and processing (177), it was hypothesized that a higher dose of antigen would trigger stronger calcium response than lower dose. In order to test this hypothesis, T cells subdivided from the same batch were stimulated with APCs loaded with L144 of 0.4μg/mL or 4μg/mL respectively. Surprisingly, while two antigen dose levels resulted in different *normalized peak fold changes* at 0.05 significance, both *normalized area under curve* and *peak time* were statistically indistinguishable between T cells subject to high and low doses of L144. Figure 4-4 d again showed similar composition of high responders between two conditions. Our results suggested T cell calcium responses were relative inert to changes in antigen dose compared to antigen potency. While this insensitivity may be due to signaling saturation to even the lower antigen dose used here, our results nevertheless supported a digital response paradigm, where individual T cell elicit either all or none response sums to a gradation of response for population (211). The different effect between antigen potency and dose may infer important physiological insight of T-cell antigen recognition, as while T cells must distinguish antigens of subtle structural differences, they need to be able to respond to a large quantity range of antigen with certain immunogenic nature. Notably, the two concentrations of L144 used here generated different levels of IL-2 production when monitored 24 hours later as reported in Kemp *et al* (177). Figure 4-5 showed the same results as Figure 4-4 with each experimental repeat listed separately (n = 4).

4.4 Antigen-Dependent Cross Regulation between Calcium and Mitochondria during Antigen Recognition

4.4.1 Metrics for Quantification of Mitochondria Dynamics

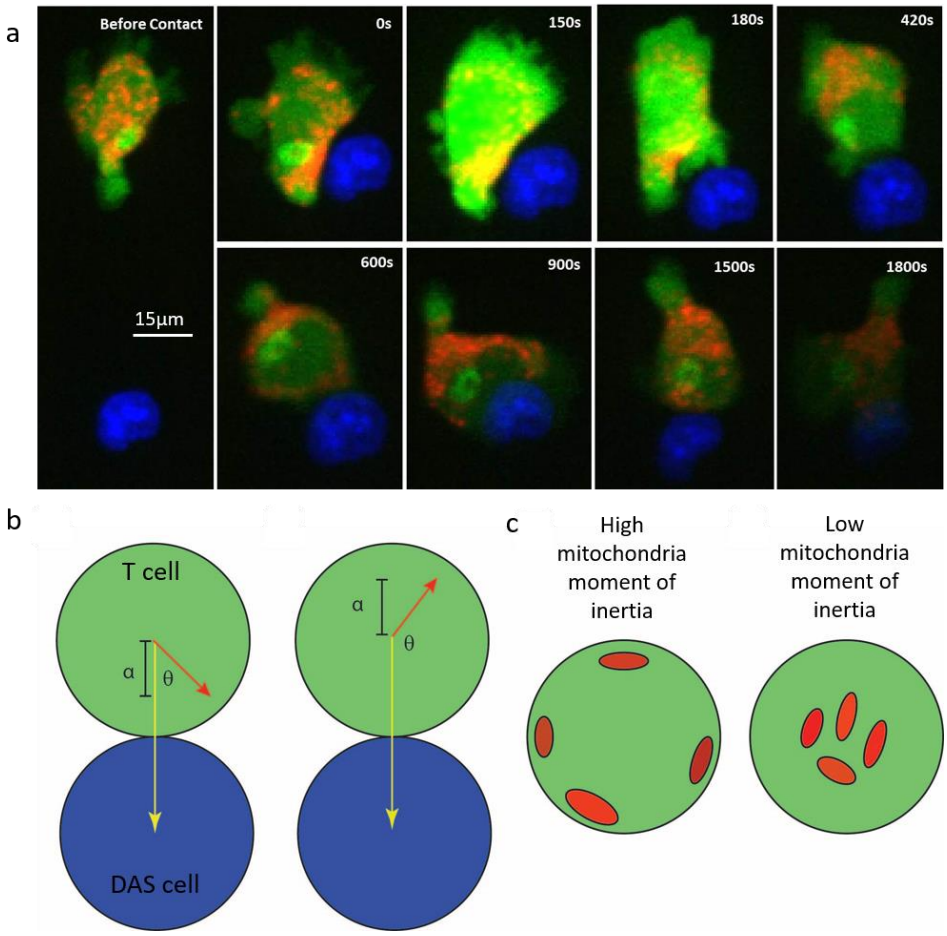

Figure 4-6 Calcium-mitochondria co-imaging and metrics for calcium-mitochondria interaction study

(a) Representative image of mitochondria (red) and calcium (green) in a T cell as activated by L144 presented on an APC (blue, nucleus). (b) Projection (α) of mitochondria vector (red vector) to intracellular vector (yellow vector). (c) *Mitochondria moment of inertia* (red regions) aims to measure the centrifuging movement of mitochondria relative to plasma membrane.

To investigate how mitochondrial movement may regulate intracellular calcium concentrations, T-cell hybridomas were labeled with Mitotracker Red and Fluo-4, AM simultaneously and monitored both signals during the initial seconds following contact (Supplemental Video 2). Figure 4-6 shows a time sequence images of a representative T

cell-APC pair captured at 40x magnification when the agonist peptide L144 was presented. In this example, the T cell hybridoma increased in calcium-sensitive fluorescence shortly after contact with an APC. Meanwhile, mitochondria morphology remodeled rapidly from a pre-contact reticular structure into a dense plaque (t = 0 to 150 sec) and finally restored a reticular texture (t = 900 to 1800 sec). Because imaging at 40x magnification only allowed two cell pairs per field of view, subsequent images were captured at 20x magnification for a larger sample size after confirming negligible loss of information at 20x magnification (Appendix Figure C-2).

Given the complex dynamics observed in these time series images, several metrics were developed to quantify mitochondrial motion. The net sum of intensity weighted projection of the *mitochondria vector* on the *intercellular vector*, *mitochondria net projection* (*NP*, Eqn. 1 in 4.2.4 Image Analysis), were used to quantify the relative position of mitochondria distribution to cell-cell interface/ immunological synapse (IS). If mitochondria congregated near the T-APC interface (Figure 4-6 b left panel), *NP* would be positive; mitochondria concentrated at the distal side of the T-cell body (Figure 4-6 b right panel), NP would be negative. However, *mitochondria net projection* alone could not quantify the position of mitochondria relative to plasma membrane (Figure 4-6 c). In order to distinguish two clearly distinct mitochondria distributions with similar *mitochondria net projection* values, another metric, *mitochondria moment of inertia* (*MC*, Eqn. 2 in in 4.2.4 Image Analysis), was devised. Increasing *MC* corresponded to mitochondria moving towards plasma membrane, while a decreasing *MC* indicated retrograde movement of mitochondria towards the nucleus. (Image-derived merics were extracted using code in Appendix D.2.1)

4.4.2 Population Average Time Series Data of Calcium-Mitochondria Dynamics

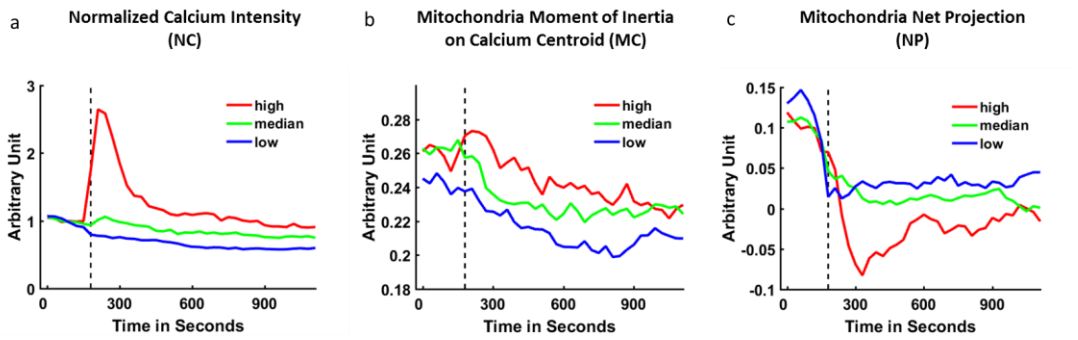

Figure 4-7. Population average of calcium and mitochondria metrics in three reponse groups

T cells are divided into three classes based on their peak fold change value: high, peak fold change > 2; median, 2 > peak fold change >1; low, peak fold change < 1. Dash line, time of contact. (a) Average *normalized calcium intensity* in three classes; (b) Average *mitochondria moment of inertia* (*MC*) indicated a graduated change in three classes; (c) Average *mitochondria net projection* (*NP*) showed a distinct pattern in high-reponder cells compared to the other two classes.

Figure 4-7 showed average traces T cells classified into three categories based on their calcium responses. T cells with *peak fold change* > 2 were labeled as high-responders, 1 < *peak fold change* < 2 as median-responders, *peak fold change* < 1 as low-responders (Figure 4-7 a). These average traces suggested a correlation between calcium dynamics and mitochondria movement. For example, high-responder cells seemed to have higher *mitochondria moment of inertia* (*MC*) following contact (Figure 4-7 b); also, high-responder cells showed a sharp negative turn in *mitochondria net projection* (*NP*) immediately following contact, which was absent in the other two groups (Figure 4-7 c). Because the highly dynamic nature of signaling processes captured in these metrics, analysis based on simple average of the entire time series eliminated the information

contained temporally, and was not able to reveal relationship between calcium response and mitochondria positioning with respect to antigen potency (Appendix Figure C-4 and Appendix Figure C-5). In addition, the profiles of each class depended on the thresholds that were selected, raising question about what thresholds should be chosen.

In these experiments, calcium intensity was used as a benchmark in order to control for calcium dynamics (Figure 4-8), which was consistent with results from study on effect of antigen potency on calcium dynamics (Figure 4-2 and Figure 4-3).

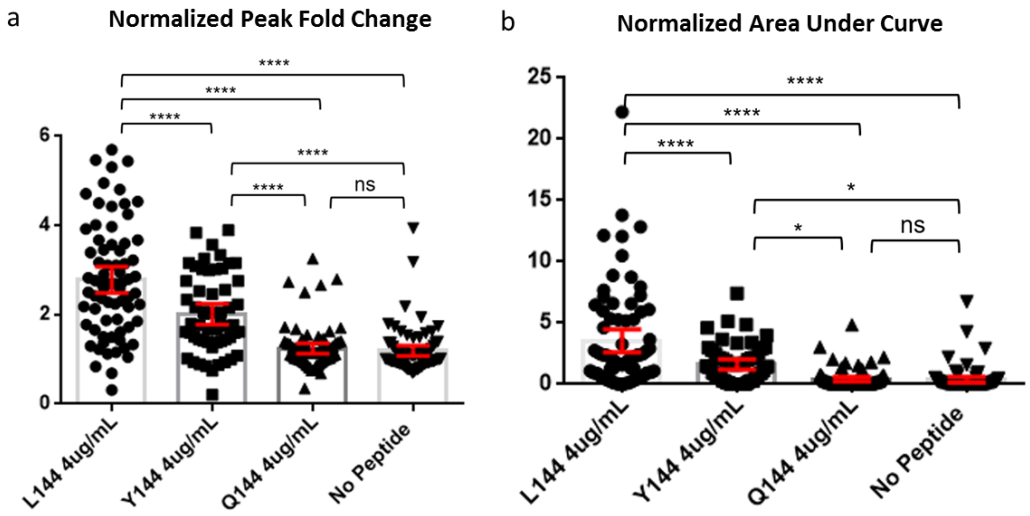

Figure 4-8 Calcium signaling benchmarking

Calcium dynamics in a calcium-mitochondria experiment were consistent with results from study on effect of antigen potency on calcium signaling (Figure 4-2 and Figure 4-3), (a) *Normalized peak fold* change as the maximum fold change of calcium intensity normalized to pre-contact intensity average. (b) *Normalized area under curve* as the total area under the normalized peak fold change curve.

4.4.3 Partial Least Square Regression Model of Calcium-Mitochondria Relationships

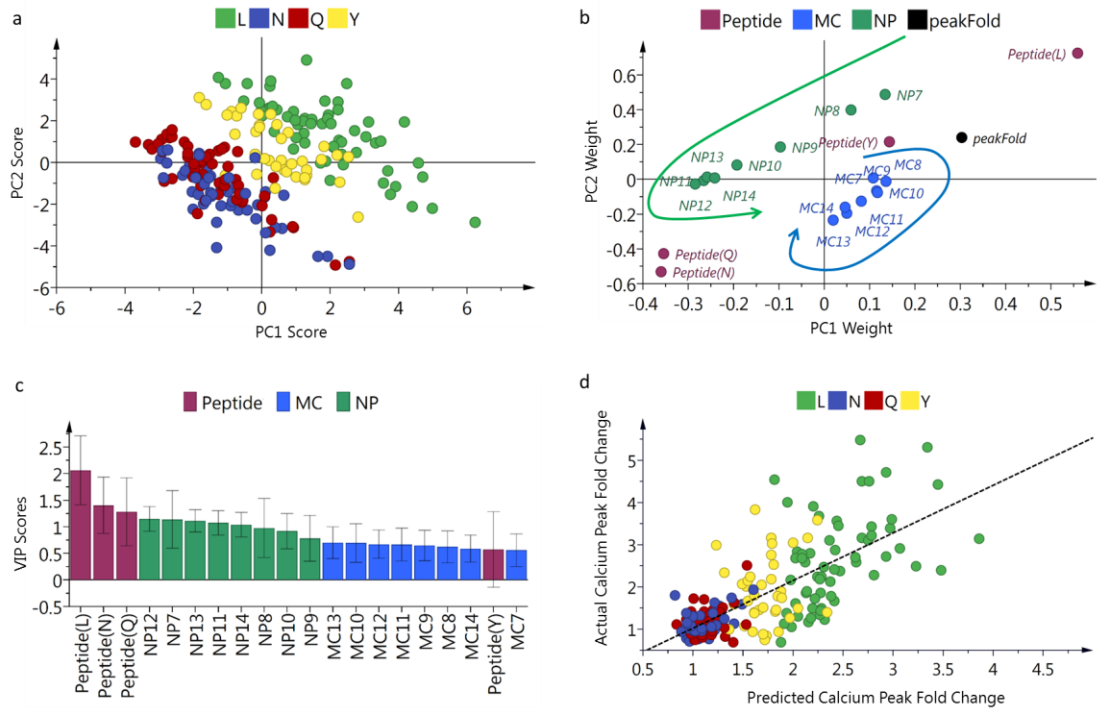

Figure 4-9 Partial least square regression model of calcium responses and mitochondria dynamics

(a) Scatter plot of scores on first two principal components. Cells subject to L144 and Y144 peptide presentation were readily seperated from Q144 and no peptide group. (b) Weight plot of mitochondria net projection (green) and moment of inertia (blue) time points in predicting calcium *peak fold change* (black dot). Only time points 7 (time of contact) to 14 (4 minutes after time of contact) were included in the model. Colored arrows reflect the change from positive correlation to negative correlation of *NP* with respect to calcium *peak fold change* as a function of time post-contact. (c) VIP score plots of X variables in order of significance. Error bars represent 95% confidence intervals. Both *MC* and *NP* between time points 7 to 14 were relevant in predicting *peak fold change.* (d) Prediction plot of calcium peak fold change versus measured calcium peak fold change.

In order to identify effective image-derived metrics and important time points among the high dimensional dataset, a partial least square regression (PLS) model was built to explore the relationship between calcium response and mitochondria dynamics in wake of APLs stimulation (Dataset was prepared using code in Appendix D.2.2). In our initial

model (Appendix Figure C-6**)**, *peakFold*, *AUC* and *peakTime* were used as Y variables and all 38 time points of all six mitochondria features as X variables. This model yielded a R^2X of 0.625, R^2Y of 0.426, and Q^2 of 0.16. The goodness of fit plot (Appendix Figure C-6 a) showed both *peakFold* and *AUC* were well modeled while *peakTime* was not. The weight plot of this model showed serval insights (Appendix Figure C-6 b): 1. Among the three response variables, *peakFold* and *AUC* were highly correlated as they located close to each other (two black dots in the bottom right quadrant). 2. Peptides were the most significant predictors as they lied furthest from the origin (pink dots). 3. L peptide was positively associated with *peakFold* and *AUC* as L peptide located on the same side of origin with these two features, while N and Q were negatively associated with *peakFold* and *AUC*. 4. *NP*, *PR*, *IR* (red, purple, orange dots) were collinear with each other and were positively associated with *peakFold* and *AUC*, while *MC*, *MM* and *AP* (blue, green, turquoise dots) were correlated with each other and were negatively associated with *peakFold* and *AUC*. 5. Time points within 4 minutes of contact time (frame 7 to 14, frame number was labeled following the metric label) were most significant in explaining *peakFold* and *AUC*, while pre-contact time points (frame 1 to 6) which clustered close to origin and latter time points (frame 15 to 38) which gradually retreated back towards origin were not significant.

After optimization, the highest quality model achieved R^2X of 0.701, R^2Y of 0.564 and Q^2 of 0.51 with three principal components (PCs), where the first two components captured most of the variance (Figure 4-9 a**)**. This model included *Peptides*, 8 time frames (from 7 to 14, 4 minutes within time of contact) of *MC* and *NP* each as predicting variables and *peak fold change* ("*peakFold"*) as the response variable. Figure 4-9 a illustrated the scores plot of cells (observations) projected on the first two PCs. In a trend consistent with

Figure 4-9 a and b, this scatter plot indicated a gradation of responses in line with APL potency. In Figure 4-9 b, the corresponding weight plot revealed relationships between all predicting variables and the response variable simultaneously. *Peptides* were the most significant predictors as they were furthest from the origin: L144 peptide was positively associated with *peakFold* as it located on the same side of origin, while N and Q were negatively associated. More interestingly, the weight plot suggested that cells with higher *peakFold* were correlated with higher *MC* (outwards movement of mitochondria relative to cell centroid) within two minutes after contact (time frame 7 to 10); cells with higher *peakFold* were initially associated with positive *NP* (mitochondria moving towards IS) immediately following contact (time frame 7 and 8), but quickly transitioned to negative *NP* (mitochondria moving towards the opposite side of cell interface), which was most significant around 2 minutes (time frame 12) after contact. The importance of the time-dependent *mitochondria net projection* was confirmed by the VIP plots (Figure 4-9 c), where all predicting variables were listed in order of significance. Lastly, the resulting PLS model was used to predict *peak fold change* from peptide and mitochondria variables. In Figure 4-9 d, the scatter of points around the diagonal line indicated agreement between observation and model prediction.

4.5 Discussion and Conclusion

4.5.1 Discussion on Calcium Response to Altered Peptide Ligands

While prior studies have identified several distinct calcium signaling patterns responding to APLs (193, 204–206, 212, 213), these patterns were described qualitatively based on visual inspection. With the metrics we developed, we are able to parameterize the

calcium response, rendering it amenable to statistical analysis. Here with the ability to monitor population responses at single T cell level, our result showed antigen potency modulated T cell activation by shifting the calcium response distribution among the population (e.g. group L and Y, Figure 4-1 a & b) (214). In addition, we observed that even a low dose of agonist peptide, a condition reported to elicit much lower levels of apoptosis or IL-2 at 24 hours (177), was nonetheless sufficient to triggering calcium response in an identical manner to a high dose. This observation is consistent with a kinetic model where engagement of a few agonist among large self pMHC background is responsible for T cell activation (49, 80). This model also explains why we observed several high responding cells subject to Q144 and no peptide: these T cells might happen to scan through a few self pMHCs that were high affinity to TCRs. While we did not directly measure phosphorylation, transcriptional and translational changes, literature using the same APLs and other studies using different altered peptide ligands have demonstrated effect of APLs on downstream processes such as cytokine production (215).

4.5.2 Discussion on Mitochondria Repositioning to Altered Peptide Ligands

The involvement of mitochondria during antigen recognition is complex. Quintana *et al.* tested the manipulation of calcium entry site with patch pipettes to establish that preferential mitochondria location at the IS in order to sustain CRAC calcium influx. In contrast, mitochondria are also postulated to transport calcium elsewhere to control duration and timing of the signal. While detailed investigations of mitochondrial positioning have elucidated the importance of this organelle for T cell activation, this body of work has largely been performed on antigen coated hard surface (microbeads, plates, glass slide, *etc.*) with Jurkat cells due to technical limitations (25, 216–218). Our cell lines

are also artificial compared to *in vivo* processes; nonetheless, MHC:peptide presentation on the APC fibroblast line with co-receptor B7.1 provided us the opportunity to monitor spatial regulation of mitochondria as a function of antigen potency within minutes of contact. The high degree of motility and surface sampling exhibited by our cells provides a physiological context with membrane interactions and small molecule exchange that cannot occur in a bead delivered system (219, 220). By showing mitochondria remodelling as a highly dynamic process, our results reconcile prior T cell studies as different phases during signaling process (25, 210, 217). We observed mitochondria translocating towards IS immediately following antigen recognition (within 1 minute of cell contact), consistent to literature reports (25, 221). In addition, our results showed mitochondria quickly move towards the opposite side of T cell body in the following 3 minutes (Figure 4-9 b). This rearward movement has also been reported by the same authors (210), where F-actin quickly accumulated around IS and elongated the T cell body towards APCs (222, 223). Interestingly, this observation coincided with a study which reported STIM1-Orai1 cap formation on the opposite side of T cell body (224), suggesting the mitochondrial role in calcium buffering (218).

4.5.3 Discussion on Partial Least Square Model

In addition, we developed new metrics to quantify highly dynamic early signaling events during T-cell antigen recognition. We developed image processing tools to automatically track cell movement and to extract image-derived features from highly dynamic mitochondria movement and corresponding calcium responses. The calcium metrics allowed us to statistically compare population responses subject to various APLs, illustrating different effects of antigen potency and dose during antigen recognition.

Similarly, the mitochondria metrics provided quantitative description of mitochondria motility and orientation within T-cell body with respect to APC engagement. Compared to experiments done in bulk where only a few time points could be measured, our study generated longitudinal time series data of coupled signaling processes, which required a new method of analysis. Here, we developed multivariate models to handle the high-dimensional data that would be difficult to dissect using conventional univariate analysis. A partial least square model revealed relationships between antigen potency, mitochondria positioning/timing and calcium response.

In our initial PLS analysis, several metrics (*NP, PR, IR*) were found to be collinear or highly correlated with each other, so these redundant metrics were excluded in our optimized model as they added little information (Appendix Figure C-6). Among these metrics, *PR* and *IR* were highly collinear with *NP*, while *MC* and *MM* were correlated with each other but yielded different information (Appendix Table C-1): *MC* measured the distribution of mitochondria relative to center of mass of the T cell body; *MM* measured the morphology of mitochondria relative to center of mass of mitochondria itself. Thus *MM* might be regarded as a metric to measure the fusion (low *MM* value) and fission (high *MM* value) of mitochondria. When we included *MM* into a model, *MM* seemed to negatively correlate with high calcium response (Appendix Figure C-7). Existing literature have suggested mitochondria fusion and fission affected bioenergetics of mitochondria, where fusion favoured oxidative phosphorylation (OXPHOS) while fission reduced electron transport chain (ETC) efficiency (225), our result might yielded insights into the role of mitochondria fusion and fission in T cell activation (221, 226).

4.5.4 Conclusion

In this Chapter, the microfluidic system developed in Chapter 3 was applied to enable synchronized interaction of T cells with antigen presenting cells in order to simultaneously monitor calcium and mitochondria dynamics during recognition of altered peptide ligands. The results confirmed that stronger antigen potency modulated T-cell calcium signaling by inducing higher percentage of responding cells. The results also showed a 10-fold change in antigen dose induced minimal effect on calcium responses in T cells, indicating different signaling mechanisms are involved in T-cell responding to antigen dose versus potency. Finally, novel metrics were developed to quantify the highly dynamic mitochondria movement during antigen recognition. The partial least square regression model revealed that high calcium responses in T cells were associated with rapid relocation of mitochondria from the region of the immunological synapse to the distal side of T cell body. This Chapter illustrated application of a microfluidic system in obtaining novel cell signaling data, which further enables use of advanced statistical techniques.

CHAPTER 5. CONCLUSION AND FUTURE DIRECTION

5.1 Conclusion

5.1.1 Thesis Contribution

As immunotherapy emerges as a promising alternative in treating multiple forms of cancer, much focus has been to improve safety and effectiveness of such therapies, where understanding of immune cell signaling is essential. Several useful methods, including bi-lipid layer, BFP, and microwell methods, were developed to study immune cell signaling. However, there is still need to incorporate advantages from all these methods to simultaneously achieve precise cell manipulation and high throughput. In this thesis, I combined microfluidics with automatic control, image processing and *in vitro* time-lapse microscopy to accomplish this goal. More specifically, new tools to perturb cell signaling by dynamic cues or through direct cell-cell interaction were developed in this thesis. The contribution of this thesis can be summarized into three categories as follows:

5.1.2 Microfluidic Device Design and Fabrication

Due to the small size of cells (on the order of 10 μm), an interface on a similar scale to a cell is required to effectively control cell movements and microenvironment. Microfluidics was proved to be effective tools in arraying, stimulating and paring of cells. In this thesis, several new microfluidic designs were created, and multiple fabrication methods were explored to enrich knowledge in microfluidic domain. In Chapter 2, a microfluidic platform for delivering of programmable dynamic chemical cues was created to interrogate calcium signaling in arrayed single T cells. In order to improve the accuracy

in fabrication of miniature structures (~2μm), a hybrid fabrication technique (silicon etching of the 2μm feature and negative photoresist for the rest) was developed. Using of single-layer on-chip valves to create arbitrary concentration level from binary input flow streams was demonstrated the first time through a microfluidic digital-to-analog converter concept. In addition, effective dispersion of chemical cues in a microfluidic cell array was characterized, where a new model was proposed to describe such phenomenon. In Chapter 3, a new microfluidic platform was designed for synchronized cell interaction using pressure induced flow. Due to the complexity involving two different cell types, a 3-layer fabrication process was developed: two silicon-etched layers with one additive photoresist layer. This process ensured the fabrication accuracy for critical features (silicon etched 3μm and 6μm layer), which was less stringent on mask resolution (10 μm maximum) and achieved high cellular imaging quality as cells were positioned at cover glass interface.

5.1.3 Experimental System Design and Automation

While microfluidics acts as good interface for working with single cell analysis, microfluidics alone is not sufficient for effective cell manipulation. Auxiliary components are required for automation of experimental processes. Previous members in Lu lab have developed tools (pressure box) to allow regulated pressure release through computer control. In Chapter 2, the pressure box was modified in controlling actuation of on-chip valves in the microfluidic chip. A custom Matlab GUI was developed for controlling the pressure box, which allowed valve actuation at specified frequencies in order to generate arbitrary concentration level. In Chapter 3, a pressure balance operation scheme was demonstrated the first time, where pressure difference between inlet and outlet was adjusted to control the movement of cells in device. Also, the original design of pressure

box was again modified because application to cells required much more precise pressure control compared to application to larger organisms (such as *C. elegans*).

5.1.4 Image Analysis and Multivariate Analysis of Cell Signaling Data

In Chapter 3, new metrics were developed to quantify calcium responses to APLs. also, several Matlab scripts including a cell tracking algorithm were developed to facilitate automatic image processing and to extract image-derived features from fast signaling dynamics in immune cells. In Chapter 4, novel metrics were designed to characterize mitochondria movement and a partial least square regression model (PLSR) was developed to reveal important relationship between calcium and mitochondria hidden in the high dimensional data. The PLSR model identified the most effective metrics and most important time points in T cell antigen recognition, with which the calcium peak fold change can be modeled as a function of antigen potency and relevant mitochondria movement metrics.

5.1.5 Biological Insight Relating to Immune Cell Signaling

In Chapter 2, system identification method was applied in studying T cell signaling. By stimulating T cells with H_2O_2 at a range of frequencies, T cells calcium dynamics were found to synchronize to the low frequency stimulus, while it did not respond to the high frequency input as in a low-path filter. Because in a physiological system all chemical signal was also limited by dispersion during transport, this observation might shed insights on limitation of many signaling processes relying on chemical signal. Also, heterogeneity of calcium response was observed among T cell population when responding to H_2O_2 stimulus. While heterogeneity was commonly observed in many biological systems, the

root cause and the biological functionality of signaling heterogeneity were still to be understood. In Chapter 4, the role of antigen potency and dose during T cell antigen recognition was systematically investigated. T cells were found to be highly sensitive to even a single amino acid change in a peptide chain; T-cell calcium response showed distinct dynamic signatures responding to peptide antigen of hierarchical potencies. Interestingly, T cells were relatively insensitive to changes in dose of antigens (10-fold difference). Both results suggested TCRs have high specificity and low detection limit, which were important to physiological functionality of T cells: T cells need to determine their effector function based on careful discrimination of antigens with subtle differences, as well as mount full-fledged response regardless of the amount of such antigens presented. Lastly, the role of mitochondria during T cell antigen recognition was studied. Our results demonstrated the first time that higher calcium response was associated with immediate (within 1 minute after contact) translocation of mitochondria towards T cell-APC interface, but was followed by rapid (within 4 minutes after contact) translocation to the opposite side of cell interface.

5.2 Future Directions

5.2.1 Future Microfluidic Fabrication Process

The conventional microfluidics fabrication technology was based on photolithography, where layers of microscale features were reductively etched or additively deposited on a silicon wafer to generate microfluidic masters. Because microfluidic devices were molded from features of a master, topologically it limited the versatility of microfluidic structures that could be achieved. Complex structure could only

be achieved through stacking of individual PDMS layers, where alignment and combining process were difficult and error-prone. In future, fabrication technology such as 3D printing may be applied to fabrication of microfluidic devices in an additive process, but current 3D printing technology cannot achieve the resolution of photolithography (~10μm) (227). Under current circumstances, a microfluidic platform designer may first evaluate experimental needs and try to avoid overcomplicated microfluidic structure.

5.2.2 Future Improvement of Dynamic Stimulus Device

In order to interrogate cellular signaling in T cells, a microfluidic platform was developed to delivery dynamic stimulus to arrayed single T cells in Chapter 2. However, to generate enough shift of flow interface by deformation of the pneumatic valves required high pressure (40 to 60 psi), which was prone to rupture of PDMS material and leakage. To reduce pressure requirement and possibility of rupture, pneumatic valves with higher aspect ratio can be designed: an additional layer can be added onto the valve structure of the master using negative photoresist. In addition, a bypass channel can be added in the design to guide the flow interface to device outlet, which further lowers the pressure required to shift the fluid interface. This channel also helps to maintain a definite positive and a negative control chamber on each side.

5.2.3 Future Improvement of Cell Interaction Device

In Chapter 3, while the final design demonstrated synchronized cell interaction, the throughput of device can be further improved. Currently, cells tended to lose their position due to pressure fluctuation in device, which was manifested as squeezing of cell into *cell interaction chamber* through *front gate* even before *transient positive pressure* was

applied. If structural change of *cell interaction units* was considered for future improvement, fluid element analysis (FEA) should be performed to access the impact of dimension changes on fluid flow, because effect of fluid resistance ratio change between *main channel* and *cell interaction unit* was multi-fold: while increasing the fluid resistance through *cell interaction unit* can help reduce squeezing of cells before application of *transient positive pressure*, it will at the same time leads to less efficient loading of cells into *front traps*. Nevertheless, there are other ways to reduce pressure fluctuation or to mitigate the effect of pressure fluctuation on cells. The easiest solution is to change for more stable pressure source. Currently an air compressor is used as transportable pressure source, but air compressor has duty cycles, which may cause pressure fluctuation in device. Alternatively, keeping the current *cell interaction unit* structure and number of units on each row unchanged, increasing the number of rows in a single *cell trap array* can reduce pressure fluctuations on each row as all rows are connected in serial fashion.

5.2.4 Measure Calcium Dynamics in Mitochondria During T-Cell Antigen Recognition

In Chapter 4, positioning of the mitochondria was discovered to be related to calcium response during T-cell antigen recognition. While the fluorescent probe used here (MitoTracker Red) could track the movement of mitochondria, it was still unknown how mitochondria exerted effect on calcium signaling. From a mass balance point of view, as calcium ion concentration fell in T-cell cytosol following initial peak, calcium ions must be either secreted to extracellular space or up taken into organelle inside cells. To visualize calcium ion concentration inside mitochondria, a fluorescent probe (Rod-2, for example) that is mitochondria-specific and responds to calcium changes must be used. An experiment that coupled mitochondria calcium measurement with mitochondria

positioning or cytosol calcium dynamics measurement can help answer whether mitochondria uptake calcium during T-cell antigen recognition.

5.2.5 Monitor ROS Signaling During T Cell Antigen Recognition

With the mitochondria as the major site of ROS generator inside a cell, it will be interesting to investigate possible cross-regulation between mitochondria produced ROS and calcium signaling during T-cell antigen recognition. It is well known calcium influx during T cell activation was conducted through CRAC channel, which were composed of STIM1 and Orai following ER calcium depletion. Studies showed ROS induced S-glutathionylation of STIM1 (228), while STIM1 further induced dimerization of Orai dimers (229). These two reports hinted that mitochondria-generated ROS may be required for formation of CRAC channels, which are necessary for sustained calcium influx during T-cell activation. The experimental system developed in Chapter 4 is well-positioned to test this hypothesis by using a mitochondria-targeted ROS indicator. The same data analysis pipeline can be followed to test the relationship between calcium and mitochondria ROS production. The challenging is however to select proper ROS indicator, as current commercially available ROS indicators have generally low signal and are sensitive to oxidation.

5.2.6 Measure Phosphorylation Signature and Transcriptome following T-Cell Antigen Recognition

While early signaling events (calcium and mitochondria) were measured in this thesis, previous studies suggested phosphorylation levels of signaling proteins also correlated with peptide antigens of various potencies and doses (177). Using on-chip

immunostaining, phosphorylation states of various signaling kinases (such as *ERK*, *AKT*, *etc*) can be measured. In addition, the single cell transcriptome can also be measured by fluorescence *in situ* hybridization (FISH) and other RNA-seq technologies. Together with early signaling events, measurement on phosphorylation signature and transcriptome will help to understand how information was transmitted along the signaling cascade during T cell antigen recognition (Figure 1-1).

5.2.7 On-Chip Investigation of Other Immune Cell Types

Antigen Presenting Cells (APCs)	T Cells
Dendritic Cell	CD8+ Cytotoxic T Cell
Macrophage/Neutrophil	CD4+ Helper T Cell
B Cell	CD4+25+ Regulatory T Cell
Abnormal/Infected somatic cell	NK Cell

Figure 5-1 The microfluidic system developed for studying cell interaction can be applied to many other immune cell types

While the microfluidic system designed in Chapter 3 has only been used for studying interaction between T cells and antigen presenting cells, its application can be readily extended to study interactions of other immune cell types (Figure 5-1). Many

processes in cell-mediated immunity rely on direct cell-cell contact: for example, CD8 T cells attack cancer cells or infected somatic cells by loading cytotoxic granules onto the target cell; similarly, B cells require CD4 helper T cells for isotope switching; and macrophages require CD4 helper T cells for clearance of engulfed bacteria.

5.2.8 Combine Gene Editing with Microfluidics for Cell Signaling Study

Using gene editing tools to alter endogenous signaling pathway provides a window for researchers to probe into properties of signaling pathways. The Vale lab genetically constituted immune cell signaling pathway components in non-immune cells, which revealed how surface co-stimulatory molecules regulated T cell signaling during activation (230). This study demonstrated the concept where isolated components of the immune cell signaling pathway can be modified using genetic tools to investigate their function. Recent advance in genetic tools such as CRISPR has improved the precision and efficiency of gene editing. Thus, our microfluidic system can be combined with this powerful gene editing tool to understand immune cell signaling by altering endogenous signaling pathways in cells.

APPENDIX A SUPPLEMENTAL MATERIAL FOR CHAPTER 2

APPENDIX A.1 Dispersion Characterization

Appendix A.1.1 Effect of Flow Rate on Stimulus Profile using FITC-BSA

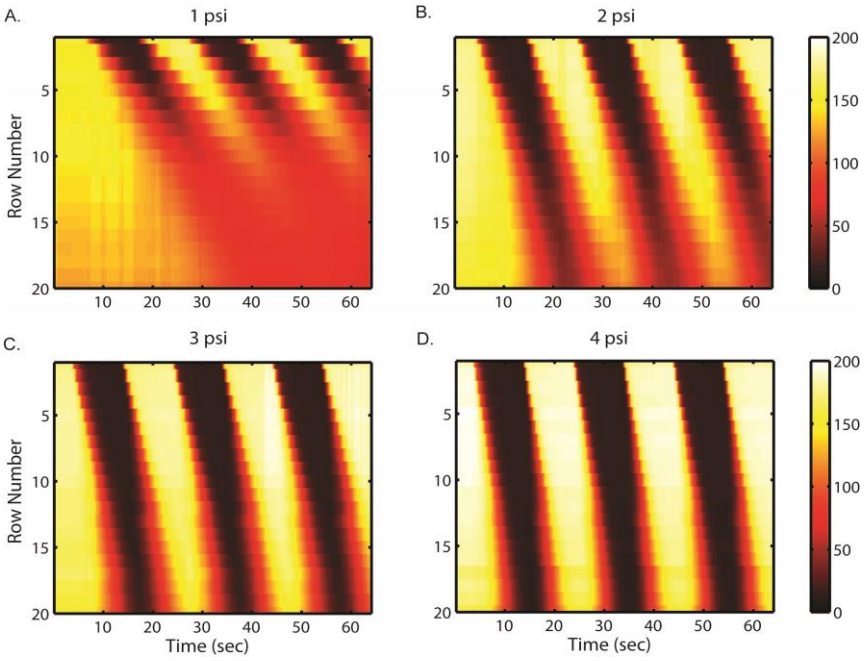

Appendix Figure A-1 The stimulus profile visualized using FITC-BSA

The stimulus profile visualized using FITC-BSA shows similar pattern to that of fluorescein, although FITC-BSA pattern was more dispersed compared to that of fluorescein. Profiles were generated by alternatively delivering FITC-BSA solution and PBS at 50 mHz driven by (a) 1psi, (b) 2psi, (c) 3psi and (d) 4psi. Heatmaps of spatial (Y axis) and temporal (X axis) show fluorescent intensity (color bar) in single observation chamber.

Appendix Table A-1 Summary of effective dispersion analysis for fluorescein and FITC-BSA

FITC-BSA dispersion

Driving Pressure	Mean Flow Velocity	Effective Dispersion Coefficient	Rise Time ***t*** *(sec)* for Row #				
(PSI)	***U*** *(m/s)*	***Deff*** *(m^2/s)*	1	5	10	15	20
1	*5.14E-04*	*5.67E-07*	*1.7*	*7.8*	*19.4*	*24.5*	*28.6*
2	*1.29E-03*	*1.73E-06*	*0.9*	*3.1*	*7.0*	*9.4*	*12.3*
3	*1.98E-03*	*2.82E-06*	*0.7*	*2.0*	*4.4*	*6.1*	*8.2*
4	*2.78E-03*	*4.36E-06*	*0.6*	*1.4*	*3.2*	*4.4*	*6.0*
5	*3.48E-03*	*5.35E-06*	*0.5*	*1.2*	*2.6*	*3.6*	*4.8*

Fluorescein dispersion

Driving Pressure	Mean Flow Velocity	Effective Dispersion Coefficient	Rise Time ***t*** *(sec)* for Row #				
(PSI)	***U*** *(m/s)*	***Deff*** *(m^2/s)*	1	5	10	15	20
1	*5.23E-04*	*1.47E-07*	*1.1*	*6.5*	*13.3*	*15.2*	*14.2*
2	*1.34E-03*	*1.11E-06*	*0.6*	*2.7*	*6.0*	*7.9*	*9.4*
3	*2.20E-03*	*2.32E-06*	*0.5*	*1.6*	*3.8*	*5.2*	*6.4*
4	*2.92E-03*	*3.61E-06*	*0.4*	*1.3*	*3.0*	*4.1*	*5.1*
5	*3.82E-03*	*5.32E-06*	*0.4*	*1.0*	*2.2*	*3.2*	*4.1*

Appendix A.1.3 Effective Dispersion Analysis is Consistent Across Experiment Repeats

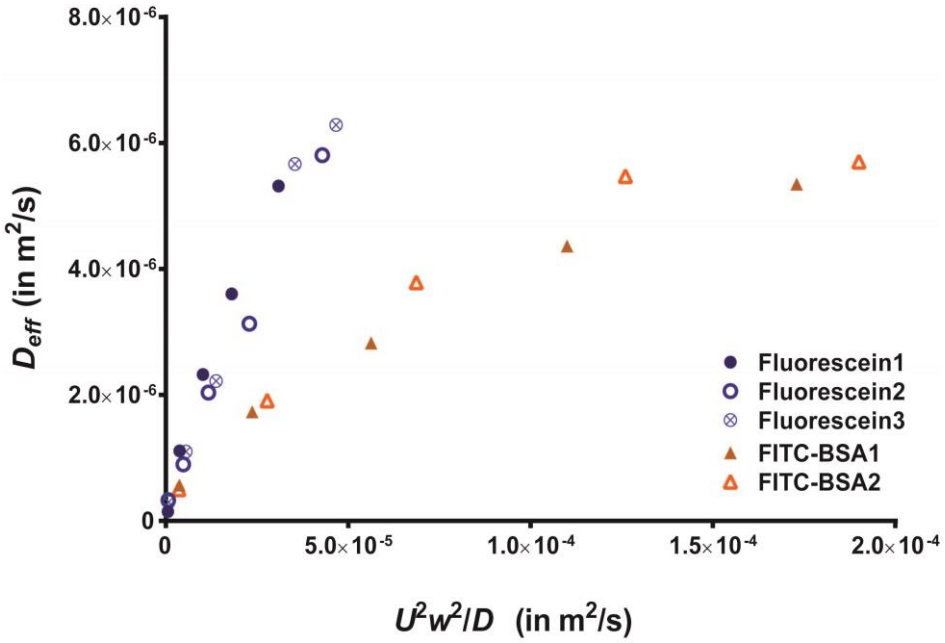

Appendix Figure A-2 The results for effective dispersion analysis are consistent across experiment repeats

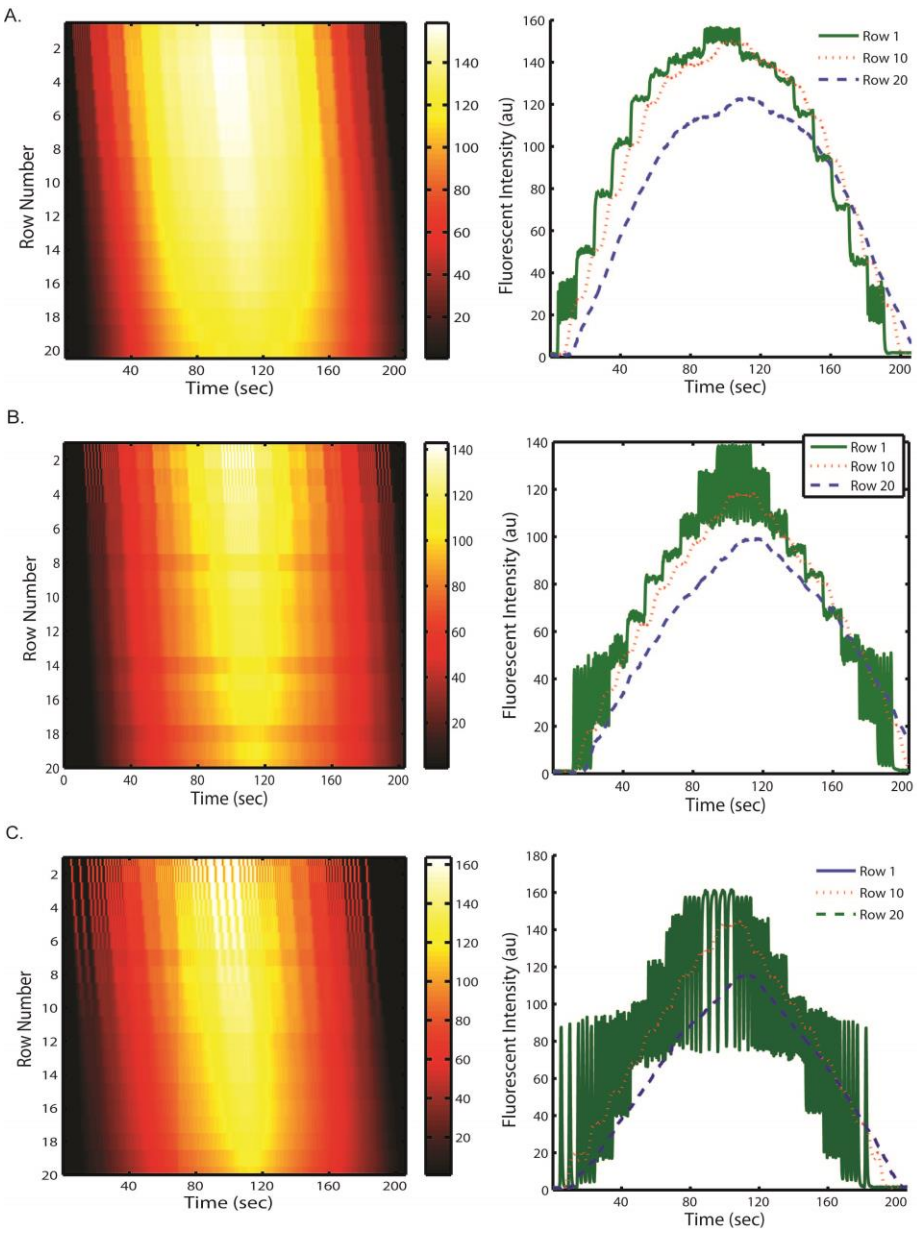

Appendix Figure A-3 The choice of base pulse duration affects stimulation profile

The spatial-temporal heat map of fluorescent intensity within an observation chamber and its corresponding fluorescent intensity profile: (a) FITC-BSA solution with base pulse of 100 ms, (b) fluorescein solution with base pulse of 200 ms, and (c) FITC-BSA solution with base base pulse of 500 ms.

APPENDIX B SUPPLEMENTAL MATERIAL FOR CHAPTER 3

APPENDIX B.1 Image Processing

Appendix B.1.1 Cell Identification Procedure

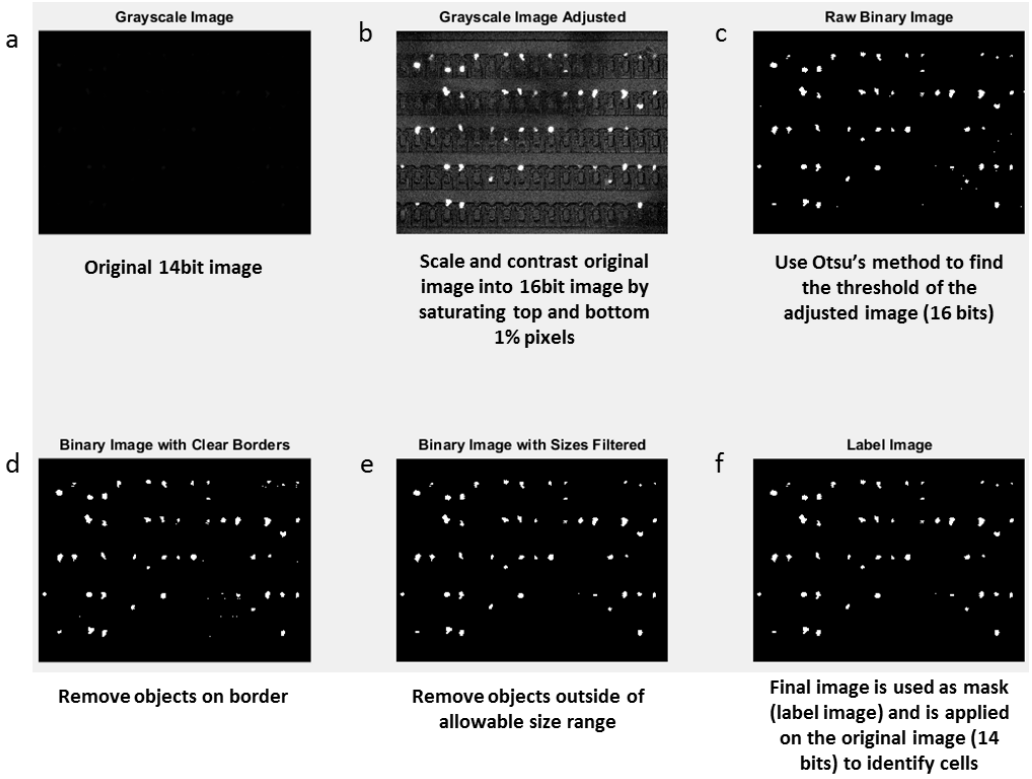

Appendix Figure B-1 Cell identification procedure

(a) Obtain the original 14 bits image. (b) Scale the image to improve contrast. (c) Find the threshold using Otsu's method and create binary image based on threshold. (d) Clear border objects. (e) Filter objects based on size. (f) Resulting image is the label image.

In order to obtain calcium signaling information, intensity values of cells were extracted from image recording. The first step was to identify cells from the original 14-bit image, shown in Appendix Figure B-1.

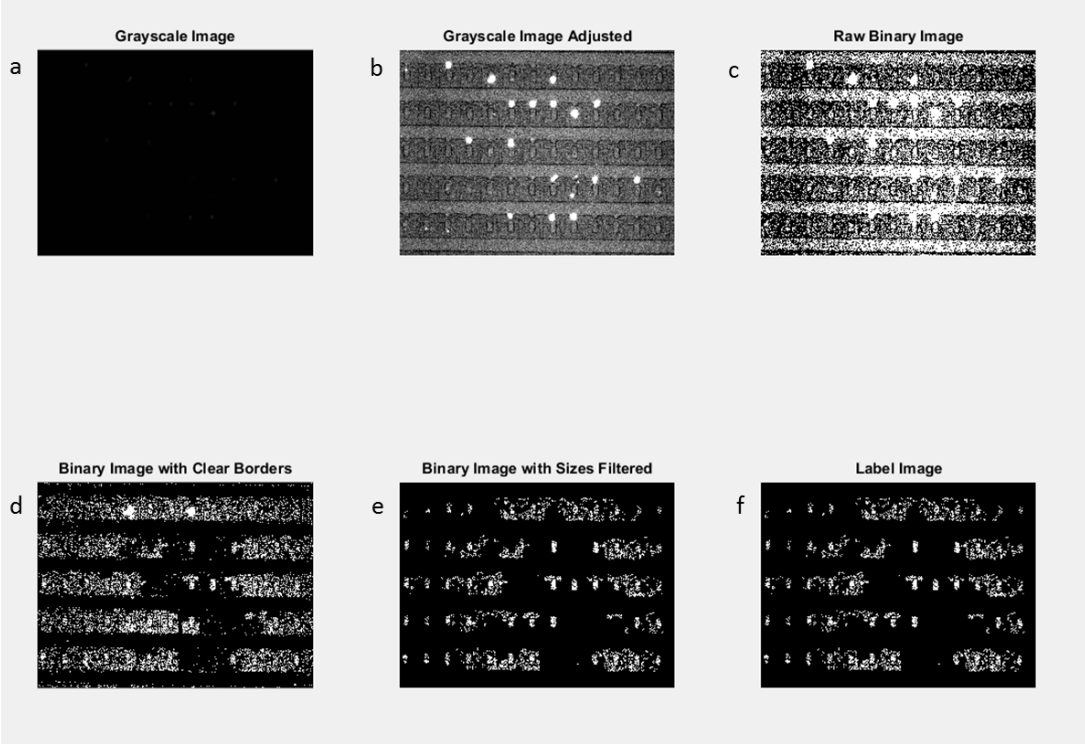

Appendix Figure B-2 Error during contrast improving step of image processing

The procedure is identical to procedure in Appendix Figure B-1.

However, sometimes errors might occur during contrast improving step (Appendix Figure B-2 b), when there were not many cells. It was caused when some background pixels among the 1% of brightest pixels were scaled to saturation. Due to this issue in image processing, a fixed threshold was adopted instead in Chapter 3 to identify the cells. Because dye loading conditions were maintained constant, this fixed threshold method was usually sufficient for cell identification.

APPENDIX B.2 Characterization of Cell Loading and Pairing Efficiency

Appendix B.2.1 Suboptimal Device Loading

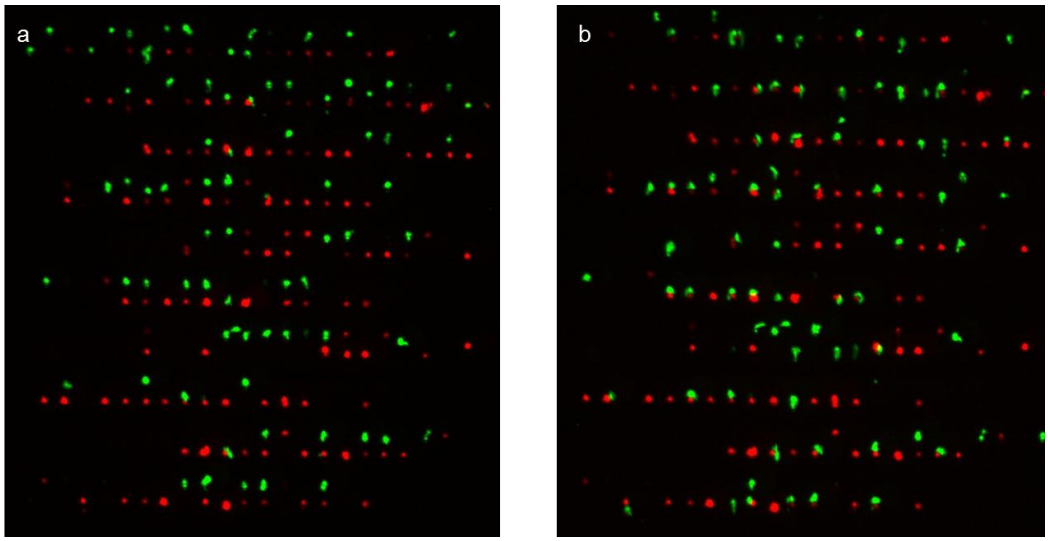

Appendix Figure B-3 Zig-zag distribution and premature contact of cell pairs

(a) Pre-contact position of both cell types (Red: DAS cells, Green: 1B6 T cells). T cells were sparsely trapped in a zig-zag fashion. Some T cells were already in contact with DAS cells even no transient pressure was applied yet. (b) Post-contact position of both cells types.

APPENDIX B.3 Optimization of Experimental Protocol

Appendix B.3.1 Effect of Temperature on Calcium Signaling of T Cells

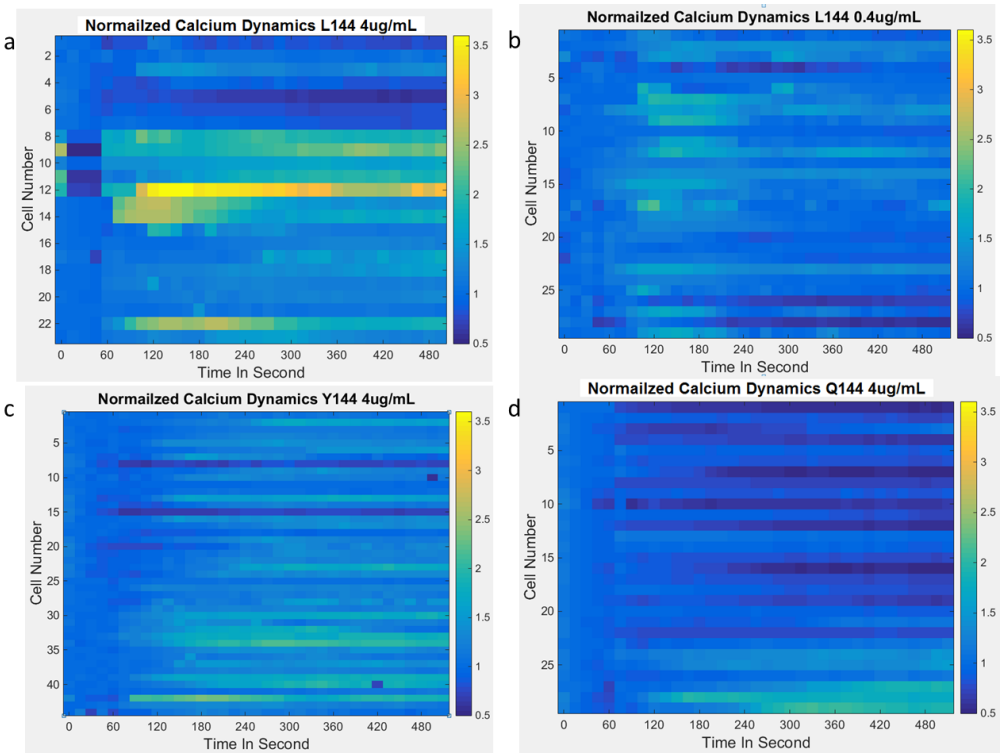

Appendix Figure B-4 Low calcium response without experimental temperature control

T cells in response to peptide antigen of various avidity presented on DAS cells, when experiments were conducted at room temperature without temperature control. The calcium responses were tepid even in response to the most potent peptide antigen L144 at high concentration of 4 μg/mL. Each row presents a single T cell's calcium signaling dynamics, which is normalized to pre-contact average with color bar indicating the normalized value. (a) L144 4 μg/mL; (b) L144 0.4 μg/mL; (c) Y144 4 μg/mL; (d) Q144 4 μg/mL.

With effect of temperature on lymphocyte signaling in literature (84, 231), it was suspected the general low response and large variation in the preliminary results was due to temperature (Appendix Figure B-4). In order to test this idea, a 12 wells plate experiment

a

b

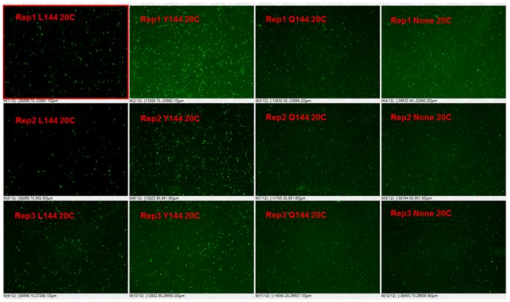

c

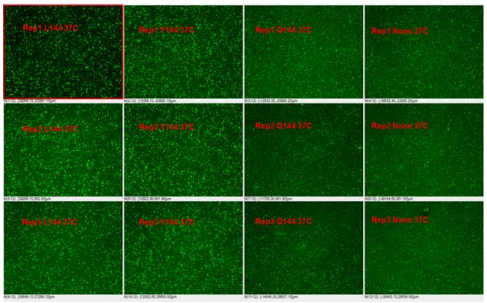

d

Treatment	Count	Total Area	Average Size	%Area	Mean
L144	1438	69508	48.34	4.8	1310.22
Y144	1777	74377	41.86	5.14	1468.81
Q144	892	13542	15.18	0.94	1337.69
No peptide	430	7073	16.45	0.49	1306.40

Appendix Figure B-5 The 12-well plate experiment for temperature effect on calcium dynamics

(a) Peptide antigens incubation layout for 12 well plate experiment. Imaging of calcium intensity of T cells at 4x magnification for plate (b) at room temperature (c) at 37 C. (d) Image analysis using imageJ. Threshold was automatically chosen to segment cells in plate image, table lists number of cells (Count), total area of counted cells (Total Area), size of cells (Average Size), percentage of cells in plate (% Area) and mean intensity (Mean).

was designed (Appendix Figure B-5). Two glass-bottom 12 well plates were used to seed and grow DAS cells into confluency. Peptide antigens of various avidities were incubated with DAS cells the same way described earlier in method's section. Without realizing effect of temperature on T cell signaling, the preliminary experiments were done without temperature control at room temperature (Appendix Figure B-4), which was contrast to results obtained after temperature control (Figure 4-1).

Appendix B.3.2 EDTA Cell Dissociation Method Does not Alter Calcium Signaling of T Cells Compared to Trypsin

a

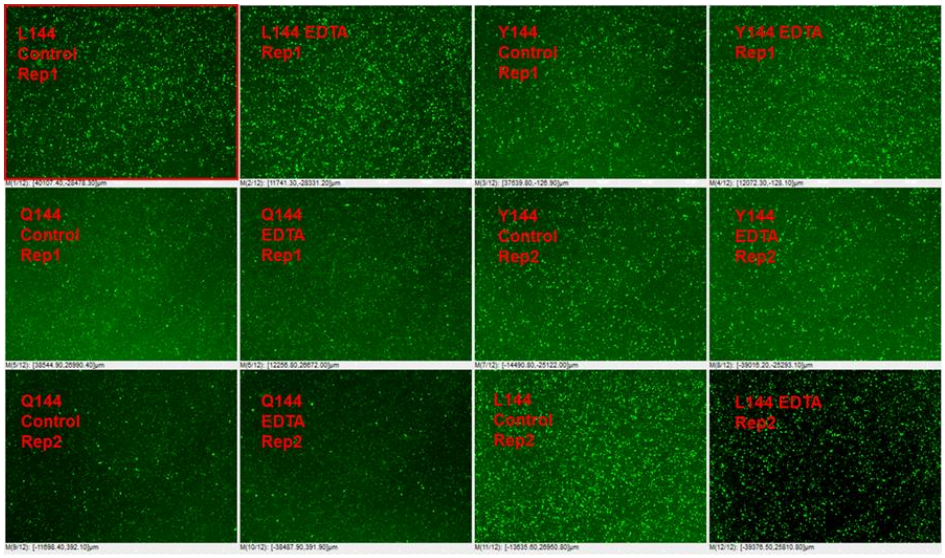

Appendix Figure B-6 Effect of EDTA on calcium dynamics

Calcium signaling in 1B6 T cells in response to peptide antigens of various avidities presented by DAS cells dissociated with EDTA versus DAS cells not dissociated. The plate was imaged at 4X magnification.

Adherent cells were usually dissociated from culture plate using trypsin. However, the enzymatic dissociation may affect the presenting of antigen on MHC complex. Especially, because trypsin's cleavage site is at the amino acid bond right after lysine, which was at the center of peptide antigens used in this study. To rule out the possibility of interference with antigen presenting, an alternative method was adopted to dissociate antigen presenting cells from culturing flask. In order to access the effect of this alternative method, a 12 well plate experiment was designed to compare calcium response of T cells in contact with EDTA dissociated DAS cells to that of non-dissociated DAS cells. The

result from EDTA dissociated DAS cells were equivalent to that of non-dissociated counterpart.

Appendix B.3.3 Effect of Dye Loading Media on Calcium Signaling of T Cells

a

b

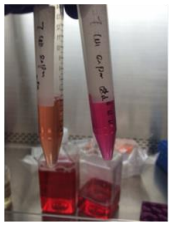

c

Media or Buffer	Description	pH value
T cell expansion media	Old, opened Dec. 2015	7.98
T cell expansion media	Fresh, opened 2/16/2016	7.24
White RPMI media	Made on 2/12/2016	7.53
RPMI base buffer	Opened on 2/12/2016	7.6
RPMI base buffer	Opened on 2/6/2016	7.8
PBS	Made on 2/2/2016	7.4
HBSS+	Hyclone, Exp Sep. 14, LOT: AXJ44035	7.95
HBSS-	Hyclone, Exp Dec. 15, LOT: AYM175561	7.7
HBSS-	Cellgro, Exp March. 18, LOT: 21022150	7.5
HBSS-	Cellgro, Exp March. 18, LOT: 21022150, open 2/3/15	8.0

Appendix Figure B-7 The aging of buffer caused drift of pH value

(a) Two bottles of commercial T cell expansion media opened within two-month range. (b) The color of old media on the right changed during this period, indicating pH drift. (c) Result of pH measurement of various media and buffer.

It was noticed that the choice of dye loading media also affected calcium signaling in T cells. After testing different choices of dye loading media, it was suspected the change of media pH might have a substantial impact on cell signaling, which tended to be ignored. Once a new media bottle was opened, the exposure of media to air and aging of the media caused drift of pH among other factors. Appendix Figure B-7 showed example of such change, included were buffer commonly used for experiments. Due to this reason, the use

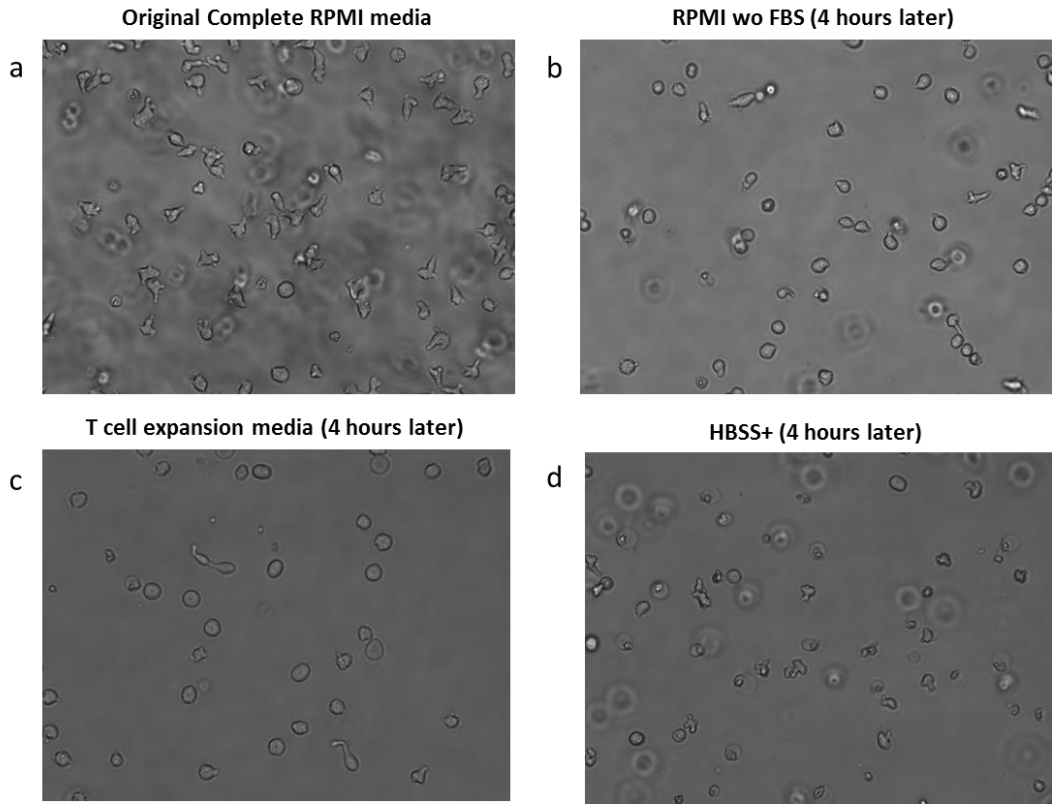

Appendix Figure B-8 The effect of dye loading media on cells

(a) Complete RPMI media. (b) RPMI 1640 buffer without any supplement. (c) Commercial T cell expansion media. (d) HBSS+.

of commercial T cell expansion media was abandoned, and regular RPMI media was used for cell culture in Chapter 3. Caution should be taken in choice of loading media.

Despite the effect of aging on pH, the aging of active ingredient in media or buffer may also have important implications on physiology of cells. In Appendix Figure B-8, 1B6 T cells originally cultured in the same flask were sub-cultured in various kinds of cell media or buffer. Generally, cells maintained the best quality in fresh growth media, with decaying viability and fitness in the order of fresh complete RPMI media > old complete RPMI

media > RPMI base buffer without FBS > HBSS+ > HBSS- = PBS. The exact reason was beyond this test, except FBS and calcium were important factors in maintaining cell physiology during incubation.

APPENDIX B.4 Reference Images of Cells

Appendix B.4.1 Benchmark Images for Healthy Cells

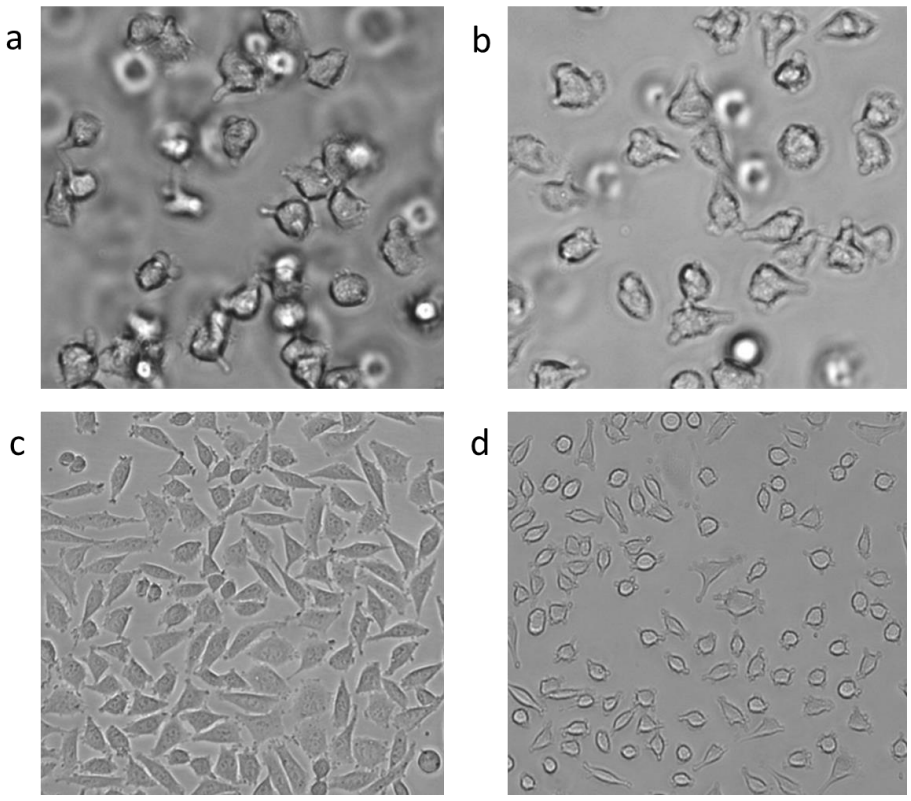

Appendix Figure B-9 Benchmark images for healthy cells

(a and b) Morphology of healthy 1B6 T cells at 20x magnification. Cells with surface protrusion extended from round, plump cell bodies. (c and d) DAS cells were grown into 80% confluency on surface of culture flask. Cells were spread out with tentacles touching each other.

Appendix B.4.2 Impact of Seeding Density on Growth of 1B6 T cells

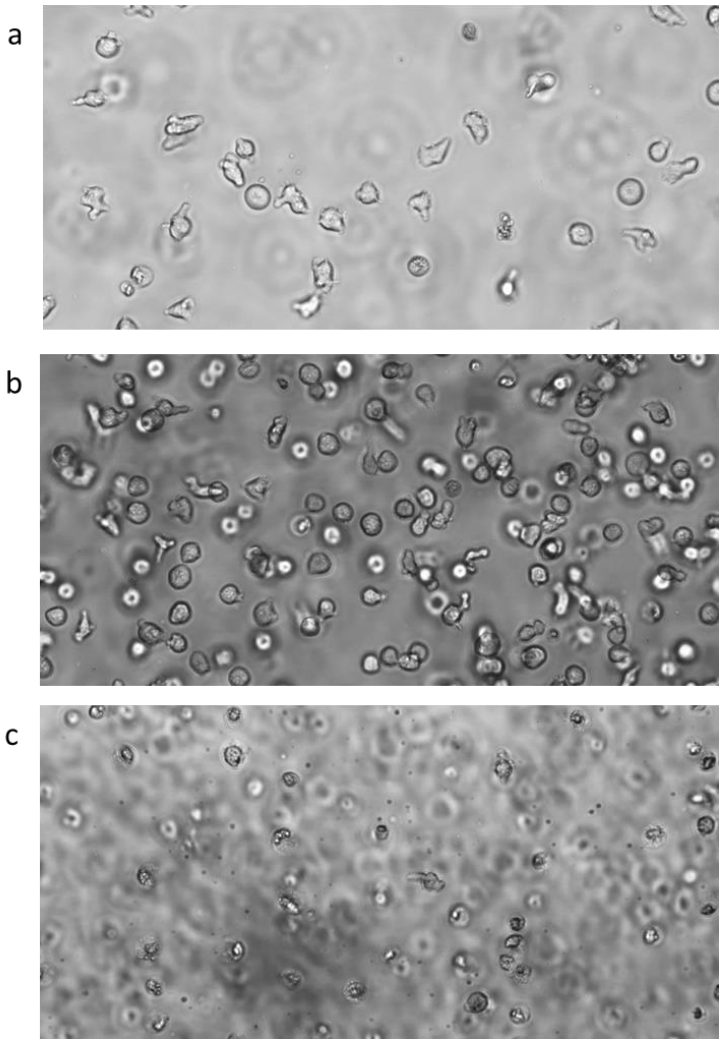

Appendix Figure B-10 Impact of Seeding Density on T cell growth

1B6 T cells were seeded at (a) 0.06 million/mL, (b) 0.08 million/mL and (c) 0.2 million/mL respectively were allowed to grow for 3 days. Notice (a) resulted in sparsely grown T cells, (b) resulted in T cells in good density with healthy morphology, (c) resulted in death of T cells characterized by small debris of T cells and cells undergoing apoptosis. Due to the difficulty in control T cell growth, instead of a 3-day culture: T cells were generally seeded around 0.1 million/mL in 5mL fresh media, allowed to grow for 2 days, and then diluted with 5mL of fresh media for a third day culture or counted to seeded at 0.2 million/mL for next day's experiment.

Appendix B.4.3 The Deterioration of T Cell Quality at Room Temperature and CO_2 level

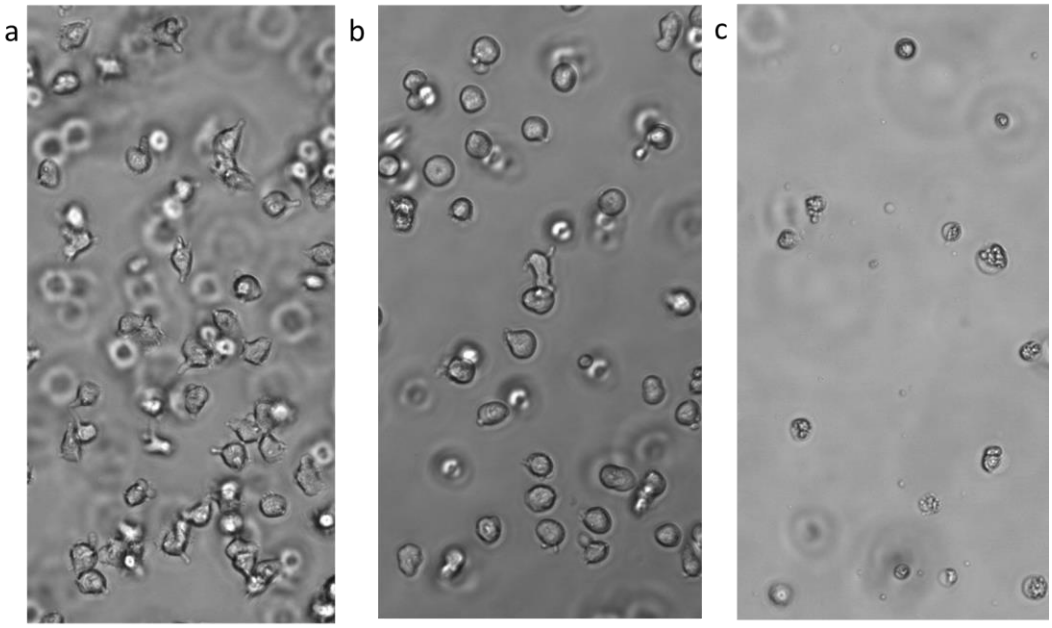

Appendix Figure B-11 Deterioration of T cell quality

(a) Healthy cells: plump cell body with protrusions. (b) Cells when left at room temperature for 30 minutes: cells started to round up and lose protrusions. (c) Cells were left for prolonged time at room temperature: cells undergoing apoptosis.

APPENDIX C SUPPLEMENTAL MATERIAL FOR CHAPTER 4

APPENDIX C.1 Experimental Condition Optimization

Appendix C.1.1 The Test on Alternative Calcium Dye

a

	Column1	Column2	Column3
Row1	Calcium Crimson 10uM	Fluo-4 2uM	Calcium Orange 10uM
	MitoTracker Green 720nM	MitoTracker Red 460nM	MitoTracker Green 720nM
Row2	Calcium Crimson 5uM	Fluo-4 2uM	Calcium Orange 5uM
	MitoTracker Green 360nM	MitoTracker Red 230nM	MitoTracker Green 360nM
Row3	Calcium Crimson 2uM	Fluo-4 2uM	Calcium Orange 2uM
	MitoTracker Green 180nM	MitoTracker Red 115nM	MitoTracker Green 180nM

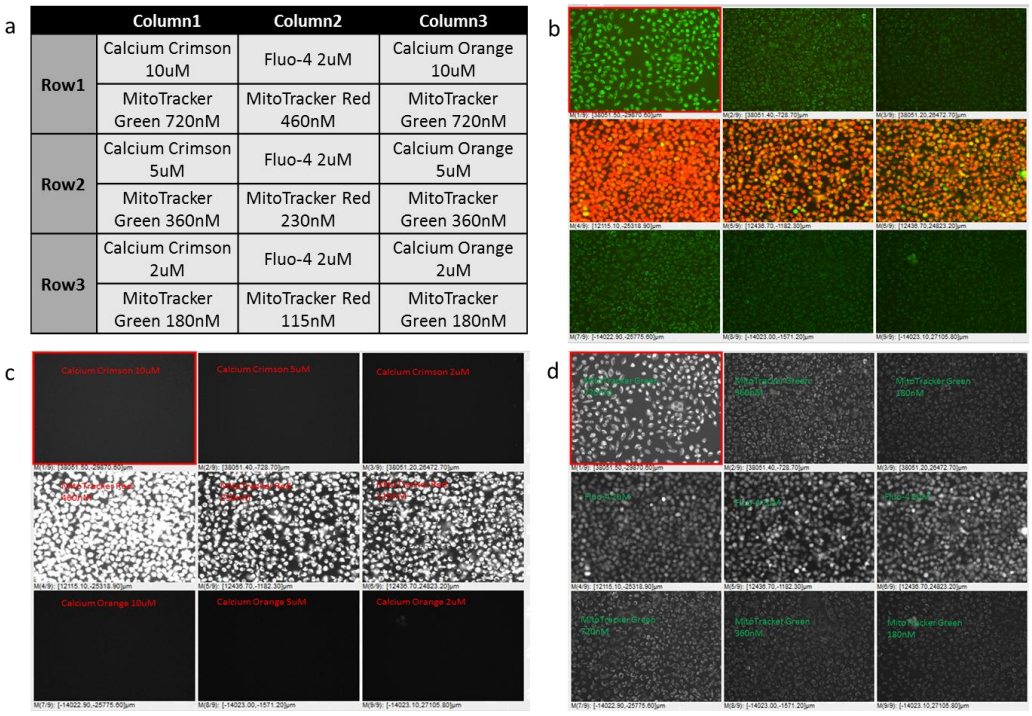

Appendix Figure C-1 12-well plate experiment on choices of calcium and mitochondria dye

Notice in b, c, d rows were transposed to columns from a. (a) Layout for 12 well plate experiments. Imaging at 4x using (b) both channels (c) TRITC channel (d) FITC channel.

In order to visualize both signaling processes (calcium and mitochondria) in both cell types (antigen presenting cells and T cells), multiple dye choices for calcium were tested (Appendix Figure C-1). Calcium Orange and Calcium Crimson were tested, however they proved to be not effective on calcium signaling monitoring because they were much dimmer than MitoTracker Red and Fluo-4, making multiplexing with other dye

impractical. On the other hand, MitoTracker Green had similar intensity compared to MitoTracker Red and Fluo-4.

Appendix C.1.2 Binned Image Maintained the Information Contained in Original Image

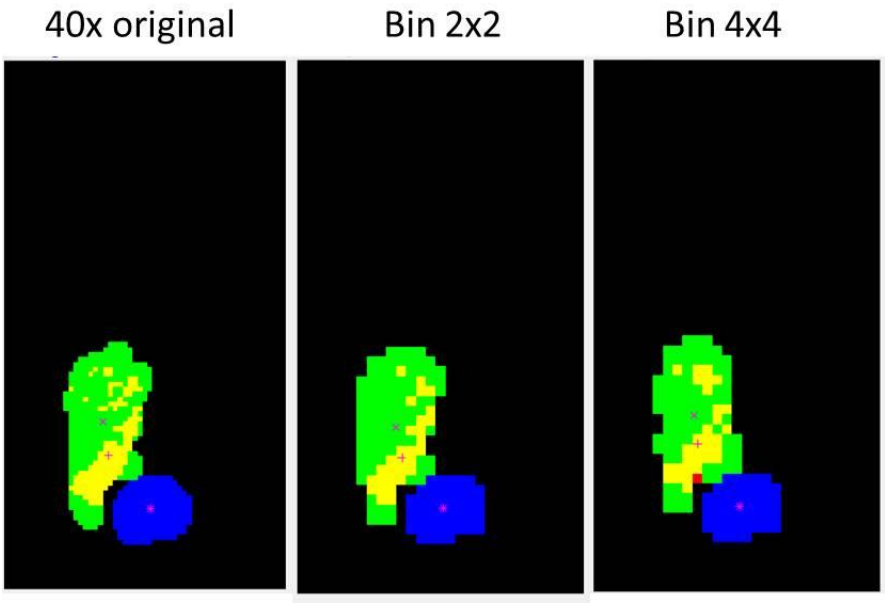

Appendix Figure C-2 Binned image maintained the information contained in the original image

(Left panel) Cells imaged at 40x magnification. (Middle panel) the 40x image was binned 2x2. (Right panel) the 40x image was binned 4x4. T cell calcium (green), mitochondria (red) and APC nucleus (blue) are shown. Plus, cross, asterisks are centroids of T cell calcium, mitochondria and APC nucleus, respectively.

APPENDIX C.2 Possible Digital Calcium Response Model to Peptide Antigen Potency

The temperature dependency of calcium signaling suggests existence of a kinetic barrier in this process that needs to be overcome by thermal energy. However, it requires future confirmation whether TCR-pMHC interaction or downstream calcium signaling cascades is the rate limiting step. Also, the digital response of T cells to various avidities of antigen suggests a different recognition model for TCR-pMHC interaction: each TCR-pMHC interaction may have multiple equilibrium states including pro-signaling states and anti-signaling states; the relative thermodynamic landscape of all equilibrium states determines distribution of T cell population into different response types; cells falling into pro-signaling state become high responder and cells falling into anti-signaling state become low or none responders.

For example, TCR-L144-MHC's pro-signaling states have lower Gibbs free energy thus more thermodynamically favorable compared to its anti-signaling states, resulting most of cells fall into high responder's group. However, TCR-Y144-MHC possesses both pro-signaling and anti-signaling states that were equally thermodynamically favorable, resulting only half of the population in high-responder group. In N or Q group, the anti-signaling states are more thermodynamically favorable, resulting most cells in non-respnoder or lower responder group. If this model is valid, then it is possible to calculate the Gibbs free energy difference of pro-signaling states versus anti-signaling states from the percentage of T cells falling into each response category. In addition, this hypothesis is consistent with my results of antigen concentration on calcium signaling, as the concentration of antigen wouldn't change the thermodynamic landscape of TCR-pMHC

interaction states, so most cells still fall into high responder despite lower L144 concentration. Also, as less pMHC presented on APCs will decrease the chance of TCR-pMHC interaction, an equal distribution between low and high concentration indicates the rate limiting step is in transition of TCR-pMHC into combination state rather than colliding of TCR with pMHC.

APPENDIX C.3 Univariate Methods to Interpret Calcium Mitochondria Interaction Data

Appendix C.3.1 Explanatory Visualization of Calcium-Mitochondria Interaction on Selected Cells

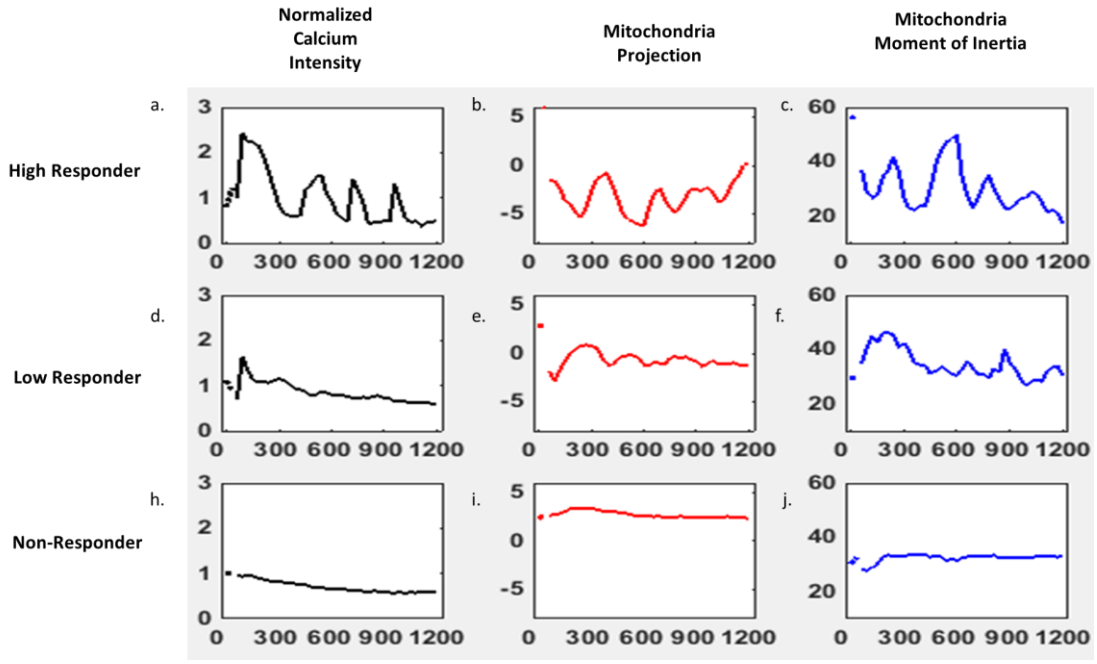

Appendix Figure C-3 Analysis of calcium mitochondria interaction on representative cells

Normalized calcium intensity, *mitochondria net projection*, *mitochondria moment of inertia* of (a to c) selected high responder cell. (d to f) selected low responder cell. (h to j) selected non-responder cell. In all cells, (a, d, h) left column showed *normalized calcium intensity*, (b, e, i) middle column showed *mitochondria net projection*, and (c, f, j) right column showed *mitochondria moment of inertia*. Y axis is the unit of respective metric, X axis is time in seconds.

Appendix Figure C-3 showed results of three representative T cells subject to L144, with each row being a different cell and each column a different metric. The three T cells were selected from three different response types classified based on calcium *peak*

foldchange. These examples suggested a correlation between calcium dynamics and mitochondria activity. However, Appendix Figure C-3 showed only 3 T cells, each from a different response type (high responder, low responder and non-responder). In order to test whether this trend could be generalized to all cells, this analysis was applied to all cells in study of calcium and mitochondria interaction, which were subjected to peptide antigens of all 4 different potencies.

Appendix C.3.2 Univariate Analysis Based on Average of Time Series Data was Not Able to Interpret Calcium-Mitochondria Dynamics

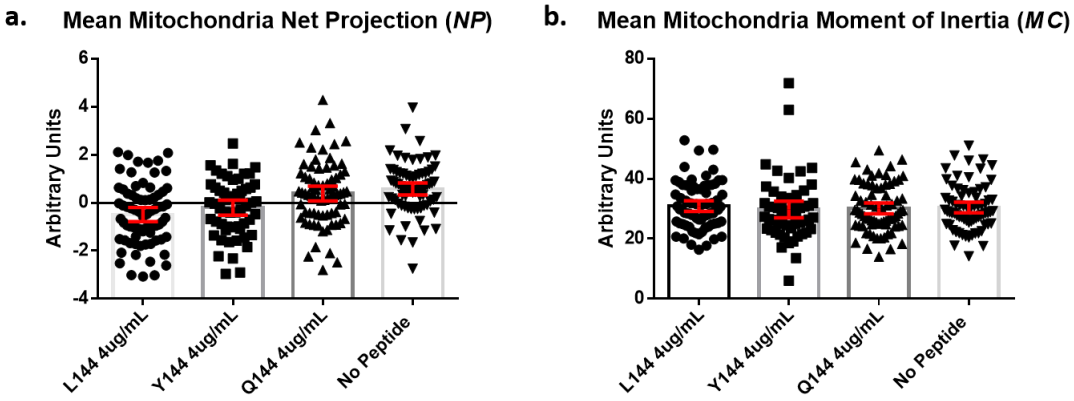

Appendix Figure C-4 Univariate analysis is not sufficient to interpret calcium-mitochondria dynamics

Time series values of (a) *NP* and (b) *MC* were averaged over the entire imaging course for each cell. The averaged value of time series measurements could not distinguish the condition cells are subject to.

Appendix C.3.3 Regression Analysis Based on Average of Time Series Data was Not Able to Interpret Calcium-Mitochondria Dynamics

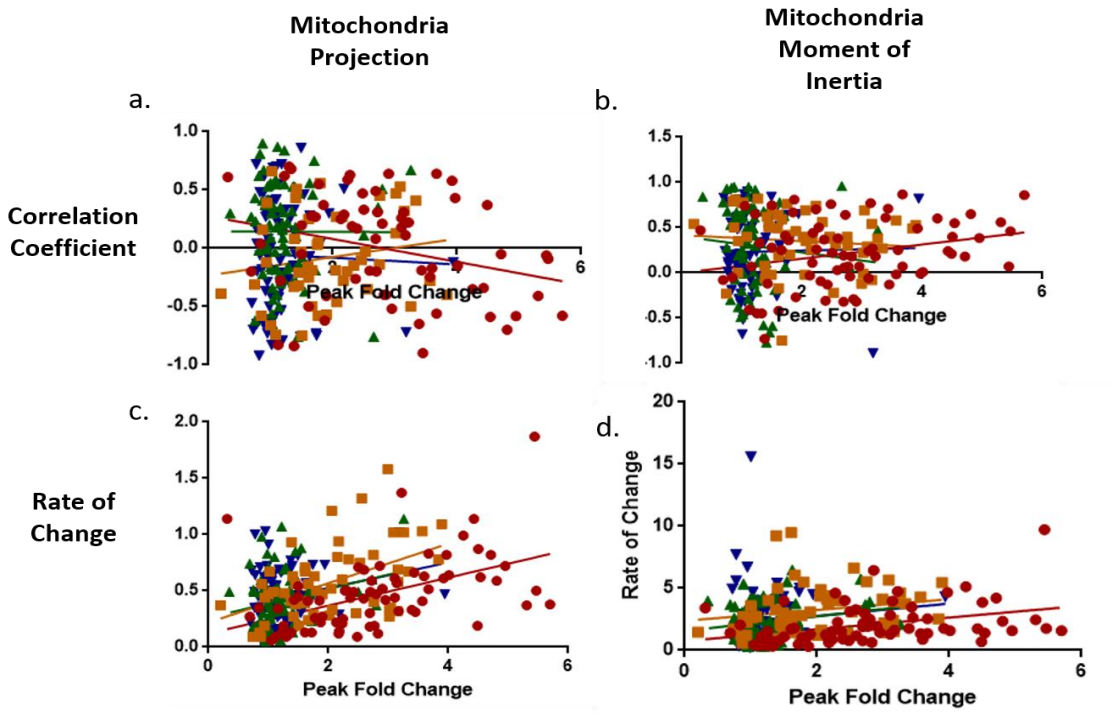

Appendix Figure C-5 Regression analysis based on time average failed to distinguish effect of antigen potency on calcium-mitochondria interaction

L144 (Red), Y144 (Yellow), Q144 (Green), No peptide (Blue). (a) Calcium peak fold intensity versus Pearson correlation coefficient between *Mitochondria net projection* (*NP*) and *Normalized Calcium Intensity* (NC). (b) Calcium peak fold intensity versus Pearson correlation coefficient between *Mitochondria Moment of Inertia* (*MC*) and *Normalized Calcium Intensity* (NC). (c) Calcium peak fold intensity versus the first derivative of *Mitochondria net projection* (*NP*) over time. (d) Calcium peak fold intensity versus the first derivative of *Mitochondria Moment of Inertia* (*MC*) over time.

APPENDIX C.4 Partial Least Square Regression Model

Appendix C.4.1 Partial Least Square Variable Table

Appendix Table C-1 MVDA variable table

MC	Mitochondria Moment of Inertia calculated on Calcium Centroid
MM	Mitochondria Moment of Inertia calculated on Mitochondria Centroid
AP	Mitochondria Absolute Projection
NP	Mitochondria Net Projection
PR	Mitochondria Projection Ratio
IR	Mitochondria Intensity Ratio

Appendix C.4.2 Initial Partial Least Square Model including All Metrics

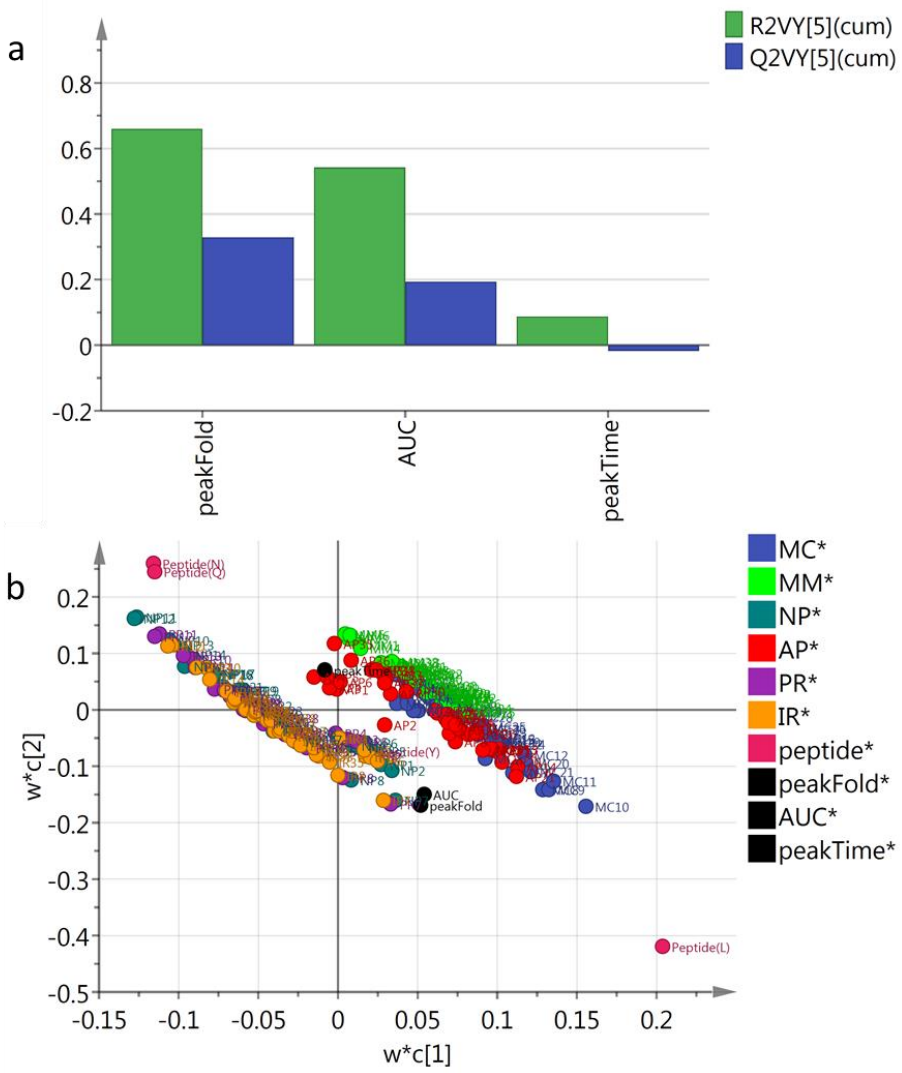

Appendix Figure C-6 Initial partial least square model including all metrics

(a) *PeakFold* and AUC were well modeled, while *peakTime* was not in the initial model. (b) Initial model containing all metrics showed *AP*, *PR*, *IR* were collinear with each other, while *MC*, *MM* and *AP* were correlated with each other.

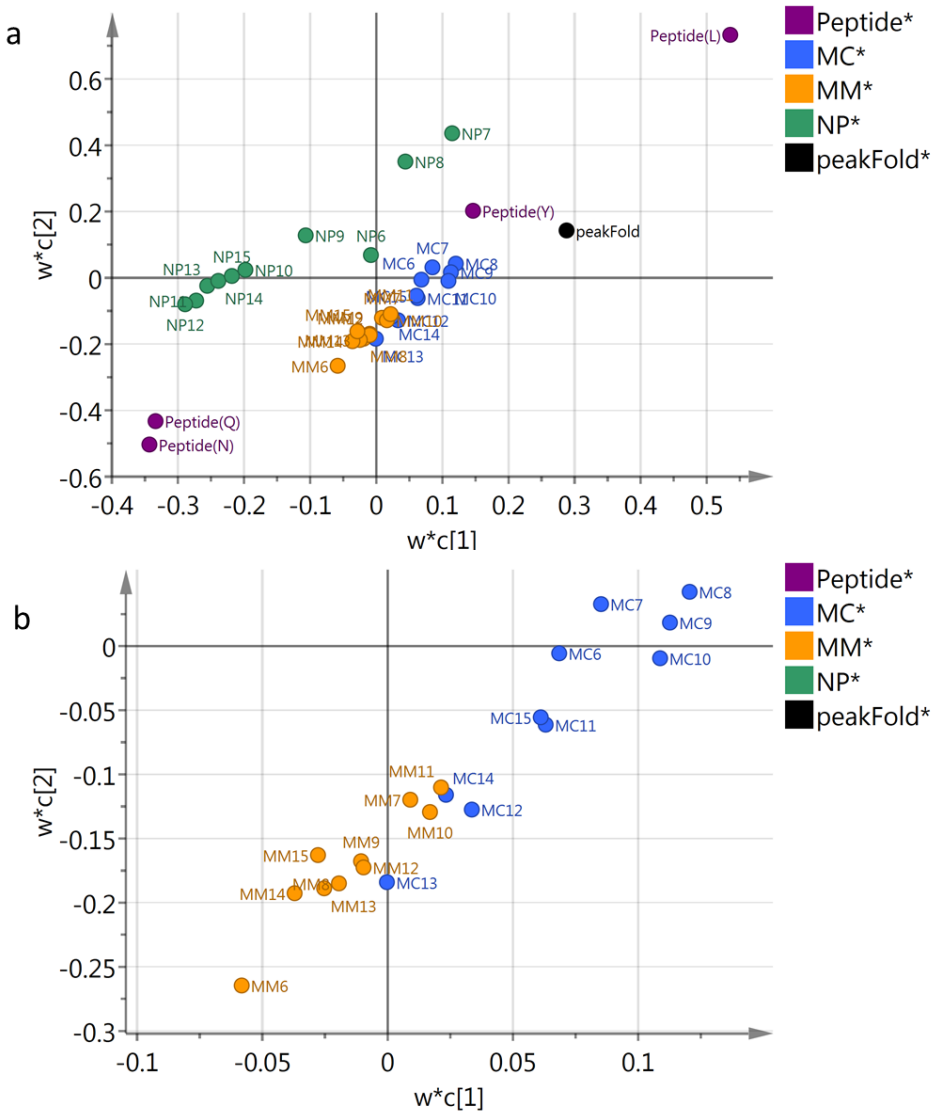

Appendix Figure C-7 Partial least square model including *MM*

(a) Weight plot including metrics of *MC*, *MM*, *NP* from time frame 6 to 15. (b) Zoom in of weight plot showed *MC* and *MM* revealed different information on movement of mitochondria (not collinear with each other).

APPENDIX D **MATLAB CODE**

APPENDIX D.1 Calcium Signalling Analysis

Appendix D.1.1 Automate Image Analysis of Multiple Video Files

```
%Luye He
%Last Edited: June 11th, 2017
%MultiLocationAnalysisScript_V2_2H

%Description:
    %The central script to run for cell tracking and information
extraction
    %on multiple field of view
    %specify parameters and assembly results for image analysis
    %Call on function "CellTracking.m" for image analysis of each field
%of view

%%%%%%%%%%%%%% Specify parameter to pass into "CellTracking"
%%%%%%%%%%%%%%
Threshold=400;
pixelarearangeT = [30 2500];                %Range of pixel area values
of T cells, used below with bwareafilt
preContactTime=2; %precontact timing in minutes
NbImages=41;    %Number of frames
ImagInterval=15;    %Imaging interval in seconds
TickSpac=floor(60/ImagInterval); %Specify the interval on image
ColorChannel=1;     %T cells' color channel in the video
AllLocations=[1 2 3 4]; %specify all the field of views to be analyzed
NbLocations=length(AllLocations);    %number of ROI recorded
OriginString='20160411_test3_y_d1c1&3%sxy%sc%s%s';     %allow modify of
string of all images in a given .tiff stack
numAvgColumn=preContactTime*floor(60/ImagInterval);    %round to lower
integer

%%%%%%%%%%%%%%Initiate variables to contain "CellTracking" results

%construct empty cells for all output from the called function later
level0List=zeros(1,NbLocations);
EMList=zeros(1,NbLocations);
thresholdList=zeros(1,NbLocations);
levelList=zeros(1,NbLocations);
ComboSet = cell(1,NbLocations);     %the record of all prompted images
for user interactive picking cells
LookUpMatrixSet = cell(1,NbLocations);  %the record of tracking of all
cells identities
CompleteLookUpMatrixSet = cell(1,NbLocations);  %the record of tracking
of only ever-existing cells identities
CompleteMeanIntensitySet = cell(1,NbLocations);     %the record of
tracking of mean intensity data of all cells
CompleteAdjustedMeanIntensitySet = cell(1,NbLocations); %the record of
tracking of relative intensity data normalized to the first few frames
as specified by user
CompleteTotalIntensitySet = cell(1,NbLocations);
```

```
CompleteAreaSet = cell(1,NbLocations);
CompleteBackgroundSet = cell(1,NbLocations);
CompleteNormalizedMeanIntensitySet = cell(1,NbLocations);
CompleteNormalizedAdjustedMeanIntensitySet = cell(1,NbLocations);
CompleteNormalizedTotalIntensitySet = cell(1,NbLocations);
CompleteNormalizedAreaSet = cell(1,NbLocations);
CompleteNormalizedBackgroundSet = cell(1,NbLocations);

%DivideLine = zeros(1,NbImages);

%constract empty matrix for combining correspoding information from all
field of views
AllLookUpMatrix = [];   %cell identity
AllCompleteLookUpMatrix = [];   %cell identity, only those ones that
ever exist
AllMeanIntensity = [];  %mean intensity
AllAdjustedMeanIntensity = [];  %normalized intensity
AllTotalIntensity = [];
AllArea = [];
AllBackground = [];
AllNormalizedMeanIntensity = [];
AllNormalizedAdjustedMeanIntensity = [];
AllNormalizedTotalIntensity = [];
AllNormalizedArea = [];
AllNormalizedBackground = [];


%%%%%%%%%%%%%%%%%%%%%%%%call function "CellTracking_V2_2D.m" as many
times as number of field of
%views

for Location=AllLocations
    InputString = sprintf(OriginString,'%s','%d','%d','%s');
    [ComboSet{Location}, LookUpMatrixSet{Location},
CompleteLookUpMatrixSet{Location},...

CompleteMeanIntensitySet{Location},CompleteAdjustedMeanIntensitySet{Loc
ation},CompleteTotalIntensitySet{Location},CompleteAreaSet{Location},Co
mpleteBackgroundSet{Location},...

CompleteNormalizedMeanIntensitySet{Location},CompleteNormalizedAdjusted
MeanIntensitySet{Location},CompleteNormalizedTotalIntensitySet{Location
},CompleteNormalizedAreaSet{Location},CompleteNormalizedBackgroundSet{L
ocation}]...
        =
CellTracking_V2_2H(Threshold,pixelarearangeT,InputString,NbImages,numAv
gColumn,ColorChannel,Location);
    AllLookUpMatrix = [AllLookUpMatrix;LookUpMatrixSet{Location}];
    AllCompleteLookUpMatrix =
[AllCompleteLookUpMatrix;CompleteLookUpMatrixSet{Location}];
    AllMeanIntensity =
[AllMeanIntensity;CompleteMeanIntensitySet{Location}];
    AllAdjustedMeanIntensity =
[AllAdjustedMeanIntensity;CompleteAdjustedMeanIntensitySet{Location}];
    AllTotalIntensity =
[AllTotalIntensity;CompleteTotalIntensitySet{Location}];
```

```
    AllArea = [AllArea;CompleteAreaSet{Location}];
    AllBackground = [AllBackground;CompleteBackgroundSet{Location}];
    AllNormalizedMeanIntensity =
[AllNormalizedMeanIntensity;CompleteNormalizedMeanIntensitySet{Location
}];
    AllNormalizedAdjustedMeanIntensity =
[AllNormalizedAdjustedMeanIntensity;CompleteNormalizedAdjustedMeanInten
sitySet{Location}];
    AllNormalizedTotalIntensity =
[AllNormalizedTotalIntensity;CompleteNormalizedTotalIntensitySet{Locati
on}];
    AllNormalizedArea =
[AllNormalizedArea;CompleteNormalizedAreaSet{Location}];
    AllNormalizedBackground =
[AllNormalizedBackground;CompleteNormalizedBackgroundSet{Location}];


end

%%%%%%%%%%%%%%%%%%% save output and visualizaiton %%%%%%%%%%%%%%%%%%
%generate file name for analysis record
FilenameString =
sprintf(OriginString,'',mat2str(AllLocations),num2str(ColorChannel),'')
;     %Indicate what filename you would like the save the results as:
Filename = [FilenameString,datestr(now,30),'.mat'];

%save file
save(Filename)

%generate tick on x axis of following figures
timeTick = 1:TickSpac:NbImages;
timeLabel = (timeTick-1)*ImagInterval;
timeSeries = linspace(0,(NbImages-1)*ImagInterval,NbImages);
NumTotalCells = size(AllNormalizedArea,1);

%generate figures for raw and relative intensity data
figure
imagesc(AllNormalizedMeanIntensity)
ax = gca;
ax.XTick = timeTick;
ax.XTickLabel = timeLabel;
xlabel('Time In Second')
ylabel('Cell Number')
title(['Normalized Mean Intensity',FilenameString])

figure
imagesc(AllNormalizedAdjustedMeanIntensity)
ax = gca;
ax.XTick = timeTick;
ax.XTickLabel = timeLabel;
xlabel('Time In Second')
ylabel('Cell Number')
title(['Normalized Adjusted Mean Intensity',FilenameString])

figure
```

```
imagesc(AllNormalizedTotalIntensity)
ax = gca;
ax.XTick = timeTick;
ax.XTickLabel = timeLabel;
xlabel('Time In Second')
ylabel('Cell Number')
title(['Normalized Total Intensity',FilenameString])
%colormap(jet)

figure;
for i = 1:size(AllNormalizedArea,1)
    plot(timeSeries,AllNormalizedArea(i,:));
    hold on;
end
ax = gca;
ax.XTick = timeLabel;
title(['Normalized Cell Size',FilenameString]);

figure;
for i = 1:size(AllNormalizedBackground,1)
    plot(timeSeries,AllNormalizedBackground(i,:));
    hold on;
end
ax = gca;
ax.XTick = timeLabel;
title(['Normalized Background',FilenameString]);
```

Appendix D.1.2 Cell Track Algorithm

```
%Luye He
%Last Edited: June 11th, 2017
%Based on CellTracking_V2_2H

%Description:
    %functions for tracking and extract cell signaling inforamtion in
time
    %series images at a given field of view
    %called by Multi_FieldofView_Analysis.m
%Features:
    %Use constant threshholding for all frames of a video instead of
changing
    %threshholding.
    %Use total intensity vs. average intensity.
    %Perform background subtraction.
    %Allow user input in choosing which cells to be analyzed
    %Allow user input in choosing how much distance cells relocated
during
    %squeezing operation
    %Allow easy identify of T cells that pair up with DAS cells
    %Normalized to first several frames as "numAvgColumn"
    %Flexible in applying to tens or hundreds of images

function [Combo, LookUpMatrix,
CompleteLookUpMatrix,CompleteMeanIntensity,CompleteAdjustedMeanIntensit
y,CompleteTotalIntensity,CompleteArea,CompleteBackground,...

CompleteNormalizedMeanIntensity,CompleteNormalizedAdjustedMeanIntensity
,CompleteNormalizedTotalIntensity,CompleteNormalizedArea,CompleteNormal
izedBackground]...
    = CellTracking(Threshold,pixelarearangeT,
InputString,NbImages,numAvgColumn,ColorChannel,Location)

%Specify filename to be saved in
FilenameString = sprintf(InputString,'',Location,ColorChannel,'');
Filename = [FilenameString,datestr(now,30),'.mat'];

if exist('NbImages', 'var')
    %Construct empty cells
    Im = cell(1,NbImages);                      %cell array for T cell
images
    ImL = cell(1,NbImages);                     %cell array for T cell
label images
    NumBlob = zeros(1,NbImages);                %vector for blob number
of each T cell image

    %read from images if less than 100 images exist in stack
if NbImages>9 && NbImages<100
    %Generate image name to be read
    FNAMEFMT1 =
sprintf(InputString,'t0%d',Location,ColorChannel,'.tif');   %T cell
image string, change these to reflect tif images from nd export
```

```
    FNAMEFMT2 =
sprintf(InputString,'t%d',Location,ColorChannel,'.tif');
    for i=1:9
      Im{i} = imread(sprintf(FNAMEFMT1,i));          %Fluorescent
images
    end
    for i = 10:NbImages
      Im{i} = imread(sprintf(FNAMEFMT2,i));
    end

    %read from images if more than 100 images exist in stack
elseif NbImages>=100
    FNAMEFMT1 =
sprintf(InputString,'t00%d',Location,ColorChannel,'.tif');      %Change
these to reflect tif images from nd export
    FNAMEFMT2 =
sprintf(InputString,'t0%d',Location,ColorChannel,'.tif');
    FNAMEFMT3 =
sprintf(InputString,'t%d',Location,ColorChannel,'.tif');
    for i=1:9
      Im{i} = imread(sprintf(FNAMEFMT1,i));          %Fluorescent
images
    end
    for i = 10:99
      Im{i} = imread(sprintf(FNAMEFMT2,i));
    end
    for i = 100:NbImages
      Im{i} = imread(sprintf(FNAMEFMT3,i));
    end

end

level=double(Threshold)/2^16; %important to convert to double,
otherwise give 0.

%Display surface plot of the first frame
figure;
t=surf(Im{1});
set(t,'LineStyle','none');
caxis([0,16383]);
zlim([0 16383]);
title(sprintf(InputString,' t1_Tcell_Processing
',Location,ColorChannel));

%Initiate important features
MeanIntensity = cell(1,NbImages);
Area = cell(1,NbImages);
BoundingBox = cell(1,NbImages);
BackGround = cell(1,NbImages);
AdjustedMeanIntensity = cell(1,NbImages);
TotalIntensity = cell(1,NbImages);

%%%%%%%%%%%%%%%%%%%%%%Image analysis for each frame
%%%%%%%%%%%%%%%%%%%%%%
for ii=1:NbImages
    %Raw image processing
```

```
    bw = im2bw(Im{ii},level);   %Convert to binary image
    bwclearborder = imclearborder(bw);  %clear any objects on the
border of image
    bwclear = bwareafilt(bwclearborder,pixelarearangeT);    %Remove
spots not in pixelrange
    [L, num] = bwlabel(bwclear);    %Label the connected components,
num returns the number of connected components, L the label matrix
    ImL{ii} = L;    %use the label image as mask
    NumBlob(ii) = num;  %how many cells in each image

    %Extract information from the original image using label image as
mask
    stats = regionprops(L,Im{ii},'MeanIntensity','Area','BoundingBox');
%extract certain property in images
    MeanIntensity{1,ii} = extractfield(stats,'MeanIntensity')';   %This
takes the values from the structure and makes a vector
    BoundingBox{1,ii} = extractfield(stats,'BoundingBox')';
    Area{1,ii} = extractfield(stats,'Area')';

    %Define bounding box for background calculation
    for i = 0:num-1
        j = i*4+1; %Bounding box has 4 values for every object: 1. x
coordinate 2. y coordinate 3. x width 4. y width
        ycoord(i+1) = round(BoundingBox{1,ii}(j+1));   %Find the y
value for all bounding boxes
        xcoord(i+1) = round(BoundingBox{1,ii}(j));     %Find the x
value for all bounding boxes
        if ycoord(i+1)-20 > 0 && xcoord(i+1)+20 < size(Im{1},2)
            BackGround{1,ii} =
[BackGround{1,ii};mean(mean(Im{ii}(ycoord(i+1)-
20:ycoord(i+1),xcoord(i+1):xcoord(i+1)+20)))]; %Take the average of
pixel intensities from the top left, a 3x3 pixel square
        else
            BackGround{1,ii} = [BackGround{1,ii};0];    %assign 0 while
the background is not available, may cause error in future
        end
    end
    AdjustedMeanIntensity{1,ii}= MeanIntensity{1,ii} -
BackGround{1,ii};
    TotalIntensity{1,ii} = AdjustedMeanIntensity{1,ii}.*Area{1,ii};

    %Display the first
    if ii==1    %if this is the first frame
        %analyze the cell size distribution in the first frame
        Area_1 = regionprops(bw,'Area');
        Area_1e = extractfield(Area_1,'Area');

%Uncomment this section if want to check image pre-processing
%         figure;
%
title(sprintf(InputString,'FirstFrameProcessing',ColorChannel,Location)
)
%         subplot(2,3,1)
%         imshow(Im{1})
%         title('Grayscale Image')
%         subplot(2,3,2)
```

```
%         imshow(Imadjust)
%         title('Grayscale Image Adjusted')
%         subplot(2,3,3)
%         imshow(bw)
%         title('Raw Binary Image')
%         subplot(2,3,4)
%         imshow(bwclearborder)
%         title('Binary Image with Clear Borders')
%         subplot(2,3,5)
%         imshow(bwclear)
%         title('Binary Image with Sizes Filtered')
%         subplot(2,3,6)
%         imshow(L)
%         title('Label Image')
%         hold on;

        %Find locations of cell positions in first frame for later
generating interactive image for user input in choosing cells to be
        %analyzed
        stats_ImL1 = regionprops(L,L,'MeanIntensity','Centroid');
%Extract values from label image of the 1st frame
        Cell_List = extractfield(stats_ImL1,'MeanIntensity')';
%Values for corresponding blobs in the label image
        Centroid_List = extractfield(stats_ImL1,'Centroid')';
%Values for define labelling circle position
        reverseL=imcomplement(L);   %reverse black and white in the
label image
        position = [];   %fomatting the labeling
        %Extract cell locations
        for i=1:NumBlob(1)
            position = [position; Centroid_List(2*i-
1),Centroid_List(2*i),20];
        end
        %Label each cell with its identity number in mask image
        Annotated_L1 =
insertObjectAnnotation(reverseL,'circle',position,Cell_List,'textcolor'
,'red','fontsize',24);

    elseif ii==NbImages %if this is the last frame
        %Analyze the cell size distribution in the last frame
        Area_end = regionprops(bw,'Area');
        Area_ende = extractfield(Area_end,'Area');

        %Generate image of cell size ditribution in both first and last
frames
%         figure;
%         title(sprintf(InputString,' [1,end]PixelDistribution
',Location,ColorChannel));
%         subplot(2,1,1)
%         histogram(Area_1e,100);
%         hold on;
%         subplot(2,1,2)
%         histogram(Area_ende,100);
%         hold on;
```

```
        %Find locations of cell positions in last frame for later
generating interactive image for user input in choosing cells to be
        %analyzed
        stats_ImLend = regionprops(L,L,'MeanIntensity','Centroid');
        Cell_List = extractfield(stats_ImLend,'MeanIntensity')';
        Centroid_List = extractfield(stats_ImLend,'Centroid')';
        reverseL=imcomplement(L);
        %Extract cell locations
        position = [];
        for i=1:NumBlob(NbImages)
            position = [position; Centroid_List(2*i-
1),Centroid_List(2*i),20];
        end
        %Label each cell with its identity number in mask image
        Annotated_Lend =
insertObjectAnnotation(reverseL,'circle',position,Cell_List,'textcolor'
,'blue','fontsize',24);

        %Prompt image for user input in choosing which cells to be
analyzed
        figure;
        Combo = imfuse(Annotated_L1,Annotated_Lend,'blend');%fuse the
first and last frame images together with identities labeled
        imshow(Combo);
        title(sprintf(InputString,' T1+end_Annotated
',Location,ColorChannel));

        %Extract coordinates of cells specified by user inputs, user
choose as
        %Many cells as they want, terminated by enter
        [x, y] = ginput;
        x = round(x);
        y = round(y);

        %Extract coorindates of two dots specified by user inputs
        [x2, y2] = ginput(2);
        x2 = round(x2);
        y2 = round(y2);
    end
end

%%%%%%%%%%%%%%%%%% user input for cell to analyze
%%%%%%%%%%%%%%%%%%%%%%%%%%%%

%Define the shift distance in terms of pixels based on user input
shiftY = abs(y2(2)-y2(1));
sizeL = size(L);        %Size of original mask
shiftMatrix = zeros(shiftY,sizeL(2));       %Construct the upper
portion of shift matrix for checking whether cells are squeezed

%construct PickMask to pick cells chosen by user input
PickMask = zeros(sizeL);
for n=1:length(x)
    PickMask(y(n),x(n)) = 1;
end
```

```
preContactPairMask = PickMask.*ImL{1};  %only identity of cells chosen
by user appear in this matrix
preContactPairMask = bwlabel(preContactPairMask); %convert to label
matrix

%%%%%%%%%%%%%%%%%%%%%%%%% cell tracking %%%%%%%%%%%%%%%%%%%%%%%%%

criteria = find(preContactPairMask);      %determine if any cells are
chosen by user
if criteria         %in case there are cells chosen
    temp1 = regionprops(preContactPairMask,ImL{1},'MeanIntensity');
%extract the identities of cells chosen by user
    preContactPair(1).pre = extractfield(temp1,'MeanIntensity')';
%this list is a starting point for cell tracking

    %determine whether cells stay still or get squeezed in adjacent
frames by matching blobs between adjacent images for all n images,
total n-1 adjecent pairs
    for ii=1: NbImages-1
        %Track squeezed cells
        newL=[shiftMatrix;ImL{ii}(1:sizeL(1)-shiftY,:)];
%Construct the shifted matrix
        squeezedCellMask = newL.*ImL{ii+1};      %select for overlaping
regions as squeezed cells appear in both the shifted image and the next
image
        squeezedCellMask = bwlabel(squeezedCellMask);       %re-number
the mask so it starts from number 1
        criteria = find(squeezedCellMask);      %judge whether there is
non-zero element
        if criteria         %in case there is overlaping region
            temp1 = regionprops(squeezedCellMask,newL,'MeanIntensity');
%use the overlapping as new mask to look for index of cells in the
earlier image of dual comparison, "mean intensity" of mask is indeed
the cell index
            squeezedCell(ii).pre =
extractfield(temp1,'MeanIntensity')';        %make up a list of
squeezed cells index in the previous image of the comparison
            temp2 =
regionprops(squeezedCellMask,ImL{ii+1},'MeanIntensity');        %use
the overlapping as new mask to look for index of cells in the latter
image of dual comparison, "mean intensity" of mask is indeed the cell
index
            squeezedCell(ii).post =
extractfield(temp2,'MeanIntensity')';       %make up a list of squeezed
cells index in the latter image of the dual comparison
        else        %in case there is no overlaping region
            squeezedCell(ii).pre=[];
            squeezedCell(ii).post=[];
        end

        %Track not squeezed cells
        stillCellMask= ImL{ii}.*ImL{ii+1};      %select for overlaping
regions as still cells appear in both the non-shifted image and the
latter image
        stillCellMask = bwlabel(stillCellMask);     %re-number the mask
so it starts from number 1
```

```
        criteria = find(stillCellMask);      %judge whether there is
non-zero element
        if criteria         %in case there is overlaping region
            temp3 = regionprops(stillCellMask,ImL{ii},'MeanIntensity');
            stillCell(ii).pre=extractfield(temp3,'MeanIntensity')';
            temp4 =
regionprops(stillCellMask,ImL{ii+1},'MeanIntensity');
            stillCell(ii).post = extractfield(temp4,'MeanIntensity')';
        else
            stillCell(ii).pre=[];
            stillCell(ii).post=[];
        end

        %combine the squeezed and still cell list to include all cells
        allCell(ii).pre = [squeezedCell(ii).pre; stillCell(ii).pre];
        allCell(ii).post = [squeezedCell(ii).post; stillCell(ii).post];
    end

    %set up matrixes for cell tracking in next part
    LookUpMatrix = [preContactPair(1).pre];%set up initial matrix
    MeanIntensityTrack = [MeanIntensity{1}(preContactPair(1).pre)];
    AdjustedMeanIntensityTrack =
[AdjustedMeanIntensity{1}(preContactPair(1).pre)];
    TotalIntensityTrack = [TotalIntensity{1}(preContactPair(1).pre)];
    BackGroundTrack = [BackGround{1}(preContactPair(1).pre)];
    AreaTrack = [Area{1}(preContactPair(1).pre)];
    rowNum=size(LookUpMatrix,1);
    colNum=size(LookUpMatrix,2);

    voidColumn = zeros(size(LookUpMatrix,1),1);

    %tracking identity of all cells by checking n-2 comparison got from
last step
    for ii=0:NbImages-2  %%flag, I change here
        n = length(allCell(ii+1).pre);      %number of cells of image
ii from latter comparison
        count=0;
        for iii=1:n         %go through each cell
            a1=allCell(ii+1).pre(iii);      %each cell of image ii from
latter comparison
            b1=LookUpMatrix(:,ii+1);       %list of cells of image ii
from earlier comparison

            [Lia1, Locb1] = ismember(a1,b1);        %determine whether
cells of image ii in latter comparison existed in earlier comparison
            %!!!There is a caveats of ismember and related functions,
it only
            %gives the lowest index, not all indexes, mess up the
duplicates
            %cases in either pre or post sets. Need to remove duplicate
            %cases!!!
            if Lia1 == 1        %the cell exits
                LookUpMatrix(Locb1,ii+2) = allCell(ii+1).post(iii);
                MeanIntensityTrack(Locb1,ii+2)=
MeanIntensity{ii+2}(allCell(ii+1).post(iii));
```

```
                AdjustedMeanIntensityTrack(Locb1,ii+2)=
AdjustedMeanIntensity{ii+2}(allCell(ii+1).post(iii));
                TotalIntensityTrack(Locb1,ii+2)=
TotalIntensity{ii+2}(allCell(ii+1).post(iii));
                BackGroundTrack(Locb1,ii+2)=
BackGround{ii+2}(allCell(ii+1).post(iii));
                AreaTrack(Locb1,ii+2)=
Area{ii+2}(allCell(ii+1).post(iii));
                count=count+1;
            else
            end
        end
        %in case not a single cell is tracked in this loop
        if count == 0
            LookUpMatrix(:,ii+2)= voidColumn;
            MeanIntensityTrack(:,ii+2)= voidColumn;
            AdjustedMeanIntensityTrack(:,ii+2)= voidColumn;
            TotalIntensityTrack(:,ii+2)= voidColumn;
            BackGroundTrack(:,ii+2)= voidColumn;
            AreaTrack(:,ii+2)= voidColumn;
        end
    end

%%%%%%%%%%%%%%%%%%% post processing of cell information %%%%%%%%%%
    %remove short trace
    CompleteLookUpMatrix=[];
    CompleteMeanIntensity=[];
    CompleteNormalizedMeanIntensity=[];
    CompleteAdjustedMeanIntensity=[];
    CompleteNormalizedAdjustedMeanIntensity=[];
    CompleteTotalIntensity=[];
    CompleteNormalizedTotalIntensity=[];
    CompleteArea=[];
    CompleteNormalizedArea=[];
    CompleteBackground=[];
    CompleteNormalizedBackground=[];

    for i=1:size(LookUpMatrix,1)
        realLength=find(LookUpMatrix(i,:));
        rowLength=length(realLength);
        if rowLength==NbImages

CompleteLookUpMatrix=[CompleteLookUpMatrix;LookUpMatrix(i,:)];

CompleteMeanIntensity=[CompleteMeanIntensity;MeanIntensityTrack(i,:)];

CompleteAdjustedMeanIntensity=[CompleteAdjustedMeanIntensity;AdjustedMe
anIntensityTrack(i,:)];

CompleteTotalIntensity=[CompleteTotalIntensity;TotalIntensityTrack(i,:)
];
            CompleteArea=[CompleteArea;AreaTrack(i,:)];

CompleteBackground=[CompleteBackground;BackGroundTrack(i,:)];
        else
        end
```

```
    end

    %generate complete relative trace, if there is one
    if CompleteLookUpMatrix

preContactMeanIntensity=mean(CompleteMeanIntensity(:,[1:numAvgColumn]),
2);

preContactAdjustedMeanIntensity=mean(CompleteAdjustedMeanIntensity(:,[1
:numAvgColumn]),2);

preContactTotalIntensity=mean(CompleteTotalIntensity(:,[1:numAvgColumn]
),2);
        preContactArea=mean(CompleteArea(:,[1:numAvgColumn]),2);

preContactBackground=mean(CompleteBackground(:,[1:numAvgColumn]),2);

        for i=1:size(CompleteLookUpMatrix,2)
            CompleteNormalizedMeanIntensity(:,i) =
CompleteMeanIntensity(:,i)./preContactMeanIntensity;
            CompleteNormalizedAdjustedMeanIntensity(:,i) =
CompleteAdjustedMeanIntensity(:,i)./preContactAdjustedMeanIntensity;
            CompleteNormalizedTotalIntensity(:,i) =
CompleteTotalIntensity(:,i)./preContactTotalIntensity;
            CompleteNormalizedArea(:,i) =
CompleteArea(:,i)./preContactArea;
            CompleteNormalizedBackground(:,i) =
CompleteBackground(:,i)./preContactBackground;
        end
    else
        CompleteNormalizedMeanIntensity=[];
        CompleteNormalizedAdjustedMeanIntensity=[];
        CompleteNormalizedTotalIntensity=[];
        CompleteNormalizedArea=[];
        CompleteNormalizedBackground=[];
    end

    save(Filename)

else        %in case there is no overlaping region, no value returned
    preContactPair(1).pre=[];
    LookUpMatrix = [];
    CompleteLookUpMatrix=[];
    CompleteMeanIntensity=[];
    CompleteAdjustedMeanIntensity=[];
    CompleteTotalIntensity=[];
    CompleteArea=[];
    CompleteBackground=[];
    CompleteNormalizedMeanIntensity=[];
    CompleteNormalizedAdjustedMeanIntensity=[];
    CompleteNormalizedTotalIntensity=[];
    CompleteNormalizedArea=[];
    CompleteNormalizedBackground=[];

end
end
```

APPENDIX D.2 Analysis of Calcium-Mitochondria Dynamics

Appendix D.2.1 Extract Multiple Image-Derived Features from Tiff File

```
%MitoTrack_V3_ReadTiff.m
close all
clearvars
ProgName='MitoTrack_V3_ReadTiff';
FileName='20161021_Test2_Q_P23.tif';
FileName
extraName='';
savedName = [FileName,'_',extraName,'_by_',ProgName,'.mat'];
channelR=1;
channelG=2;
channelB=3;
thresholdR=3000;
thresholdG=3000;
thresholdB=3000;
xySpace=0.72; %xy resolution at 20x
%xySpace=0.36; %xy resolution at 40x
%xySpace=1.44; %xy resolution at 20x
zSpace=3; %3um between each z stacks
sizeRrangeG=[20 3000];
cellDistThreshold=20;
channelDistThreshold=10;
A1 = imread(FileName,'index',1);
ImHeight=size(A1,1);
ImWidth=size(A1,2);
numTimePt=41;
numChannel=3;
numZstacks=10;
% yDimension = Dimension(1);
% xDimension = Dimension(2);
M=zeros(ImHeight,ImWidth,numZstacks,numChannel,numTimePt);
for time=1:numTimePt
    for channel=1:numChannel
        for zstack=1:numZstacks
            frame=zstack+numZstacks*(channel-
1)+numZstacks*numChannel*(time-1);
            M(:,:,zstack,channel,time)=imread(FileName,'index',frame);
        end
    end
end

% %bin 2x2
% yDimension = size(M,1);
% xDimension = size(M,2);
% if rem(yDimension,2) > 0
%     M = [M;M(end,:,:,:,:)];
% end % Make duplicate of last row for n odd
% newM = (M(1:2:end,:,:,:,:) + M(2:2:end,:,:,:,:))/2; % Add pairs of
rows
% if rem(xDimension,2) > 0
%     newM = [newM,newM(:,end,:,:,:)];
% end % Make duplicate of last row for n odd
```

```
% new2M = (newM(:,1:2:end,:,:,:) + newM(:,2:2:end,:,:,:))/2; % Add
pairs of rows
% M=new2M;
%
% %bin 4x4
% yDimension = size(M,1);
% xDimension = size(M,2);
% if rem(yDimension,2) > 0
%     M = [M;M(end,:,:,:,:)];
% end % Make duplicate of last row for n odd
% newM = (M(1:2:end,:,:,:,:) + M(2:2:end,:,:,:,:))/2; % Add pairs of
rows
% if rem(xDimension,2) > 0
%     newM = [newM,newM(:,end,:,:,:)];
% end % Make duplicate of last row for n odd
% new2M = (newM(:,1:2:end,:,:,:) + newM(:,2:2:end,:,:,:))/2; % Add
pairs of rows
% M=new2M;

Dimension = size(M);
yDimension = Dimension(1);
xDimension = Dimension(2);
zDimension = Dimension(3);
NumTimePt = Dimension(5);
zVector = (0:zSpace:(zDimension-1)*zSpace)'; %column of z vector
RGB=zeros(yDimension,xDimension,3);
count=1;
series=1:zDimension;

CentroidZR=zeros(zDimension,2,NumTimePt);
CentroidZG=zeros(zDimension,2,NumTimePt);
CentroidZB=zeros(zDimension,2,NumTimePt);
CentroidWeightedZR=zeros(zDimension,2,NumTimePt);
CentroidWeightedZG=zeros(zDimension,2,NumTimePt);
CentroidWeightedZB=zeros(zDimension,2,NumTimePt);

% CentroidsZ=zeros(zDimension,2,3,NumTimePt);
% CentroidsZWeighted=zeros(zDimension,2,3,NumTimePt);
totalIntensityZ=zeros(zDimension,NumTimePt,3);
Centroid=zeros(3,NumTimePt,3);
CentroidWeighted = zeros(3,NumTimePt,3);

MomentR=zeros(zDimension,NumTimePt);
totalAxDistSQR=zeros(zDimension,NumTimePt);
MomentG=zeros(zDimension,NumTimePt);
totalAxDistSQG=zeros(zDimension,NumTimePt);
MOI3DRtoR=zeros(1,NumTimePt);
totalRadSQ3DRtoR=zeros(1,NumTimePt);
MOI3DRtoG=zeros(1,NumTimePt);
totalRadSQ3DRtoG=zeros(1,NumTimePt);

BoundPixelSeperateR=cell(NumTimePt,1);
IntensitySeperateR3=cell(NumTimePt,1);

VecMitoSeperateR3=cell(NumTimePt,1);
MOI3DBoundRtoR=zeros(1,NumTimePt);
```

```
totalRadSQ3DBoundRtoR=zeros(1,NumTimePt);
MeanMitoMOI3DBoundRtoR=zeros(1,NumTimePt);

VecMitoSeperateG3=cell(NumTimePt,1);
MOI3DBoundRtoG=zeros(1,NumTimePt);
totalRadSQ3DBoundRtoG=zeros(1,NumTimePt);
MeanMitoMOI3DBoundRtoG=zeros(1,NumTimePt);

BoundPixelSeperateG=cell(NumTimePt,1);
IntensitySeperateG3=cell(NumTimePt,1);

PixelG=cell(NumTimePt,1);
IntensityPixelG=cell(NumTimePt,1);
ShapeG=zeros(zDimension,NumTimePt,5);

VecInterCell = zeros(3,NumTimePt);
VecMito = zeros(3,NumTimePt);
VecInterCellWeighted = zeros(3,NumTimePt);
VecMitoWeighted = zeros(3,NumTimePt);

Angle = zeros(1,NumTimePt);
cellDistance = zeros(1,NumTimePt);
sProjection=zeros(1,NumTimePt);
AngleWeighted = zeros(1,NumTimePt);
cellDistWeighted = zeros(1,NumTimePt);
channelDistWeighted = zeros(1,NumTimePt);
sProjWeighted=zeros(1,NumTimePt);

CentroidSeperateR=cell(NumTimePt,1);
IntensitySeperateR1=cell(NumTimePt,1);
PixelSeperateR=cell(NumTimePt,1);
IntensitySeperateR2=cell(NumTimePt,1);
IntensityBoundR=zeros(1,NumTimePt);

projSeperate1=cell(NumTimePt,1);
VecMitoSeperateG1=cell(NumTimePt,1);
VecMitoSeperateR2=cell(NumTimePt,1);
VecMitoSeperateG2=cell(NumTimePt,1);
projPos1=zeros(3,NumTimePt);
projNeg1=zeros(3,NumTimePt);

projSeperate2=cell(NumTimePt,1);
VecMitoSeperate2=cell(NumTimePt,1);
projPos2=zeros(3,NumTimePt);
projNeg2=zeros(3,NumTimePt);

maxIntZ=zeros(1,NumTimePt);
maxIndexZ=zeros(1,NumTimePt);
% CellEccentr1=zeros(1,NumTimePt);
% CellMajorAxis1=zeros(1,NumTimePt);
% CellMinorAxis1=zeros(1,NumTimePt);
% CellArea1=zeros(1,NumTimePt);
% CellDia1=zeros(1,NumTimePt);
CellEccentr2= zeros(1,NumTimePt);
CellMajorAxis2= zeros(1,NumTimePt);
```

```
CellMinor2= zeros(1,NumTimePt);
CellArea2=zeros(1,NumTimePt);
CellDia2= zeros(1,NumTimePt);
IntensityBoundG=zeros(1,NumTimePt);
minDistSQ3DAllPixelG=zeros(1,NumTimePt);
maxDistSQ3DAllPixelG=zeros(1,NumTimePt);
medianDistSQ3DAllPixelG=zeros(1,NumTimePt);
meanDistSQ3DAllPixelG=zeros(1,NumTimePt);
CalcMOI3DAllPixelG=zeros(1,NumTimePt);
totalDistSQ3DAllPixelG=zeros(1,NumTimePt);
MeanCalcMOI3DAllPixelG=zeros(1,NumTimePt);
CalcMOI3DBoundG=zeros(1,NumTimePt);
minDistSQ3DG=zeros(1,NumTimePt);
maxDistSQ3DG=zeros(1,NumTimePt);
medianDistSQ3DG=zeros(1,NumTimePt);
meanDistSQ3DG=zeros(1,NumTimePt);
NumBoundR=zeros(1,NumTimePt);
NumBoundG=zeros(1,NumTimePt);
NumAllPixelG=zeros(1,NumTimePt);
NumAllPixelR=zeros(1,NumTimePt);
MeanCalcMOI3DBoundG=zeros(1,NumTimePt);
IntensityAllPixelG=zeros(1,NumTimePt);
totalRadSQ3DBoundGtoG=zeros(1,NumTimePt);
numOutHalfG=zeros(1,NumTimePt);
numOutHalfR=zeros(1,NumTimePt);
numOutHalfG0=zeros(1,NumTimePt);
numOutHalfR0=zeros(1,NumTimePt);
IntenOutHalfG=zeros(1,NumTimePt);
IntenOutHalfR=zeros(1,NumTimePt);
IntenOutHalfG0=zeros(1,NumTimePt);
IntenOutHalfR0=zeros(1,NumTimePt);

for t=1:NumTimePt

    for z=[floor(median(series)):-
1:min(series),floor(median(series))+1:max(series)]
        %green channel
        %figure;
        Green=M(:,:,z,channelG,t)>thresholdG;
        Green = bwareafilt(Green,sizeRrangeG);
        Green = bwareafilt(Green,1);
        %imshow(Green);
        criteriaG = any(any(Green));
        if criteriaG

            sG =
regionprops(Green,M(:,:,z,channelG,t),{'Centroid','WeightedCentroid','A
rea','MeanIntensity',...

'Eccentricity','MajorAxisLength','MinorAxisLength','EquivDiameter','Pix
elValues','PixelList'});

            CentroidG = cat(1, sG.Centroid);
            AreaG = cat(1, sG.Area);
            MeanIntensityG = cat(1, sG.MeanIntensity);
            WeightedCentroidG = cat(1,sG.WeightedCentroid);
```

```
            EccentricityG=cat(1,sG.Eccentricity);
            MajorAxisLengthG=cat(1,sG.MajorAxisLength);
            MinorAxisLengthG=cat(1,sG.MinorAxisLength);
            EquivDiameterG=cat(1,sG.EquivDiameter);
            PixelValuesG=cat(1,sG.PixelValues);
            PixelListG=cat(1,sG.PixelList);
            numPixelG=size(PixelListG,1);

PixelG{t}=[PixelG{t};cat(2,xySpace*PixelListG,zVector(z)*ones(numPixelG
,1))];
            IntensityPixelG{t}=cat(1,
IntensityPixelG{t},double(PixelValuesG));
            BoundPixelG=bwboundaries(Green);
            BoundPixelListG2=[BoundPixelG{1}(:,2),BoundPixelG{1}(:,1)];
            [BoundPixelListG,ja,jb] =
intersect(PixelListG,BoundPixelListG2,'rows');
            numBoundG=size(BoundPixelListG,1);

BoundPixelSeperateG{t}=[BoundPixelSeperateG{t};cat(2,xySpace*BoundPixel
ListG,zVector(z)*ones(numBoundG,1))];
            IntensitySeperateG3{t}=cat(1,
IntensitySeperateG3{t},double(PixelValuesG(ja)));
            totalIntensityG=MeanIntensityG.*AreaG;
            numG=size(AreaG,1);
            totalIntensityZ(z,t,2) = sum(totalIntensityG);

            if numG>1
                CentroidZG(z,:,t) =
(CentroidG'*totalIntensityG/sum(totalIntensityG))';
                CentroidWeightedZG(z,:,t) =
(WeightedCentroidG'*totalIntensityG/sum(totalIntensityG))';
                ShapeG(z,t,1) =
(EccentricityG'*totalIntensityG/sum(totalIntensityG))';
                ShapeG(z,t,2) =
(MajorAxisLengthG'*totalIntensityG/sum(totalIntensityG))';
                ShapeG(z,t,3) =
(MinorAxisLengthG'*totalIntensityG/sum(totalIntensityG))';
                ShapeG(z,t,4) =
(AreaG'*totalIntensityG/sum(totalIntensityG))';
                ShapeG(z,t,5) =
(EquivDiameterG'*totalIntensityG/sum(totalIntensityG))';
            else
                CentroidZG(z,:,t) = CentroidG;
                CentroidWeightedZG(z,:,t) = WeightedCentroidG;
                ShapeG(z,t,1) = EccentricityG;
                ShapeG(z,t,2) = MajorAxisLengthG;
                ShapeG(z,t,3) = MinorAxisLengthG;
                ShapeG(z,t,4) = AreaG;
                ShapeG(z,t,5) = EquivDiameterG;
            end

        else

            %CentroidZG(z,:,t) = [NaN NaN];
            BoundPixelListG=[NaN,NaN];
            totalIntensityZ(z,t,2) = 0;
```

```
            %CentroidWeightedZG(z,:,t)=[NaN NaN];
        end

        %Red channel
        Red=M(:,:,z,channelR,t)>thresholdR;
        %imshow(Red)
        criteriaR = any(any(Red));
        if criteriaR
            sR =
regionprops(Red,M(:,:,z,channelR,t),{'Centroid','WeightedCentroid','Are
a','MeanIntensity','PixelValues','PixelList'});
            CentroidR = cat(1, sR.Centroid);
            AreaR = cat(1, sR.Area);
            MeanIntensityR = cat(1, sR.MeanIntensity);
            WeightedCentroidR = cat(1,sR.WeightedCentroid);
            PixelValuesR=cat(1,sR.PixelValues);
            PixelListR=cat(1,sR.PixelList);
            numR=size(AreaR,1);
            sizeR=sum(AreaR);
            totalIntensityR=MeanIntensityR.*AreaR;

            [BoundPixelListR,ia,ib] =
intersect(PixelListR,BoundPixelListG,'rows');
            numBoundR=size(BoundPixelListR,1);

BoundPixelSeperateR{t}=[BoundPixelSeperateR{t};cat(2,xySpace*BoundPixel
ListR,zVector(z)*ones(numBoundR,1))];
            IntensitySeperateR3{t}=cat(1,
IntensitySeperateR3{t},double(PixelValuesR(ia)));

CentroidSeperateR{t}=[CentroidSeperateR{t};cat(2,xySpace*CentroidR,zVec
tor(z)*ones(numR,1))];
            IntensitySeperateR1{t}=cat(1,
IntensitySeperateR1{t},totalIntensityR);

PixelSeperateR{t}=[PixelSeperateR{t};cat(2,xySpace*PixelListR,zVector(z
)*ones(sizeR,1))];
            IntensitySeperateR2{t}=cat(1,
IntensitySeperateR2{t},double(PixelValuesR));
            totalIntensityZ(z,t,1)=sum(totalIntensityR);

            if numR>1
                CentroidZR(z,:,t) =
(CentroidR'*totalIntensityR/sum(totalIntensityR))';

CentroidWeightedZR(z,:,t)=(WeightedCentroidR'*totalIntensityR/sum(total
IntensityR))';
            else
                CentroidZR(z,:,t) = CentroidR;
                CentroidWeightedZR(z,:,t)= WeightedCentroidR;

            end


ArrayCentroidR=[CentroidWeightedZR(z,1,t)*ones(sizeR,1),CentroidWeighte
dZR(z,2,t)*ones(sizeR,1)];
```

```
            VecAxDistR=xySpace*(PixelListR-ArrayCentroidR);
            AxDistSQR=sum(VecAxDistR.*VecAxDistR,2);
            MomentR(z,t)=sum(AxDistSQR.*double(PixelValuesR));
            totalAxDistSQR(z,t)=sum(AxDistSQR,1);

            if criteriaG

ArrayCentroidsG=[CentroidWeightedZG(z,1,t)*ones(sizeR,1),CentroidWeight
edZG(z,2,t)*ones(sizeR,1)];
                VecAxDistG=xySpace*(PixelListR-ArrayCentroidsG);
                AxDistSQG=sum(VecAxDistG.*VecAxDistG,2);
                MomentG(z,t)=sum(AxDistSQG.*double(PixelValuesR));
                totalAxDistSQG(z,t)=sum(AxDistSQG,1);
            else
                MomentG(z,t)=0;
                totalAxDistSQG(z,t)=0;
            end

        else
            totalIntensityZ(z,t,1)=0;
            %CentroidsR=[0 0];
            %WeightedCentroidsR=[0 0];
            MomentR(z,t)=0;
            totalAxDistSQR(z,t)=0;
            MomentG(z,t)=0;
            totalAxDistSQG(z,t)=0;
            CentroidSeperateR{t}=CentroidSeperateR{t};
            IntensitySeperateR1{t}=IntensitySeperateR1{t};
            PixelSeperateR{t}=PixelSeperateR{t};
            IntensitySeperateR2{t}=IntensitySeperateR2{t};
        end

        %Blue channel
        Blue=M(:,:,z,channelB,t)>thresholdB;
        criteriaB = any(any(Blue));
        if criteriaB
            %Blue = bwareafilt(Blue,1);
            sB =
regionprops(Blue,M(:,:,z,channelB,t),{'Centroid','WeightedCentroid','Ar
ea','MeanIntensity'});
            CentroidB = cat(1, sB.Centroid);
            AreaB = cat(1, sB.Area);
            MeanIntensityB = cat(1, sB.MeanIntensity);
            WeightedCentroidB = cat(1,sB.WeightedCentroid);

            totalIntensityB=MeanIntensityB.*AreaB;
            totalIntensityZ(z,t,3)=sum(totalIntensityB);

            numB=size(AreaB,1);

            if numB>1
                CentroidZB(z,:,t) =
(CentroidB'*totalIntensityB/sum(totalIntensityB))';

CentroidWeightedZB(z,:,t)=(WeightedCentroidB'*totalIntensityB/sum(total
IntensityB))';
```

```
            else
                CentroidZB(z,:,t) = CentroidB;
                CentroidWeightedZB(z,:,t)= WeightedCentroidB;

            end

        else
            totalIntensityZ(z,t,3) =0;
            %CentroidsB=[0 0];
            %WeightedCentroidsB=[0 0];
        end

    end

    Centroid(:,t,1) =
(cat(2,xySpace*CentroidZR(:,:,t),zVector)'*totalIntensityZ(:,t,1))./sum
(totalIntensityZ(:,t,1));
    Centroid(:,t,2) =
(cat(2,xySpace*CentroidZG(:,:,t),zVector)'*totalIntensityZ(:,t,2))./sum
(totalIntensityZ(:,t,2));
    Centroid(:,t,3) =
(cat(2,xySpace*CentroidZB(:,:,t),zVector)'*totalIntensityZ(:,t,3))./sum
(totalIntensityZ(:,t,3));

    CentroidWeighted(:,t,1) =
(cat(2,xySpace*CentroidWeightedZR(:,:,t),zVector)'*totalIntensityZ(:,t,
1))./sum(totalIntensityZ(:,t,1));
    CentroidWeighted(:,t,2) =
(cat(2,xySpace*CentroidWeightedZG(:,:,t),zVector)'*totalIntensityZ(:,t,
2))./sum(totalIntensityZ(:,t,2));
    CentroidWeighted(:,t,3) =
(cat(2,xySpace*CentroidWeightedZB(:,:,t),zVector)'*totalIntensityZ(:,t,
3))./sum(totalIntensityZ(:,t,3));

    VecInterCell(:,t) = Centroid(:,t,3)-Centroid(:,t,2);
    VecMito(:,t) = Centroid(:,t,1)-Centroid(:,t,2);
    %cellDistance(t)=norm(VecVecMito(:,t));
    %channelDistance(t)=norm(VecInterCell(:,t));

Angle(t)=acosd(dot(VecInterCell(:,t),VecMito(:,t))./(norm(VecInterCell(
:,t))*norm(VecMito(:,t))));

sProjection(t)=dot(VecInterCell(:,t),VecMito(:,t))./norm(VecInterCell(:
,t));

    VecInterCellWeighted(:,t) = CentroidWeighted(:,t,3)-
CentroidWeighted(:,t,2);
    VecMitoWeighted(:,t) = CentroidWeighted(:,t,1)-
CentroidWeighted(:,t,2);
    cellDistWeighted(t)=norm(VecInterCellWeighted(:,t));
    channelDistWeighted(t)=norm(VecMitoWeighted(:,t));

AngleWeighted(t)=acosd(dot(VecInterCellWeighted(:,t),VecMitoWeighted(:,
t))./(norm(VecInterCellWeighted(:,t))*norm(VecMitoWeighted(:,t))));
```

```
    sProjWeighted(t)=
dot(VecInterCellWeighted(:,t),VecMitoWeighted(:,t))./norm(VecInterCellW
eighted(:,t));

    [maxIntZ(t),maxIndexZ(t)]=max(totalIntensityZ(:,t,2));
    CellEccentr2(t)= ShapeG(maxIndexZ(t),t,1);
    CellMajorAxis2(t)= ShapeG(maxIndexZ(t),t,2);
    CellMinor2(t)= ShapeG(maxIndexZ(t),t,3);
    CellArea2(t)=ShapeG(maxIndexZ(t),t,4);
    CellDia2(t)= ShapeG(maxIndexZ(t),t,5);
    NumSeperateR1=size(CentroidSeperateR{t},1);
    if NumSeperateR1
        projSeperate1{t}=zeros(NumSeperateR1,1);

ArrayCentroidG1=[CentroidWeighted(1,t,2).*ones(NumSeperateR1,1),
CentroidWeighted(2,t,2).*ones(NumSeperateR1,1),CentroidWeighted(3,t,2).
*ones(NumSeperateR1,1)];
        VecMitoSeperateG1{t}=CentroidSeperateR{t}-ArrayCentroidG1;

        for i=1:NumSeperateR1

projSeperate1{t}(i)=dot(VecInterCellWeighted(:,t),VecMitoSeperateG1{t}(
i,:))./norm(VecInterCellWeighted(:,t));
            if projSeperate1{t}(i)>0
                projPos1(1,t)= projPos1(1,t)+ projSeperate1{t}(i);
                projPos1(2,t)= projPos1(2,t)+
IntensitySeperateR1{t}(i);
                projPos1(3,t)= projPos1(3,t)+
projSeperate1{t}(i)*IntensitySeperateR1{t}(i);
            elseif projSeperate1{t}(i)<0
                projNeg1(1,t)= projNeg1(1,t)+ projSeperate1{t}(i);
                projNeg1(2,t)= projNeg1(2,t)+
IntensitySeperateR1{t}(i);
                projNeg1(3,t)= projNeg1(3,t)+
projSeperate1{t}(i)*IntensitySeperateR1{t}(i);
            end
        end
    else
        projSeperate1{t}=0;
        projPos1(:,t)=NaN;
        projNeg1(:,t)=NaN;
    end
%
    NumAllPixelR(t)=size(PixelSeperateR{t},1);
    if NumAllPixelR(t)
        %sizeAllR(t)=NumSeperateR2;
        projSeperate2{t}=zeros(NumAllPixelR(t),1);

ArrayCentroidR2=[CentroidWeighted(1,t,1).*ones(NumAllPixelR(t),1),
CentroidWeighted(2,t,1).*ones(NumAllPixelR(t),1),CentroidWeighted(3,t,1
).*ones(NumAllPixelR(t),1)];

ArrayCentroidG2=[CentroidWeighted(1,t,2).*ones(NumAllPixelR(t),1),
CentroidWeighted(2,t,2).*ones(NumAllPixelR(t),1),CentroidWeighted(3,t,2
).*ones(NumAllPixelR(t),1)];
        VecMitoSeperateR2=PixelSeperateR{t}-ArrayCentroidR2;
```

```
        VecMitoSeperateG2=PixelSeperateR{t}-ArrayCentroidG2;

DistSQ3DR=sum(VecMitoSeperateR2(:,:).*VecMitoSeperateR2(:,:),2);
        MOI3DRtoR(t)=sum(DistSQ3DR.*IntensitySeperateR2{t});
        totalRadSQ3DRtoR(t)=sum(DistSQ3DR,1);

MeanMitoMOI3DRtoR=sum(MOI3DRtoR,1)./sum(totalIntensityZ(:,:,1),1);

DistSQ3DG=sum(VecMitoSeperateG2(:,:).*VecMitoSeperateG2(:,:),2);
        MOI3DRtoG(t)=sum(DistSQ3DG.*IntensitySeperateR2{t});
        minDistSQ3DG(t)=min(DistSQ3DG);
        maxDistSQ3DG(t)=max(DistSQ3DG);
        medianDistSQ3DG(t)=median(DistSQ3DG);
        meanDistSQ3DG(t)=mean(DistSQ3DG);

%minMoment3DG(t)=min(DistSQ3DG.*IntensitySeperateR2{t}./sum(IntensitySe
perateR2{t}));
        %maxMoment3DG(t)=max(DistSQ3DG.*IntensitySeperateR2{t});
        %medianMoment3DG(t)=median(DistSQ3DG.*IntensitySeperateR2{t});
        totalRadSQ3DRtoG(t)=sum(DistSQ3DG,1);

MeanMitoMOI3DRtoG=sum(MOI3DRtoG,1)./sum(totalIntensityZ(:,:,1),1);

        for ii=1:NumAllPixelR(t)


projSeperate2{t}(ii)=dot(VecInterCellWeighted(:,t),VecMitoSeperateG2(ii
,:))./norm(VecInterCellWeighted(:,t));
            if projSeperate2{t}(ii)>0
                projPos2(1,t)= projPos2(1,t)+ projSeperate2{t}(ii);
                projPos2(2,t)= projPos2(2,t)+
IntensitySeperateR2{t}(ii);
                projPos2(3,t)= projPos2(3,t)+
projSeperate2{t}(ii)*IntensitySeperateR2{t}(ii);
            elseif projSeperate2{t}(ii)<0
                projNeg2(1,t)= projNeg2(1,t)+ projSeperate2{t}(ii);
                projNeg2(2,t)= projNeg2(2,t)+
IntensitySeperateR2{t}(ii);
                projNeg2(3,t)= projNeg2(3,t)+
projSeperate2{t}(ii)*IntensitySeperateR2{t}(ii);
            end

            if norm(VecMitoSeperateG2(ii,:))>CellDia2(t)/4
                numOutHalfG(t)=numOutHalfG(t)+1;

IntenOutHalfG(t)=IntenOutHalfG(t)+IntensitySeperateR2{t}(ii);
            end
            if norm(VecMitoSeperateR2(ii,:))>CellDia2(t)/4
                numOutHalfR(t)=numOutHalfR(t)+1;

IntenOutHalfR(t)=IntenOutHalfR(t)+IntensitySeperateR2{t}(ii);
            end
            if norm(VecMitoSeperateG2(ii,:))>CellDia2(1)/4
                numOutHalfG0(t)=numOutHalfG0(t)+1;

IntenOutHalfG0(t)=IntenOutHalfG0(t)+IntensitySeperateR2{t}(ii);
```

```
            end
            if norm(VecMitoSeperateR2(ii,:))>CellDia2(1)/4
                numOutHalfR0(t)=numOutHalfR0(t)+1;

IntenOutHalfR0(t)=IntenOutHalfR0(t)+IntensitySeperateR2{t}(ii);
            end
        end
    else
        projSeperate2{t}=0;
        projPos2(:,t)=NaN;
        projNeg2(:,t)=NaN;

    end

    NumBoundR(t)=size(BoundPixelSeperateR{t},1);
    if NumBoundR(t)
        %sizeBoundR(t)=NumSeperateR3;
        ArrayCentroidR3=[CentroidWeighted(1,t,1).*ones(NumBoundR(t),1),
CentroidWeighted(2,t,1).*ones(NumBoundR(t),1),CentroidWeighted(3,t,1).*
ones(NumBoundR(t),1)];
        ArrayCentroidG3=[CentroidWeighted(1,t,2).*ones(NumBoundR(t),1),
CentroidWeighted(2,t,2).*ones(NumBoundR(t),1),CentroidWeighted(3,t,2).*
ones(NumBoundR(t),1)];
        VecMitoSeperateR3=BoundPixelSeperateR{t}-ArrayCentroidR3;
        VecMitoSeperateG3=BoundPixelSeperateR{t}-ArrayCentroidG3;
        IntensityBoundR(t)=sum(IntensitySeperateR3{t},1);

DistSQ3DBoundR=sum(VecMitoSeperateR3(:,:).*VecMitoSeperateR3(:,:),2);

MOI3DBoundRtoR(t)=sum(DistSQ3DBoundR.*IntensitySeperateR3{t},1);
        totalRadSQ3DBoundRtoR(t)=sum(DistSQ3DBoundR,1);

MeanMitoMOI3DBoundRtoR(t)=MOI3DBoundRtoR(t)./IntensityBoundR(t);

DistSQ3DBoundRtoG=sum(VecMitoSeperateG3(:,:).*VecMitoSeperateG3(:,:),2)
;

MOI3DBoundRtoG(t)=sum(DistSQ3DBoundRtoG.*IntensitySeperateR3{t});
        totalRadSQ3DBoundRtoG(t)=sum(DistSQ3DBoundRtoG,1);

MeanMitoMOI3DBoundRtoG(t)=MOI3DBoundRtoG(t)./IntensityBoundR(t);
    else
        MeanMitoMOI3DBoundRtoG(t)=NaN;
        IntensityBoundR(t)=0;
    end

    NumBoundG(t)=size(BoundPixelSeperateG{t},1);
    if NumBoundG(t)
        %sizeBoundG(t)=NumSeperateG3;

%ArrayCentroidR3=[CentroidWeighted(1,t,1).*ones(NumSeperateR3,1),
CentroidWeighted(2,t,1).*ones(NumSeperateR3,1),CentroidWeighted(3,t,1).
*ones(NumSeperateR3,1)];
        ArrayCentroidG4=[CentroidWeighted(1,t,2).*ones(NumBoundG(t),1),
CentroidWeighted(2,t,2).*ones(NumBoundG(t),1),CentroidWeighted(3,t,2).*
ones(NumBoundG(t),1)];
```

```
        %VecMitoSeperateR3{t}=BoundPixelSeperateR{t}-ArrayCentroidR3;
        VecCenterBoundG=BoundPixelSeperateG{t}-ArrayCentroidG4;
        IntensityBoundG(t)=sum(IntensitySeperateG3{t},1);

DistSQ3DBoundGG=sum(VecCenterBoundG(:,:).*VecCenterBoundG(:,:),2);

CalcMOI3DBoundG(t)=sum(DistSQ3DBoundGG.*IntensitySeperateG3{t},1);
        totalRadSQ3DBoundGtoG(t)=sum(DistSQ3DBoundGG,1);
        MeanCalcMOI3DBoundG(t)=CalcMOI3DBoundG(t)./IntensityBoundG(t);
    else
        IntensityBoundG(t)=0;
        CalcMOI3DBoundG(t)=0;
        totalRadSQ3DBoundGtoG(t)=0;
        MeanCalcMOI3DBoundG(t)=0;
    end

    NumAllPixelG(t)=size(PixelG{t},1);
    if NumAllPixelG(t)
        %sizeAllPixelG(t)=NumAllPixelG;

%ArrayCentroidR3=[CentroidWeighted(1,t,1).*ones(NumSeperateR3,1),
CentroidWeighted(2,t,1).*ones(NumSeperateR3,1),CentroidWeighted(3,t,1).
*ones(NumSeperateR3,1)];

ArrayCentroidG5=[CentroidWeighted(1,t,2).*ones(NumAllPixelG(t),1),
CentroidWeighted(2,t,2).*ones(NumAllPixelG(t),1),CentroidWeighted(3,t,2
).*ones(NumAllPixelG(t),1)];
        %VecMitoSeperateR3{t}=BoundPixelSeperateR{t}-ArrayCentroidR3;
        VecCenterAllPixelG=PixelG{t}-ArrayCentroidG5;

        IntensityAllPixelG(t)=sum(IntensityPixelG{t},1);


DistSQ3DAllPixelG=sum(VecCenterAllPixelG(:,:).*VecCenterAllPixelG(:,:),
2);
        minDistSQ3DAllPixelG(t)=min(DistSQ3DAllPixelG);
        maxDistSQ3DAllPixelG(t)=max(DistSQ3DAllPixelG);
        medianDistSQ3DAllPixelG(t)=median(DistSQ3DAllPixelG);
        meanDistSQ3DAllPixelG(t)=mean(DistSQ3DAllPixelG);

CalcMOI3DAllPixelG(t)=sum(DistSQ3DAllPixelG.*IntensityPixelG{t},1);
        totalDistSQ3DAllPixelG(t)=sum(DistSQ3DAllPixelG,1);

MeanCalcMOI3DAllPixelG(t)=CalcMOI3DAllPixelG(t)./IntensityAllPixelG(t);
    else
        IntensityAllPixelG(t)=0;
        minDistSQ3DAllPixelG(t)=0;
        maxDistSQ3DAllPixelG(t)=0;
        medianDistSQ3DAllPixelG(t)=0;
        meanDistSQ3DAllPixelG(t)=0;
        CalcMOI3DAllPixelG(t)=0;
        totalDistSQ3DAllPixelG(t)=0;
        MeanCalcMOI3DAllPixelG(t)=0;
    end

end
```

```
tContact=find(cellDistWeighted<cellDistThreshold,1);
time=1:NumTimePt;

CaTotalInt=sum(totalIntensityZ(:,:,2),1);
MitoTotalInt=sum(totalIntensityZ(:,:,1),1);
IntenFractBoundR=IntensityBoundR./MitoTotalInt;
IntenFractBoundG=IntensityBoundG./CaTotalInt;
SizeFractBoundR=NumBoundR./NumAllPixelR;
SizeFractBoundG=NumBoundG./NumAllPixelG;
MOIFractBoundR=MOI3DBoundRtoG./MOI3DRtoG;
MOIFractBoundG=CalcMOI3DBoundG./CalcMOI3DAllPixelG;

OutHalfFractG=numOutHalfG./NumAllPixelR;
OutHalfFractR=numOutHalfR./NumAllPixelR;
OutHalfFractG0=numOutHalfG0./NumAllPixelR;
OutHalfFractR0=numOutHalfR0./NumAllPixelR;
IntenOutHalfFractG=IntenOutHalfG./MitoTotalInt;
IntenOutHalfFractR=IntenOutHalfR./MitoTotalInt;
IntenOutHalfFractG0=IntenOutHalfG0./MitoTotalInt;
IntenOutHalfFractR0=IntenOutHalfR0./MitoTotalInt;

NormalOutHalfFractG=OutHalfFractG./mean(OutHalfFractG(1:tContact-1));
NormalOutHalfFractR=OutHalfFractR./mean(OutHalfFractR(1:tContact-1));
NormalOutHalfFractG0=OutHalfFractG0./mean(OutHalfFractG0(1:tContact-
1));
NormalOutHalfFractR0=OutHalfFractR0./mean(OutHalfFractR0(1:tContact-
1));
NormalIntenOutHalfFractG=IntenOutHalfFractG./mean(IntenOutHalfFractG(1:
tContact-1));
NormalIntenOutHalfFractR=IntenOutHalfFractR./mean(IntenOutHalfFractR(1:
tContact-1));
NormalIntenOutHalfFractG0=IntenOutHalfFractG0./mean(IntenOutHalfFractG0
(1:tContact-1));
NormalIntenOutHalfFractR0=IntenOutHalfFractR0./mean(IntenOutHalfFractR0
(1:tContact-1));
NormalMeanCalcMOI3DAllPixelG=MeanCalcMOI3DAllPixelG./mean(MeanCalcMOI3D
AllPixelG(1:tContact-1));

EffMeanIntBoundG=CalcMOI3DBoundG./totalRadSQ3DBoundGtoG;

TotalMitoMOI2DRtoR=sum(MomentR,1);
MeanMitoMOI2DRtoR=sum(MomentR,1)./sum(totalIntensityZ(:,:,1),1);
TotalRadSQ2DRtoR=sum(totalAxDistSQR,1);
EffMeanIntR=sum(MomentR,1)./sum(totalAxDistSQR,1);

TotalMitoMOI2DRtoG=sum(MomentG,1);
MeanMitoMOI2DRtoG=sum(MomentG,1)./sum(totalIntensityZ(:,:,1),1);
TotalRadSQ2DRtoG=sum(totalAxDistSQG,1);
EffMeanIntG=sum(MomentG,1)./sum(totalAxDistSQG,1);

projPosFractWeighted=projPos2(3,:)./MitoTotalInt;
projNegFractWeighted=projNeg2(3,:)./MitoTotalInt;

projPosMean=projPos2(3,:)./projPos2(2,:);
```

```
projNegMean=projNeg2(3,:)./projNeg2(2,:);

projPosFract=projPos2(2,:)./MitoTotalInt;
projNegFract=projNeg2(2,:)./MitoTotalInt;

%intensity weighted eccentricity
CellEccentr1=sum(ShapeG(:,:,1).*totalIntensityZ(:,:,2),1)./sum(totalInt
ensityZ(:,:,2));
CellMajorAxis1=sum(ShapeG(:,:,2).*totalIntensityZ(:,:,2),1)./sum(totalI
ntensityZ(:,:,2));
CellMinorAxis1=sum(ShapeG(:,:,3).*totalIntensityZ(:,:,2),1)./sum(totalI
ntensityZ(:,:,2));
CellArea1=sum(ShapeG(:,:,4).*totalIntensityZ(:,:,2),1)./sum(totalIntens
ityZ(:,:,2));
CellDia1=sum(ShapeG(:,:,5).*totalIntensityZ(:,:,2),1)./sum(totalIntensi
tyZ(:,:,2));

CellVolume=sum(ShapeG(:,:,4),1);

NormalCaTotalInt=CaTotalInt./mean(CaTotalInt(1:tContact-1));
NormalMeanMitoMOI2DRtoR=MeanMitoMOI2DRtoR./mean(MeanMitoMOI2DRtoR(1:tCo
ntact-1));
NormalMeanMitoMOI2DRtoG=MeanMitoMOI2DRtoG./mean(MeanMitoMOI2DRtoG(1:tCo
ntact-1));
NormalMeanMitoMOI3DRtoR=MeanMitoMOI3DRtoR./mean(MeanMitoMOI3DRtoR(1:tCo
ntact-1));
NormalMeanMitoMOI3DRtoG=MeanMitoMOI3DRtoG./mean(MeanMitoMOI3DRtoG(1:tCo
ntact-1));
%CellEccentricity=sum(ShapeG(:,:,1).*totalIntensityZplane(:,:,2),1)./su
m(totalIntensityZplane(:,:,2));
% [Ma,I]=max(totalIntensityZplane(:,:,2));
% for i=1:42
%     CellEccentricity2(i)= ShapeG(I(i),i,1);
% end
% figure;
k = find(channelDistWeighted>channelDistThreshold)
channelDistWeighted
%k=size(k,2);
if k
    AngleWeighted(k)=NaN;
    sProjWeighted(k)=NaN;
    TotalMitoMOIG(k)=NaN;
%     MeanMitoMOIG(k)=NaN;
%     TotalRadSQG(k)=NaN;
%     EffMeanIntG(k)=NaN;
    %projSeperate{k}=NaN;
    projPos2(:,k)=NaN;
    projNeg2(:,k)=NaN;

    IntenOutHalfFractR(k)=NaN;
    IntenOutHalfFractG(k)=NaN;
    IntenOutHalfFractR0(k)=NaN;
    IntenOutHalfFractG0(k)=NaN;
    MOIFractBoundR(k)=NaN;
    MOIFractBoundG(k)=NaN;
```

```
    MeanCalcMOI3DAllPixelG(k)=NaN;
    MeanMitoMOI3DRtoG(k)=NaN;
    MeanCalcMOI3DBoundG(k)=NaN;
    MeanMitoMOI3DBoundRtoG(k)=NaN;
    MeanCalcMOI3DBoundG(k)=NaN;
    MeanMitoMOI3DBoundRtoG(k)=NaN;
    MOI3DRtoG(k)=NaN;
    MOI3DRtoR(k)=NaN;
    totalRadSQ3DRtoG(k)=NaN;
    totalRadSQ3DRtoR(k)=NaN;
    MeanMitoMOI3DRtoG(k)=NaN;
    MeanMitoMOI3DRtoR(k)=NaN;
    MeanMitoMOI2DRtoG(k)=NaN;
    MeanMitoMOI2DRtoR(k)=NaN;
    TotalRadSQ2DRtoG(k)=NaN;
    TotalRadSQ2DRtoR(k)=NaN;
    TotalMitoMOI2DRtoG(k)=NaN;
    TotalMitoMOI2DRtoR(k)=NaN;
    projPosMean(k)=NaN;
    projNegMean(k)=NaN;
    projPosFractWeighted(k)=NaN;
    projNegFractWeighted(k)=NaN;
    projPosFract(k)=NaN;
    projNegFract(k)=NaN;
    NormalMeanMitoMOI3DRtoR(k)=NaN;
    NormalMeanMitoMOI3DRtoG(k)=NaN;
    NormalMeanMitoMOI2DRtoR(k)=NaN;
    NormalMeanMitoMOI2DRtoG(k)=NaN;
    NormalMeanCalcMOI3DAllPixelG(k)=NaN;
else
end



% k = find(channelDistWeighted>channelDistThreshold);
% %j=size(k,2)
% if k
%     AngleWeighted(k)=NaN;
%     sProjWeighted(k)=NaN;
%     TotalMitoMOIG(k)=NaN;
%     MeanMitoMOIG(k)=NaN;
%     TotalRadSQG(k)=NaN;
%     EffMeanIntG(k)=NaN;
%     %projSeperate{k}=NaN;
%     projPos(:,k)=NaN;
%     projNeg(:,k)=NaN;
%
% else
% end

% p1=CellEccentr1(tContact:end);
% p2=CellEccentr2(tContact:end);
figure;
subplot(3,3,9);
%plot(time,IntensityBoundG)
```

```
p1Post9=plot(time(tContact:end),NormalMeanMitoMOI3DRtoR(tContact:end),'
r-x',time(tContact:end),NormalMeanMitoMOI3DRtoG(tContact:end),'b-x');
hold on
p1Pre9=plot(time(1:tContact-1),NormalMeanMitoMOI3DRtoR(1:tContact-
1),'r:x',time(1:tContact-1),NormalMeanMitoMOI3DRtoG(1:tContact-
1),'b:x');
legend(p1Post9,'C on Mito','C on Ca');
%plot(time,IntensityBoundG./CaTotalInt,time,sizeBoundG./CellVolume);
title('Normalized 3D MOI Centered on Mito Vs. Calcium')

subplot(3,3,8);
%plot(time,IntensityBoundG)
p1Post8=plot(time(tContact:end),NormalMeanMitoMOI2DRtoR(tContact:end),'
r-x',time(tContact:end),NormalMeanMitoMOI2DRtoG(tContact:end),'b-x');
hold on
p1Pre8=plot(time(1:tContact-1),NormalMeanMitoMOI2DRtoR(1:tContact-
1),'r:x',time(1:tContact-1),NormalMeanMitoMOI2DRtoG(1:tContact-
1),'b:x');
legend(p1Post8,'C on Mito','C on Ca');
%plot(time,IntensityBoundG./CaTotalInt,time,sizeBoundG./CellVolume);
title('Normalized 2D MOI Centered on Mito Vs. Calcium')

subplot(3,3,7);
%plot(time,IntensityBoundG)
p1Post7=plot(time(tContact:end),NormalCaTotalInt(tContact:end),'r-
x',time(tContact:end),NormalMeanCalcMOI3DAllPixelG(tContact:end),'b-
x');
hold on
p1Pre7=plot(time(1:tContact-1),NormalCaTotalInt(1:tContact-
1),'b:x',time(1:tContact-1),NormalMeanCalcMOI3DAllPixelG(1:tContact-
1),'b:x');
legend(p1Post7,'Intensity','MOI');
%plot(time,IntensityBoundG./CaTotalInt,time,sizeBoundG./CellVolume);
title('Normalized Calcium Intensity Vs. 3D MOI')

%plot(time,AngleWeighted)
subplot(3,3,3);
plot(time(1:tContact-1),AngleWeighted(1:tContact-1),'b-
x',time(tContact:end),AngleWeighted(tContact:end),'r-x')
title('Angle Weighted')

% figure;
subplot(3,3,6);
%plot(time,sProjWeighted)
plot(time(1:tContact-1),sProjWeighted(1:tContact-1),'b-
x',time(tContact:end),sProjWeighted(tContact:end),'r-x')
title('Scalar Projection Weighted')



% figure;
% %plot(time,TotalMitoMOI)
% plot(time(1:tContact-1),TotalMitoMOIG(1:tContact-1),'b-
x',time(tContact:end),TotalMitoMOIG(tContact:end),'r-x')
% title('Total Mito Moment of Inertia')
```

```
% figure;

subplot(3,3,1);
%plot(time,MitoTotalInt)
plot(time(1:tContact-1),MitoTotalInt(1:tContact-1),'b-
x',time(tContact:end),MitoTotalInt(tContact:end),'r-x')
title('Mito Total Intensity')


% figure;
subplot(3,3,2);
%plot(time,CaTotalInt)
plot(time(1:tContact-1),CaTotalInt(1:tContact-1),'b-
x',time(tContact:end),CaTotalInt(tContact:end),'r-x')
title('Calcium Total Intensity')

subplot(3,3,4);
%plot(time,CellArea1,time,CellArea2);
plot(time(tContact:end),CellArea1(tContact:end),'r-
x',time(tContact:end),CellArea2(tContact:end),'r:x',...
     time(1:tContact-1),CellArea1(1:tContact-1),'b-x',time(1:tContact-
1),CellArea2(1:tContact-1),'b:x')
title('Cell Size')
legend('Intensity Weighted','Maximum Projection')


%figure;
subplot(3,3,5);
%plot(time,CellEccentr1,time,CellEccentr2);
plot(time(tContact:end),CellEccentr1(tContact:end),'r-
x',time(tContact:end),CellEccentr2(tContact:end),'r:x',...
     time(1:tContact-1),CellEccentr1(1:tContact-1),'b-
x',time(1:tContact-1),CellEccentr2(1:tContact-1),'b:x')
title('Cell Eccentricity')
legend('Intensity Weighted','Maximum Projection')


figure;
%plot(time,Moment3DBoundG./Moment3DG);
%plot(time,MeanCalcMOI3DAllPixelG,time,MeanMitoMOI3DG);
subplot(3,3,9);
%plot(time,IntensityBoundG)
p4Post9=plot(time(tContact:end),IntenOutHalfFractR(tContact:end),'r-
x',time(tContact:end),IntenOutHalfFractG(tContact:end),'b-
x',time(tContact:end),IntenOutHalfFractR0(tContact:end),'m-
x',time(tContact:end),IntenOutHalfFractG0(tContact:end),'c-x');
hold on
p4Pre9=plot(time(1:tContact-1),IntenOutHalfFractR(1:tContact-
1),'r:x',time(1:tContact-1),IntenOutHalfFractG(1:tContact-
1),'b:x',time(1:tContact-1),IntenOutHalfFractR0(1:tContact-
1),'m:x',time(1:tContact-1),IntenOutHalfFractG0(1:tContact-1),'c:x');
legend(p4Post9,'MiC','CaC','CMiC','CCaC','Location','best');
%plot(time,IntensityBoundG./CaTotalInt,time,sizeBoundG./CellVolume);
title('Fraction of Mito Intensity in Outter Half of Diameter')
```

```
% subplot(3,3,9);
% %plot(time,IntensityBoundG)
% pCalPost5=plot(time(tContact:end),minDistSQ3DG(tContact:end),'r-
x',time(tContact:end),minDistSQ3DAllPixelG(tContact:end),'r:x');
% hold on
% pCalPre5=plot(time(1:tContact-1),minDistSQ3DG(1:tContact-1),'b-
x',time(1:tContact-1),minDistSQ3DAllPixelG(1:tContact-1),'b:x');
% legend(pCalPost5,'Mito','Calcium');
% %plot(time,IntensityBoundG./CaTotalInt,time,sizeBoundG./CellVolume);
% title('Minimum Radius Square')

subplot(3,3,8);
%plot(time,IntensityBoundG)
p4Post8=plot(time(tContact:end),MOIFractBoundR(tContact:end),'r-
x',time(tContact:end),MOIFractBoundG(tContact:end),'b-x');
hold on
p4Pre8=plot(time(1:tContact-1),MOIFractBoundR(1:tContact-
1),'r:x',time(1:tContact-1),MOIFractBoundG(1:tContact-1),'b:x');
legend(p4Post8,'Mito C on Ca','Ca C on Ca');
%plot(time,IntensityBoundG./CaTotalInt,time,sizeBoundG./CellVolume);
title('Boundary/Total MOI Fraction')


%plot(time,IntenFractBoundR,time,sizeBoundR./sizeAllR,time,sizeBoundG./
CellVolume);
subplot(3,3,7);
%plot(time,IntensityBoundG)
p4Post7=plot(time(tContact:end),IntenFractBoundR(tContact:end),'r-
x',time(tContact:end),SizeFractBoundR(tContact:end),'m-
x',time(tContact:end),IntenFractBoundG(tContact:end),'b-
x',time(tContact:end),SizeFractBoundG(tContact:end),'c-x');
hold on
p4Pre7=plot(time(1:tContact-1),IntenFractBoundR(1:tContact-
1),'r:x',time(1:tContact-1),SizeFractBoundR(1:tContact-
1),'m:x',time(1:tContact-1),IntenFractBoundG(1:tContact-
1),'b:x',time(1:tContact-1),SizeFractBoundG(1:tContact-1),'c:x');
legend(p4Post7,'Mito Intensity','Mito Size','Caclium
Intensity','Caclium Size','Location','best');
%plot(time,IntensityBoundG./CaTotalInt,time,sizeBoundG./CellVolume);
title('Boundary/Total Intensity or Size Fraction')


%plot(time,MeanCalcMOI3DAllPixelG,time,MeanMitoMOI3DG);
subplot(3,3,2);
%plot(time,IntensityBoundG)
p4Post2=plot(time(tContact:end),MeanCalcMOI3DAllPixelG(tContact:end),'b
-x',time(tContact:end),MeanMitoMOI3DRtoG(tContact:end),'r-x');
hold on
p4Pre2=plot(time(1:tContact-1),MeanCalcMOI3DAllPixelG(1:tContact-
1),'b:x',time(1:tContact-1),MeanMitoMOI3DRtoG(1:tContact-1),'r:x');
legend(p4Post2,'Ca C on Ca','Mito C on Ca');
%plot(time,IntensityBoundG./CaTotalInt,time,sizeBoundG./CellVolume);
title('Mean Pan Cell 3D MOI')
```

```
subplot(3,3,5);
%plot(time,IntensityBoundG)
p4Post5=plot(time(tContact:end),MeanCalcMOI3DBoundG(tContact:end),'b-
x',time(tContact:end),MeanMitoMOI3DBoundRtoG(tContact:end),'r-x');
hold on
p4Pre5=plot(time(1:tContact-1),MeanCalcMOI3DBoundG(1:tContact-
1),'b:x',time(1:tContact-1),MeanMitoMOI3DBoundRtoG(1:tContact-
1),'r:x');
legend(p4Post5,'Ca C on Ca','Mito C on Ca');
%plot(time,IntensityBoundG./CaTotalInt,time,sizeBoundG./CellVolume);
title('Mean Boundary 3D MOI')

%subplot(2,3,1);
%plot(time,CaTotalInt)
% plot(time(1:tContact-1),EffMeanIntBoundG(1:tContact-1),'b-
x',time(tContact:end),EffMeanIntBoundG(tContact:end),'r-x');
% title('Mean Effective Intensity of Calcium at Boundary');


subplot(3,3,1);
%plot(time,CaTotalInt)
plot(time(1:tContact-1),CaTotalInt(1:tContact-1),'b-
x',time(tContact:end),CaTotalInt(tContact:end),'r-x');
title('Total Intensity of Calcium');

subplot(3,3,4);
%plot(time,CaTotalInt)
plot(time(1:tContact-1),IntensityBoundG(1:tContact-
1),'b:x',time(tContact:end),IntensityBoundG(tContact:end),'r:x');
title('Boundary Intensity of Calcium');

% subplot(3,3,2);
% %plot(time,CalcMOI3DBoundG)
% plot(time(1:tContact-1),CalcMOI3DBoundG(1:tContact-1),'b-
x',time(tContact:end),CalcMOI3DBoundG(tContact:end),'r-x');
% title('Total 3D Moment of Inertia of Calcium Boundary Intensity');


% subplot(2,3,6);
% %plot(time,totalRadSQ3DBoundG)
% plot(time(1:tContact-1),totalRadSQ3DBoundG(1:tContact-1),'b-
x',time(tContact:end),totalRadSQ3DBoundG(tContact:end),'r-x');
% title('Total 3D Radius Square of Calcium Boundary Intensity');

% subplot(3,3,3);
% %plot(time,totalRadSQ3DBoundG)
% plot(time(1:tContact-1),EffMeanIntBoundG(1:tContact-1),'b-
x',time(tContact:end),EffMeanIntBoundG(tContact:end),'r-x');
% title('Effective Calcium Boundary Intensity');

subplot(3,3,6);
%plot(time,MeanCalcMOI3DBoundG)
%plot(time(1:tContact-1),MeanCalcMOI3DBoundG(1:tContact-1),'b-
x',time(tContact:end),MeanCalcMOI3DBoundG(tContact:end),'r-x');
```

```
pCalPost6=plot(time(tContact:end),MeanCalcMOI3DBoundG(tContact:end),'c-
x',time(tContact:end),MeanCalcMOI3DAllPixelG(tContact:end),'b-
x',time(tContact:end),meanDistSQ3DAllPixelG(tContact:end),'r-
x',time(tContact:end),medianDistSQ3DAllPixelG(tContact:end),'m-x');
hold on
pCalPre6=plot(time(1:tContact-1),MeanCalcMOI3DBoundG(1:tContact-
1),'c:x',time(1:tContact-1),MeanCalcMOI3DAllPixelG(1:tContact-
1),'b:x',time(1:tContact-1),meanDistSQ3DAllPixelG(1:tContact-
1),'r:x',time(1:tContact-1),medianDistSQ3DAllPixelG(1:tContact-
1),'m:x');
legend(pCalPost6,'Boundary Weighted','Mean Weighted','Mean','Median');
%plot(time,IntensityBoundG./CaTotalInt,time,sizeBoundG./CellVolume);
%title('Boundary/Total Intensity or Size Fraction')
title('3D MOI of Calcium by Category')

subplot(3,3,3);
%plot(time,MeanCalcMOI3DBoundG)
%plot(time(1:tContact-1),MeanCalcMOI3DBoundG(1:tContact-1),'b-
x',time(tContact:end),MeanCalcMOI3DBoundG(tContact:end),'r-x');
pCalPost7=plot(time(tContact:end),MeanMitoMOI3DBoundRtoG(tContact:end),
'c-x',time(tContact:end),MeanMitoMOI3DRtoG(tContact:end),'b-
x',time(tContact:end),meanDistSQ3DG(tContact:end),'r-
x',time(tContact:end),medianDistSQ3DG(tContact:end),'m-x');
hold on
pCalPre7=plot(time(1:tContact-1),MeanMitoMOI3DBoundRtoG(1:tContact-
1),'c:x',time(1:tContact-1),MeanMitoMOI3DRtoG(1:tContact-
1),'b:x',time(1:tContact-1),meanDistSQ3DG(1:tContact-
1),'r:x',time(1:tContact-1),medianDistSQ3DG(1:tContact-1),'m:x');
legend(pCalPost7,'Boundary Weighted','Mean Weighted','Mean','Median');
%plot(time,IntensityBoundG./CaTotalInt,time,sizeBoundG./CellVolume);
%title('Boundary/Total Intensity or Size Fraction')
title('3D MOI of Mito by Category')



% subplot(3,3,6);
% %plot(time,IntensityBoundG)
%
pCalPost2=plot(time(tContact:end),IntensityBoundG(tContact:end)./CaTota
lInt(tContact:end),'r-
x',time(tContact:end),sizeBoundG(tContact:end)./CellVolume(tContact:end
),'r:x');
% hold on
% pCalPre2=plot(time(1:tContact-1),IntensityBoundG(1:tContact-
1)./CaTotalInt(1:tContact-1),'b-x',time(1:tContact-
1),sizeBoundG(1:tContact-1)./CellVolume(1:tContact-1),'b:x');
% legend(pCalPost2,'Fraction of Intensity','Fraction of Size');
% %plot(time,IntensityBoundG./CaTotalInt,time,sizeBoundG./CellVolume);
% title('Fraction Intensity vs. Area of Calcium at Boundary')




% subplot(3,3,9);
```

```
% %plot(time,CellArea1,time,CellArea2);
% p1=plot(time(tContact:end),Moment3DBoundG(tContact:end),'r-
x',time(tContact:end),Moment3DBoundR(tContact:end),'r:x');
% hold on
% p2=plot(time(1:tContact-1),Moment3DBoundG(1:tContact-1),'b-
x',time(1:tContact-1),Moment3DBoundR(1:tContact-1),'b:x');
% title('Total Boundary Intensity')
% legend(p1,'Green Centroid','Red Centroid')
%
% subplot(3,3,9);
% %plot(time,CellArea1,time,CellArea2);
% plot(time(tContact:end),IntenFractBound(tContact:end),'r-
x',time(tContact:end),IntenFractBound(tContact:end),'r:x',...
%      time(1:tContact-1),IntenFractBound(1:tContact-1),'b-
x',time(1:tContact-1),IntenFractBound(1:tContact-1),'b:x')
% title('Total Boundary Mito 3D Moment of Inertia')
% legend('Green','Red')
%
% subplot(3,3,9);
% %plot(time,CellArea1,time,CellArea2);
% plot(time(tContact:end),Moment3DBoundG(tContact:end),'r-
x',time(tContact:end),Moment3DBoundR(tContact:end),'r:x',...
%      time(1:tContact-1),Moment3DBoundG(1:tContact-1),'b-
x',time(1:tContact-1),Moment3DBoundR(1:tContact-1),'b:x')
% title('Total Boundary Mito 3D Moment of Inertia')
% legend('Green','Red')
figure;
subplot(3,3,9);
%plot(time,CellArea1,time,CellArea2);
plot(time(tContact:end),MOI3DBoundRtoG(tContact:end),'b-
x',time(tContact:end),MOI3DBoundRtoR(tContact:end),'r-x',...
     time(1:tContact-1),MOI3DBoundRtoG(1:tContact-
1),'b:x',time(1:tContact-1),MOI3DBoundRtoR(1:tContact-1),'r:x')
title('Total Boundary Mito 3D Moment of Inertia')
legend('C on Ca','C on Mito')


subplot(3,3,8);
%plot(time,CellArea1,time,CellArea2);
plot(time(tContact:end),totalRadSQ3DBoundRtoG(tContact:end),'b-
x',time(tContact:end),totalRadSQ3DBoundRtoR(tContact:end),'r-x',...
     time(1:tContact-1),totalRadSQ3DBoundRtoG(1:tContact-
1),'b:x',time(1:tContact-1),totalRadSQ3DBoundRtoR(1:tContact-1),'r:x')
title('Total Boundary Mito 3D Radius Square')
legend('C on Ca','C on Mito')


subplot(3,3,7);
%plot(time,CellArea1,time,CellArea2);
plot(time(tContact:end),MeanMitoMOI3DBoundRtoG(tContact:end),'b-
x',time(tContact:end),MeanMitoMOI3DBoundRtoR(tContact:end),'r-x',...
     time(1:tContact-1),MeanMitoMOI3DBoundRtoG(1:tContact-
1),'b:x',time(1:tContact-1),MeanMitoMOI3DBoundRtoR(1:tContact-1),'r:x')
title('Mean Boundary Mito 3D Moment of Inertia')
legend('C on Ca','C on Mito')
```

```
subplot(3,3,6);
%plot(time,CellArea1,time,CellArea2);
plot(time(tContact:end),MOI3DRtoG(tContact:end),'b-
x',time(tContact:end),MOI3DRtoR(tContact:end),'r-x',...
     time(1:tContact-1),MOI3DRtoG(1:tContact-1),'b:x',time(1:tContact-
1),MOI3DRtoR(1:tContact-1),'r:x')
title('Total 3D Mito Moment of Inertia')
legend('C on Ca','C on Mito')


subplot(3,3,5);
%plot(time,CellArea1,time,CellArea2);
plot(time(tContact:end),totalRadSQ3DRtoG(tContact:end),'b-
x',time(tContact:end),totalRadSQ3DRtoR(tContact:end),'r-x',...
     time(1:tContact-1),totalRadSQ3DRtoG(1:tContact-
1),'b:x',time(1:tContact-1),totalRadSQ3DRtoR(1:tContact-1),'r:x')
title('Total 3D Radius Square')
legend('C on Ca','C on Mito')


subplot(3,3,4);
%plot(time,CellArea1,time,CellArea2);
plot(time(tContact:end),MeanMitoMOI3DRtoG(tContact:end),'b-
x',time(tContact:end),MeanMitoMOI3DRtoR(tContact:end),'r-x',...
     time(1:tContact-1),MeanMitoMOI3DRtoG(1:tContact-
1),'b:x',time(1:tContact-1),MeanMitoMOI3DRtoR(1:tContact-1),'r:x')
title('Mean 3D Mito Moment of Inertia')
legend('C on Ca','C on Mito')


subplot(3,3,1);
%plot(time,CellArea1,time,CellArea2);
plot(time(tContact:end),MeanMitoMOI2DRtoG(tContact:end),'b-
x',time(tContact:end),MeanMitoMOI2DRtoR(tContact:end),'r-x',...
     time(1:tContact-1),MeanMitoMOI2DRtoG(1:tContact-
1),'b:x',time(1:tContact-1),MeanMitoMOI2DRtoR(1:tContact-1),'r:x')
title('Mean Mito 2D Moment of Inertia')
legend('C on Ca','C on Mito')


subplot(3,3,2);
%plot(time,CellArea1,time,CellArea2);
plot(time(tContact:end),TotalRadSQ2DRtoG(tContact:end),'b-
x',time(tContact:end),TotalRadSQ2DRtoR(tContact:end),'r-x',...
     time(1:tContact-1),TotalRadSQ2DRtoG(1:tContact-
1),'b:x',time(1:tContact-1),TotalRadSQ2DRtoR(1:tContact-1),'r:x')
title('Total 2D Radius Square')
legend('C on Ca','C on Mito')


subplot(3,3,3);
%plot(time,CellArea1,time,CellArea2);
plot(time(tContact:end),TotalMitoMOI2DRtoG(tContact:end),'b-
x',time(tContact:end),TotalMitoMOI2DRtoR(tContact:end),'r-x',...
```

```
     time(1:tContact-1),TotalMitoMOI2DRtoG(1:tContact-
1),'b:x',time(1:tContact-1),TotalMitoMOI2DRtoR(1:tContact-1),'r:x')
title('Total 2D Mito Moment of Inertia')
legend('Green','Red')

% subplot(2,2,1);
% %plot(time,CaTotalInt)
% plot(time(1:tContact-1),CaTotalInt(1:tContact-1),'b-
x',time(tContact:end),CaTotalInt(tContact:end),'r-x')
% title('Calcium Total Intensity')


figure;
%figure;
subplot(2,3,3);
%plot(time,projPos(3,:),time,projNeg(3,:))
plot(time(1:tContact-1),projPos2(3,(1:tContact-1)),'b-
x',time(tContact:end),projPos2(3,(tContact:end)),'r-x',...
     time(1:tContact-1),projNeg2(3,(1:tContact-
1)),'b:x',time(tContact:end),projNeg2(3,(tContact:end)),'r:x')
title('Total Intensity Weighted Projection')

% %figure;
subplot(2,3,1);
%plot(time,projPos(1,:),time,projNeg(1,:))
plot(time(1:tContact-1),projPos2(1,(1:tContact-1)),'b-
x',time(tContact:end),projPos2(1,(tContact:end)),'r-x',...
     time(1:tContact-1),projNeg2(1,(1:tContact-1)),'b--
x',time(tContact:end),projNeg2(1,(tContact:end)),'r--x')
title('Total Projection')

%figure;
subplot(2,3,6);
%plot(time,projPos(3,:)./MitoTotalInt,time,projNeg(3,:)./MitoTotalInt)
plot(time(1:tContact-1),projPosMean(1:tContact-1),'b-
x',time(tContact:end),projPosMean(tContact:end),'r-x',...
     time(1:tContact-1),projNegMean(1:tContact-
1),'b:x',time(tContact:end),projNegMean(tContact:end),'r:x')
title('Mean Intensity Weighted Projection')

%figure;
subplot(2,3,5);
%plot(time,projPos(3,:),time,projNeg(3,:))
plot(time(1:tContact-1),projPosFractWeighted(1:tContact-1),'b-
x',time(tContact:end),projPosFractWeighted(tContact:end),'r-x',...
     time(1:tContact-1),projNegFractWeighted(1:tContact-
1),'b:x',time(tContact:end),projNegFractWeighted(tContact:end),'r:x')
title('Intensity Fraction Weighted Projection')

% figure;
subplot(2,3,4);
%plot(time,projPos(3,:),time,projNeg(3,:))
plot(time(1:tContact-1),(projPos2(3,(1:tContact-
1))+projNeg2(3,(1:tContact-1)))./MitoTotalInt(1:tContact-1),'b-
```

```
x',time(tContact:end),(projPos2(3,(tContact:end))+projNeg2(3,(tContact:
end)))./MitoTotalInt(tContact:end),'r-x')
title('Mean Net Fraction Weighted Projection')

%figure;
subplot(2,3,2);
%plot(time,projPos(2,:)./MitoTotalInt,time,projNeg(2,:)./MitoTotalInt)
plot(time(1:tContact-1),projPosFract(1:tContact-1),'b-
x',time(tContact:end),projPosFract(tContact:end),'r-x',...
     time(1:tContact-1),projNegFract(1:tContact-
1),'b:x',time(tContact:end),projNegFract(tContact:end),'r:x');
title('Projection Fraction')

% figure;
% plot(time,projPos(1,:),time,projNeg(1,:))
% title('Total Projection')
%
% figure;
% plot(time,projPos(2,:),time,projNeg(2,:))
% title('Projection')

% figure
% %plot(time,cellDistWeighted)
% plot(time(1:tContact-1),cellDistWeighted(1:tContact-1),'b-
x',time(tContact:end),cellDistWeighted(tContact:end),'r-x')
% title('Cell Distance Weighted')




% figure;
% subplot(2,3,4);
% %plot(time,MeanMitoMOI)
% plot(time(1:tContact-1),MeanMitoMOI2DRtoR(1:tContact-1),'b-
x',time(tContact:end),MeanMitoMOI2DRtoR(tContact:end),'r-x')
% title('Mean Mito Moment of Inertia Red')

% figure;
% %plot(time,TotalRadSQ)
% plot(time(1:tContact-1),TotalRadSQR(1:tContact-1),'b-
x',time(tContact:end),TotalRadSQR(tContact:end),'r-x')
% title('Total Radius Square')

% figure;
% %plot(time,EffMeanInt)
% plot(time(1:tContact-1),EffMeanIntR(1:tContact-1),'b-
x',time(tContact:end),EffMeanIntR(tContact:end),'r-x')
% title('Effective Mean Intensity')

% figure;
% subplot(2,3,5);
% %plot(time,MeanMitoMOI)
% plot(time(1:tContact-1),MeanMitoMOI2DRtoG(1:tContact-1),'b-
x',time(tContact:end),MeanMitoMOI2DRtoG(tContact:end),'r-x')
% title('Mean Mito Moment of Inertia Green')
```

```
% figure;
% %plot(time,TotalRadSQ)
% plot(time(1:tContact-1),TotalRadSQG(1:tContact-1),'b-
x',time(tContact:end),TotalRadSQG(tContact:end),'r-x')
% title('Total Radius Square')
%
% figure;
% %plot(time,EffMeanInt)
% plot(time(1:tContact-1),EffMeanIntG(1:tContact-1),'b-
x',time(tContact:end),EffMeanIntG(tContact:end),'r-x')
% title('Effective Mean Intensity')

% figure;
% plot(time,sum(MomentR,1)-
sum(totalAxDistSQ,1).*sum(totalIntensityZplane(:,:,1),1))
% title('Mito Moment of Inertia - Total Radius Square x Mito Total
Intensity')



% figure;
% plot(time,Angle)
% title('Angle')
% figure
% plot(time,cellDistance)
% title('Cell Distance')
% figure;
% plot(time,sProjection)
% title('Scalar Projection')
%
[maxMeanCalciumMOIG,nMaxAllPixelG]=max(MeanCalcMOI3DAllPixelG(tContact:
end));
nMaxAllPixelG=nMaxAllPixelG+tContact-1;
Red=max(M(:,:,:,channelR,nMaxAllPixelG),[],3)>thresholdR;
Green=max(M(:,:,:,channelG,nMaxAllPixelG),[],3)>thresholdG;
Blue=max(M(:,:,:,channelB,nMaxAllPixelG),[],3)>thresholdB;
RGB(:,:,1)= Red;
RGB(:,:,2)= Green;
RGB(:,:,3)= Blue;
% figure;
% imshow(RGB);
% hold on
% plot(Centroids(1,15,1)/xySpace,Centroids(2,15,1)/xySpace,
'm+',Centroids(1,15,2)/xySpace,Centroids(2,15,2)/xySpace,
'mx',Centroids(1,15,3)/xySpace,Centroids(2,15,3)/xySpace, 'm*')
% title('centroids')
figure;
subplot(2,5,1);
imshow(RGB);
hold on
plot(CentroidWeighted(1,nMaxAllPixelG,1)/xySpace,CentroidWeighted(2,nMa
xAllPixelG,1)/xySpace,
```

```
'm+',CentroidWeighted(1,nMaxAllPixelG,2)/xySpace,CentroidWeighted(2,nMa
xAllPixelG,2)/xySpace,
'mx',CentroidWeighted(1,nMaxAllPixelG,3)/xySpace,CentroidWeighted(2,nMa
xAllPixelG,3)/xySpace, 'm*')
title1=title(['Max Calcium MOI at Frame ',num2str(nMaxAllPixelG)]);
title1.Color = 'green';



[minMeanCalciumMOIG,nMinAllPixelG]=min(MeanCalcMOI3DAllPixelG(tContact:
end));
nMinAllPixelG=nMinAllPixelG+tContact-1;
Red=max(M(:,:,:,channelR,nMinAllPixelG),[],3)>thresholdR;
Green=max(M(:,:,:,channelG,nMinAllPixelG),[],3)>thresholdG;
Blue=max(M(:,:,:,channelB,nMinAllPixelG),[],3)>thresholdB;
RGB(:,:,1)= Red;
RGB(:,:,2)= Green;
RGB(:,:,3)= Blue;
% figure;
% imshow(RGB);
% hold on
% plot(Centroids(1,15,1)/xySpace,Centroids(2,15,1)/xySpace,
'm+',Centroids(1,15,2)/xySpace,Centroids(2,15,2)/xySpace,
'mx',Centroids(1,15,3)/xySpace,Centroids(2,15,3)/xySpace, 'm*')
% title('centroids')
subplot(2,5,2);
imshow(RGB);
hold on
plot(CentroidWeighted(1,nMinAllPixelG,1)/xySpace,CentroidWeighted(2,nMi
nAllPixelG,1)/xySpace,
'm+',CentroidWeighted(1,nMinAllPixelG,2)/xySpace,CentroidWeighted(2,nMi
nAllPixelG,2)/xySpace,
'mx',CentroidWeighted(1,nMinAllPixelG,3)/xySpace,CentroidWeighted(2,nMi
nAllPixelG,3)/xySpace, 'm*')
title1=title(['Min Calcium MOI at Frame ',num2str(nMinAllPixelG)]);
title1.Color = 'green';



% [maxMeanMitoMOIR,nMaxR]=max(MeanMitoMOI2DRtoR(tContact:end));
% Red=max(M(:,:,:,channelR,nMaxR),[],3)>thresholdR;
% Green=max(M(:,:,:,channelG,nMaxR),[],3)>thresholdG;
% Blue=max(M(:,:,:,channelB,nMaxR),[],3)>thresholdB;
% RGB(:,:,1)= Red;
% RGB(:,:,2)= Green;
% RGB(:,:,3)= Blue;
% % figure;
% % imshow(RGB);
% % hold on
% % plot(Centroids(1,15,1)/xySpace,Centroids(2,15,1)/xySpace,
'm+',Centroids(1,15,2)/xySpace,Centroids(2,15,2)/xySpace,
'mx',Centroids(1,15,3)/xySpace,Centroids(2,15,3)/xySpace, 'm*')
% % title('centroids')
%
% subplot(2,4,1);
% imshow(RGB);
```

```
% hold on
%
plot(CentroidWeighted(1,nMaxR,1)/xySpace,CentroidWeighted(2,nMaxR,1)/xy
Space,
'm+',CentroidWeighted(1,nMaxR,2)/xySpace,CentroidWeighted(2,nMaxR,2)/xy
Space,
'mx',CentroidWeighted(1,nMaxR,3)/xySpace,CentroidWeighted(2,nMaxR,3)/xy
Space, 'm*')
% title1=title(['Maximum Mito 2D MOI Red at Frame ',num2str(nMaxR)]);
% title1.Color = 'red';

[maxMeanMitoMOIR,nMaxR]=max(MeanMitoMOI3DRtoR(tContact:end));
nMaxR=nMaxR+tContact-1;
Red=max(M(:,:,:,channelR,nMaxR),[],3)>thresholdR;
Green=max(M(:,:,:,channelG,nMaxR),[],3)>thresholdG;
Blue=max(M(:,:,:,channelB,nMaxR),[],3)>thresholdB;
RGB(:,:,1)= Red;
RGB(:,:,2)= Green;
RGB(:,:,3)= Blue;
% % figure;
% % imshow(RGB);
% % hold on
% % plot(Centroids(1,15,1)/xySpace,Centroids(2,15,1)/xySpace,
'm+',Centroids(1,15,2)/xySpace,Centroids(2,15,2)/xySpace,
'mx',Centroids(1,15,3)/xySpace,Centroids(2,15,3)/xySpace, 'm*')
% % title('centroids')
subplot(2,5,3);
imshow(RGB);
hold on
plot(CentroidWeighted(1,nMaxR,1)/xySpace,CentroidWeighted(2,nMaxR,1)/xy
Space,
'm+',CentroidWeighted(1,nMaxR,2)/xySpace,CentroidWeighted(2,nMaxR,2)/xy
Space,
'mx',CentroidWeighted(1,nMaxR,3)/xySpace,CentroidWeighted(2,nMaxR,3)/xy
Space, 'm*')
title1=title(['Max Mito 3D MOI Red at Frame ',num2str(nMaxR)]);
title1.Color = 'red';

[minMeanMitoMOIR,nMinR]=min(MeanMitoMOI3DRtoR(tContact:end));
nMinR=nMinR+tContact-1;
Red=max(M(:,:,:,channelR,nMinR),[],3)>thresholdR;
Green=max(M(:,:,:,channelG,nMinR),[],3)>thresholdG;
Blue=max(M(:,:,:,channelB,nMinR),[],3)>thresholdB;
RGB(:,:,1)= Red;
RGB(:,:,2)= Green;
RGB(:,:,3)= Blue;
% % figure;
% % imshow(RGB);
% % hold on
% % plot(Centroids(1,15,1)/xySpace,Centroids(2,15,1)/xySpace,
'm+',Centroids(1,15,2)/xySpace,Centroids(2,15,2)/xySpace,
'mx',Centroids(1,15,3)/xySpace,Centroids(2,15,3)/xySpace, 'm*')
% % title('centroids')
subplot(2,5,4);
imshow(RGB);
hold on
```

```
plot(CentroidWeighted(1,nMinR,1)/xySpace,CentroidWeighted(2,nMinR,1)/xy
Space,
'm+',CentroidWeighted(1,nMinR,2)/xySpace,CentroidWeighted(2,nMinR,2)/xy
Space,
'mx',CentroidWeighted(1,nMinR,3)/xySpace,CentroidWeighted(2,nMinR,3)/xy
Space, 'm*')
title1=title(['Min Mito 3D MOI Red at Frame ',num2str(nMinR)]);
title1.Color = 'red';
%
% [minMeanMitoMOIR,nMinR]=min(MeanMitoMOI2DRtoR(tContact:end));
% Red=max(M(:,:,:,channelR,nMinR),[],3)>thresholdR;
% Green=max(M(:,:,:,channelG,nMinR),[],3)>thresholdG;
% Blue=max(M(:,:,:,channelB,nMinR),[],3)>thresholdB;
% RGB(:,:,1)= Red;
% RGB(:,:,2)= Green;
% RGB(:,:,3)= Blue;


[maxEccentr1,nCellEccentr1]=max(CellEccentr1(tContact:end));
nCellEccentr1=nCellEccentr1+tContact-1;
Red=max(M(:,:,:,channelR,nCellEccentr1),[],3)>thresholdR;
Green=max(M(:,:,:,channelG,nCellEccentr1),[],3)>thresholdG;
Blue=max(M(:,:,:,channelB,nCellEccentr1),[],3)>thresholdB;
RGB(:,:,1)= Red;
RGB(:,:,2)= Green;
RGB(:,:,3)= Blue;

subplot(2,5,5);
imshow(RGB);
hold on
plot(CentroidWeighted(1,nCellEccentr1,1)/xySpace,CentroidWeighted(2,nCe
llEccentr1,1)/xySpace,
'm+',CentroidWeighted(1,nCellEccentr1,2)/xySpace,CentroidWeighted(2,nCe
llEccentr1,2)/xySpace,
'mx',CentroidWeighted(1,nCellEccentr1,3)/xySpace,CentroidWeighted(2,nCe
llEccentr1,3)/xySpace, 'm*')
title2=title(['Max Cell Eccentricity at Frame
',num2str(nCellEccentr1)]);
title2.Color = 'black';


[maxCellArea2,nCellArea2]=max(CellArea2(tContact:end));
nCellArea2=nCellArea2+tContact-1;
Red=max(M(:,:,:,channelR,nCellArea2),[],3)>thresholdR;
Green=max(M(:,:,:,channelG,nCellArea2),[],3)>thresholdG;
Blue=max(M(:,:,:,channelB,nCellArea2),[],3)>thresholdB;
RGB(:,:,1)= Red;
RGB(:,:,2)= Green;
RGB(:,:,3)= Blue;
subplot(2,5,10);
imshow(RGB);
hold on
plot(CentroidWeighted(1,nCellArea2,1)/xySpace,CentroidWeighted(2,nCellA
rea2,1)/xySpace,
'm+',CentroidWeighted(1,nCellArea2,2)/xySpace,CentroidWeighted(2,nCellA
rea2,2)/xySpace,
```

```
'mx',CentroidWeighted(1,nCellArea2,3)/xySpace,CentroidWeighted(2,nCellA
rea2,3)/xySpace, 'm*')
title2=title(['Max Cell Size at Frame ',num2str(nCellArea2),' is
',num2str(maxCellArea2)]);
title2.Color = 'black';



[maxprojPosFractWeighted,nprojPosFractWeighted]=max(projPosFractWeighte
d(tContact:end));
nprojPosFractWeighted=nprojPosFractWeighted+tContact-1;
Red=max(M(:,:,:,channelR,nprojPosFractWeighted),[],3)>thresholdR;
Green=max(M(:,:,:,channelG,nprojPosFractWeighted),[],3)>thresholdG;
Blue=max(M(:,:,:,channelB,nprojPosFractWeighted),[],3)>thresholdB;
RGB(:,:,1)= Red;
RGB(:,:,2)= Green;
RGB(:,:,3)= Blue;
subplot(2,5,6);
imshow(RGB);
hold on
plot(CentroidWeighted(1,nprojPosFractWeighted,1)/xySpace,CentroidWeight
ed(2,nprojPosFractWeighted,1)/xySpace,
'm+',CentroidWeighted(1,nprojPosFractWeighted,2)/xySpace,CentroidWeight
ed(2,nprojPosFractWeighted,2)/xySpace,
'mx',CentroidWeighted(1,nprojPosFractWeighted,3)/xySpace,CentroidWeight
ed(2,nprojPosFractWeighted,3)/xySpace, 'm*')
title2=title(['Max Positive Projection at Frame
',num2str(nprojPosFractWeighted)]);
title2.Color = 'black';



[maxprojNegFractWeighted,nprojNegFractWeighted]=min(projNegFractWeighte
d(tContact:end));
nprojNegFractWeighted=nprojNegFractWeighted+tContact-1;
Red=max(M(:,:,:,channelR,nprojNegFractWeighted),[],3)>thresholdR;
Green=max(M(:,:,:,channelG,nprojNegFractWeighted),[],3)>thresholdG;
Blue=max(M(:,:,:,channelB,nprojNegFractWeighted),[],3)>thresholdB;
RGB(:,:,1)= Red;
RGB(:,:,2)= Green;
RGB(:,:,3)= Blue;
subplot(2,5,7);
imshow(RGB);
hold on
plot(CentroidWeighted(1,nprojNegFractWeighted,1)/xySpace,CentroidWeight
ed(2,nprojNegFractWeighted,1)/xySpace,
'm+',CentroidWeighted(1,nprojNegFractWeighted,2)/xySpace,CentroidWeight
ed(2,nprojNegFractWeighted,2)/xySpace,
'mx',CentroidWeighted(1,nprojNegFractWeighted,3)/xySpace,CentroidWeight
ed(2,nprojNegFractWeighted,3)/xySpace, 'm*')
title2=title(['Max Negative Projection at Frame
',num2str(nprojNegFractWeighted)]);
title2.Color = 'black';
```

```
% figure;
% imshow(RGB);
% hold on
% plot(Centroids(1,15,1)/xySpace,Centroids(2,15,1)/xySpace,
'm+',Centroids(1,15,2)/xySpace,Centroids(2,15,2)/xySpace,
'mx',Centroids(1,15,3)/xySpace,Centroids(2,15,3)/xySpace, 'm*')
% title('centroids')
% figure;
% subplot(1,4,3);
% imshow(RGB);
% hold on
%
plot(CentroidWeighted(1,nMinR,1)/xySpace,CentroidWeighted(2,nMinR,1)/xy
Space,
'm+',CentroidWeighted(1,nMinR,2)/xySpace,CentroidWeighted(2,nMinR,2)/xy
Space,
'mx',CentroidWeighted(1,nMinR,3)/xySpace,CentroidWeighted(2,nMinR,3)/xy
Space, 'm*')
% title2=title(['centroids weighted at minimum MOI Red of frame
',num2str(nMinR)]);
% title2.Color = 'red';

% [maxMeanMitoMOIG,nMaxG]=max(MeanMitoMOI2DRtoG(tContact:end));
% Red=max(M(:,:,:,channelR,nMaxG),[],3)>thresholdR;
% Green=max(M(:,:,:,channelG,nMaxG),[],3)>thresholdG;
% Blue=max(M(:,:,:,channelB,nMaxG),[],3)>thresholdB;
% RGB(:,:,1)= Red;
% RGB(:,:,2)= Green;
% RGB(:,:,3)= Blue;
% % figure;
% % imshow(RGB);
% % hold on
% % plot(Centroids(1,15,1)/xySpace,Centroids(2,15,1)/xySpace,
'm+',Centroids(1,15,2)/xySpace,Centroids(2,15,2)/xySpace,
'mx',Centroids(1,15,3)/xySpace,Centroids(2,15,3)/xySpace, 'm*')
% % title('centroids')
% % figure;
% subplot(2,4,2);
% imshow(RGB);
% hold on
%
plot(CentroidWeighted(1,nMaxG,1)/xySpace,CentroidWeighted(2,nMaxG,1)/xy
Space,
'm+',CentroidWeighted(1,nMaxG,2)/xySpace,CentroidWeighted(2,nMaxG,2)/xy
Space,
'mx',CentroidWeighted(1,nMaxG,3)/xySpace,CentroidWeighted(2,nMaxG,3)/xy
Space, 'm*')
% title3=title(['Maximum Mito 2D MOI Green at Frame ',num2str(nMaxG)]);
% title3.Color = [0 0 1];



[maxMeanMitoMOIG,nMaxG]=max(MeanMitoMOI3DRtoG(tContact:end));
nMaxG=nMaxG+tContact-1;
Red=max(M(:,:,:,channelR,nMaxG),[],3)>thresholdR;
```

```
Green=max(M(:,:,:,channelG,nMaxG),[],3)>thresholdG;
Blue=max(M(:,:,:,channelB,nMaxG),[],3)>thresholdB;
RGB(:,:,1)= Red;
RGB(:,:,2)= Green;
RGB(:,:,3)= Blue;
% figure;
% imshow(RGB);
% hold on
% plot(Centroids(1,15,1)/xySpace,Centroids(2,15,1)/xySpace,
'm+',Centroids(1,15,2)/xySpace,Centroids(2,15,2)/xySpace,
'mx',Centroids(1,15,3)/xySpace,Centroids(2,15,3)/xySpace, 'm*')
% title('centroids')
% figure;
subplot(2,5,8);
imshow(RGB);
hold on
plot(CentroidWeighted(1,nMaxG,1)/xySpace,CentroidWeighted(2,nMaxG,1)/xy
Space,
'm+',CentroidWeighted(1,nMaxG,2)/xySpace,CentroidWeighted(2,nMaxG,2)/xy
Space,
'mx',CentroidWeighted(1,nMaxG,3)/xySpace,CentroidWeighted(2,nMaxG,3)/xy
Space, 'm*')
title3=title(['Max Mito 3D MOI Green at Frame ',num2str(nMaxG)]);
title3.Color = [0 0 1];



[minMeanMitoMOIG,nMinG]=min(MeanMitoMOI3DRtoG(tContact:end));
nMinG=nMinG+tContact-1;
Red=max(M(:,:,:,channelR,nMinG),[],3)>thresholdR;
Green=max(M(:,:,:,channelG,nMinG),[],3)>thresholdG;
Blue=max(M(:,:,:,channelB,nMinG),[],3)>thresholdB;
RGB(:,:,1)= Red;
RGB(:,:,2)= Green;
RGB(:,:,3)= Blue;

subplot(2,5,9);
imshow(RGB);
hold on
plot(CentroidWeighted(1,nMinG,1)/xySpace,CentroidWeighted(2,nMinG,1)/xy
Space,
'm+',CentroidWeighted(1,nMinG,2)/xySpace,CentroidWeighted(2,nMinG,2)/xy
Space,
'mx',CentroidWeighted(1,nMinG,3)/xySpace,CentroidWeighted(2,nMinG,3)/xy
Space, 'm*')
title3=title(['Min Mito 3D MOI Green at Frame ',num2str(nMinG)]);
title3.Color = [0 0 1];
% figure;
% imshow(RGB);
% hold on
% plot(Centroids(1,15,1)/xySpace,Centroids(2,15,1)/xySpace,
'm+',Centroids(1,15,2)/xySpace,Centroids(2,15,2)/xySpace,
'mx',Centroids(1,15,3)/xySpace,Centroids(2,15,3)/xySpace, 'm*')
% title('centroids')
% figure;
% subplot(1,4,4);
```

```
% imshow(RGB);
% hold on
%
plot(CentroidWeighted(1,nMinG,1)/xySpace,CentroidWeighted(2,nMinG,1)/xy
Space,
'm+',CentroidWeighted(1,nMinG,2)/xySpace,CentroidWeighted(2,nMinG,2)/xy
Space,
'mx',CentroidWeighted(1,nMinG,3)/xySpace,CentroidWeighted(2,nMinG,3)/xy
Space, 'm*')
% title4=title(['centroids weighted at minimum MOI Green of frame
',num2str(nMinG)]);
% title4.Color = [0 0 1];


DateString = datestr(datetime('now'));
%savedName = [FileName,' ',DateString,'.mat'];

save(savedName)
```

Appendix D.2.2 Generation of Various Forms of Datasets for Further Analysis

```
%%5/8/2017
%Luye He
%combine time frames to give various form of dataset
%and perform simple analysis tasks

%%
%%prepare workspace
close all
clearvars
BaseString='20160706_Test2_N';
peptideString = 'N';
extraName='';
InputString=[BaseString,'_P%d.tif',extraName,' by
MitoTrack_V3_ReadTiff.mat'];
vectorP=[1:8];
numP=size(vectorP,2);
timeInterval=30;
ds_all=[];
%% import data of all cells into the dataset
for iP=1:numP
    vectorP(iP)
    fileSelect = sprintf(InputString,vectorP(iP));
    load(fileSelect);
    disp(fileSelect)

    [peakFold,peakIndex]=max(NormalCaTotalInt(tContact:end));

AreaUnderCurve=sum((NormalCaTotalInt(tContact:end)>1).*NormalCaTotalInt
(tContact:end)-(NormalCaTotalInt(tContact:end)>1))*timeInterval/100;
    peakTime=timeInterval*(peakIndex-1);
    PosMitoWeightProj=projPos2(3,:);
    NegMitoWeightProj=projNeg2(3,:);
    PosMitoInt=projPos2(2,:);
    NegMitoInt=projNeg2(2,:);
    CellRad=CellDia2/2;
    ds_1 = mat2dataset(NormalCaTotalInt);
    ds_2 = mat2dataset(MeanMitoMOI3DRtoG);
    ds_3 = mat2dataset(MeanMitoMOI3DRtoR);
    ds_4 = mat2dataset(PosMitoWeightProj);
    ds_5 = mat2dataset(NegMitoWeightProj);
    ds_6 = mat2dataset(PosMitoInt);
    ds_7 = mat2dataset(NegMitoInt);
    ds_8 = mat2dataset(CellRad);
    ds_merge=[mat2dataset(vectorP(iP)),mat2dataset(peakFold),
mat2dataset(AreaUnderCurve), mat2dataset(peakTime),
mat2dataset(tContact), ds_1, ds_2, ds_3, ds_4, ds_5, ds_6,ds_7,ds_8];
    ds_all=[ds_all;ds_merge];
end
ds_all.Properties.VarNames{1} = 'cellNum';
%% final touch of the dataset by adding two description columns and
export
n = size(ds_all,1);
peptide = dataset(repmat(peptideString,n,1));
peptide.Properties.VarNames{1} = 'peptide';
```

```
file = dataset(repmat(BaseString,n,1));
file.Properties.VarNames{1} = 'file';
ds_all=[file,peptide,ds_all];
export(ds_all,'file',[BaseString,'_8features.csv'],'Delimiter',',');
%% dataset from individual experiment day
clearvars
ds_new1 =
dataset('File','20161011_Test1_N_8features.csv','Delimiter',',');
ds_new2 =
dataset('File','20161011_Test2_L_8features.csv','Delimiter',',');
ds_new3 =
dataset('File','20161014_Test2_L_8features.csv','Delimiter',',');
ds_new4 =
dataset('File','20161018_Test1_L_8features.csv','Delimiter',',');
ds_new5 =
dataset('File','20161018_Test2_Q_8features.csv','Delimiter',',');
ds_new6 =
dataset('File','20161021_Test1_N_8features.csv','Delimiter',',');
ds_new7 =
dataset('File','20161021_Test2_Q_8features.csv','Delimiter',',');
%%
ds_old1 =
dataset('File','20160910_Test2_L_8features.csv','Delimiter',',');
ds_old2 =
dataset('File','20160728_Test1_L_8features.csv','Delimiter',',');
ds_old3 =
dataset('File','20160728_Test2_L_8features.csv','Delimiter',',');
ds_old4 =
dataset('File','20160808_Test2_Y_8features.csv','Delimiter',',');
ds_old5 =
dataset('File','20160811_Test1_Y_8features.csv','Delimiter',',');
ds_old6 =
dataset('File','20160906_Test1_Y_8features.csv','Delimiter',',');
ds_old7 =
dataset('File','20160913_Test2_Y_8features.csv','Delimiter',',');
ds_old8 =
dataset('File','20160811_Test2_Q_8features.csv','Delimiter',',');
ds_old9 =
dataset('File','20160830_Test1_Q_8features.csv','Delimiter',',');
ds_old10 =
dataset('File','20160903_Test2_Q_8features.csv','Delimiter',',');
ds_old11 =
dataset('File','20160920_Test1_Q_8features.csv','Delimiter',',');
ds_old12 =
dataset('File','20160706_Test2_N_8features.csv','Delimiter',',');
ds_old13 =
dataset('File','20160827_Test1_N_8features.csv','Delimiter',',');
ds_old14 =
dataset('File','20160906_Test2_N_8features.csv','Delimiter',',');
ds_old15 =
dataset('File','20160910_Test1_N_8features.csv','Delimiter',',');
%% new dataset only
ds_combine_new =
[ds_new1;ds_new2;ds_new3;ds_new4;ds_new5;ds_new6;ds_new7];
ds_clean = ds_combine_new(~any(ismissing(ds_combine_new),2),:);
```

```
ds_clean =
ds_clean(ds_clean.tContact1==6|ds_clean.tContact1==7|ds_clean.tContact1
==8,:);
export(ds_clean,'file','newData_clean.csv','Delimiter',',');
%%
ds = dataset('File','newData_clean.csv','Delimiter',',');
p = ds_old15.Properties.VarNames(:);
ds=ds(:,p);
%% Combine all cell traces into one dataset
p = ds_old15.Properties.VarNames(:);
ds_combine_new =
[ds_new1;ds_new2;ds_new3;ds_new4;ds_new5;ds_new6;ds_new7];
ds_combine_all = [ds_combine_new(:,p);...

ds_old1(:,p);ds_old2(:,p);ds_old3(:,p);ds_old4(:,p);ds_old5(:,p);ds_old
6(:,p);ds_old7(:,p);...

ds_old8(:,p);ds_old9(:,p);ds_old10(:,p);ds_old11(:,p);ds_old12(:,p);ds_
old13(:,p);ds_old14(:,p);ds_old15(:,p)];
export(ds_combine_all,'file','allData.csv','Delimiter',',');
%% Reload the all cell dataset
ds = dataset('File','allData.csv','Delimiter',',');
ds_clean = ds(~any(ismissing(ds),2),:);
ds_clean =
ds_clean(ds_clean.tContact1==6|ds_clean.tContact1==7|ds_clean.tContact1
==8,:);
%%
export(ds_clean,'file','allData_clean.csv','Delimiter',',');
%% load all cell traces
ds = dataset('File','allData_clean.csv','Delimiter',',');
%% load new cell traces
ds_old15 =
dataset('File','20160910_Test1_N_8features.csv','Delimiter',',');
p = ds_old15.Properties.VarNames(:);
ds = dataset('File','newData_clean.csv','Delimiter',',');
ds=ds(:,p);
%% select time frames
startPT=1;
endPT=38;
timePT=endPT-startPT+1;
pCalInt= ds.Properties.VarNames(8+startPT-1:8+endPT-1);
pMitoMOIRtoG = ds.Properties.VarNames(46+startPT-1:46+endPT-1);
pMitoMOIRtoR = ds.Properties.VarNames(84+startPT-1:84+endPT-1);
pPosMitoWeightProj = ds.Properties.VarNames(122+startPT-1:122+endPT-1);
pNegMitoWeightProj = ds.Properties.VarNames(160+startPT-1:160+endPT-1);
pPosMitoInt = ds.Properties.VarNames(198+startPT-1:198+endPT-1);
pNegMitoInt = ds.Properties.VarNames(236+startPT-1:236+endPT-1);
pCellDia = ds.Properties.VarNames(274+startPT-1:274+endPT-1);

%% if sample balanced high and low cells
threshold=3;
ds_high=datasample(ds(ds.peakFold1>threshold,:),30);
ds_low=datasample(ds(ds.peakFold1<threshold,:),30);
ds=[ds_high;ds_low];
%% Divide cells by response types
%ds_clean.responseType = ds_clean.peakFold1 > 2.5;
%x=1:1:41;
```

```
% pCalInt= ds_clean.Properties.VarNames(7:47);
% pMitoMOIRtoG = ds_clean.Properties.VarNames(48:88);
% pMitoMOIRtoR = ds_clean.Properties.VarNames(89:129);
% pMitoPosProj = ds_clean.Properties.VarNames(130:170);
% pMitoNegProj = ds_clean.Properties.VarNames(171:211);
% pCellDia = ds_clean.Properties.VarNames(212:252);
%% Calculate pre-contact average size, choose normalize or not

n=size(ds,1);
doNormalize=1;
avgRad=ones(n,1);
peptideLabel=ones(n,1);

for i=1:n
    if doNormalize
        avgRad(i)=mean(double(ds(i,274:274+ds.tContact1(i)-2)));

    end
    if ds.peptide{i}=='N'
        peptideLabel(i)=0;
    elseif ds.peptide{i}=='Q'
        peptideLabel(i)=1;
    elseif ds.peptide{i}=='Y'
        peptideLabel(i)=2;
    elseif ds.peptide{i}=='L'
        peptideLabel(i)=3;
    end

end
test=[ds(:,2),dataset(peptideLabel)];
avgRadSquare=avgRad.*avgRad;
%% Define features
t=1:1:timePT;
peptide_matrix=repmat(peptideLabel,1,timePT);
CaInt_normal=double(ds(:,pCalInt));
MitoMOIRtoG_normal=double(ds(:,pMitoMOIRtoG))./repmat(avgRadSquare,1,ti
mePT);
MitoMOIRtoR_normal=double(ds(:,pMitoMOIRtoR))./repmat(avgRadSquare,1,ti
mePT);
MitoNetProj=(double(ds(:,pPosMitoWeightProj))+double(ds(:,pNegMitoWeigh
tProj)))./(double(ds(:,pPosMitoInt))+double(ds(:,pNegMitoInt)));
MitoNetProj_normal=MitoNetProj./repmat(avgRad,1,timePT);
MitoAbsProj=(double(ds(:,pPosMitoWeightProj))-
double(ds(:,pNegMitoWeightProj)))./(double(ds(:,pPosMitoInt))+double(ds
(:,pNegMitoInt)));
MitoAbsProj_normal=MitoAbsProj./repmat(avgRad,1,timePT);
MitoRatioProj=double(ds(:,pPosMitoWeightProj))./(double(ds(:,pPosMitoWe
ightProj))-double(ds(:,pNegMitoWeightProj)));
MitoRatioInt=double(ds(:,pPosMitoInt))./(double(ds(:,pNegMitoInt))+doub
le(ds(:,pPosMitoInt)));
%%
featureSet={CaInt_normal,MitoMOIRtoG_normal,MitoMOIRtoR_normal,MitoNetP
roj_normal,MitoAbsProj_normal,MitoRatioProj,MitoRatioInt};
```

```
%ylabelSet={'Normalized Calcium','MitoMOI on CaCentroid','MitoMOI on
MitoCentroid','MitoNetProjection','MitoAbsProjection','MitoProjectionRa
tio','MitoIntensityRatio'};
titleSet={'Normalized_Calcium','MitoMOI_on_CaCentroid','MitoMOI_on_Mito
Centroid','Mito_Net_Projection','Mito_Abs_Projection','Mito_Projection_
Ratio','Mito_Intensity_Ratio'};

title=[];
all=[];

for ii=1:size(featureSet,2)
    ii
    feature=featureSet{ii};
    total=[];
    for i=1:n
        i
        pre=ds.tContact1(i);
        sec1=mean(feature(i,1:pre-1));
        sec2=mean(feature(i,pre:pre+5));
        sec3=mean(feature(i,pre+6:pre+11));
        sec4=mean(feature(i,pre+12:pre+17));
        sec5=mean(feature(i,pre+18:pre+23));
        sec6=mean(feature(i,pre+24:end));
        test=[sec1,sec2,sec3,sec4,sec5,sec6];
        total=[total;test];
    end
    all=[all,total];

title=[title,strcat(titleSet(ii),'_',num2str(1)),strcat(titleSet(ii),'_
',num2str(2)),strcat(titleSet(ii),'_',num2str(3))...

,strcat(titleSet(ii),'_',num2str(4)),strcat(titleSet(ii),'_',num2str(5)
),strcat(titleSet(ii),'_',num2str(6))];
end

ds_blockAverage=mat2dataset(all);
ds_blockAverage.Properties.VarNames= title;
ds_blockAverage=[ds(:,1:7),ds_blockAverage];
%sprintf('PeakFold_Theshold_%d',threshold)

%%
export(ds_blockAverage,'file','allData_NormalizeRadius_blockAverage_reg
ular_addHead.csv','Delimiter',',');

%% if not doing the blocking
featureSet={CaInt_normal,MitoMOIRtoG_normal,MitoMOIRtoR_normal,MitoNetP
roj_normal,MitoAbsProj_normal,MitoRatioProj,MitoRatioInt};
%ylabelSet={'Normalized Calcium','MitoMOI on CaCentroid','MitoMOI on
MitoCentroid','MitoNetProjection','MitoAbsProjection','MitoProjectionRa
tio','MitoIntensityRatio'};
%titleSet={'Normalized_Calcium','MitoMOI_on_CaCentroid','MitoMOI_on_Mit
oCentroid','Mito_Net_Projection','Mito_Abs_Projection','Mito_Projection
_Ratio','Mito_Intensity_Ratio'};
titleSet={'NC','MC','MM','NP','AP','PR','IR'};
title2=[];
total2=[];
```

```
for ii=1:size(featureSet,2)
    ii
    feature=featureSet{ii};
    for i=1:timePT
        i

        total2=[total2,feature(:,i)];
        title2=[title2,strcat(titleSet(ii),num2str(i))]
    end
end

ds_timeSeries=mat2dataset(total2);
ds_timeSeries.Properties.VarNames= title2;
ds_timeSeries=[mat2dataset((1:size(ds_timeSeries,1))'),ds(:,1:7),ds_tim
eSeries];
ds_timeSeries.Properties.VarNames(1:8)={'ID','File','Peptide','cellNum'
,'peakFold','AUC','peakTime','tContact'};

%%
export(ds_timeSeries,'file','allData_NormalizeRadius_timeSeries_regular
_addHead_abbrev.csv','Delimiter',',');
%% normalize for PCA
all=[];
featureSet={MitoMOIRtoG_normal,MitoMOIRtoR_normal,MitoNetProj_normal,Mi
toAbsProj_normal,MitoRatioProj,MitoRatioInt};
for ii=1:size(featureSet,2)
    all=[all,featureSet{ii}];
end



%% unit variate normalization
norm=[];
M = mean(all,1);
S = std(all,0,1);
norm=(all-repmat(M,n,1))./repmat(S,n,1);
%% block normalization
norm=[];
for i=1:7
    i;
    (i-1)*6+1:i*6;
    block=all(:,(i-1)*6+1:i*6);
    M = mean(mean(block));
    S = std(reshape(block,[n*6,1]));
    temp=(block-repmat(M,n,6))./repmat(S,n,6);
    norm=[temp,norm];
end

%%
norm=[];
for i=1:6
    i;
    (i-1)*38+1:i*38;
    block=all(:,(i-1)*38+1:i*38);
```

```
    M = mean(mean(block));
    S = std(reshape(block,[n*38,1]));
    temp=(block-repmat(M,n,38))./repmat(S,n,38);
    norm=[temp,norm];
end


%% pcaa
[coeff,score,latent] = pca(norm(:,1:end));
idx = kmeans(score(:,1:2),2);
%%
figure;

plot(cumsum(latent/sum(latent)));
xlabel('Number of Priciple Components');
ylabel('Variation captured');
title('Efficiency of PCA');
%%
figure;
scatter(score(:,1),score(:,2),'.');
xlabel('PC1');
ylabel('PC2');
title('Projection on first two components');
%%
threshold=2;
matrix=[ds.peakFold1>threshold,idx-1];
if (sum(matrix(:,1)==matrix(:,2))/size(matrix,1))<0.5
    matrix(:,2)=~matrix(:,2);
end
testScore=sum(matrix(:,1)==matrix(:,2))/size(matrix,1)


%matrix2(:,2)=matrix2(:,2);
%%
featureSet={CaInt_normal,MitoMOIRtoG_normal,MitoMOIRtoR_normal,MitoNetP
roj_normal,MitoAbsProj_normal,MitoRatioProj,MitoRatioInt};
ylabelSet={'Normalized Calcium','MitoMOI on CaCentroid','MitoMOI on
MitoCentroid','MitoNetProjection','MitoAbsProjection','MitoProjectionRa
tio','MitoIntensityRatio'};
titleSet={'Normalized_Calcium','MitoMOI_on_CaCentroid','MitoMOI_on_Mito
Centroid','Mito_Net_Projection','Mito_Abs_Projection','Mito_Projection_
Ratio','Mito_Intensity_Ratio'};
featureSize=size(featureSet,2);
ds_head=[];
matrix_timeFlat=[];
for i=1:n

matrix=[CaInt_normal(i,:)',MitoMOIRtoG_normal(i,:)',MitoMOIRtoR_normal(
i,:)',MitoNetProj_normal(i,:)',MitoAbsProj_normal(i,:)',MitoRatioProj(i
,:)',MitoRatioInt(i,:)'];
    matrix_timeFlat=[matrix_timeFlat;matrix];
    ds_head=[ds_head;repmat(ds(i,1:7),timePT,1)];
end
ds_timeFlat=mat2dataset(matrix_timeFlat);

ds_timeFlat.Properties.VarNames= titleSet;
```

```
ds_timeFlat_new=[ds_head,ds_timeFlat];
%%

export(ds_timeFlat,'file','newData_NormalizeRadius_timeFlat_regular&dif
f1&2_addpeptide.csv','Delimiter',',');

%% first order derivative


CaInt_diff=(diff([CaInt_normal(:,1),CaInt_normal],1,2)+diff([CaInt_norm
al,CaInt_normal(:,end)],1,2))/2;
MitoMOIRtoG_diff=(diff([MitoMOIRtoG_normal(:,1),MitoMOIRtoG_normal],1,2
)+diff([MitoMOIRtoG_normal,MitoMOIRtoG_normal(:,end)],1,2))/2;
MitoMOIRtoR_diff=(diff([MitoMOIRtoR_normal(:,1),MitoMOIRtoR_normal],1,2
)+diff([MitoMOIRtoR_normal,MitoMOIRtoR_normal(:,end)],1,2))/2;
MitoNetProj_diff=(diff([MitoNetProj_normal(:,1),MitoNetProj_normal],1,2
)+diff([MitoNetProj_normal,MitoNetProj_normal(:,end)],1,2))/2;
MitoAbsProj_diff=(diff([MitoAbsProj_normal(:,1),MitoAbsProj_normal],1,2
)+diff([MitoAbsProj_normal,MitoAbsProj_normal(:,end)],1,2))/2;
MitoRatioProj_diff=(diff([MitoRatioProj(:,1),MitoRatioProj],1,2)+diff([
MitoRatioProj,MitoRatioProj(:,end)],1,2))/2;
MitoRatioInt_diff=(diff([MitoRatioInt(:,1),MitoRatioInt],1,2)+diff([Mit
oRatioInt,MitoRatioInt(:,end)],1,2))/2;

%% second order derivative
CaInt_diff2=[CaInt_normal(:,1),CaInt_normal(:,1:end-
1)]+[CaInt_normal(:,2:end),CaInt_normal(:,end)]-2*CaInt_normal;
MitoMOIRtoG_diff2=[MitoMOIRtoG_normal(:,1),MitoMOIRtoG_normal(:,1:end-
1)]+[MitoMOIRtoG_normal(:,2:end),MitoMOIRtoG_normal(:,end)]-
2*MitoMOIRtoG_normal;
MitoMOIRtoR_diff2=[MitoMOIRtoR_normal(:,1),MitoMOIRtoR_normal(:,1:end-
1)]+[MitoMOIRtoR_normal(:,2:end),MitoMOIRtoR_normal(:,end)]-
2*MitoMOIRtoR_normal;
MitoNetProj_diff2=[MitoNetProj_normal(:,1),MitoNetProj_normal(:,1:end-
1)]+[MitoNetProj_normal(:,2:end),MitoNetProj_normal(:,end)]-
2*MitoNetProj_normal;
MitoAbsProj_diff2=[MitoAbsProj_normal(:,1),MitoAbsProj_normal(:,1:end-
1)]+[MitoAbsProj_normal(:,2:end),MitoAbsProj_normal(:,end)]-
2*MitoAbsProj_normal;
MitoRatioProj_diff2=[MitoRatioProj(:,1),MitoRatioProj(:,1:end-
1)]+[MitoRatioProj(:,2:end),MitoRatioProj(:,end)]-2*MitoRatioProj;
MitoRatioInt_diff2=[MitoRatioInt(:,1),MitoRatioInt(:,1:end-
1)]+[MitoRatioInt(:,2:end),MitoRatioInt(:,end)]-2*MitoRatioInt;

%%

titleSet={'Normalized_Calcium','MitoMOI_on_CaCentroid','MitoMOI_on_Mito
Centroid','Mito_Net_Projection','Mito_Abs_Projection','Mito_Projection_
Ratio','Mito_Intensity_Ratio',...

'Normalized_Calcium_diff','MitoMOI_on_CaCentroid_diff','MitoMOI_on_Mito
Centroid_diff','Mito_Net_Projection_diff','Mito_Abs_Projection_diff','M
ito_Projection_Ratio_diff','Mito_Intensity_Ratio_diff',...

'Normalized_Calcium_diff2','MitoMOI_on_CaCentroid_diff2','MitoMOI_on_Mi
```

```
toCentroid_diff2','Mito_Net_Projection_diff2','Mito_Abs_Projection_diff
2','Mito_Projection_Ratio_diff2','Mito_Intensity_Ratio_diff2'};
matrix_timeFlat=[];
ds_head=[];
for i=1:n

matrix=[CaInt_normal(i,:)',MitoMOIRtoG_normal(i,:)',MitoMOIRtoR_normal(
i,:)',MitoNetProj_normal(i,:)',MitoAbsProj_normal(i,:)',MitoRatioProj(i
,:)',MitoRatioInt(i,:)',...

CaInt_diff(i,:)',MitoMOIRtoG_diff(i,:)',MitoMOIRtoR_diff(i,:)',MitoNetP
roj_diff(i,:)',MitoAbsProj_diff(i,:)',MitoRatioProj_diff(i,:)',MitoRati
oInt_diff(i,:)',...

CaInt_diff2(i,:)',MitoMOIRtoG_diff2(i,:)',MitoMOIRtoR_diff2(i,:)',MitoN
etProj_diff2(i,:)',MitoAbsProj_diff2(i,:)',MitoRatioProj_diff2(i,:)',Mi
toRatioInt_diff2(i,:)'];
    matrix_timeFlat=[matrix_timeFlat;matrix];
    ds_head=[ds_head;repmat(ds(i,1:7),timePT,1)];
end
ds_timeFlat=mat2dataset(matrix_timeFlat);
ds_timeFlat.Properties.VarNames= titleSet;
ds_timeFlat_new=[ds_head,ds_timeFlat];

%%
export(ds_timeFlat_new,'file','allData_NormalizeRadius_timeFlat_regular
&diff1&2_addHead.csv','Delimiter',',');
%%
a1=[a(:,1),a];
a2=[a,a(:,end)];
b1=diff(a1,1,2);
b2=diff(a2,1,2);
d=(b1+b2);

%%
threshold=3;
ds_regress=[ds(:,4),mat2dataset(MitoMOIRtoG_normal),mat2dataset(MitoMOI
RtoR_normal),mat2dataset(MitoNetProj_normal),mat2dataset(MitoAbsProj_no
rmal),mat2dataset(MitoRatioProj)];

%%

export(ds_regress,'file','allData_normalizeRadius.csv','Delimiter',',')
;

%%
% r=zeros(n,1);
% lags=zeros(n,1);
% for i=1:n
%     [r,lag] = xcorr(CaInt_normal(i,:),MitoMOIRtoG_normal(i,:));
%     [~,I] = max(abs(r));
%     lags(i) = lag(I);
% end
```

```
%%
%
% close all;
% figure;
% for i=1:n
%     plot(t,MitoNetProj_normal,'-')
%     hold on
% end
%% prepare for analysis
close all;
featureSet={CaInt_normal,MitoMOIRtoG_normal,MitoMOIRtoR_normal,MitoNetP
roj_normal,MitoAbsProj_normal,MitoRatioProj,MitoRatioInt};
ylabelSet={'Normalized Calcium','MitoMOI on CaCentroid','MitoMOI on
MitoCentroid','MitoNetProjection','MitoAbsProjection','MitoProjectionRa
tio','MitoIntensityRatio'};
titleSet={'Normalized Calcium','MitoMOI on CalCentroid','MitoMOI on
MitoCentroid','MitoNetProjection','MitoAbsProjection','MitoProjectionRa
tio','MitoIntensityRatio'};
featureSize=size(featureSet,2);
coeff=cell(featureSize,1);
score=cell(featureSize,1);
latent=cell(featureSize,1);
idx=zeros(n,featureSize);

%% calculate the lag between features
lags=zeros(n,featureSize);
for ii=1:featureSize
    feature=featureSet{ii};
    for i=1:n
        [r,lag] = xcorr(CaInt_normal(i,:),feature(i,:));
        [~,I] = max(abs(r));
        lags(i,ii) = lag(I);
    end
end
mean(lags)
%% PCA analysis
close all;
low=[0,0,0,-1,0,0,0];
high=[6,1,1,1,1,1,1];
for ii=1:featureSize
    feature=featureSet{ii};
    [coeff{ii},score{ii},latent{ii}] = pca(feature);
    idx(:,ii) = kmeans(score{ii}(:,1:10),2);

    figure;
    subplot(2,2,1)
    plot(cumsum(latent{ii}/sum(latent{ii})));
    xlabel('Number of Priciple Components')
    ylabel('Variation captured')
    title('Efficiency of PCA')

    subplot(2,2,2)
    scatter(score{ii}(:,1),score{ii}(:,2),'.')
    xlabel('PC1')
    ylabel('PC2')
    title('Projection on first two components')
```

```
%     figure;
%     subplot(2,2,3)
%     for i = 1:n
%         if idx(i,ii) == 1
%            plot(t,feature(i,:),'b')
%            hold on;
%         else
%            plot(t,feature(i,:),'r')
%            hold on;
%         end
%     end
%     legend('low','high')
%     xlabel('Time in 30sec')
%     ylabel(ylabelSet{ii})
%     title(titleSet{ii})

    subplot(2,2,3)
    for i = 1:n
        if idx(i,ii) == 1
           plot(t,feature(i,:),'b')
           if doNormalize
            ylim([low(ii) high(ii)])
           end
           hold on;
        end
    end
    legend(sprintf('cluster %d',1))
    xlabel('Time in 30sec')
    ylabel(ylabelSet{ii})
    title(titleSet{ii})

    subplot(2,2,4)
    for i = 1:n
        if idx(i,ii) == 2
           plot(t,feature(i,:),'r')
           if doNormalize
            ylim([low(ii) high(ii)])
           end
           hold on;
        end
    end
    legend(sprintf('cluster %d',2))
    xlabel('Time in 30sec')
    ylabel(ylabelSet{ii})
    title(titleSet{ii})
end
%% make testing error matrix based on manual thresholding

threshold=3;
matrix=[ds.peakFold1>threshold,idx-1];

%sum((idx-1)==(ds_clean.peakFold1>threshold))/size(matrix,1)
%sum((idx2-1)==(ds_clean.peakFold1>threshold))/size(matrix,1)
%sum(idx-1)
%sum(idx2-1)
```

```
clc;
score=zeros(featureSize+1,1);
for iii=1:featureSize+1
    if (sum(matrix(:,iii)==matrix(:,1))/size(matrix,1))<0.5
        matrix(:,iii)=~matrix(:,iii);
        score(iii)=sum(matrix(:,iii)==matrix(:,1))/size(matrix,1);
    else
        score(iii)=sum(matrix(:,iii)==matrix(:,1))/size(matrix,1);
    end
end
score
avgScore=mean(score)
matrix(:,9)=mode(matrix(:,3:end),2);
MajorityScore=sum(matrix(:,end)==matrix(:,1))/size(matrix,1)
ds_matrix=[ds(:,2),ds(:,4),mat2dataset(matrix)];
ds_matrix.Properties.VarNames(3:end) =
{sprintf('PeakFold_Theshold_%d',threshold),'Normalized_Calcium','MitoMO
I_on_CaCentroid','MitoMOI_on_MitoCentroid','MitoNetProjection',...

'MitoAbsProjection','MitoProjectionRatio','MitoIntensityRatio','MitoMaj
orityVote'};

%% make testing error matrix based on clustering on calcium traces

threshold=3;
matrix=[ds.peakFold1>threshold,idx-1];

%sum((idx-1)==(ds_clean.peakFold1>threshold))/size(matrix,1)
%sum((idx2-1)==(ds_clean.peakFold1>threshold))/size(matrix,1)
%sum(idx-1)
%sum(idx2-1)

clc;
score=zeros(featureSize+1,1);
for iii=1:featureSize+1
    if (sum(matrix(:,iii)==matrix(:,2))/size(matrix,1))<0.5
        matrix(:,iii)=~matrix(:,iii);
        score(iii)=sum(matrix(:,iii)==matrix(:,2))/size(matrix,1);
    else
        score(iii)=sum(matrix(:,iii)==matrix(:,2))/size(matrix,1);
    end
end
score
avgScore=mean(score)
matrix(:,9)=mode(matrix(:,3:end),2);
MajorityScore=sum(matrix(:,end)==matrix(:,2))/size(matrix,1)
ds_matrix=[ds(:,2),ds(:,4),mat2dataset(matrix)];
ds_matrix.Properties.VarNames(3:end) =
{sprintf('PeakFold_Theshold_%d',threshold),'Normalized_Calcium','MitoMO
I_on_CaCentroid','MitoMOI_on_MitoCentroid','MitoNetProjection',...

'MitoAbsProjection','MitoProjectionRatio','MitoIntensityRatio','MitoMaj
orityVote'};
```

```
%%
export(ds_matrix,'file','allData_designMatrix.csv','Delimiter',',');

%%
allFeature=[MitoMOIRtoG_normal,MitoMOIRtoR_normal,MitoNetProj_normal,Mi
toAbsProj_normal,MitoRatioProj,MitoRatioInt];

[coeff,score,latent] = pca(allFeature);
idx = kmeans(score(:,1:10),2);
%%

figure;
subplot(2,2,1)
plot(cumsum(latent/sum(latent)));
xlabel('Number of Priciple Components')
ylabel('Variation captured')
title('Efficiency of PCA')

subplot(2,2,2)
scatter(score(:,1),score(:,2),'.')
xlabel('PC1')
ylabel('PC2')
title('Projection on first two components')

%     figure;
%     subplot(2,2,3)
%     for i = 1:n
%         if idx(i,ii) == 1
%            plot(t,feature(i,:),'b')
%            hold on;
%         else
%            plot(t,feature(i,:),'r')
%            hold on;
%         end
%     end
%     legend('low','high')
%     xlabel('Time in 30sec')
%     ylabel(ylabelSet{ii})
%     title(titleSet{ii})

subplot(2,2,3)
for i = 1:n
    if idx(i) == 1
       plot(allFeature(i,:),'b')

       hold on;
    end
end
legend(sprintf('cluster %d',1))

subplot(2,2,4)
for i = 1:n
    if idx(i) == 2
       plot(t,allFeature(i,:),'r')
```

```
        hold on;
    end
end
legend(sprintf('cluster %d',2))
%%
matrix2=[ds.peakFold1>threshold,idx-1];
score2=1-sum(matrix2(:,2)==matrix2(:,1))/size(matrix2,1)
matrix2(:,2)=matrix2(:,2);
% sum(matrix(:,2)==matrix(:,1))/size(matrix,1)
% sum(matrix(:,3)==matrix(:,1))/size(matrix,1)
% sum(matrix(:,4)==matrix(:,1))/size(matrix,1)
% sum(matrix(:,5)==matrix(:,1))/size(matrix,1)
% sum(matrix(:,6)==matrix(:,1))/size(matrix,1)
% sum(matrix(:,7)==matrix(:,1))/size(matrix,1)
% sum(matrix(:,8)==matrix(:,1))/size(matrix,1)
```

REFERENCES

1. Murphy, K. M. 2011. *Janeway's Immunobiology*, 8th ed. Garland Science.

2. Metchnikoff, E. 1905. *Immunity in infective diseases*, reprint. University Press.

3. Dudley, M., J. Wunderlich, and J. Yang. 2005. Adoptive cell transfer therapy following non-myeloablative but lymphodepleting chemotherapy for the treatment of patients with refractory metastatic melanoma. *J. Clin. Oncol.* 23: 2346–2357.

4. Morris, E., A. Tsallios, and G. Bendle. 2005. A critical role of T cell antigen receptor-transduced MHC class I-restricted helper T cells in tumor protection. *Proc. Natl. Acad. Sci.* 102: 7934–7939.

5. Bruggen, P. Van Der, Y. Zhang, and P. Chaux. 2002. Tumor-specific shared antigenic peptides recognized by human T cells. *Immunol. Rev.* 188: 51–64.

6. Gubin, M. M., X. Zhang, H. Schuster, E. Caron, J. P. Ward, T. Noguchi, Y. Ivanova, J. Hundal, C. D. Arthur, W.-J. Krebber, G. E. Mulder, M. Toebes, M. D. Vesely, S. S. K. Lam, A. J. Korman, J. P. Allison, G. J. Freeman, A. H. Sharpe, E. L. Pearce, T. N. Schumacher, R. Aebersold, H.-G. Rammensee, C. J. M. Melief, E. R. Mardis, W. E. Gillanders, M. N. Artyomov, and R. D. Schreiber. 2014. Checkpoint blockade cancer immunotherapy targets tumour-specific mutant antigens. *Nature* 515: 577–581.

7. Moynihan, K., C. Opel, G. Szeto, A. Tzeng, and E. Zhu. 2016. Eradication of large established tumors in mice by combination immunotherapy that engages innate and adaptive immune responses. *Nat. Med.* .

8. Feldmann, M. 2009. Translating molecular insights in autoimmunity into effective therapy. *Annu. Rev. Immunol.* 27: 1–27.

9. Curtiss, R. 2002. Bacterial infectious disease control by vaccine development. *J. Clin. Invest.* 110: 1061–1066.

10. Kappe, S., A. Vaughan, and J. Boddey. 2010. That was then but this is now: malaria research in the time of an eradication agenda. *Science* 328: 862–866.

11. Virgin, H., and B. Walker. 2010. Immunology and the elusive AIDS vaccine. *Nature* 464: 224–231.

12. Reshef, D., Y. Reshef, H. Finucane, S. Grossman, G. Mcvean, P. Turnbaugh, E. Lander, M. Mitzenmacher, and P. Sabeti. 2011. in Large Data Sets. *Sci. Transl. Med.* 334: 1518–1524.

13. Lemaitre, B., E. Nicolas, L. Michaut, J.-M. Reichhart, and J. A. Hoffmann. 1996. The dorsoventral regulatory gene cassette spätzle/Toll/cactus controls the potent antifungal response in Drosophila adults. *Cell* 86: 973–983.

14. Beutler, B. 2009. Microbe sensing, positive feedback loops, and the pathogenesis of inflammatory diseases. *Immunol. Rev.* 227: 248–263.

15. Janeway, C. A., and R. Medzhitov. 2002. Innate immune recognition. *Annu. Rev. Immunol.* 20: 197–216.

16. Kawai, T., and S. Akira. 2009. The roles of TLRs, RLRs and NLRs in pathogen recognition. *Int. Immunol.* 21: 317–37.

17. Landsteiner, K. 1990. *The specificity of serological reactions,*. Courier Corporation.

18. Burnet, S. F. M. 1959. *The clonal selection theory of acquired immunity,*. Nashville: Vanderbilt University Press.

19. Dustin, M. 2003. Coordination of T cell activation and migration through formation of the immunological synapse. *Ann. N. Y. Acad. Sci.* 987: 51–59.

20. Heath, W., and F. Carbone. 2009. Dendritic cell subsets in primary and secondary T cell responses at body surfaces. *Nat. Immunol.* 10: 1237–1244.

21. Tseng, S., and M. Dustin. 2002. T-cell activation: a multidimensional signaling network. *Curr. Opin. Cell Biol.* 14: 575–580.

22. Fooksman, D.R., Vardhana, S., Vasiliver-Shamis, G., Liese, J., Blair, D.A., Waite, J., Sacristán, C., Victora, G.D., Zanin-Zhorov, A. and Dustin, M. L. 2009. Functional anatomy of T cell activation and synapse formation. *Annu. Rev. Immunol.* 28: 79–105.

23. Grakoui, Arash, et al. 1999. The immunological synapse: a molecular machine controlling T cell activation. *Science* 285: 221–227.

24. Huppa, J. B., and M. M. Davis. 2003. T-cell-antigen recognition and the immunological synapse. *Nat. Rev. Immunol.* 3: 973–83.

25. Quintana, A., C. Schwindling, A. S. Wenning, U. Becherer, J. Rettig, E. C. Schwarz, and M. Hoth. 2007. T cell activation requires mitochondrial translocation to the immunological synapse. *Proc. Natl. Acad. Sci.* 104: 14418–14423.

26. Huse, M., E. J. Quann, and M. M. Davis. 2010. Shouts, whispers and the kiss of death: directional secretion in T cells. 9: 1105–1111.

27. Bodmer, J. G., S. G. E. Marsh, E. D. Albert, W. F. Bodmer, B. Dupont, H. A. Erlich, B. Mach, W. R. Mayr, P. Parham, T. Sasazuki, G. M. T. Schreuder, J. L. Strominger, A. Svejgaard, and P. I. Terasaki. 1994. Nomenclature for factors of the HLA system, 1994. *Hum. Immunol.* 41: 1–20.

28. Germain, R. N. 1994. MHC-dependent antigen processing and peptide presentation: Providing ligands for T lymphocyte activation. *Cell* 76: 287–299.

29. Grommé, M., and J. Neefjes. 2002. Antigen degradation or presentation by MHC class I molecules via classical and non-classical pathways. *Mol. Immunol.* 39: 181–202.

30. Chaudhuri, J., U. Basu, A. Zarrin, C. Yan, and S. Franco. 2007. Evolution of the immunoglobulin heavy chain class switch recombination mechanism. *Adv. Immunol.* 94: 157–214.

31. Fugmann, S., A. Lee, and P. Shockett. 2000. The RAG proteins and V (D) J recombination: complexes, ends, and transposition. *Annu. Rev. Immunol.* 18: 495–527.

32. Schatz, D., and M. Oettinger. 1992. V (D) J recombination: molecular biology and regulation. *Annu. Rev. Immunol.* 18: 495–527.

33. Gorbulev, S., R. Abele, and R. Tampé. 2001. Allosteric crosstalk between peptide-binding, transport, and ATP hydrolysis of the ABC transporter TAP. *Proc. Natl. Acad. Sci.*

U. S. A. 98: 3732–7.

34. Shastri, N., S. Schwab, and T. Serwold. 2002. Producing nature's gene-chips: the generation of peptides for display by MHC class I molecules. *Annu. Rev. Immunol.* 20: 463–493.

35. Hiltbold, E. M., and P. A. Roche. 2002. Trafficking of MHC class II molecules in the late secretory pathway. *Curr. Opin. Immunol.* 14: 30–35.

36. Bouvier, M. 2003. Accessory proteins and the assembly of human class I MHC molecules: a molecular and structural perspective. *Mol. Immunol.* 39: 697–706.

37. Fremont, D., W. Henderickson, and P. Marrack. 1996. Structures of an MHC class II molecule with covalently bound single peptides. *Science* 272: 1001.

38. Steimle, V., C. Siegrist, and A. Mottet. 1994. Regulation of MHC Class II Expression by Interferon-(Gamma). *Science* 265: 106.

39. Garcia, K., M. Degano, L. Pease, and M. Huang. 1998. Structural basis of plasticity in T cell receptor recognition of a self peptide-MHC antigen. *Science* 279: 1166–1172.

40. Sant'Angelo, D., G. Waterbury, and P. Preston-Hurlburt. 1996. The specificity and orientation of a TCR to its peptide–MHC class II ligands. *Immunity* 4: 367–376.

41. Teng, M., A. Smolyar, A. Tse, J. Liu, and J. Liu. 1998. Identification of a common docking topology with substantial variation among different TCR–peptide–MHC complexes. *Curr. Biol.* 8: 409–414.

42. Sykulev, Y., M. Joo, I. Vturina, T. J. Tsomides, and H. N. Eisen. 1996. Evidence that a Single Peptide–MHC Complex on a Target Cell Can Elicit a Cytolytic T Cell Response. *Immunity* 4: 565–571.

43. Henrickson, S., T. Mempel, I. Mazo, B. Liu, M. Artomov, H. Zheng, A. Peixoto, M. Flynn, B. Senman, T. Junt, H. Wong, A. Chakraborty, and U. von Andrian. 2008. T cell sensing of antigen dose governs interactive behavior with dendritic cells and sets a threshold for T cell activation. *Nat. Immunol.* 9: 282.

44. Sykulev, Y., A. Brunmark, M. Jackson, R. J. Cohen, P. A. Peterson, and H. N. Eisen. 1994. Kinetics and affinity of reactions between an antigen-specific T cell receptor and peptide-MHC complexes. *Immunity* 1: 15–22.

45. Corse, E., R. A. Gottschalk, and J. P. Allison. 2017. Strength of TCR–Peptide/MHC Interactions and In Vivo T Cell Responses. *J Immunol Ref.* 186: 5039–5045.

46. Savage, P. A., J. J. Boniface, and M. M. Davis. 1999. A Kinetic Basis For T Cell Receptor Repertoire Selection during an Immune Response. *Immunity* 10: 485–492.

47. Kersh, G. J., E. N. Kersh, D. H. Fremont, and P. M. Allen. 1998. High- and Low-Potency Ligands with Similar Affinities for the TCR: The Importance of Kinetics in TCR Signaling. *Immunity* 9: 817–826.

48. Rosette, C., G. Werlen, M. A. Daniels, P. O. Holman, S. M. Alam, P. J. Travers, N. R. . Gascoigne, E. Palmer, and S. C. Jameson. 2001. The Impact of Duration versus Extent of TCR Occupancy on T Cell Activation: A Revision of the Kinetic Proofreading Model. *Immunity* 15: 59–70.

49. Rabinowitz, J. D., C. Beeson, D. S. Lyonst, M. M. Davist, and H. M. Mcconnell. 1996.

Kinetic discrimination in T-cell activation. *Immunology* 93: 1401–1405.

50. Wong, P., G. M. Barton, K. A. Forbush, and A. Y. Rudensky. 2001. Dynamic Tuning of T Cell Reactivity by Self-Peptide–Major Histocompatibility Complex Ligands. *J. Exp. Med.* 193: 1179–1188.

51. Bour-Jordan, H., and J. Bluestone. 2002. CD28 function: a balance of costimulatory and regulatory signals. *J. Clin. Immunol.* 22: 1–7.

52. Kapsenberg, M. 2003. Dendritic-cell control of pathogen-driven T-cell polarization. *Nat. Rev. Immunol.* 3: 984–993.

53. Gonzalo, J., T. Delaney, and J. Corcoran. 2001. Cutting edge: the related molecules CD28 and inducible costimulator deliver both unique and complementary signals required for optimal T cell activation. *J. Immunol.* 166: 1–5.

54. O'Shea, J., and W. Paul. 2010. Mechanisms underlying lineage commitment and plasticity of helper CD4+ T cells. *Science* 327: 1098–1102.

55. Gomperts, B., I. Kramer, and P. Tatham. 2009. *Signal transduction*,. Academic Press.

56. Marks, F., U. KlingmÙller, and K. Müller-Decker. 2008. *Cellular signal processing: an introduction to the molecular mechanisms of signal transduction*,. Garland Science.

57. Lin, J., and A. Weiss. 2001. T cell receptor signalling. *J. Cell Sci.* 114.

58. Smith-Garvin, J. E., G. A. Koretzky, and M. S. Jordan. 2009. T cell activation. *Annu. Rev. Immunol.* 27: 591–619.

59. Call, M. E., J. Pyrdol, M. Wiedmann, and K. W. Wucherpfennig. 2002. The Organizing Principle in the Formation of the T Cell Receptor-CD3 Complex. *Cell* 111: 967–979.

60. Exley, M., C. Terhorst, and T. Wileman. 1991. Structure, assembly and intracellular transport of the T cell receptor for antigen. *Semin. Immunol.* 3: 283–97.

61. Li, Q.-J., A. R. Dinner, S. Qi, D. J. Irvine, J. B. Huppa, M. M. Davis, and A. K. Chakraborty. 2004. CD4 enhances T cell sensitivity to antigen by coordinating Lck accumulation at the immunological synapse. *Nat. Immunol.* 5: 791–799.

62. Acuto, O., and F. Michel. 2003. CD28-mediated co-stimulation: a quantitative support for TCR signalling. *Nat. Rev. Immunol.* 3: 939–951.

63. Pawson, T. 2004. Specificity in Signal Transduction: From Phosphotyrosine-SH2 Domain Interactions to Complex Cellular Systems. *Cell* 116: 191–203.

64. Irving, B. A., and A. Weiss. 1991. The cytoplasmic domain of the T cell receptor ζ chain is sufficient to couple to receptor-associated signal transduction pathways. *Cell* 64: 891–901.

65. Chan, A. C., M. Dalton, R. Johnson, G. H. Kong, T. Wang, R. Thoma, and T. Kurosaki. 1995. Activation of ZAP-70 kinase activity by phosphorylation of tyrosine 493 is required for lymphocyte antigen receptor function. *EMBO J.* 14: 2499–508.

66. Jordan, M. S., A. L. Singer, and G. A. Koretzky. 2003. Adaptors as central mediators of signal transduction in immune cells. *Nat. Immunol.* 4: 110–116.

67. Berg, L. J., L. D. Finkelstein, J. A. Lucas, and P. L. Schwartzberg. 2005. Tec family kinases in T lymphocyte development and function. *Annu. Rev. Immunol.* 23: 549–600.

68. Hogan, P. G., L. Chen, J. Nardone, and A. Rao. 2003. Transcriptional regulation by calcium, calcineurin, and NFAT. *Genes Dev.* 17: 2205–32.

69. Macian, Fernando, Cristina Lopez-Rodriguez, A. R. 2001. Partners in transcription: NFAT and AP-1. *Oncogene* 20: 2476.

70. Picard, C., C.-A. McCarl, A. Papolos, S. Khalil, K. Lüthy, C. Hivroz, F. LeDeist, F. Rieux-Laucat, G. Rechavi, A. Rao, A. Fischer, and S. Feske. 2009. *STIM1* Mutation Associated with a Syndrome of Immunodeficiency and Autoimmunity. *N. Engl. J. Med.* 360: 1971–1980.

71. Prakriya, M., S. Feske, Y. Gwack, S. Srikanth, A. Rao, and P. G. Hogan. 2006. Orai1 is an essential pore subunit of the CRAC channel. *Nature* 443: 230–233.

72. Simula, L., F. Nazio, and S. Campello. 2017. The mitochondrial dynamics in cancer and immune-surveillance. *Semin. Cancer Biol.* .

73. Bonifaz, L. C., M. P. Cervantes-Silva, E. Ontiveros-Dotor, E. O. López-Villegas, and F. J. Sánchez-García. 2015. A role for mitochondria in antigen processing and presentation. *Immunology* 144: 461–471.

74. Quintana, A., and M. Hoth. 2012. Mitochondrial dynamics and their impact on T cell function. *Cell Calcium* 52: 57–63.

75. Saris, N.-E. L., and E. Carafoli. 2005. A historical review of cellular calcium handling, with emphasis on mitochondria. *Biochem.* 70: 187–194.

76. Hoth, M., C. M. Fanger, and R. S. Lewis. 1997. Mitochondrial Regulation of Store-operated Calcium Signaling in T Lymphocytes. *J. Cell Biol.* 137: 633–648.

77. Borner, C. 2003. The Bcl-2 protein family: sensors and checkpoints for life-or-death decisions. *Mol. Immunol.* 39: 615–647.

78. Hildeman, D., Y. Zhu, T. Mitchell, and J. Kappler. 2002. Molecular mechanisms of activated T cell death in vivo. *Curr. Opin. Immunol.* 14: 354–359.

79. Chesla, S. E., P. Selvaraj, and C. Zhu. 1998. Measuring Two-Dimensional Receptor-Ligand Binding Kinetics by Micropipette. *Biophys. J.* 75: 1553–1572.

80. Huang, J., V. I. Zarnitsyna, B. Liu, L. J. Edwards, N. Jiang, B. D. Evavold, and C. Zhu. 2010. The kinetics of two-dimensional TCR and pMHC interactions determine T-cell responsiveness. *Nature* 464: 932–936.

81. Marshall, B. T., M. Long, J. W. Piper, T. Yago, R. P. McEver, and C. Zhu. 2003. Direct observation of catch bonds involving cell-adhesion molecules. *Nature* 423: 190–193.

82. Zhu, C., G. Bao, and N. Wang. 2000. Cell Mechanics: Mechanical Response, Cell Adhesion, and Molecular Deformation. *Annu. Rev. Biomed. Eng.* 2: 189–226.

83. Liu, B., W. Chen, B. D. Evavold, and C. Zhu. 2014. Accumulation of dynamic catch bonds between TCR and agonist peptide-MHC triggers T cell signaling. *Cell* 157: 357–368.

84. Pryshchep, S., V. I. Zarnitsyna, J. Hong, B. D. Evavold, and C. Zhu. 2014. Accumulation of Serial Forces on TCR and CD8 Frequently Applied by Agonist Antigenic Peptides Embedded in MHC Molecules Triggers Calcium in T Cells. *J. Immunol.* 193: 68–76.

85. Glasebrook, A. L., and F. W. Fitch. 1980. Alloreactive cloned T cell lines. I. Interactions between cloned amplifier and cytolytic T cell lines. *J. Exp. Med.* 151: 876–895.

86. Ju, S.T., Panka, D.J., Cui, H., Ettinger, R., Maan, E.K., Sherr, D.H., Stanger, B.Z. and Marshak-Rothstein, A. 1995. Fas(CD95)/FasL interactions required for programmed cell death after T-cell activation. *Nature* 373: 444–448.

87. Brunner, T., Mogil, R.J., LaFace, D., Yoo, N.J., Mahboubi, A., Echeverri, F., Martin, S.J., Force, W.R., Lynch, D.H., Ware, C.F. and Green, D. R. 1995. Cell-autonomous Fas (CD95)/Fas-ligand interaction mediates activation-induced apoptosis in T-cell hybridomas. *Nature* 373: 441–444.

88. Whitesides, G. M. 2006. The origins and the future of microfluidics. *Nature* 442: 368.

89. Squires, T.M. and Quake, S. R. 2005. Microfluidics : Fluid physics at the nanoliter scale. *Rev. Mod. Phys.* 77: 977.

90. El-Ali, Jamil, Peter K. Sorger, and K. F. J. 2006. Cells on chips. *Nature* 442: 403.

91. Sims, C. E., and N. L. Allbritton. 2007. Analysis of single mammalian cells on-chip. *Lab Chip* 7: 423–40.

92. Duffy, D. C., J. C. McDonald, O. J. Schueller, and G. M. Whitesides. 1998. Rapid Prototyping of Microfluidic Systems in Poly(dimethylsiloxane). *Anal. Chem.* 70: 4974–84.

93. Hooshangi, S., S. Thiberge, and M. Luxr. 2005. Dynamics of Drosophila embryonic patterning network perturbed in space and time using microfluidics. *Nature* 434: 1134.

94. Figueroa, X.A., Cooksey, G.A., Votaw, S.V., Horowitz, L.F. and Folch, A. 2010. Large-scale investigation of the olfactory receptor space using a microfluidic microwell array. *Lab Chip* 10: 1120–1127.

95. Yamamura, S., H. Kishi, Y. Tokimitsu, S. Kondo, R. Honda, S. R. Rao, M. Omori, E. Tamiya, and A. Muraguchi. 2005. Single-cell microarray for analyzing cellular response. *Anal. Chem.* 77: 8050–6.

96. Rettig, J. R., and A. Folch. 2005. Large-scale single-cell trapping and imaging using microwell arrays. *Anal. Chem.* 77: 5628–34.

97. Park, M. C., J. Y. Hur, H. S. Cho, S.-H. Park, and K. Y. Suh. 2011. High-throughput single-cell quantification using simple microwell-based cell docking and programmable time-course live-cell imaging. *Lab Chip* 11: 79–86.

98. Voldman, J., M. L. Gray, M. Toner, and M. A. Schmidt. 2013. A Microfabrication-Based Dynamic Array Cytometer parallel luminescent single-cell assays that can sort popu-. 74: 3984–3990.

99. Taff, B. M., and J. Voldman. 2005. A scalable addressable positive-dielectrophoretic cell-sorting array. *Anal. Chem.* 77: 7976–83.

100. Tan, W.-H., and S. Takeuchi. 2007. A trap-and-release integrated microfluidic system for dynamic microarray applications. *Proc. Natl. Acad. Sci.* 104: 1146–51.

101. Oh, K.W., Lee, K., Ahn, B. and Furlani, E. P. 2012. Design of pressure-driven microfluidic networks using electric circuit analogy. *Lab Chip* 12: 515–545.

102. Faley, S., K. Seale, J. Hughey, D. K. Schaffer, S. VanCompernolle, B. McKinney, F. Baudenbacher, D. Unutmaz, and J. P. Wikswo. 2008. Microfluidic platform for real-time signaling analysis of multiple single T cells in parallel. *Lab Chip* 8: 1700–12.

103. Hirsch, A. M., C. A. Rivet, B. Zhang, M. L. Kemp, and H. Lu. 2009. Parallel multi-time point cell stimulation and lysis on-chip for studying early signaling events in T cell activation. *Lab Chip* 9: 536–544.

104. Chung, K., C. A. Rivet, M. L. Kemp, and H. Lu. 2011. Imaging single-cell signaling dynamics with a deterministic high-density single-cell trap array. *Anal. Chem.* 83: 7044–7052.

105. Dertinger, S. K. W., D. T. Chiu, N. L. Jeon, and G. M. Whitesides. 2001. Generation of Gradients Having Complex Shapes Using Microfluidic Networks. *Anal. Chem.* 73: 1240–1246.

106. Jeon, N. L., S. K. W. Dertinger, D. T. Chiu, I. S. Choi, A. D. Stroock, and G. M. Whitesides. 2000. Generation of Solution and Surface Gradients Using Microfluidic Systems. *Langmuir* 16: 8311–8316.

107. Lee, K., C. Kim, B. Ahn, R. Panchapakesan, A. R. Full, L. Nordee, J. Y. Kang, and K. W. Oh. 2009. Generalized serial dilution module for monotonic and arbitrary microfluidic gradient generators. *Lab Chip* 9: 709–17.

108. Li Jeon, N., H. Baskaran, S. K. W. Dertinger, G. M. Whitesides, L. Van de Water, and M. Toner. 2002. Neutrophil chemotaxis in linear and complex gradients of interleukin-8 formed in a microfabricated device. *Nat. Biotechnol.* 20: 826–30.

109. Azizi, F., and C. H. Mastrangelo. 2008. Generation of dynamic chemical signals with pulse code modulators. *Lab Chip* 8: 907–12.

110. Bennett, M. R., W. L. Pang, N. a Ostroff, B. L. Baumgartner, S. Nayak, L. S. Tsimring, and J. Hasty. 2008. Metabolic gene regulation in a dynamically changing environment. *Nature* 454: 1119–22.

111. Dolmetsch, R. E., K. Xu, and R. S. Lewis. 1998. Calcium oscillations increase the efficiency and specificity of gene expression. *Nature* 392: 933–6.

112. Hersen, P., M. N. McClean, L. Mahadevan, and S. Ramanathan. 2008. Signal processing by the HOG MAP kinase pathway. *Proc. Natl. Acad. Sci.* 105: 7165–70.

113. King, K. R., S. Wang, A. Jayaraman, M. L. Yarmush, and M. Toner. 2008. Microfluidic flow-encoded switching for parallel control of dynamic cellular microenvironments. *Lab Chip* 8: 107–16.

114. Mettetal, J. T., D. Muzzey, C. Gómez-Uribe, and A. van Oudenaarden. 2008. The frequency dependence of osmo-adaptation in Saccharomyces cerevisiae. *Science* 319: 482–4.

115. Olofsson, J., H. Bridle, J. Sinclair, D. Granfeldt, E. Sahlin, and O. Orwar. 2005. A chemical waveform synthesizer. *Proc. Natl. Acad. Sci. U. S. A.* 102: 8097–102.

116. Unger, Marc A., Hou-Pu Chou, Todd Thorsen, Axel Scherer, and S. R. Q. 2000. Monolithic microfabricated valves and pumps by multilayer soft lithography. *Science* 288: 113–116.

117. VanDersarl, J. J., A. M. Xu, and N. a Melosh. 2011. Rapid spatial and temporal controlled signal delivery over large cell culture areas. *Lab Chip* 11: 3057–63.

118. Wheeler, A. R., W. R. Throndset, R. J. Whelan, A. M. Leach, R. N. Zare, Y. H. Liao, K. Farrell, I. D. Manger, and A. Daridon. 2003. Microfluidic device for single-cell analysis. *Anal. Chem.* 75: 3581–6.

119. Abate, a. R., and D. a. Weitz. 2008. Single-layer membrane valves for elastomeric microfluidic devices. *Appl. Phys. Lett.* 92: 243509.

120. Guldevall, K., B. Vanherberghen, and T. Frisk. 2010. Imaging immune surveillance of individual natural killer cells confined in microwell arrays. *PLoS One* 5: e15453.

121. Biggs, M.J.P., Milone, M.C., Santos, L.C., Gondarenko, A. and Wind, S. J. 2011. High-resolution imaging of the immunological synapse and T-cell receptor microclustering through microfabricated substrates. *J. R. Soc. Interface* rsif20110025.

122. Şen, M., K. Ino, J. Ramón-Azcón, H. Shiku, and T. Matsue. 2013. Cell pairing using a dielectrophoresis-based device with interdigitated array electrodes. *Lab Chip* 13: 3650–2.

123. Frimat, J.P., Becker, M., Chiang, Y.Y., Marggraf, U., Janasek, D., Hengstler, J.G., Franzke, J. and West, J. 2011. A microfluidic array with cellular valving for single cell co-culture. *Lab Chip* 11: 231–237.

124. Lee, P. J., P. J. Hung, R. Shaw, L. Jan, and L. P. Lee. 2005. Microfluidic application-specific integrated device for monitoring direct cell-cell communication via gap junctions between individual cell pairs. *Appl. Phys. Lett.* 86: 223902.

125. Skelley, A. M., O. Kirak, H. Suh, R. Jaenisch, and J. Voldman. 2009. Microfluidic control of cell pairing and fusion. *Nat Methods* 6: 147–152.

126. Dura, B., S. K. Dougan, M. Barisa, M. M. Hoehl, C. T. Lo, H. L. Ploegh, and J. Voldman. 2015. Profiling lymphocyte interactions at the single-cell level by microfluidic cell pairing. *Nat. Commun.* 6: 1–13.

127. Dura, B., Y. Liu, and J. Voldman. 2014. Deformability-based microfluidic cell pairing and fusion. *Lab Chip* 14: 2783–90.

128. Fixture Failure Diagnosis for Auto Body Assembly... - Google Scholar. .

129. Janes, K. A., and M. B. Yaffe. 2006. Data-driven modelling of signal-transduction networks. *Nat. Rev. Mol. Cell Biol.* 7: 820–828.

130. Mehmood, T., K. H. Liland, L. Snipen, and S. Sæbø. 2012. A review of variable selection methods in Partial Least Squares Regression. *Chemom. Intell. Lab. Syst.* 118: 62–69.

131. Janes, K. A., J. R. Kelly, S. Gaudet, J. G. Albeck, P. K. Sorger, and D. A. Lauffenburger. 2004. Cue-Signal-Response Analysis of TNF-Induced Apoptosis by Partial Least Squares Regression of Dynamic Multivariate Data. *J. Comput. Biol.* 11: 544–561.

132. Choe, G., Horvath, S., Cloughesy, T.F., Crosby, K., Seligson, D., Palotie, A., Inge, L., Smith, B.L., Sawyers, C.L. and Mischel, P. S. 2003. Analysis of the phosphatidylinositol 3′-kinase signaling pathway in glioblastoma patients in vivo. *Cancer Res.* 63: 2742–2746.

133. Smith-Garvin, J., and G. Koretzky. 2009. T cell activation. *Annu. Rev. Immunol.* 27: 591–619.

134. Feske, S. 2007. Calcium signalling in lymphocyte activation and disease. *Nat. Rev. Immunol.* 7: 690–702.

135. Dolmetsch, R. E., R. S. Lewis, C. C. Goodnow, and J. I. Healy. 1997. Differential activation of transcription factors induced by Ca2+ response amplitude and duration. *Nature* 386: 855–858.

136. Dolmetsch, R., K. Xu, and R. Lewis. 1998. Calcium oscillations increase the efficiency and specificity of gene expression. *Nature* 392: 933–6.

137. Finotto, S., Neurath, M.F., Glickman, J.N., Qin, S., Lehr, H.A., Green, F.H., Ackerman, K., Haley, K., Galle, P.R., Szabo, S.J. and Drazen, J. M. 2002. Development of spontaneous airway changes consistent with human asthma in mice lacking T-bet. *Science* 295: 336–338.

138. Zhu, J., and W. Paul. 2008. CD4 T cells: fates, functions, and faults. *Blood* 112: 1557–1569.

139. Dipaolo, R. J., C. Brinster, T. S. Davidson, J. Andersson, D. Glass, and E. M. Shevach. 2007. Autoantigen-specific TGFβ-induced Foxp3+ regulatory T cells prevent autoimmunity by inhibiting dendritic cells from activating autoreactive T cells. *J. Immunol.* 179: 4685–4693.

140. Perl, A., R. Hanczko, and E. Doherty. 2012. Assessment of mitochondrial dysfunction in lymphocytes of patients with systemic lupus erythematosus. *Autoimmun. Methods Protoc.* 61–89.

141. Zhu, J., H. Yamane, and W. Paul. 2010. Differentiation of effector CD4 T cell populations. *Annu. Rev. Immunol.* 28: 445–489.

142. Mettetal, J. T., D. Muzzey, C. Gómez-Uribe, and A. van Oudenaarden. 2008. The frequency dependence of osmo-adaptation in Saccharomyces cerevisiae. *Science* 319: 482–4.

143. Hersen, P., M. N. McClean, L. Mahadevan, and S. Ramanathan. 2008. Signal processing by the HOG MAP kinase pathway. *Proc. Natl. Acad. Sci.* 105: 7165–70.

144. Bennett, M. R., W. L. Pang, N. a Ostroff, B. L. Baumgartner, S. Nayak, L. S. Tsimring, and J. Hasty. 2008. Metabolic gene regulation in a dynamically changing environment. *Nature* 454: 1119–22.

145. LeDuc, P., and W. Messner. 2011. How do control-based approaches enter into biology? *Annu. Rev. Biomed. Eng.* 13: 369–96.

146. Toettcher, J., O. Weiner, and W. Lim. 2013. Using optogenetics to interrogate the dynamic control of signal transmission by the Ras/Erk module. *Cell* 155: 1422–34.

147. Spiller, D., C. Wood, D. Rand, and M. White. 2010. Measurement of single-cell dynamics. *Nature* 465: 736–45.

148. Altschuler, S., and L. Wu. 2010. Cellular heterogeneity: do differences make a difference? *Cell* 141: 559–63.

149. Bennett, M., and J. Hasty. 2009. Microfluidic devices for measuring gene network

dynamics in single cells. *Nat. Rev. Genet.* 10: 628.

150. 2008. Microfluidic platform for real-time signaling analysis of multiple single T cells in parallel. *Lab Chip* 8: 1700–12.

151. Love, J. Christopher, Jehnna L. Ronan, Gijsbert M. Grotenbreg, Annemarthe G. van der Veen, and H. L. P. 2006. A microengraving method for rapid selection of single cells producing antigen-specific antibodies. *biotechnology* 24: 703.

152. Carlo, D., and L. Lee. 2006. Dynamic single-cell analysis for quantitative biology. *Anal. Chem.* 78: 7918–7925.

153. Jeon, N. L., S. K. W. Dertinger, D. T. Chiu, I. S. Choi, A. D. Stroock, and G. M. Whitesides. 2000. Generation of solution and surface gradients using microfluidic systems. *Langmuir* 16: 8311–8316.

154. Lipan, O., and W. Wong. 2005. The use of oscillatory signals in the study of genetic networks. *Proc. Natl. Acad.* 102: 7063–7068.

155. Kuczenski, B., W. Ruder, W. Messner, and P. LeDuc. 2009. Probing cellular dynamics with a chemical signal generator. *PLoS One* 4: e4847.

156. Azizi, F., and C. Mastrangelo. 2008. Generation of dynamic chemical signals with pulse code modulators. *Lab Chip* 8: 907–912.

157. Abate, A., and D. Weitz. 2008. Single-layer membrane valves for elastomeric microfluidic devices. *Appl. Phys. Lett.* 92: 243509.

158. Unger, Marc A., Hou-Pu Chou, Todd Thorsen, Axel Scherer, and S. R. Q. 2000. Monolithic microfabricated valves and pumps by multilayer soft lithography. *Science* 288: 113–116.

159. Bontoux, N., A. Pépin, Y. Chen, A. Ajdari, and H. Stone. 2006. Experimental characterization of hydrodynamic dispersion in shallow microchannels. *Lab Chip* 6: 930–935.

160. Ajdari, A., N. Bontoux, and H. Stone. 2006. Hydrodynamic dispersion in shallow microchannels: the effect of cross-sectional shape. *Anal. Chem.* 78: 387–392.

161. Taylor, G. 1953. Dispersion of soluble matter in solvent flowing slowly through a tube. *Proc. R. Soc. London A Math. Phys. Eng. Sci.* 219: 186–203.

162. Aris, R. 1956. On the dispersion of a solute in a fluid flowing through a tube. *Proc. R. Soc. London A Math. Phys. Eng. Sci.* 235: 67–77.

163. Omilusik, K., L. Nohara, and S. Stanwood. 2013. Weft, warp, and weave: the intricate tapestry of calcium channels regulating T lymphocyte function. *Front. Immunol.* 4.

164. Skupin, A., H. Kettenmann, and M. Falcke. 2010. Calcium signals driven by single channel noise. *PLoS Comput Biol* 6: e1000870.

165. Skupin, A., H. Kettenmann, U. Winkler, and M. Wartenberg. 2008. How does intracellular Ca 2+ oscillate: by chance or by the clock? *Biophys. J.* 94: 2404–2411.

166. Kwon, J., K. E. Shatynski, H. Chen, S. Morand, X. de Deken, F. Miot, T. L. Leto, and M. S. Williams. 2010. The nonphagocytic NADPH oxidase Duox1 mediates a positive feedback loop during T cell receptor signaling. *Sci. Signal.* 3: ra59.

167. Sena, L. a, S. Li, A. Jairaman, M. Prakriya, T. Ezponda, D. a Hildeman, C.-R. Wang, P. T. Schumacker, J. D. Licht, H. Perlman, P. J. Bryce, and N. S. Chandel. 2013. Mitochondria are required for antigen-specific T cell activation through reactive oxygen species signaling. *Immunity* 38: 225–236.

168. Reth, M. 2002. Hydrogen peroxide as second messenger in lymphocyte activation. *Nat. Immunol.* 3: 1129–1134.

169. Bekker, L.-G., S. Freeman, P. J. Murray, B. Ryffel, and G. Kaplan. 2001. TNF-α Controls Intracellular Mycobacterial Growth by Both Inducible Nitric Oxide Synthase-Dependent and Inducible Nitric Oxide Synthase-Independent Pathways. *J. Immunol.* 166: 6728–6734.

170. Breitfeld, Dagmar, Lars Ohl, Elisabeth Kremmer, Joachim Ellwart, Federica Sallusto, Martin Lipp, and R. F. 2000. Follicular B helper T cells express CXC chemokine receptor 5, localize to B cell follicles, and support immunoglobulin production. *J. Exp. Med.* 192: 1545–1552.

171. Nurieva, R., and Y. Chung. 2010. Understanding the development and function of T follicular helper cells. *Cell. Mol. Immunol.* 7: 190.

172. Underhill, D. M., M. Bassetti, A. Rudensky, and A. Aderem. 1999. Dynamic Interactions of Macrophages with T Cells during Antigen Presentation. *J. Exp. Med.* 190: 1909–1914.

173. Bossi, G., C. Trambas, S. Booth, and R. Clark. 2002. The secretory synapse: the secrets of a serial killer. *Immunol. Rev.* 189: 152–160.

174. Trambas, C., and G. Griffiths. 2003. Delivering the kiss of death. *Nat. Immunol.* 4: 399–403.

175. Russell, J., and T. Ley. 2002. Lymphocyte-mediated cytotoxicity. *Annu. Rev. Immunol.* 20: 323–370.

176. Stinchcombe, J., and G. Griffiths. 2007. Secretory mechanisms in cell-mediated cytotoxicity. *Annu. Rev. Cell Dev. Biol.* 23: 495–517.

177. Kemp, M. L., L. Wille, C. L. Lewis, L. B. Nicholson, and D. a Lauffenburger. 2007. Quantitative network signal combinations downstream of TCR activation can predict IL-2 production response. *J. Immunol.* 178: 4984–4992.

178. Fooksman, D.R., Vardhana, S., Vasiliver-Shamis, G., Liese, J., Blair, D.A., Waite, J., Sacristán, C., Victora, G.D., Zanin-Zhorov, A. and Dustin, M. L. 2009. Functional Anatomy of T Cell Activation and Synapse Formation David. *Annu. Rev. Immunol.* 28: 79–105.

179. Biggs, M.J.P., Milone, M.C., Santos, L.C., Gondarenko, A. and Wind, S. J. 2011. High-resolution imaging of the immunological synapse and T-cell receptor microclustering through microfabricated substrates. *J. R. Soc. Interface* rsif20110025.

180. Whitesides, G. 2006. The origins and the future of microfluidics. *Nature* 442: 368.

181. El-Ali, Jamil, Peter K. Sorger, and K. F. J. 2006. Cells on chips. *Nature* 442: 403.

182. Guldevall, K., B. Vanherberghen, T. Frisk, and J. Hurtig. 2010. Imaging immune surveillance of individual natural killer cells confined in microwell arrays. *PLoS One* 5:

e15453.

183. Jang, J., Y. Huang, P. Zheng, and M. Jo. 2015. Imaging of Cell–Cell Communication in a Vertical Orientation Reveals High-Resolution Structure of Immunological Synapse and Novel PD-1 Dynamics. *J. Immunol.* 195: 1320–1330.

184. Şen, M., K. Ino, J. Ramón-Azcón, H. Shiku, and T. Matsue. 2013. Cell pairing using a dielectrophoresis-based device with interdigitated array electrodes. *Lab Chip* 13: 3650–3652.

185. Lee, P., P. Hung, R. Shaw, L. Jan, and L. Lee. 2005. Microfluidic application-specific integrated device for monitoring direct cell-cell communication via gap junctions between individual cell pairs. *Appl. Phys. Lett.* 86: 223902.

186. Skelley, A., O. Kirak, H. Suh, R. Jaenisch, and J. Voldman. 2009. Microfluidic control of cell pairing and fusion. *Nat. Methods* 6: 147–152.

187. Dura, B., M. M. Servos, R. M. Barry, H. L. Ploegh, S. K. Dougan, and J. Voldman. 2016. Longitudinal multiparameter assay of lymphocyte interactions from onset by microfluidic cell pairing and culture. *Proc. Natl. Acad. Sci.* 113: E3599–E3608.

188. Laermer, F. and Urban, A. 2003. Challenges, developments and applications of silicon deep reactive ion etching. *Microelectron. Eng.* 67: 349–355.

189. Nicholson, L.B., Waldner, H., Carrizosa, A.M., Sette, A., Collins, M. and Kuchroo, V. K. 1998. Heteroclitic proliferative responses and changes in cytokine profile induced by altered peptides: implications for autoimmunity. *Proc. Natl. Acad. Sci.* 95: 264–269.

190. Munder, M., E. Bettelli, L. Monney, and J. Slavik. 2002. Reduced self-reactivity of an autoreactive T cell after activation with cross-reactive non–self-ligand. *J. Exp. Med.* 196: 1151–1162.

191. Tan, W., and S. Takeuchi. 2007. A trap-and-release integrated microfluidic system for dynamic microarray applications. *Proc. Natl. Acad. Sci.* 104: 1146–1151.

192. Liu, C., and T. Hermann. 1978. Characterization of ionomycin as a calcium ionophore. *J. Biol. Chem.* 235: 5892–5894.

193. Sloan-Lancaster, J., and P. M. Allen. 1996. Altered peptide ligand–induced partial T cell activation: molecular mechanisms and role in T cell biology. *Annu. Rev. Immunol.* 14: 1–27.

194. Kersh, B. G. J., and P. M. Allen. 1996. Structural basis for T cell recognition of altered peptide ligands: a single T cell receptor can productively recognize a large continuum of related ligands. *J. Exp. Med.* 184: 1259–1268.

195. Sloan-Lancaster, Joanne, Brian D. Evavold, and P. M. A. 1993. Induction of T-cell anergy by altered T-cell-receptor ligand on live antigen-presenting cells. *Nature* 363: 156–159.

196. Pfeiffer, B. C., J. Stein, S. Southwood, H. Ketelaar, A. Sette, and K. Bottomly. 1995. Altered peptide ligands can control CD4 T lymphocyte differentiation in vivo. *J. Exp. Med.* 181: 1569–1574.

197. Chen, Y.Z., Lai, Z.F., Nishi, K. and Nishimura, Y. 2017. TCR-Independent Pathways Mediate the Effects of Antigen Dose and Altered Peptide Ligands on Th Cell Polarization.

J. Immunol. 162: 1923–1930.

198. Nicholson, L. B., a Murtaza, B. P. Hafler, a Sette, and V. K. Kuchroo. 1997. A T cell receptor antagonist peptide induces T cells that mediate bystander suppression and prevent autoimmune encephalomyelitis induced with multiple myelin antigens. *Proc. Natl. Acad. Sci. U. S. A.* 94: 9279–84.

199. Kuchroo, V. K., A. C. Anderson, H. Waldner, M. Munder, E. Bettelli, and L. B. Nicholson. 2002. T cell response in experimental autoimmune encephalomyelitis (EAE): role of self and cross-reactive antigens in shaping, tuning, and regulating the autopathogenic T cell repertoire. *Annu. Rev. Immunol.* 20: 101–23.

200. Munder, M., E. Bettelli, L. Monney, J. M. Slavik, L. B. Nicholson, and V. K. Kuchroo. 2002. Reduced Self-Reactivity of an Autoreactive T Cell After Activation with Cross-reactive Non-Self-Ligand. *J. Exp. Med.* 196: 1151–1162.

201. Nicholson, L. B., J. M. Greer, R. a Sobel, M. B. Lees, and V. K. Kuchroo. 1995. An altered peptide ligand mediates immune deviation and prevents autoimmune encephalomyelitis. *Immunity* 3: 397–405.

202. Nicholson, L.B., Waldner, H., Carrizosa, A.M., Sette, A., Collins, M. and Kuchroo, V. K. 1998. Heteroclitic proliferative responses and changes in cytokine profile induced by altered peptides : Implications for autoimmunity. *Proc. Natl. Acad. Sci.* 95: 264–269.

203. Sloan-lancaster, B., T. H. Steinberg, and P. M. Allen. 1996. Selective activation of the calcium signaling pathway by altered peptide ligands. *J. Exp. Med.* 184: 1525–1530.

204. Chen, Yu-Zhen, Zhong-Fang Lai, Katsuhide Nishi, and Y. N. 1998. Modulation of calcium responses by altered peptide ligands in a human T cell clone. *Eur. J. Immunol.* 28: 3929–3939.

205. Wülfing, C., J. D. Rabinowitz, C. Beeson, M. D. Sjaastad, H. M. Mcconnell, and M. M. Davis. 1997. Kinetics and Extent of T Cell Activation as Measured with the Calcium Signal. *J. Exp. Med* 185: 1815–1825.

206. Mariathasan, S., D. Bouchard, D. E. Speiser, and P. S. Ohashi. 1997. Four types of Ca2+ signals in naive CD8+ cytotoxic T cells after stimulation with T cell agonists, partial agonists and antagonists. *Eur. J. Immunol.* 27: 3414–3419.

207. Feske, S. 2007. Calcium signalling in lymphocyte activation and disease. *Nat. Rev. Immunol.* 7: 690–702.

208. Feske, S., M. Prakriya, A. Rao, and R. S. Lewis. 2005. A severe defect in CRAC Ca2+ channel activation and altered K+ channel gating in T cells from immunodeficient patients. *J. Exp. Med.* 202: 651–662.

209. Barr, V. A., K. M. Bernot, S. Srikanth, Y. Gwack, L. Balagopalan, C. K. Regan, D. J. Helman, C. L. Sommers, M. Oh-Hora, A. Rao, and L. E. Samelson. 2008. Dynamic Movement of the Calcium Sensor STIM1 and the Calcium Channel Orai1 in Activated T-Cells: Puncta and Distal Caps. *Mol. Biol. Cell* 19: 2802–2817.

210. Yog, R., R. Barhoumi, D. N. McMurray, R. S. Chapkin, J. Whitelegge, Y. Gwack, D. Griesemer, B. Strauss, M. Wolfs, A. Quintana, M. Hoth, B. A. Niemeyer, and M. Hoth. 2010. Calcium microdomains at the immunological synapse: how ORAI channels, mitochondria and calcium pumps generate local calcium signals for efficient T-cell

activation. *J. Immunol.* 184: 5865–73.

211. Altan-Bonnet, G., and R. N. Germain. 2005. Modeling T Cell Antigen Discrimination Based on Feedback Control of Digital ERK Responses. *PLoS Biol.* 3: e356.

212. Boutin, Y., D. Leitenberg, X. Tao, and K. Bottomly. 1997. Distinct biochemical signals characterize agonist- and altered peptide ligand-induced differentiation of naive CD4+ T cells into Th1 and Th2 subsets. *J. Immunol.* 159: 5802–5809.

213. Rabinowitz, J.D., Beeson, C., Wülfing, C., Tate, K., Allen, P.M., Davis, M.M. and McConnell, H. M. 1996. Altered T Cell Receptor Ligands Trigger a Subset of Early T Cell Signals. *Immunity* 5: 125–135.

214. Henrickson, S. E., T. R. Mempel, I. B. Mazo, B. Liu, M. N. Artyomov, H. Zheng, A. Peixoto, M. P. Flynn, B. Senman, T. Junt, H. C. Wong, A. K. Chakraborty, and U. H. Von Andrian. 2008. T cell sensing of antigen dose governs interactive behavior with dendritic cells and sets a threshold for T cell activation. *Nat. Immunol.* 9: 282.

215. Windhagen, A., C. Schooz, P. Höllsberg, H. Fukaura, A. Sette, and D. A. Hafler. 1995. Modulation of cytokine patterns of human autoreactive T cell clones by a single amino acid substitution of their peptide ligand. *Immunity* 2: 373–380.

216. Hoth, M., C. Schwindling, A. Quintana, and E. Krause. 2017. Mitochondria positioning controls local calcium influx in T cells. *J. Immunol.* 184: 184–190.

217. Quintana, A., E. C. Schwarz, C. Schwindling, P. Lipp, L. Kaestner, and M. Hoth. 2006. Sustained activity of calcium release-activated calcium channels requires translocation of mitochondria to the plasma membrane. *J. Biol. Chem.* 281: 40302–9.

218. Naghdi, S., M. Waldeck-Weiermair, I. Fertschai, M. Poteser, W. F. Graier, and R. Malli. 2010. Mitochondrial Ca2+ uptake and not mitochondrial motility is required for STIM1-Orai1-dependent store- operated Ca2+ entry. *J. Cell Sci.* 123: 2553–2564.

219. Groves, J. T., and M. L. Dustin. 2003. Supported planar bilayers in studies on immune cell adhesion and communication. *J. Immunol. Methods* 278: 19–32.

220. Bromley, S.K., Burack, W.R., Johnson, K.G., Somersalo, K., Sims, T.N., Sumen, C., Davis, M.M., Shaw, A.S., Allen, P.M. and Dustin, M. L. 2001. The immunological synapse. *Annu. Rev. Immunol* 19: 375–96.

221. Baixauli, F., N. B. Martín-Có freces, G. Morlino, Y. R. Carrasco, C. Calabia-Linares, E. Veiga, J. M. Serrador, and F. Sá nchez-Madrid. 2011. The mitochondrial fission factor dynamin-related protein 1 modulates T-cell receptor signalling at the immune synapse. *EMBO J.* 30: 1238–1250.

222. Lin, W., Y. Suo, Y. Deng, Z. Fan, Y. Zheng, X. Wei, and Y. Chu. 2012. Morphological change of CD4 + T cell during contact with DC modulates T-cell activation by accumulation of F-actin in the immunology synapse. *BMC Immunol.* 16: 49.

223. Martín-Cófreces, N. B., B. Alarcón, and F. Sánchez-Madrid. 2011. Tubulin and actin interplay at the T cell and antigen-presenting cell interface. *Front. Immunol.* 2: 24.

224. Barr, V. A., K. M. Bernot, S. Srikanth, Y. Gwack, L. Balagopalan, C. K. Regan, D. J. Helman, C. L. Sommers, M. Oh-Hora, A. Rao, and L. E. Samelson. 2008. Dynamic movement of the calcium sensor STIM1 and the calcium channel Orai1 in activated T-

cells: puncta and distal caps. *Mol. Biol. Cell* 19: 2802–17.

225. Buck, M. D. D., D. O'Sullivan, R. I. I. Klein Geltink, J. D. D. Curtis, C. H. Chang, D. E. E. Sanin, J. Qiu, O. Kretz, D. Braas, G. J. J. W. van der Windt, Q. Chen, S. C. C. Huang, C. M. M. O'Neill, B. T. T. Edelson, E. J. J. Pearce, H. Sesaki, T. B. B. Huber, A. S. S. Rambold, and E. L. L. Pearce. 2016. Mitochondrial Dynamics Controls T Cell Fate through Metabolic Programming. *Cell* 166: 63–76.

226. Junker, C., and M. Hoth. 2011. Immune synapses: mitochondrial morphology matters. *EMBO J. EMBO J. Eur. Mol. Biol. Organ. | All Rights Reserv.* 30: 1187–1189.

227. Chia, H. N., B. M. Wu, V. Cristini, J. Kim, J. Lowengrub, and S. Singh. 2015. Recent advances in 3D printing of biomaterials. *J. Biol. Eng.* 9: 4.

228. Hawkins, B. J., K. M. Irrinki, K. Mallilankaraman, Y. C. Lien, Y. Wang, C. D. Bhanumathy, R. Subbiah, M. F. Ritchie, J. Soboloff, Y. Baba, T. Kurosaki, S. K. Joseph, D. L. Gill, and M. Madesh. 2010. S-glutathionylation activates STIM1 and alters mitochondrial homeostasis. *J. Cell Biol.* 190: 391–405.

229. Penna, A., A. Demuro, A. V Yeromin, S. L. Zhang, O. Safrina, I. Parker, and M. D. Cahalan. 2008. The CRAC channel consists of a tetramer formed by Stim-induced dimerization of Orai dimers. *Nature* 456: 116.

230. James, J. R., and R. D. Vale. 2012. Biophysical mechanism of T-cell receptor triggering in a reconstituted system. *Nature* 487: 64–69.

231. Xiao, B., B. Coste, J. Mathur, and A. Patapoutian. 2011. Temperature-dependent STIM1 activation induces Ca^{2}+ influx and modulates gene expression. *Nat. Chem. Biol.* 7: 351–8.